Processing of organic waste by Catalytic Supercritical Water Gasification

by

Boris Fotso Tapah

A thesis submitted to

The University of Birmingham

for the degree of

DOCTOR OF PHILOSOPHY (PhD)

13/08/2013

Supercritical Fluids Technology

Research Group

School of Chemical Engineering

The University of Birmingham

Abstract

The objective of this work was to investigate the processing of organic waste by catalytic supercritical water gasification into gases and valuable compounds. The organic wastes that have been considered were pure, crude glycerol and to a less extent digestate, a by-product from biogas production by anaerobic digestion. Above its critical point [>221 barg, >374°C], the properties of water, such as the low relative permittivity (ratio of the permittivity of a substance to that of free space) and high ionic product enhance the dissolving capability of most compounds including non-polar organic compounds, by allowing high reactivity, and the ability to act as an acid/base catalyst. Converting glycerol, a by-product from biodiesel production in the most cost-effective routes into useful products and energy could contribute to a positive life cycle for the biodiesel process. One kg of glycerol is produced for every 10 kg of biodiesel and has the potential to be used as a source of H_2, syngas or CH_4 by an appropriate conversion process. Catalytic Supercritical Water Gasification (CSCWG) for the processing of crude glycerol solutions is one such viable option. In this work, the degradation of glycerol by CSCWG at temperatures [400-550°C], pressures [170-270 barg], feed concentrations [2-30 wt %], flowrates [10-65 $mLmin^{-1}$] or/and WHSV [38 -125 h^{-1}] was investigated using a packed bed reactor (PBR) containing a known amount (10.1 g at optimal loading) of Fe_2O_3+Cr_2O_3 or Fe_3O_4 catalysts. The results of the degradation of glycerol in supercritical water show that conversion of pure glycerol (58 % at 550°C) without a catalyst can be achieved, but complete conversion of pure glycerol over Fe_2O_3+Cr_2O_3 or Fe_3O_4 catalysts (at 550°C, 250 barg, <15 wt% feed concentration, 10.1 g catalyst loading (3.5 mm cylinder with 4 mm diameter) can be reached. When crude glycerol was used, the conversion decreases from 100 to 67 mole% and 100 to 74 mole% over the same catalysts and conditions. The amount of catalyst loading over the same experimental conditions does not significantly affect product gas yield, but selectivity for hydrogen increased from 41 to 49 mole% with reducing Fe_2O_3+Cr_2O_3 loading (3.5 mm cylinder with 4 mm diameter) from 32.3 to 10.1 g (representing 12 vol% of the 30 mL reactor capacity), respectively. Hydrogen yield was as high as 61 mole% and 49 mole % when crude glycerol was gasified over Fe_3O_4 and Fe_2O_3+Cr_2O_3, respectively. 64 mole% of syngas was obtained with minimum 4:1 mole ratio of H_2:CO. Syngas yield remains low for both catalysts due to low yield of CO, which suggests a poor reforming of carbon oxides. Hydrocarbon yields (69 mole% for ethylene and 22 mole% for methane) were obtained and this decreased with temperature as a result of

thermal cracking. The catalytic cracking of hydrocarbons cannot be limited to one single reaction. Depending of the catalyst selection and the operating conditions such as temperature, pressure, feed concentration, WHSV and reaction time; a mixture of gaseous (H_2, CO, CO_2, CH_4, C_2H_4), liquid products (ethanol, methanol, allyl-alcohol, formaldehyde, acetaldehyde, propionaldehyde and acrolein) and char are formed. These formations resulted from various reactions (WGS, methanation, gas-solid reaction) and their mechanism of formation. Small amounts of char (< 3.1 wt%) and carbon deposition on the catalyst surface and inside the reactor wall was observed. Lower yield of tar and char by-products were formed, mainly with increased feed concentration above 20 wt %, which was due to polymerisation reactions. The condensate liquid effluent was found to have little COD value (< 21 %), and due to an initially slow reaction, its colour changed with run time from brown (0 to 20 min) into a clear (35 to 80 min) and transparent in the case of crude glycerol. Prolonged exposure of Fe_2O_3+Cr_2O_3 to 172 h on-stream under supercritical conditions resulted in fragmentation of the surface from metal sintering, which reduced activity for H_2 production. No sign of deactivation was observed on both catalysts after 9 h on-stream. However, Fe_3O_4 was found to have better activity on hydrogen production than Fe_2O_3+Cr_2O_3 probably due to its high iron content, enhancing its thermal conduction. Neither catalysts were able to promote a good balance syngas ratio of 2:1 for H_2:CO that is suitable for FTS into mixed alcohols; minimum of 4:1 ratio was obtained. This demonstrated that the utilisation of effective and low cost-effective iron oxide catalysts (Fe_2O_3+Cr_2O_3 or Fe_3O_4) in a high pressure SCWG of glycerol can be carried out successfully at a temperature up to 550°C when compared to non-catalytic SCWG, which is usually carried out at 700-800°C to produce H_2-rich gases. Preliminary results of the digestate show that 69.6 wt% of product gas containing 42.3 mole% of H_2 can be obtained by CSCWG of 2 wt% digestate over Fe_3O_4 at the same conditions.

Acknowlegments

I wish to express my appreciation to Dr. Gary Leeke whose supervise and guide me throughout this research program and has contributed immensely to the success of this work. I am also indebted to my co-supervisor Dr. Regina Santos, who gave me valuable suggestions throughout this research program and for providing crude glycerol for the research studies. I would like to thank my internal and external examiners, Dr. Neil Rowson and Prof. Paul Williams, respecivetly for their advices and suggestions on the thesis.

I would like to thank Dave Boylin and the Mechanical Engineering workshop teams for their assistance on manufacturing the mini-cooler, mini-reactor, and LEV Extraction system, which were used for the construction of the laboratory and pilot plant rigs. I would like to thank John Bowden at minelco.com Ltd for providing magnetite catalyst for this research studies. I would like to thank Graham Burns and Peter Hachton at the chemistry department for helping me in GC-MS analysis. I would like to thank John Wedderburn and Paul stanley both at the metallurgic and microscopic centre for their helps on the BET and ESEM-EDS analysis, respectively. Also, i would like to thank Alireza Bahari a former fellows research student at the Chemical Engineering Department for his help with the GC studies and Lynn Drapper for her administrative assistance.

I express my sincere appreciation to Dr. Teijun Lu and to all the members of the supercritical fluids groups, for all the discussions and suggestions. I thank all my friends for supporting me to complete this research work successfully.

I thank EPSRC for providing me with a scholarship. The Chemical Engineering Department for their financial assistance during struggling time, which i gratefully acknowledged.

Last but not the least, thanks to my wife, kids, parents, brother and sisters for their enthusiastic support which encouraged me throughout my academic pursuits.

This work is dedicated to

My Parents, My kids

And

To the memory of my youngest brother; Elvis

To the memory of my older brother; Benjamin

Table of Contents

List of Figures

List of Tables

Abbreviations

Symbol	Description	Unit
BET	Brunauer-Emmett-Teller	
GC	Gas chromatography	
SC	Supercritical	
SCW	Supercritical water	
SCWG	Supercritical water gasification	
CSCWG	Catalytic supercritical water gasification	
XRD	X-ray diffraction	
ESEM	emission scanning electron microscope	
EDS	energy-dispersive spectrometer	
ICP-MS	Inductively coupled plasma mass spectrometry	
TCD	thermal conductivity detector	
FID	Flame ionised detector	
SCF	Supercritcal Fluid	
SRM	Steam reforming of methane	
SOFC	Solid oxide fuel cell	
P	Pressure	barg
T	Temperature	°C
F	Flowrate	$ml.min^{-1}$

WHSV	Weight hourly space velocity	h^{-1}
LHSV	Liquid hourly space velocity	h^{-1}
STP	Standard Temperature and pressure *(0^oC* and under a pressure of *1,013 mbar)*	
SS	Stainless Steel	
o.d	Outside diameter	
UV	Ultraviolet	
GHG	GreenHouse Gases	
d_{50}	Catalyst particle size	

Symbol	**Description**	**Unit**
γ	Activity coefficient	
y	Intercept of the calibration equation	
x	Concentration variable	$mg.mL^{-1}$
η	Dynamic viscosity	mPa s
ρ	Density	$g\ cm^{-3}$
ϵ	Dielectric constant	Fm^{-1}
Φ	Volume fraction	
C_P	Specific heat capacity	$J.mole.K^{-1}$
τ	Residence time	s
ε	Bed porosity	fraction
$C_{g,\,i}$	Concentration of the component (i) in the gas sample	$mg.mL^{-1}$
C_S	Concentration of the external standard	$mg.mL^{-1}$

$C_{l,\,i'}$	Concentration of the component (i') in the liquid	$mg.mL^{-1}$
$A_{g,i}$	Peak areas of the gas component (i) in the gas sample	Area unit
A_S	Peak areas of the external standard gas	Area unit
$A_{S'}$	Peak areas of the internal standard in the liquid sample	Area unit
$A_{l,\,i'}$	Peak areas of the component(i') in the liquid sample	Area unit

Subscripts

Symbol	**Description**
E	Excess properties
C	Combinatorial
R	Residual
L	Liquid
V	(vapour)
Sat.	Saturated

CHAPTER 1. INTRODUCTION AND AIMS

1.1 Organic waste problems and solution approaches

As the world population continues to increase from a current number of 6 billion (2012) to a projection of 9 billion in the year of 2050, the amount of organic waste generated by human, animal and agricultural activity would also increase causing more pollution problems to the environment. Disposing of waste organics in landfill only exacerbates the environmental problems of greenhouse gases (GHG) gases, dust and occupation of viable landfill that could be used for food production.

In addition, the demand for energy and chemicals are increasing, while concomitantly fossil fuel resources are depleting. The growing demand for foods due to the growing world population, the productivity of forest and energy crops, the increased use of biomaterials and the need to reduce the environmental impact of energy/chemicals production are the crucial factors for the utilisation of alternatives source for energy and chemicals production. One of these is the low cost conversion of organic waste/ biomass into fuel gas (e.g. H_2-rich light alkanes).

The utilisation of biodiesel has become more attractive recently because of its environmental benefits and the fact that it is biodegradable, made from renewable resources and the growing interest in using vegetable oil fuels for diesel engines. However, the production cost of biodiesel (US$0.53L ($2.00/gal) is significantly higher compared to fossil derived diesel (US$0.0022/L ($0.0085/gal) [**1**], which constitutes a barrier for its commercial development. Because of the mass transfer limitation between the oil and alcohols during the continuous transesterification process, significant amount of by-product (crude glycerol) can be produced. Finding a suitable and cost effective route for the conversion of crude glycerol into valuable products such as H_2-rich gas could contribute to lower the cost of biodiesel.

Digestate is another organic waste of research interest. It is recovered as a waste residue from anaerobic digestion to produce biogas either by acidogenesis (if plant wastes containing fibres, grass or lignocellulosic (LC) biomass are used as feed or by methanogenesis (if sludge from liquor is used). The digestate can be used as fertiliser. However, the problem is the high transport cost of this material from the plant to the agricultural land and the seasonal factor that restricted its utilisation in the landfill to a few months in order to avoid run off the fertiliser, which could potentially contaminate local water.

Because of these issues, an ideal solution for handling the liquid digestate is currently being investigated.

Supercritical water gasification (SCWG) of organic wastes has been studi

as the most promising routes for organic waste processing. However, little progress has been achieved to exploit the technologies at a commercial scale because of the remaining unsolved engineering problems (such as salt deposition, corrosion issues and high cost of metals catalyst) and the absence of reliable kinetic data for the decomposition by SCWG of organic wastes have not been yet established .

Supercritical water gasification is an innovative thermo-chemical method for converting biomass and organic wastes into hydrogen and light alkanes gaseous products. However, at present, there are remarkably few reports in the literature on the SCWG of "real organic wastes" and this work will provide valuable data together with addressing some of the problems reported in catalytic supercritical water gasification (CSCWG) processes:

- Reduce the operating cost by investigating the conversion at a temperature below 550°C under high pressure (>250 barg).
- Exploring a low cost iron oxide catalyst that has the potential to be effective, when compared to the high cost metals (Ni, Pt). Their integrity in hydrothermal processes, and their capability to break the glycerol and crude glycerol into light gases, such as H_2, CO, CO_2, and CH_4.
- Mitigating the salt issues in SCW by pre-treatment (ion removal in deionised water production) of the water used in preparation of the feed slurry.
- Utilisation of a flow reactor, which is more suitable for high-pressure systems over other reactor configurations, as it provides uniform heat transfer, better conversion per unit volume, and has the potential for high catalyst loading.

1.2 Background of SCWG

SCWG processes are currently being investigated both as a novel technique for waste treatment processes, and as a means of energy and materials recovery from biomass and biodegradable organic wastes. The process takes place above the critical pressure (>221 barg) and temperature of water (>374°C) although the processes are also operated in the sub-critical conditions. On the approach to supercritical conditions and above, the thermo-physical properties of water such as the density, viscosity, thermal conductivity, specific heat capacity, ionic product, diffusivity and solvent ability change drastically compared to ambient, and are often in orders of magnitude different with respect to subcritical conditions [**2, 3, 4**]. Organic compounds have high solubility [**5, 6, 7**] in water at elevated

temperatures. More often than not the vapour-liquid phases become indistinguishable (only one phase exists in SC conditions) and the water behaves as a dense gas, which enhances the elimination of barriers to inter-phase mass transport and thus provides opportunities conditions by just changing the pressure or/and temperature.

The catalytic supercritical water gasification (CSCWG) process has many advantages, when compared to high temperature non-CSCWG and conventional gasification. This is because; higher gasification efficiencies can be achieved at much lower temperatures of approximately 550°C. Simple flow reactors can be used to yield the product gas at high pressure, which can be stored directly in pressurised storage tanks resulting in a significant energy saving.

A number of studies have reported on the utilisation of model compounds (cellulose, alcohols and pure glycerol) [**8 -12**] and real organic wastes (animal waste, sewage sludge, sawdust, rice straw and waste from the food industry) [**13-17**] in SCWG. Depending on the materials' of choice and primary source, the organic wastes may contain minerals and metal elements (e.g., nitrates, phosphates, carbonates, halides, silicates and sulfides) that could interfere with the reaction mechanism. For instance, under supercritical conditions, the solubility of minerals (salt) in water is reduced drastically, leading to mineral precipitation and crystals in the SCWG process. These solid deposits ultimately lead to clogging of the gasification process and corrosion.

This work reports on the CSCWG of a model compound (pure glycerol), and real organic waste (crude glycerol and digestate) over iron oxide and magnetite catalysts. The influence of the operating conditions (reactor temperature, feed concentration, pressure, WHSV, time on-stream) and catalyst parameters (catalyst loading, particle size) were studied using model compounds to establish the optimal conditions for the high product gas yield and H_2-rich gases. The second part of the study investigated the CSCWG of crude glycerol and digestate over the same catalyst; the results of pure glycerol and crude glycerol are compared, as well as the influence of iron oxide-based catalysts.

1.3 The aim and objectives of the work

The overall aim of this PhD study was to investigate the hydrothermal processing of organic wastes by CSCWG over low cost catalysts, into higher product gas yields or/and H_2-rich gases. This aim was accomplished by meeting the following objectives:

- Construction of bespoke CSCWG equipment at laboratory and pilot scales.
- Studying decomposition of pure glycerol in SCW to understand the reactions involved, the reactions conditions and the impact of cheap metal oxide catalysts.

- Establishing the optimal operational and catalytic conditions for the maximisation of products gas and H_2-rich gas
- Evaluation of CSCWG of crude glycerol based on the optimal conditions obtained and to report preliminary data for CSCWG of digestate.
- Conducting various analytical techniques to investigate the product gas, liquid and char phase of the process, as well as the characterisation of the catalysts used.

1.4 Layout of this thesis

This thesis consists of 8 chapters. Chapter 1 is the introduction. The literature review presented in chapter 2 provides an overview of the work done in the field of organic waste processing by SCWG. Detailed literature specific to chemical reactions in SCW is included in subsections 2.3 and 2.4. Chapter 3 describes the materials and the experimental methods used for both laboratory and pilot scale rigs. Chapter 4 presents the results and discussion of the catalyst characterisation. Chapter 5 presents the results and discussion of SCWG and CSCWG of the model compounds glycerol over Fe_2O_3-Cr_2O_3. Chapter 6 studies the processing of crude glycerol by CSCWG over Fe_2O_3-Cr_2O_3 and Fe_3O_4. Preliminary work of CSCWG of digestate is also described. Chapter 7 evaluates the engineering problems of the SCWG process and key areas for optimisation of the existing process. Chapter 8 lists the conclusions of the thesis and proposed future work.

CHAPTER 2. LITERATURE REVIEW

2.1 Introduction to SCF technologies and SCWG

Scientists have intensively studied supercritical fluids (SCF) since the past century, and they continue to receive more attention in order to establish their full potential benefits to chemistry and industry. A supercritical fluid is any substance compressed to a pressure higher than the critical pressure (P_c) above the critical temperature (T_c). SCFs have different properties when compared to ordinary liquids or/and gases; these properties can be modified by changing the pressure and temperature. For instance, density and viscosity change drastically at conditions close to the critical point. Because of their unique characteristics, SCFs also offer a series of technical advantages including exploitation in chromatography (e.g. separations of compounds can be based on a user programmed density profile with the supercritical fluid being used as the mobile phase) and chemical engineering (e.g. particle production, chemical reactions, extraction and separation processes). Performing chemical reactions at supercritical conditions provides opportunities to manipulate the reaction environment (solvent properties) by modifying the pressure; to enhance the solubility of reactants and products, and to eliminate inter-phase transport limitations on reaction rates [**18**]. In addition, SCFs can form single-phase mixtures (liquid + gaseous) of reactants, creating no barrier to rate-limiting mass-transfer and thus enhancing reaction rates. Using SCFs in large-scale chemical manufacturing could lead to pollution prevention; since they can be used as solvents instead of volatile organic solvents, such as chlorinated hydrocarbons. For example, supercritical carbon dioxide ($scCO_2$), [T_c = 31 °C and a P_c = 73 barg] has excellent potential for achieving this goal. Although, $scCO_2$'s ability to dissolve polar, ionic or polymeric compounds is limited, it is widely available, inexpensive, non-flammable, nontoxic, and environmentally friendly if captured and recycled. It has solubility toward non-polar organic compounds and upon depressurisation; it can facilitate the separation process of reactants, catalysts and products as it returns to a gaseous state. Supercritical water (scH_2O), [T_c = 374°C and P_c = 221 barg] is another ideal SCF medium. Supercritical fluids based on water can simplify separation processes, and solvent strength can be manipulated to improve its extraction capability for polar and non-polar compounds. Chemicals dissolved in supercritical water only require the pressure to be reduced to allow water to return to its normal properties thereby facilitating the separation of organic compounds.

Although, SCFs have multiple merits (refer to sub-section 2.2), they are still under-exploration and have not been fully exploited by industry. This may be because of the limitation of knowledge on certain phenomena surrounding SCF or because of its disadvantages such as high capital process costs. Salt deposition, corrosion issues and an elevated pressure process, which has its associated safety concerns.

Over the last two decades, researchers have explored the conversion of organic wastes in order to find alternatives sources to produce chemicals, fuels and other bio-based products. A study reported that most organic wastes could be converted into useful biofuels and bio-chemicals by upgrading (fractionation, liquefaction, pyrolysis, hydrolysis, fermentation, and gasification) and biorefinery technologies [**19**]. Amount these three key technologies are continuously receiving more attention: hydrolysis, pyrolysis and gasification. The aim is to combine these three technologies in a single platform known as bio-refining, which could facilitate the large-scale manufacturing of low cost bio-products and bio-fuels. In spite of the economic, environmental and sustainable potential, the technologies still face many challenges. One of these limitations is the ability to deal with heterogeneous feedstocks, which means that the technology must make use of a wider variety of processing techniques. Other limitations may be the cost of capital equipment, and the scale-up to commercial scale.

Hydrothermal processes have the potential to address most of these limitations, and have attracted worldwide attention because of the fascinating characteristics of water as a reaction medium at elevated temperatures and pressures [**20**]. Among the hydrothermal processes, it is possible to highlight Supercritical Water Gasification (SCWG), a process that occurs in the partial or total absence of dissolved oxygen. Supercritical water is used as reagent, and oxidant to gasify selected organic compounds to produce a mixture of product gas (H_2, CO, CO_2, CH_4), condensate liquid product and char. This process can be accomplished both in supercritical and near-supercritical water [**21**]. Water changes its character from a solvent for ionic species at ambient conditions, into a solvent for non-ionic species at supercritical conditions, enabling non-polar substances to be readily dissolved and extracted. An electrochemical property, e.g. relative permittivity decreases from 75 at ambient conditions to 5 at SCF conditions [**22**]. The reactivity of water increases in the neighbourhood of the critical point without the presence of a catalyst. scH_2O is relatively non-polar but highly acidic; the pH-value decreases by three units in SCW regions, which provides more hydroniums (H_3O^+) ions for acid catalysed reactions. Thus, most organic compounds can be easily fractionated in supercritical conditions. In comparison to other thermal processes, SCWG is reported to reduce the cost of organic materials or biomass conversion to £1.86 /GJ [**23**]. This hydrothermal process is favoured over vapour phase processes as it overcomes the low volatility of carbohydrates and negates the need for a dry

feedstock, which would otherwise require an energy intensive drying step. SCWG technology is set to receive more attention in order to determine its full economical and technical viability in comparison to other thermal processes.

This chapter reviews the SCFs technology, with detailed studies on the SCWG of organic wastes. The process, feedstock, chemical reactions, the used of catalyst, and design issues in SCWG are discussed.

2.2 Supercritical fluids

Two groups of properties make a supercritical fluid (SCF) an attractive solvent or/ and a reaction medium from a chemical engineering viewpoint. Firstly, because of its adaptable thermodynamic properties (e.g. low density, high solvation capacity); it is possible to match the solubility parameter of the fluid to that of the solute by modest changes in pressure, temperature, or both. These properties determine the capacity and selectivity of a fluid as a solvent for extraction or chemical reactions processes. Secondly, SCF has a favourable transport property (low viscosity and high diffusivity), which results in large Peclet (P_e = f (*Re, Pr*) and Prandtl (*Pr)* numbers, hence large Sherwood numbers (*Sh =f(Re,Sc))*; these factors contribute to large dissolving rates for a number of compounds. This section reviews SCFs with focus on their properties that most influence chemical reactions. e.g diffusion, transition-state, pressure, and selected solvent effects.

2.2.1 Basic physical properties of SCFs

Table 2.1 shows typical properties of SCF (density, viscosity and diffusivity), compared to gases and liquids. It can be seen that the density and transport properties are intermediate between those of a liquid and gas.

Table 2.1. Comparison of a typical physical and transport properties of gases, liquids and SCFs [**24**].

Property	Density ($kg.m^{-3}$)	Viscosity (cP)	Diffusivity ($mm^2. s^{-1}$)
Gas	1	0.01	1-10
SCF	100-800	0.05-0.1	0.01-0.1
Liquid	1000	0.5-1.0	0.001

The density, viscosity, and diffusivity values are dependent on temperature and pressure change. The SCF density is closer to that of organic liquids and its solvent power increases with density at a given temperature. On the other hand, the viscosities and diffusivities of SCF's are closer to that of gases.

Thus, a SCF can diffuse faster in a solid matrix than a liquid, while at the same time it possesses a solvent strength to extract the solute from the solid matrix. Carbon dioxide is the most commonly used SCF, primarily due to its low critical parameters (31.1°C, 73.8 barg), low cost and non-toxicity. SCW is another captivating SCF's, which is usually used to conduct chemical reactions for the gasification of organic wastes. These reactions can be accomplished in sub-critical, above CP of water (>221 barg, >371°C) or at high temperature (600 to 800°C). However, several other SCFs, including water have been used in both commercial and development processes.

2.2.2 Phase behaviour in SCF and its importance in SCF technologies

Phase behaviour is best illustrated in a phase diagram, where critical points (CP) are defined. The CP represents the highest temperature and pressure at which the substance can exist as a vapour and liquid in equilibrium. Figure 2.2 (refer to sub-section 2.3.2) shows phase diagram of water where a gas, liquid, solid or SCF phase boundaries are present. At the triple point, (TP), the three phases coexist. However, above CP point, only one phase exists, which is known as the supercritical (SC). In SCF technologies, the effect of pressure plays a crucial role as the driving force for the change of properties and phase behaviour. For instance, the pressure effect on chemical reaction is to stimulate the selectivity and the rate of reaction. By enhancing the solubility and phase condition of the component involved; e.g., SCWO at high pressure is an efficient method for the decontamination of wastes [**25**]. $ScCO_2$, if used as solvent can be applied in number of processes including SC extraction, fractionation, dyeing, cleaning, degreasing and crystallisation.

2.2.3 Solubility and factors affecting solubility in SCF

The solubility parameter and relative permittivity are also density dependent properties. The solubility increases with increasing density (i.e. with increasing pressure at constant temperature). The main factors that affect solubility in a SCF include solvent selection, chemical functionality of the solute and temperature or/and pressure. The reduced effect of hydrogen bonding is responsible for the change in solubility properties of supercritical water. Hydrogen bonding is a weak force, and its effect decreases with a decrease in the density of water under supercritical conditions. A study has demonstrated that a spectroscopic and computer simulation technique can be used to evaluate the number of hydrogen bonds per water molecule in SCW, which are about one-third that at numbers at ambient conditions [**26**]. Hydrogen bonding is important to determine how a SCF will interact with potential solutes and whether a single phase can be formed.

An intermolecular interaction between the solvent and the solute depends on the functional groups present in its molecular structure [**27**]. This factors, as well as vapour pressure determine solubility in a

given SCF. In addition, a change in pressure and temperature will affect the solubility of reactants and products, as well as the phase behaviour, diffusivity of the solute, the reaction rate and its activation energy. Because of the unique solubility properties of SCFs, compounds that are largely insoluble in a fluid at ambient conditions can become soluble in the fluid at supercritical conditions. Conversely, some compounds that are soluble at ambient conditions can become less soluble at supercritical if water is considered; organic compounds are highly soluble in SCW, whereas the solubility of salts and inorganic are reduced in the same region. Increasing temperature at constant density would decrease the relative permittivity, as a result of the breakage of hydrogen bonds. The association of H-O-H bonding depends strongly upon pressure and temperature under SCW conditions. This association influences the solubility phenomena, the reaction chemistry, and the corrosion. Stillinger F. et al have investigated extensively the molecular dynamics of hydrogen bonding at high temperature [**28**]. Their study indicate that the system density (>50 barg) leads to a shortening of the hydrogen bond, and exhibited a temperature dependence for liquid-like densities (ρ>0.6 g.cm^{-3}), but not for vapour-like densities; with a phase transition around the critical density.

2.2.4 Diffusion and mass transfer effects in SCFs

Diffusion is a random thermal movement of a molecule from high to the low concentration zones in a given volume until the system reaches equilibrium (net flux is zero). A profound understanding of diffusion in SCFs is of considerable importance for reaction control, design of SC equipments, SC process development and its exploitation in extraction processes. However, there are currently little available fundamental diffusion data in the supercritical region. This is due to two mains reasons: (i) sampling difficulties encountered in high-pressure systems as a result of accurately measuring and maintaining the pressures and (ii) the challenge posed by the design of apparatus for the measurement of diffusion coefficients in SCF.

Factors affecting this challenge are mainly due to the limitation in measuring transport properties at high pressures and the difficulty in obtaining a representative sample without disturbing the system from equilibrium. A good control of these factors is necessary in order to limit convective effects. Natural convection effects should be accounted for when measuring diffusion in SCFs; because SCFs exhibit exceptionally drop in viscosities with temperature increased towards SC [**29**]. The conversion bulk flow (forced convection) usually results from forces on the system. However, this can be occasionally caused by diffusion, which plays a critical role on phase transformations (mass transport during phase change resulting from random molecular motion).

In a heterogeneous system where a catalyst is used, diffusion occurs across the surface of the catalyst (external diffusion) and inside of the catalyst through the pores (internal diffusion). The analysis of

internal diffusion is complicated by many factors such as the shape of the particles, distribution in size and shape of the catalyst pores and total volume of the pores with respect to the particle volume (porosity). In addition, the depth to which the pores penetrate the particles, and the tortuosity of the route through the pores where the reactants or substrate encounters, as well as the effective diffusivity of the reactants and products profoundly influence the internal diffusion.

Experimental data for diffusion in SCF are extremely valuable in order to establish theoretical and empirical models for the prediction of diffusion coefficients in SCF. However, the lack of experimental data due to complication in sample collection at high pressure make it difficult to model diffusion coefficients in SCF. Nevertheless, some studies have reported diffusion coefficients measurements in SCF [**30, 31**]. The diffusion expressions are given in appendix A.

The mass transfer in SCFs is improved significantly due to a single-phase, which minimises barrier to mass transfer and because of their favourable transport properties (low viscosity and high diffusivity). Various studies have reported the most common correlations for mass transfer at low pressure and supercritical conditions [**32**], and some of these are summarised in table 2.2.

Table 2.2: Most common correlations for mass transfer at low pressure and SC conditions.

Authors	Application	Range of validity	Correlation
Dwivedi and Upadhyay [**33**]	Gases and liquid at low pressures	*Re* = 0.01-15000 *Sc* = 1 -1000	$\varepsilon j_D = \frac{0.765}{\mathrm{Re}^{0.82}} + \frac{0.365}{\mathrm{Re}^{0.386}}$
Wakao and Kaguei [**34**]	Solid and liquid or gases at low pressures	Re = 3-3000 *Sc* = 0.5-10000	$Sh=2 + 1.1Re^{0.6} Sc^{1/3}$
Lee *et al.* [**35**]	Oils /SCF	uSCF=$4x10^{-5}$ $-2.8x10^{-3}$ m/s *Sc* = *8*	$K_Ga= 1.55 (\frac{u}{\varepsilon})^{0.54}$
Tan *et al.* [**36**]	Solids/SCF	*Re* = 2-40 *Sc* = 2-20	$Sh=0.38Re^{0.83} Sc^{1/3}$
Lim *et al.* [**37**]	Solids/SCF	*Re* = 2 -70 *Gr* = 78-3.25 × 107	$\frac{Sh}{ScGr^{0.25}} = 1.692 \left[\frac{\mathrm{Re}}{Gr^{1/2}}\right]^{0.356}$
Lim *et al.* [**38**]	Solids/SCF, natural convection	*Re* = 4-140 *Sc* = *2-11*	$\frac{Sh}{ScGr^{0.25}} = 0.1813\left[\frac{\mathrm{Re}^{0.5} Sc^{1/3}}{Gr}\right]^{3/4}$ *$(Re^{1/2}Sc^{1/3})^{3/4}$ + 1.2149 $\left[(\frac{\mathrm{Re}^2 Sc^{1/3}}{Gr})^{3/4} - 0.0165\right]^{1/3}$
Lee and Holder [**39**]	Toluene and naphthalene from silica gel/SCF	*Re* = *0.3-135* +2.48	$\frac{Sh}{ScGr^{0.25}} = 0.526\left(\frac{\mathrm{Re}^{0.5} Sc^{1/3}}{ScGr^{1/4}}\right)^{1.68}$ $\left[(\frac{\mathrm{Re}^2 Sc^{1/3}}{Gr})^{0.643} - 0.8768\right]^{\frac{1}{0.6439}}$
Zehnder and Trepp [**40**]	Natural substances (flat layer)/SCF	*Re* = 100 -2000 *Sc* = 1- 10	$Sh=0.13 Re^{0.5} Sc^{0.632} (d_h/L)^{0.3}$

It can be seen in table 2.2 that few researchers [**34, 36, 40**] were able to establish a standard correlation of the type *Sh =f(Re, Sc),* specific for SCF in packed beds. Other studies [**41**] have

investigated the contribution to mass transfer due from forced convection (inertial forces) separately from that of free convection (buoyancy forces) much like in heat transfer studies. Although they studied the free convection effects separately by performing up flow and down flow experiments, they did not reach a general correlation, only Lim et al. [**37, 38**], Lee and Holder [**39**] correlated the Sherwood number in terms of the Schmidt and Grashof numbers to account for natural convection effects on the dissolution rate.

2.2.5 Transition-state theory applied to SCF_S

This sub-section gives an overview of transition-state theory, pressure, and solvent effects on chemical reactions. However, its does not provide a comprehensive reviewed of the topic as more detailed information is given in the references cited. The kinetics of elementary reactions are best explained by Transition-state theory, which is the state of maximum energy along the reaction coordinate, where the reaction coordinate is the minimum energy pathway between the reactants and products on the potential-energy surface. This theory views a chemical reaction as occurring via a transition-state (M) species. For instance, Cellulose (A) + water (B) → glucose (M) → product gas). The chemical reaction is shown in equation 2.5.

$$aA + bB \rightarrow [M] \rightarrow \text{Products} \qquad (2.5)$$

A study [**42**] defined, the transition-state theory rate constant (k) as

$$k = K\frac{K_B T}{h}K_C \qquad (2.6)$$

Where K_B is the Boltzmann constant, K is the transition coefficient, (h) is Planck's constant, T is the absolute temperature, and K_C is the concentration-based equilibrium constant for the reaction involving the reactants and the transition state. In principle, the properties and structure of water under any thermodynamic conditions can be determined by intermolecular interactions scaled by the thermal energy $K_B T$ as the Boltzmann factor. In theory, Kc can be related to the equilibrium constant and to the difference in Gibb's free energy (ΔG) between the activated complex and the reactants. The rate constant in equation 2.6 can therefore be written as follows:

$$k = K\frac{K_B T}{h} * \exp\left(\frac{\Delta G}{RT}\right) \qquad (2.7)$$

Where, *R* is the gas constant. The rate constant for an elementary reaction step is a function of the difference in Gibb's free energies between the reactants and the transition state. The solvent strength of a SCF may be manipulated by changing pressure and/or temperature to adjust reaction rates by changing equilibrium constants (K_C), or concentrations of reactants and products and transition-state

rate constant (k). In SC region, the concentrations of reactants and products are drastically changed as a result of increasing reactivity.

As showed in equation 2.5 and assuming that the reactants (A and B), and transition state (M) are in equilibrium, the thermodynamic solvent effects on reaction rate constants (k) can be explained using transition state theory, where the activation volume can be expressed as

$$\Delta v = -RT\left(\frac{\partial lnk}{\partial P}\right)_T = v_M - v_A - v_B \qquad (2.8)$$

It can be seen that the activation volume is also function of the rate constant and pressure changed. At the lowest pressures, the magnitude of the activation volume and isothermal compressibility increase with pressure. Beyond the point of maximum compressibility, the compressibility and thus the magnitude of the activation volume decrease sharply with pressure [**43**]. Because of these changes, the selectivity to certain products can be controlled by adjusting pressure or/and temperature to influence the activation volume.

2.2.5.1 Pressure effects on chemical reactions

Various studies have demonstrated that the properties of SCF (e.g., relative permittivity, diffusivity) near its critical point, unlike the properties of a liquid, can change remarkably with pressure and that these changes can also influence kinetics [**44, 45**]. At low pressures, water behaves as a non-polar solvent with low self-dissociation. High pressures can increase the ionic product to values above those found for water at ambient conditions. In addition, solubility of a reactant increases with increasing pressure, enhances with increasing in density. From the transition-state theory rate constant point, the rate constant k is related to the activation volume (Δv), which is the difference between the partial molar volumes (v_m, v_A and v_B) of the activated complex and the reactants [**46**] following equation 2.10:

$$k = K\frac{K_B T}{h} * \exp\left(\frac{\Delta G}{RT}\right) = -\frac{\Delta v}{RT} * \frac{\delta \ln K}{\Delta P} \qquad (2.9)$$

$$\Delta v = v_m - v_A - v_B \qquad (2.10)$$

Where $\frac{\delta * \ln K}{\Delta P}$ is the transition coefficient, which is dependent to the pressure influence that also contributes to speed up the reaction by reducing the space between molecules in a chemical reaction. Iyer and Klein [**47**] have reported on the effect of pressure on the hydrolysis rate of reaction, and their data were used to calculate the effective activation volumes. Van Eldik et al [**48**] works indicated that it is crucial to account Δv, for volume changes arising from changes in bond lengths and angles, and for volume changes arising from electrostriction and other solvent effects.

2.2.5.2 Solvent effects on chemical reactions

Solvent effects are especially valuable for a reaction in SCFs because solvation has effects on both energy transfer and chemical reactions (refer to section 2.3.3). In some cases, these effects can be manipulated to influence the state of the SCF fluid, whereas in other cases, these effects can be used to infer molecular-level information. For instance, if SCWG is conducted with the aim of producing a selective product gas such as H_2, or/and 2:1 ratio of H_2:CO. It is therefore necessary to control the chemical reaction in the process by defining the basic variables such as solute: solvent dosing in the feed, as well as system pressure, residence time, and process temperature. This could contribute to steer the reaction conditions toward the desired product gas.

2.3 Chemical Reaction with SCF

Many fundamentals questions in relation to chemical reactions in SCF are still unanswered. Some of these questions include: how the phase behaviour of the initial reactants affected by product formation?. How does critical and near-critical operation affect the adsorption, diffusion, reaction, and desorption steps involved in heterogeneous fluid-solid catalysis? How does the SCF condition affect the equilibrium rates and chemical reactions? More attention is being given in this field in order to address most of these challenges. Conducting a chemical reaction at SCW conditions has the potential to benefit from the exceptional physico-chemical properties, such as low relative permittivity, high ionic products, low density and low viscosity. These provide opportunities to manipulate the reaction environment (solvent properties) by changing pressure, to enhance the solubility of reactants and products, to eliminate inter-phase transport limitations on reaction rates [**49**].

2.3.1 Chemical reactions at supercritical conditions using water

The ease of manipulating the physical properties of the SCFs enables easier control of the reaction conditions and easier solvent removal after the reaction. Using SCF as reaction medium can offer a variety of advantages, which include its ability to act as reagent and to catalyse reactions, to improve mass transfer, to control ionic reactions and improve catalyst lifetime by reducing undesired reaction such as coke formation.

SCFs can act as reagent, or as solvent. Solvent effects are especially valuable for reactions in SCFs because their interaction with a solute (solvation effect) can influence the rate of reaction. For instance, if the reactants interact with the solvent and are solvated, it might lead to lowering the potential energy

of the reactants then the activation energy increases; in this way, it would contribute to lowering the reaction rate. On the other hand, if the activated complex interacts with the solvent and is solvated, it induces to lowering the potential energy; the activation energy decreases, which implies that the rate of the reaction would increase. Mass transfer for heterogeneous reactions is improved due to single-phase behaviour, and heterogeneous reactions can effectively be transformed into homogeneous reactions. SCW reacts well as a medium with heterogeneous catalysts due to its unique properties; its diffusivity properties are higher when compared to liquid (refer to table 2.1), which reduces the mass transfer barrier. For example, using SCW for organic wastes reaction occurs in an homogeneous phase because the mixture exists as single phase in the SC region [**50**]; therefore eliminating the interface mass transfer barriers that occurred in multiple phase reactions.

The relative permittivity of the reaction medium can be used to control ionic reactions. In the case of SCW, the ion product, or self-ionization constant, is defined as the product of the concentrations of the acidic and basic forms of water, $K_w = [H_3O^+][OH^-]$; these properties are heavily dependent on the density and temperature. They can be used to optimize acid-base-catalysed reactions, given that the logarithm of the rate constant of an ionic reaction varies inversely with the relative permittivity at a given temperature. Another advantage is to improve catalyst life for heterogeneous reactions by mitigating the formation of by-products such as coke on the catalysts pores and tar from polymerisation reaction. This is possible because high pressure contributes to favour certain reactions (selectivity) over others. SCF_S have unique solubility properties (refer to section 2.2.3); for example, organic compounds are highly soluble in SCW, whereas salt has lowered solubility in SCW. This enhanced solubility can accelerate reaction rates and facilitate the synthesis of novel organometallic compounds [**51**]. This effect can also be exploited to overcome potential interphase transport limitations, to reduce carbon deposition on heterogeneous catalysts, or to simplify downstream separation and purification of reaction products and unreacted reactants.

In addition, the reaction environment can be manipulated by changing pressure or temperature or both, in order to influence the solubility as showed for example in Fig.2.1. A study has reported [**52**] on the measurement of the solubility of aluminum sulphate in sub- and supercritical water using flow system at temperatures and pressures ranging between 619 to 675 K and 15 to 29.2 MPa, respectively.

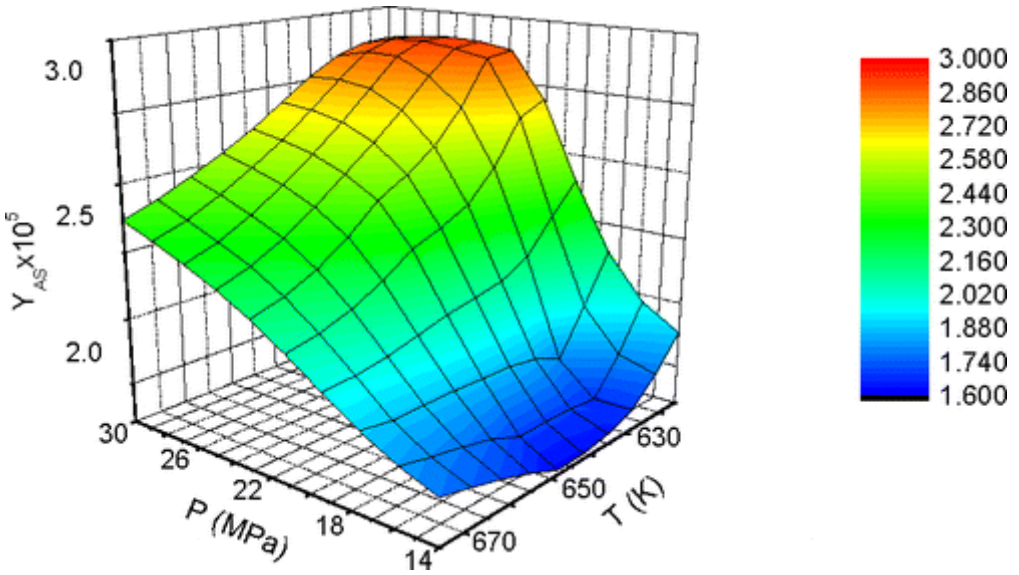

Fig.2.1 Solubility of aluminum sulfate in sub- and supercritical water as a function of T an P [**52**]

It can be seen that the solubility of aluminum sulphate varied from $1.61 \cdot 10^{-5}$ to $2.94 \cdot 10^{-5}$ (in terms of mole fraction) at the reported conditions. This is because the properties of the SCFs vary with density, which is a strong function of temperature and pressure in the critical region.

2.3.2 Water at supercritical conditions

Important physicochemical properties of water are presented in Table 2.3 as a function of pressure and temperature. The density of SCW can be changed continuously from high (liquid-like) to low (gas-like) values without phase transition by varying the pressure and temperature as shown in Figure 2.2.

Table 2.3. Physicochemical properties of water as a function of temperature and pressure [**53, 54**]

Physicochemical properties	Normal water	Subcritical water	Supercritical Water	Supercritica water	Superheated water
T (°C)	25	250	400	400	400
P (bar)	1	50	250	500	1
Density [gcm^{-3}]	0.997	0.80	0.17	0.58	0.0003
Dielectric constant,	78.5	27.1	5.9	10.5	1
The ion product, pK_W	14.0	11.2	19.4	11.9	-
Specific heat capacity Cp [kJ kg^{-1} K^{-1}]	4.22	4.86	13	6.8	2.1
Viscosity [mPas]	0.89	0.11	0.03	0.07	0.02
Thermal conductivity [$Wm^{-1}K^{-1}$]	608	620	160	438	55

The high relative static dielectric constant of water; 78.5 at 25.8 °C drops to a value of about 5.9 at the CP, thus clarifying the difference in the solution properties of SCW by comparison with normal water

[**55**]. The reasons for the relatively low value of the dielectric constant are found in the reduced number of hydrogen bonds [**56, 57**] brought about by the density and temperature. At high-pressure (i.e. high-density) substances with ionic bonds such as KCl, Na_2SO_4, and NaOH can be dissolved, and at low density, non-polar organic substances (e.g. cyclohexane, glycerol, and biomass) and gases can be dissolved. In the latter case, SCW behaves almost like a non-aqueous solvent. According to quantum-mechanical calculations, the molecules of supercritical water take part in the breakage and formation of chemical bonds by significantly lowering the activation energy [**58**].

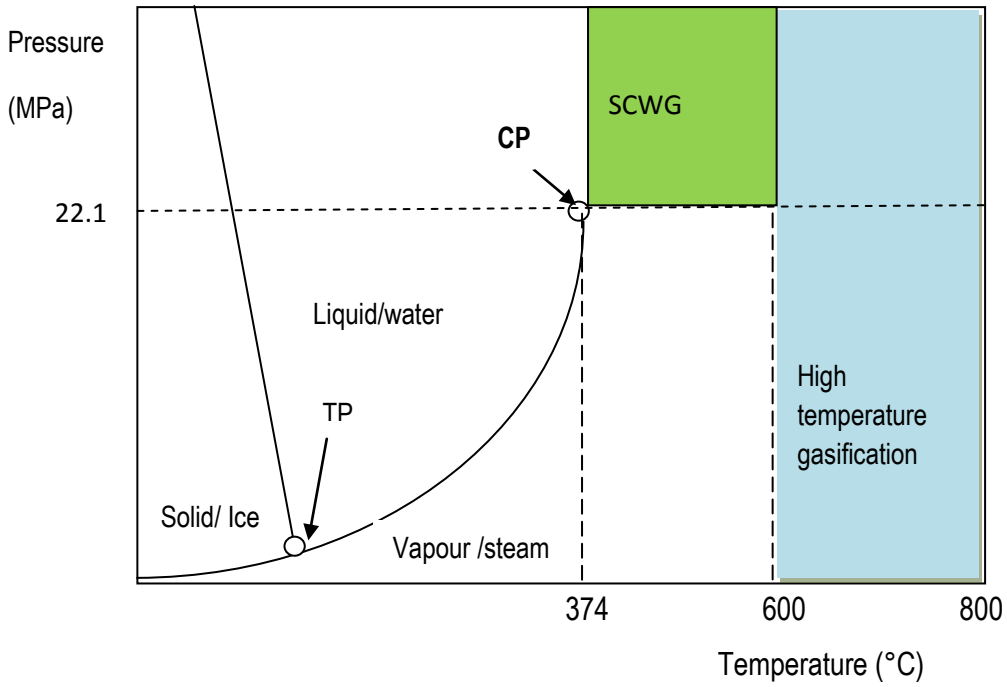

Fig.2.2. Phase diagram of water

SCW exhibits remarkably high specific heat capacities (e.g. Cp=29.2 kJ $kg^{-1}K^{-1}$ at 400°C and 29 MPa) and this can vary continuously over a wide range depending on the pressure and temperature. In highly exothermic reactions, such as partial oxidations in SCW, this could diminish the problem of hot spots. The dynamic viscosity decreases with temperature at high density (due to collisional transfer of momentum) and increases with temperature at low density (due to translational transfer of momentum). At moderate supercritical temperatures, the density is only a tenth to a twentieth of its value under normal conditions [**59**]. This leads to the expectation of advantages with regard to selectivity and space-time yield, especially in the case of heterogeneously catalyzed reactions, in which mass transfer on the catalyst active sites often limits the overall reaction rate. The attribution of a physical effect as the cause for the course of a chemical reaction in SCW is complicated since all the physical properties are highly dependent on temperature and pressure. Moreover, water can appear as a reactive component

as well as a catalyst [**60, 61**]. Thermodynamic data for pure water are available over a wide range of pressures and temperatures [**62, 63**]. However, apart from a few binary systems that have been investigated, corresponding data for aqueous multi-component systems are often lacking due to lack of pressure and temperature-dependent data for given volumes. These would allow the exact determination of residence times in continuously operated reactors. Nevertheless, data can be determined only by means of many experiments.

2.3.3 Influence of water properties on chemical reaction in SCWG

At high temperatures and pressures, pure liquid water becomes a surprisingly effective medium for the reactions of organic compounds. It may function simultaneously as a convenient solvent, a reagent for reactions, and a catalyst (acid or base). However, the role of supercritical water in organic processing is not fully understood. The low cost of water and its environmental friendliness are incentives for the growing interest in its utilisation in hydrothermal gasification of organic wastes. Water takes advantage of favourable changes in its chemical and physical properties at high temperatures and pressures [**64, 65, 66**]. Thus, temperature and pressure effects can drive the reaction toward preferred pathways; for example, in order to improve yield and selectivity toward a selective product. Chemical reaction in SCW can occur in single phase by adjusting the conditions of the reaction and rapid diffusion accelerates diffusion-controlled reactions. In addition, SCW used as solvent in the reaction can allow separation of phases (gas/liquid) for efficient product removal.

Various studies have reported on the use of SCW as a medium for the complete destruction of hazardous and toxic wastes by SCWO process [**67, 68**]. A similar approach has been exploited to decompose organic wastes by SCWG process. However, the full chemistry of this is still under investigation. For instance, SCW is capable of breaking bonds of non-polar compounds such as polymer sugars into gaseous products, due to its high reactivity. Above its critical point (CP); water undergoes significant structural changes due to the loss of its ionic strength, because of the weakening of the hydrogen bonds. There is also a significant reduction in its density; viscosity and dielectric constant (refer to table 2.3). In the sub-critical region, water is polar, whereas above CP water exhibits enormous changes in solvation behaviour where it transforms from a polar, highly hydrogen-bonded solvent to behavior more typical of a non-polar solvent like hexane. The relative permittivity or dielectric constant decreases from about 80 at ambient conditions (25°C) to less than 2 at 450°C. Dielectric constants between 2 to 30 cover solvents from hexane (non-polar) to methanol (polar). The reduced dielectric constant combined with a considerably diminished number of hydrogen bonds gives an organic like solvent. A gradual decrease in the dielectric constant of water with increasing temperatures [**69**] is paralleled by increasing water solubility of organic compounds. For many organic compounds,

high solubility can be achieved in near critical water, and complete miscibility can be attained in supercritical water. Moreover, gases are also fully miscible in supercritical water. On the other hand, salts will hardly dissolve in supercritical water, because of the low dielectric constant. The ion product (K_w), or dissociation constant (K_w) for water as it approaches the critical point, is about 3 orders of magnitude higher than it is for ambient liquid water. In fact, the ion product (K_w) first increases from 10^{-14} to 10^{-11} just below 350 °C and then decreases by five orders of magnitude or more above 500°C [**70**]. Near the critical point, the ion-product can be as high as 10^{-11} [**70**]; As a result, the H^+ ions concentration is about thirty times higher than at ambient conditions, which enhances the acidity in SCW. This indicates that near the critical point, water possesses the properties of an acid / base catalyst. In the high-temperature range of the supercritical region, the ion-product decreases again to unusually low values. In fact, Kw is about 9 orders of magnitude lower at 600°C and 250 barg than at ambient conditions. Consequently, acid and base-catalyzed reactions that cannot occur readily at ordinary temperatures could be promoted due to its excellent transport characteristics (low density, low viscosity and high diffusibility) of the SCW. For example, at 300°C, the polarity and density of water approach those of acetone at room temperature [**71**]. These changes in density correlate with other macroscopic properties to reflect changes at the molecular level such as solvation power, degree of hydrogen bonding, polarity, dielectric strength, molecular diffusivity, and viscosity [**72**]. A slight change in pressure or temperature can generate a massive change in the physical properties, which facilitates fast control over the properties, allowing a "switching" operation mode [**73**]. Above its CP, the reactivity of SCW increases due to it dissolving capability, which makes it an ideal reaction medium for organic compounds conversion. Moreover, SCW exhibits a relatively high heat capacity that gives to efficient heat transfer. A study has reported that the fundamental reactions that can occur in SCW are the same as those that occur in gasification, including pyrolysis, hydrolysis, steam reforming, and water-gas shift, and methanation [**74**]. The chemical reactions in SCW can be classified in two groups: chemical synthesis and chemical conversion, and are discussed in the following sections.

2.3.3.1 Chemical synthesis

2.3.3.1.1 Hydrolysis

Hydrolysis reaction involves water where it interacts with the compounds in the mixture to form another compound. Several different compounds readily hydrolyse in SCW. For example, esters can undergo an autocatalytic hydrolysis to form carboxylic acids and alcohols. Researchers have investigated hydrolysis over acid catalyst, and have reported that this feature is the source of the autocatalysis [**75, 76**]. A typical example of hydrolysis reaction is the lignocelluloses hydrolysis into

polymer sugars. Another simple hydrolysis reaction is (cellulose + water →glucose). A hydrolysis is one of the principal processing reactions of polysaccharides in which the glycosidic bonds between the sugar units are cleaved to form uncomplicated sugars molecule like glucose, fructose, and xylose and partially hydrolysed dimer, trimers, and other oligomers. The challenge is often to identify the reaction conditions and catalysts to convert a diverse set of polysaccharides (such as cellulose, hemicellulose, starch and xylene) obtained from a variety of biomass sources. Hydrolysis reactions are typically carried out using acid or base catalysts at temperatures ranging from 370 to 570 K [**77**], depending on the structure and nature of the polysaccharides. Acid-hydrolysis is more commonly practiced because base-hydrolysis leads to more side reactions and thus lower yields; whereas, acid hydrolysis proceeds by C−O−C bond cleavage at the intermediate oxygen atom between two sugar molecules [**78**]. Often the reaction conditions can lead to further degradation of sugars to products such as furfural and Hydroxymethylfurfural (HMF) that may be undesirable. Cellulose, the most abundant polysaccharide with glycosidic bonds are the most difficult material to hydrolyze because of its high crystallinity. However, it has been reported that both mineral acids and enzymatic catalysts can be used for cellulose hydrolysis [**79**], with enzymatic catalysts being more selective.

2.3.3.1.2 Water gas shift (WGS) and reverse -WGS

The water-gas shift ($CO + H_2O \longleftrightarrow CO_2 + H_2$) is a prominent reaction in SCW. It is a reversible, exothermic chemical reaction, and a catalyst usually assists its promotion. Carbon monoxide is reformed in SCW, which lead to the formation of carbon dioxide and hydrogen gas. The reverse-WGS reaction also occurs by catalytic hydrogenation of CO_2 according to the reaction

$$CO_2 + H_2 \leftrightarrow CO + H_2O \quad (2.11)$$

2.3.3.1.3 Partial oxidation

Methane is one of the gaseous products from SCWG and it is stable in SCW up to a temperature of 450°C [**80**]. However, methane could undergo partial oxidation to form methanol depending on the temperature and pressure. In this context, partial oxidation of methane in SCW around 400°C has been examined as a potential route to methanol. The extent to which methane reacts easily rises with increasing temperature and pressure. The products of methane oxidation include carbon monoxide, carbon dioxide, methanol, and small quantities of formaldehyde and formic acid [**80, 81, 82**].

2.3.3.1.4 Hydration

In hydration, a substance is gaining water for its reaction and this can occur without the presence of a catalyst. However, temperature plays a prominent role on product yield. Typical examples of hydration reactions in SCW conditions are SRM and SRC:

Steam reforming of methane (SRM), $CH_4 + H_2O \rightarrow 4H_2 + CO$ (2.12)

Steam reforming of char (SRC) = steam-carbon reaction, $C + H_2O \rightarrow H_2 + CO$ (2.13)

2.3.3.1.5 Dehydration

In a dehydration reaction, water is usually produced as part of the product formation. Antal and co-workers [**82**] have been pioneers in studying the dehydration of alcohols to olefins in near-critical and supercritical water. For instance, the dehydration of ethanol to form ethylene has been reported to occur at a significant rate only at elevated temperatures [**83**]. In addition, ethanol has been proven to be kinetically stable in SCW. Because dehydration reactions usually proceed rapidly with a high degree of specificity, they appear to be good candidates for industrial exploitation.

2.3.3.2 Chemical conversion reactions

Chemical conversion reactions tend to involve the movement of electrons leading to the formation and breaking of chemical bonds. The reactants chemically change to form a product different from the starting materials. The main processing routes of organic wastes for chemicals and energy production are by chemical conversion reactions. The concept of organic wastes processing can be well defined in the context of bio-refining, which is to integrate the production of higher value chemicals and commodities, as well as fuels and energy, and also optimise use of resources, maximise profitability, benefits and minimise wastes [**84**]. In this approach, two mains concepts can be distinguished: Product –driven and energy-driven organic wastes processing. The first leads to the production of bio-based products (food, chemicals, and materials) and the latter to produce biofuels (H_2, synthesis fuels), and indirectly power and heat using process residues. In product-driven processes, the organic waste is primary converted into bio-based products with minimal environmental impact. Secondary products and residues such as char are re-used for heat and/or power production. In an energy-driven process, the organic waste is mainly used for the direct production of energy carriers such as biofuels (H_2). Various techniques for promoting bio-based chemical reactions are reviewed and summarised in Table 2.4.

Table 2.4: Evaluation of the main processing techniques for organic materials

Techniques	Advantages	Disadvantages
Biological routes	Wet feed is acceptable	○ Sensitive process conditions ○ Slow processes and more selective ○ Bacteria is required, less versatile
Pyrolysis	○ No air is required ○ Various products (liquid, char, gases and tar). Liquid products are easy to store and to transport ○ Moderate temperature (≈500°C), good control of temperature. ○ Relative fast process depending on the type of pyrolysis.	○ Presence of tar hence difficulty of separation ○ High cost ○ Liquid quality is poor ○ Unusual properties of liquid (viscosity increase with time, volatility decreases with time)
Aerobic Gasification	○ Lower temperature ○ if air is used→reduced cost ○ various product application (suitable for boiler, engine and turbine operation)	○ Only dry feed required; energy intensive if O_2 is used→extra cost ○ More selective and ash formation ○ If O_2 is used→ syngas, [CV≈12-27] MJ/Nm^3 [**85**] ○ If air is used→producer gas (high in N_2), Low CV≈4 –12 MJ/Nm^3 [**86**]
Gasification using SCW	○ Wet feed (various feedstocks) ○ Less selective-Mixed products ○ More versatile in term of variety of products and applications. Fast processes and low cost process. ○ The reaction rates of thermochemical processes are orders of magnitude higher and can be used to process a wide range of feedstocks (forest residues, animal wastes, *etc.*) into a syngas mixture of reasonably consistent composition	○ Severe process conditions due to high pressure and high temperature. ○ Salt solubility is reduced, hence solid deposition on the reactor wall that can lead to corrosion problem

CV = calorific value

2.3.3.2.1 Pyrolysis

In pyrolysis reactions, materials or organic compounds are rapidly heated at a temperature between 450 to 500°C under ambient pressure and under absence of oxygen, followed by rapid cooling (< 2 s); in order to decompose the starting materials into gases, small quantities of liquid, and a solid residue containing carbon and ash. The product concentration is dependent on the choice of pyrolysis used (fast, intermediate or slow pyrolysis) and the type of feedstock. For example, slow pyrolysis could be used to break down polymer sugars and degrade organic materials at 450°C into gaseous product (35 wt %) of (CO, H_2, CO_2, CH_4), 30 wt% liquid and char. Depending on the operating conditions, the three types of pyrolysis are described:

- ★ Fast pyrolysis. Moderate temperature is applied (500°C), fast heating rate and the residence time is less than 2 seconds. Products: 75% liquid, 12% char and 13 %gas [**87**].
- ★ Intermediate pyrolysis. Moderate temperature (450 to 500°C) is used with moderate residence time (few seconds).
- ★ Slow pyrolysis. Low temperature (400 to 450°C) is required, slow heating rate and long residence time (>2 seconds). Products: 30% liquid, 35% char and 35 % gas [**87**].

2.3.3.2.2 Oxidation

Oxidation of organic compounds in a supercritical water medium has undoubtedly received the most attention [**88**]. Its chemistry forms the basis for a waste treatment technology known as supercritical water oxidation (SCWO). The technology takes advantage of the complete miscibility of organic compounds and oxygen with SCW, enhancing a single fluid phase formation at reaction conditions. In the case of waste treatment, SCW is used to oxidize hazardous waste, thus eliminating production of toxic combustion products that are produced from burning materials. Moreover, when temperatures are significantly higher (400-600°C), the reaction rates proceed rapidly and essentially complete conversion of organic carbon to CO_2 occurs on the time scale of a few minutes. Several studies have reported on the applications and developments of SCWO technology [**89-92**].

2.3.3.2.3 Decomposition by Gasification

Organic materials can be decomposed in SCW, in the absence of oxygen. Many other complex materials such as polymers, vegetable oils, fats and biomass can also decompose in SCW at a variable rate depending on the complexity of their chemical structure and composition. Chemical decomposition in SCW is reviewed herein

Gasification is a thermochemical process that has been exploited for more than 200 years for converting solid feedstocks to gaseous energy carriers. Virtually all of the energy derived from biomass

(98% by one estimate) [**93**] is currently produced by direct combustion. Gasification process offers a number of advantages for organic waste processing; for instance the reaction rates and thermal efficiency can be higher [**94**]. Among the gasification techniques, two main groups of gasification can be distinguished: hydrothermal gasification and aerobic gasification. One chemical of interest, for example is formaldehyde, which can be formed as by-product of SCWG in the liquid phase, but it easily decomposes in SCW at sufficient temperature. At temperatures above the critical, formaldehyde reacts to completion to form methanol, formic acid, carbon monoxide, and carbon dioxide. Carbon monoxide is the main product at higher reaction temperatures and methanol at lower reaction temperatures [**95**]. However, it is not fully established whether the products of the decomposition of organic compounds are formed directly from the C-H-O bond breakage or if the organic molecules decompose into intermediates before gaseous products are indirectly formed.

2.3.3.2.3.1 Aerobic Gasification

Aerobic gasification allows the utilisation of oxidant such as air or oxygen for the conversion of different organic compounds including biomass feedstocks to a more convenient gaseous fuel known as producer gas, which can then be used in conventional equipment (e.g., boilers, engines, and turbines) or advanced equipment (e.g., fuel cells) for the generation of heat and electricity. Conventional gasification requires a dry feedstock, so energy is needed to vaporise the moisture content, hence increasing cost of production. Large scale biomass gasification plants ranging in size from 15–70 MWth [**96**] are being developed in Europe, primarily for power generation. One key problem of the process is to deal with the high level of tar. Tar formation and mitigation are a serious topic of gasification development. Tar is formed from polymerisation reactions, and condenses at reduced temperature, leading to the blocking and fouling process equipments such as fittings, tubing, engines and turbines. Considerable efforts have been directed on tar removal from fuel gas. Tar removal technologies can broadly be divided into two approaches; hot gas cleaning after the gasifier (secondary methods), and treatments inside the gasifier (primary methods) [**97**]. More importantly, the selection of the gasifier can play a significant role on tar reduction. For instance, tar concentration in the product gas at the outlet of the updraft-fixed bed gasifier can be higher compared to a downdraft gasifier [**98**]. This is due to the mechanism of air flowing (counter current versus co-current), which can influence the reaction conditions in the combustion zone.

2.3.3.2.3.2 Hydrothermal Gasification

In hydrothermal gasification, steam or SCW are used as an oxidant for the rapid decomposition of the organic wastes. SCW is used to gasify organic materials to produce a mixture of H_2, CO, CO_2,

CH_4, and char. This can be accomplished in both supercritical and near-supercritical water [**99**]. Modell and co-workers were the first to use supercritical water to gasify biomass when they gasified maple sawdust and water to produce a high BTU gas containing CO, CO_2, H_2, and CH_4 as the major components [**100,101**].

Supercritical water attracts many scientists and engineers to research its properties as a clean reaction medium, which provides alternative routes to hazardous organic solvents. Non-polar organic compounds, which are insoluble or poorly soluble in ambient water, can become fully miscible in high-temperature and high-pressure water, enabling many unusual reactions to take place.

A number of waste biomass feedstocks have been used as feeds, including manure solids, saw dust, corn fibre, and wood residue. The product gas can be reformed into a H_2-rich stream by water gas shift reaction ($CO + H_2O \rightarrow CO_2 + H_2$) or into syngas by steam reforming ($H_2O + CH_4 \rightarrow CO + 3H_2$). Other gas products can be produced by varying the process conditions and by using an appropriate catalyst. Mixtures of H_2 and CH_4 can also be produced, and this can be used as a substitute natural gas. One advantage of this process is that the water in the organic material or biomass is not vaporised in the feed, thereby improving the Process Thermal Efficiency (PTE). Therefore, wet feedstocks can efficiently be processed with super/subcritical water. Most organic wastes can be fractionated easily or/and decomposed in SCW conditions. Other advantages of SCWG allow complete gasification in short residence time/reaction time. For example, it takes between 30 to 120 seconds for glucose reaction with SCW to produce H_2-rich gases, and this is obtained at high pressures in a simple step process [**102**]. The extended benefit of this is that the product gas obtained at high pressure can mitigate the cost of expensive gas compression if needed. In addition, a wide range of organic wastes can be processed by SCWG, hence less selective on feedstock. It has been reported that supercritical gasification can occur at both high temperature 600-800°C [**103, 104**], and at lower temperatures ranging from 350 to 600°C with the addition of a heterogeneous catalyst such as Ru/TiO_2 [**105**]. The product of gasification is commercially viable at various degrees depending on the conversion routes. The process, products, conversion routes and the potential market of the gasification are reviewed and summarised in Fig.2.3.

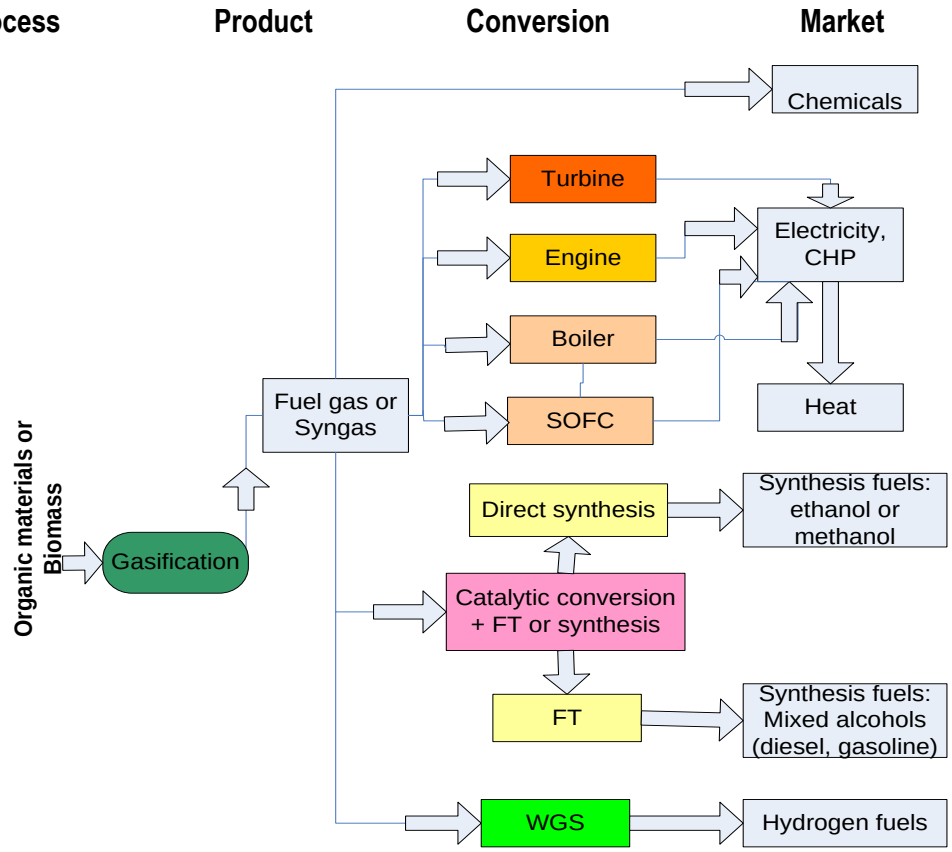

Fig.2.3. Gasification of biomass; process, product, conversion and market.

Syngas to synthesise fuels: It can be seen in Fig.2.3 that syngas produced from the thermochemical routes such as gasification can be used to produce higher alcohols from biomass. Synthesis gas (a mixture consisting primarily of CO/ H_2, CO_2, and H_2O) can be used to produce a range of products using well-established technologies, such as liquid fuels *via* the Fischer–Tropsch process [**106, 107, 108**] or by direct synthesis. However, the use of organic wastes-derived syngas to produce higher alcohols has received relatively little attention, despite the potential to produce valuable compounds such as ethanol [**109, 110**]. The main challenge is to find suitable catalyst designs for large scale biomass conversion processes. In addition, finding a suitable reforming catalyst for downstream adjustment of the H_2/CO ratio for a selective end products could significantly improve this process. Various studies have reported on the direct synthesis of alcohols from syngas [**111, 112**]. This has showed to be one of the most promising process routes for producing fuels and raw chemicals. For instance, the production of ethanol is thermodynamically feasible at temperatures below 350°C at 30 bar [**111**], and with a selective catalyst to achieve high conversion to alcohols. However, if methane is allowed as a reaction product, the conversion to ethanol (or other oxygenates) is extremely limited. The most promising catalysts for the synthesis of ethanol are based on Rh, and some other formulations (such as modified methanol synthesis catalysts) [**113**].

Synthesis of alcohols from synthesis gas remains an economically attractive method for making fuels and chemicals. Higher alcohol synthesis is of interest due to increasing petroleum prices, environmental concerns, and gasoline additive octane demands. Many researchers developed several catalytic systems for higher alcohol synthesis through CO hydrogenation. These catalysts for higher alcohol synthesis can be categorized into two groups [**114, 115**]: (i) Catalysts for the production of methanol and branched alcohols, such as modified methanol synthesis catalysts (e.g. ZnO/Cr_2O_3, $CuZnO/Al_2O_3$) and (ii) molybdenum sulfide and Co/Cu-based catalysts to form straight chain alcohols. Among these molybdenum based catalysts are more attractive due to their excellent resistance to sulfur poisoning and high activity for the water–gas shift reaction [**116**].

Fischer -Tropsch synthesis (FTS): synthesis fuels made of mixed alcohols such as gasoline and diesel can be obtained from syngas through FTS route. The FTS step can be carried out subsequent to organic wastes or glycerol conversion step [**117**]. In this manner, the method may involve two reactions, one exothermic and the other endothermic. The heat from the exothermic reaction could be used to supply (at least in part) the energy required to drive the endothermic reaction. A study has established that both reactions can be coupled by integrating the active sites for each reaction within a single catalyst bed [**117**]. In such invention, the conversion of the reactant feedstock to synthesis gas is accomplished using a catalyst containing Pt-Re on a carbon support, whereas the carbon-carbon bond-forming reaction is accomplished using a Ru/TiO_2 catalyst.

In practice, FTS is part of gas to liquid (GTL) techniques [**118**]. The fuels produced by FT processes are environmentally superior to conventional crude oil derived fuels because of virtually zero sulphur content. Others studies have demonstrated that FTS is a surface catalyzed stepwise growth process using CHx monomers, which are formed by the hydrogenation of CO in the presence of a transition metal catalyst [**119, 120**]. Among the metal catalysts used, cobalt is the preferred FT active metal for conversion synthesis gases (syngas H_2/CO of 2:1 ratio) because of its high activity, high selectivity for long chain hydrocarbons and low water-gas shift (WGS) activity [**121, 122**].

2.4 SCWG of organic wastes for H_2 or/and syngas products

SCWG of organic wastes can be accomplished at high temperature 700-800°C without catalyst, or at lower temperature (<600°C) with the utilisation of effective catalysts. CSCWG has continued to receive more attention from scientists in order to establish full understanding of all the chemistry and to reduce the operating cost. Organic materials can be efficiently decomposed to produce a mixture of gases and value-added liquid products depending on the process conditions. The gas mixture can contain hydrogen, carbon monoxide, carbon dioxide, methane, ethylene, and the liquid fraction, can

contain value added products (e.g. acetaldehyde, acetic acid, acetone, methanol and ethanol); char can also be obtained [**123, 124**]. As discussed in section 2.3, Water above its critical point [≥221 barg, ≥374 °C], has low relative permittivity (6 compared to 80 at ambient), high ionic product (10^{-11} as compared to 10^{-14} for subcritical) [**125**], which can be manipulated by changing pressure and temperature. These properties offer a number of advantages for organic material decomposition, such as enhanced capability to dissolve non-polar compounds, high reactivity and the ability to act as an acid/base catalyst. This section reviews the SCWG process, feedstock, reaction steps, chemistry and the design considerations of SCWG.

2.4.1 The SCWG process

The process of SCWG is mainly made of the upstream process (feed pump, pre-heater, and reactor) and downstream process (condenser, separator, gas purification system). Section 3 discusses the process and equipments used in this work in more detail.

2.4.2 The feedstock for SCWG process

Five broad categories of biomass can be identified as suitable feedstock: woody biomass, aquatic biomass and forest residues, agricultural residues, directly fermentable crop-grown biomass, and municipal solid waste and sewage [**126**]. Table 2.5 presents the broad categories and some examples of biomass type.

Lignocellulosic (LC) biomass and, to a lesser extent, crude glycerol have received much attention in the literature as a suitable feedstocks for SCWG and, have been the focus and are reviewed here. These feedstocks have the potential to address certain issues related to wastes transformation into viable products; for example, a selected feedstock for organic material processing should not create competition with human source of food and energy. Table 2.6 summarises the main driving force for the increased use of organic wastes for the production of bio-based products and bio-energy.

Table 2.5. Category of biomass and examples

Category of biomass	*Examples*
Energy crops	Dedicated energy crops, Herbaceous energy crops, Woody energy crops, Industrial crops, Agricultural crops, Aquatic crops
Agricultural wastes and residues	Crop waste, Animal waste
Forestry waste and residues	Mill wood waste, Logging residues, Trees, Shrub residues
Industrial and municipal wastes	Municipal solid waste (MSW), Sewage sludge, Industry waste
Aquatic biomass	Marine or freshwater algae; macro-algae (blue, green, blue-green, brown, red) or microalgae; seaweed, kelp, lake weed, water hyacinth, others

Table 2.6. Main reasons for the increased processing of organic wastes.

Main reasons	Details
Depletion of the fossil resources	o Increasing prices of energy o Difficult approach o High sophisticated technologies (oil sands) o Increase of political dependency
Biomass is readily available at low prices ≈1.65 to 2.48 £/GJ [**127**] (Hence low production cost. For example H_2 production from biomass cost ≈ 6.1 to 10.69 £/GJ) [**128**]	o Widely available in different forms o More reliable and cheaper o Competitive for H_2 production o Can be a sustainable source of chemicals.
Environmental concerns	Rio agreement, The Hague, The Bali, Kyoto protocols. Copenhagen accord (2009) [**129**] Most governments have pledged to reduce CO_2 emissions from fossil fuels by substituting renewable (biomass and others). Biomass is the only source of renewable with fixed carbon, which is essential for many fuels, chemicals and goods.
Almost CO_2 neutral	Small quantity of CO_2 is produced during processing of biomass in comparison to fossil fuels. CO_2 can be captured and reused to grow the plant.
Directives ,	European Commission (EC) has set the target to 20 % CO_2 reduction by 2020. UK target is 60% CO_2 reduction by 2050 [**130**]

2.4.2.1 Lignocellulosic (LC) biomass

LC-biomass is the most abundant material in the world. Its sources range from trees to agricultural residues. The chemical components of lignocellulosic can be divided into four main components as

shown in column 1 in the Table 2.7. Note, that the difference in chemical composition of the LC-biomass is influenced by genetic and environmental factors.

Table 2.7. Distribution of lignocellulosic biomass [**131**]

LC components and generic molecular formulas	Amount	Composition	Function
Cellulose $CH_{1.7}O_{0.83}$	40-55 (%)	Long Macromolecule C_6, Glucose units	Cell wall structure Semi-crystalline
Hemicelluloses $CH_{1.6}O_{0.8}$	15-35 (%)	Short, linked macromolecule C_5,Pentose Units	Cell wall structure
Lignin $CH_{1.4}O_{0.66}$	28-41 % if Softwood 18-25% if Hardwood	Three dimensional macromolecule Methoxyphenyl propane units	Filler in cells reason for wooden character
Extractives	0.2 – 8.5 % if Softwood 0.1 – 7.7 % if Hardwood Up to 10.6% for banana stem	Low molecular weight compounds (resins, fats, fatty acids, alcohols, proteins)	

Fig.2.4 shows the chemical structure of LC-biomass, which is essentially, composed of celluloses, hemicelluloses, lignin and extractives materials as also shown in Fig.2.4.

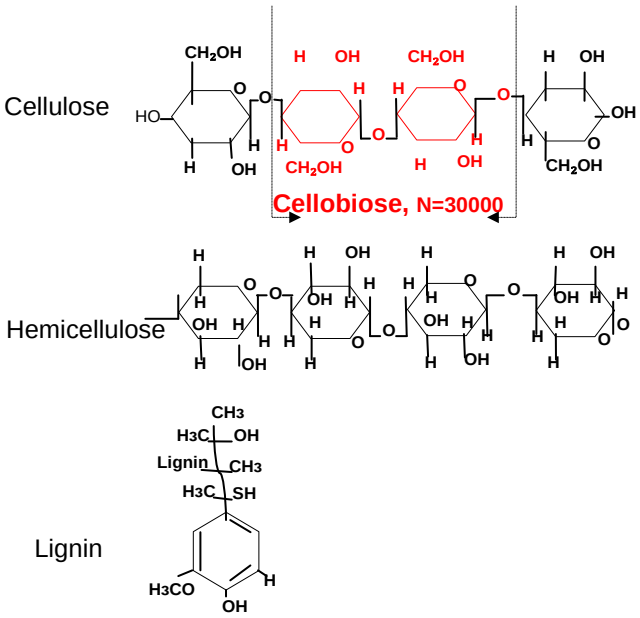

Fig.2.4. Chemical structure of LC-biomass

Lignin is a phenolic polymer that surrounds the polysaccharides. Its presence makes the biomass structure resistant to enzymatic digestion. It is the hardest component to break due to its molecular structure. Hemicellulose is a polymer of hexoses, pentose and sugar acids which surrounds the cellulose via hydrogen bonds. Cellulose is a semi-crystalline structure formed from linkage of glucose chains.

2.4.2.2 Crude glycerol

Glycerol is a polyalcohol with several commercial applications in food and cosmetics, but due to the increasing demand for biodiesel, massive amounts of crude glycerol are being obtained as by-product during the manufacture of fatty acids and biodiesel. The surplus amount generated from biodiesel is so large, that more than 600 000 tonnes were generated as surplus in Europe in 2006 [**132**]. In 2009, the biodiesel product from the European Union and United States reached a massive share of 9 and 2.7 million tons respectively, from a total of 16 million tons worldwide. Hence, 1.6 million tons of glycerol were produced as an obligatory by-product [**133**]. Because of this rapid increase of surplus, the crude glycerol market price has decreased to less that 0.05 €/kg [**134**]. Due to its low purity, crude glycerol from biodiesel cannot be used in cosmetics or food unless a costly refining process is undertaken, but its wide availability and cheap price offer new opportunities for chemistry and energy [**135**]. Among

these, the production of hydrogen by supercritical water processing of crude glycerol solutions is a considerable option.

Biodiesel has become a renewable source of energy, and alternative fuel. This is because of low environmental impacts such as net zero carbon dioxide emission and less emission of SO_x and NO_x. Biodiesel can be produced in four different ways namely direct use or blending, micro-emulsions, pyrolysis and transesterification [**136**]. Among these methods, transesterification process is most commonly used to produce biodiesel from vegetable oil or animal fats by reacting them with alcohol in the presence of a catalyst [**137, 138**]. In this process, about 10 wt% of vegetable oil or animal fats is usually converted to biodiesel as the primary product and crude glycerol as by-product [**139**]. The increased yield of glycerol by-product is largely attributed to poor mass transfer between alcohol and oil. To improve the biodiesel economy and the glycerol market, it would be extremely beneficial to find useful applications for crude glycerol.

Glycerol has the potential to produce hydrogen, syngas (H_2 + CO) and hydrocarbons using processing techniques such as pyrolysis, steam gasification and catalytic SCW reaction [**140, 141**]. However, glycerol is also a potential feedstock for other processes including the production of 1,3-propanediol, polyglycerol and polyurethanes [**142**]. These main processes and derived products that use crude glycerol as raw material are summarised in table 2.8.

Table 2.8. Main Processes that Use Glycerol as Raw Material

Process	Catalyst	Main products	Main applications	References
Carboxylation	Zeolites, Zn-based, or under supercritical conditions	Glycerol carbonate	Production of polycarbonates and polyurethanes	[**143**]
Dehydration	Acid catalysts	Acrolein	Chemical intermediate	[**144, 145**]
	Acid catalysts	Acrylic acid	Polymers, resins, paints, acrylic fibers, etc.	[**146, 147**]
	Sb-V-O	Acrylonitrile	Polymers, resins, paints, acrylic fibers, etc.	[**148, 149**]
Esterification	Mesoporous materials	Glycerides, polyglycerol esters	Emulsifiers	[**150, 151**]
	Mesoporous materials	Diacetylglycerol (DAG) and Triacetylglycerol (TAG)	Fuel additives	[**152, 153**]
	Chlorides, sulfates	Monolaurin, dilaurin	Pharmaceutical industry	[**154**]
Esterification	Mesoporous materials	Glycerol Ter Butyl Ether(GTBE)	Fuel additives	[**155, 156**]
	Sulfates	Monoether glyceryl ethers (MAGEs)	Pharmaceutical industry	[**157**]
	CaO-based	Di- and tri- glycerol	Pharmaceutical industry	[**158**]
Epicerol	Carboxylic acids	Epichlorohydrin	Production of epoxy resins	[**159, 160**]
Fermentation	Enzymes	1,3 (propanediol)	Manufacture of polyesters	[**161, 162**]
Hydrogenolysis	Ru/C or Cu-based	1,2 (propanediol)	Chemical intermediate, antifreeze	[**163, 164**]
Oxidation	Pt-Bi/C Catalyst	Dihydroxyacetone	Active ingredient of sunless tanning skincare preparations	[**165**]
Reforming	Pt-Re /C	Syngas	FT synthesis	[**166, 167**]
	Pt or Ni based-catalysts	H_2	Energy, fuel cells	[**168, 169**]
Telomerization	Homogenous catalysts	C8 chain Ethers	Surfactant chemistry	[**170**]

2.4.2.2.1 Main advantages of processing glycerol for chemicals

There are many advantages for using crude glycerol as the main feedstock for large-scale organic waste processing:

- ✧ The availability of crude glycerol is growing as a consequence of the increase in biodiesel production. Thus, processes using glycerol as starting material represent an economic advantage with respect to traditional processes.
- ✧ Crude Glycerol from biodiesel is a renewable material that does not contribute to global warning. This is especially attractive for hydrogen production since hydrogen represents an alternative energy vector for next future and its production from renewable resources is recommended.
- ✧ In some cases, the use of glycerol constitutes a new route to chemicals. For example, glyceric acid and dihydroxyacetone have a limited market because they are either produced using costly and polluting oxidation processes or low-productivity fermentation. This is one of many reasons why alternative routes are being explored for the conversion of glycerol into chemicals. In this manner, combining the use of glycerol and clean oxidizing agents, it is possible to achieve the economic and clean production of chemical derivates [**171**] as well as low heating value fuels.

2.4.2.2.2 Chemical structure of glycerol

Glycerol molecule is an oxygenated hydrocarbon that contains 3-OH as shown in Fig.2.5. These hydroxyl groups are responsible for its solubility in water and its hygroscopic nature. Because of the 3-OH group attached to each of its 3 carbon atoms, glycerol is also known as a trihydric alcohol or 1,2,3 propanetriol, glycyl alcohol or tri-hydroxy propane with a relative molecular mass (RMM) of 92.09 g/mole.

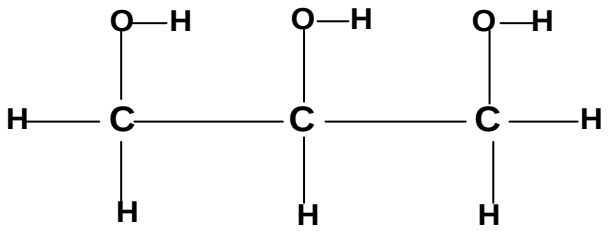

Fig.2.5. Chemical structure of glycerol

2.4.2.2.3 Element and Energy content in glycerol

The most prominent chemical elements in glycerol are C, H and O. However, depending on the level of purity and the primary feedstock for its production, other elements such as alkali salt (K), ash and S could also be presented. The energy content of pure glycerol is about 19.0 $MJ.kg^{-1}$, and for crude glycerol is 25.30 $MJ.kg^{-1}$ [**172**]. It can be noted that the HV of crude glycerol is higher than that of pure glycerol. This is due to the presence of methanol and traces of biodiesel in the crude glycerol sample. Compared to petro-diesel, whose energy content is around 43.33 $MJ.kg^{-1}$, biodiesel (B-100) energy content is about 38.02 $MJ.kg^{-1}$, which represents 12% lower energy content, as expected [**173**].

2.4.2.2.4 Review of glycerol processing in SCW

A number of researchers have demonstrated that crude glycerol can also be efficiently converted into hydrogen with steam or SCW according to the following overall reaction $C_3H_8O_3 + 4H_2O \rightarrow 3CO_2 + 7H_2 + H_2O$. If the reaction takes place at atmospheric pressure, extremely high temperatures(700-800°C) are required [**174**]. Non-catalytic glycerol decomposition in SCW proceeds through a complex reaction mechanism that can be summarised in two competing pathways: ionic and free-radical, whose predominance depends on water density and acidity [**175, 176**]. At low temperature(<550 °C) and high pressure(>250 barg), hence high water density, a catalyst is needed, and a set of ionic reactions forming acetaldehyde, formaldehyde and acrolein as main products [**177**] are expected. At low water density, a free-radical pathway leads to the preferential formation of allyl alcohol and methanol. Gases are typical products of the free-radical reactions, and their yield is favoured by low water density.

The main products of the glycerol degradation in SCWG are usually methanol, acetaldehyde, propionaldehyde, acrolein, allyl alcohol, ethanol, formaldehyde, carbon monoxide, carbon dioxide, hydrogen and char [**178**].

Noble metals such as Pd and Pt are effective for aqueous reforming of oxygenated hydrocarbons [**179, 180**], but such catalysts are not common in industrial applications because of their high cost. A typical catalytic system for aqueous reforming is mainly based on nickel as an active component [**181**], although it is more susceptible to carbon formation during the reaction than Pt based catalysts [**182**]. Several heterogeneous catalysts have been studied to promote hydrogen yield and reduce the formation of tars and char [**182-185**] in SCWG. Among those, Ruthenium-based catalysts have been shown to offer the best results for SCW gasification of biomass feedstocks [**186, 187**], but still temperatures above 700°C are required in order to have a high selectivity towards hydrogen if high feed (>30 wt% glycerol) concentration is used. In fact, no catalyst capable of reaching complete

conversion of glycerol and a hydrogen yield close to the stoichiometric value at a temperature below 550°C has been found yet, partially because of the formation of methane as competing final product.

2.4.3 Reaction Steps in SCWG

SCWG is fundamentally similar to other thermal gasification in terms of the possible reaction step and the variety of associated chemical reactions as shown in Fig.2.6. The reaction proceeds probably in four steps, which include hydrolysis, pyrolysis, gas-solid reactions that consume char, and gas-phase reactions, which enhance the final chemical composition of the product gas.

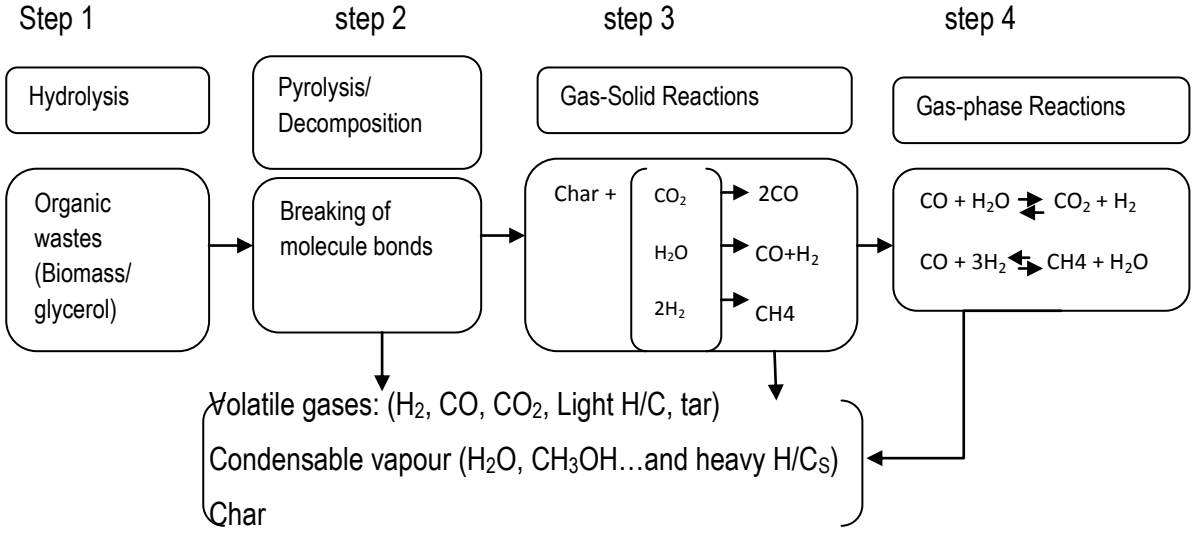

Fig.2.6. Reaction steps in SCWG

Step 1: Hydrolysis

If LC-biomass is used as the feedstock; then the hydrolysis reaction is as follows:

LC-biomass (cellulose + hemicellulose + lignin) + H_2O⟶ polymer sugar + lignin.

The hydrolysis of cellulose produces glucose. This reaction step is explained in more detail in sub-section 2.3.3.

Step 2: Pyrolysis / hydrothermal gasification

Pyrolysis has been reviewed in section 2.3.3.2.1. However, it could play an important part in the overall SCWG processes. In the case of hydrothermal gasification, pyrolysis step is dominated by steam or SCW gasification but occurs to some extent to allow degradation of reactants. Steam or SCW is used as oxidant in order to decompose by breaking down the molecule structure of the materials. Thus, for glycerol decomposition by hydrothermal gasification, the overall reaction is as followed:

$$C_3H_8O_3 + 3H_2O \xrightarrow{k_1} 3CO_2 + 7H_2 + H_2O \qquad (2.14)$$

Step 3: Gas-solid reactions

This step of the products formation results from side reactions; solid (char) is converted into gaseous (CO, H_2, CH_4) by reacting with gases (usually CO_2,H_2).

Main reactions in this step of the gasification are:

Boudouard reaction: $C + CO_2 \xrightarrow{k_2} 2CO$ (2.15) ΔH_R = 172.4 MJ kmol^{-1} [**188**]

Carbon water reaction: $C + H_2O \xrightarrow{k_3} CO + H_2$ (2.16) ΔH_R = 131.3 MJ kmol^{-1}

Hydrogenation reaction: $C + 2H_2 \xrightarrow{k_4} CH4$ (2.17) ΔH_R = -74.8 MJ kmol^{-1}

The conversion of organic waste by gasification in SCW is strongly driven by temperature. This is because high temperature leads to increase the reaction rate, and higher conversions while reducing the formation of char and tars that result from polymerisation due to incomplete conversion of the feed materials. In addition, gas composition is more likely to vary with temperature increase due to increasing side reactions such as gas phase reactions e.g. methanation and reverse WGS (see step 4 below).

For lower temperature gasification; catalyst is usually used, and temperature can be varied up to 600°C, whereas for high temperature gasification; temperature can be varied from 600 to 800°C. An increasing temperature contributes to increased H_2 and CO_2 yield while hydrocarbons such as CH_4 yield decreases [**189**]. However, high feed concentration would profoundly influence the thermal efficiency of organic waste gasification in SCW. A high temperature and catalyst may therefore be required in order to achieve high efficiency gasification or complete conversion of organic wastes. Increasing the feed concentration has been coupled with a decrease in the yield of hydrogen and an accompanying increase in the methane yield, which is attributed to the presence of less water at higher feed concentrations of solute, giving low steam/carbon ratios [**190**]. Thus, CO is more likely to produce methane by consuming hydrogen. A number of studies have also reported that high feed concentration increases the risk of plugging the reactor and fittings [**191, 192**] due to increase in polymerisation reactions, which lead to tar /char.

Pressure is expected to have little influence on the gas composition because most reactions are kinetically driven [**193, 194**]. However, high pressure may favour certain reactions such as WGS. Hydrogen yield could increase therefore with increasing pressure while CH_4 and CO yields would have a tendency to decrease with pressure.

Step 4: gas-phase reactions

This step determines the final mix of gaseous products

WGS and R-WGS reactions: $CO + H_2O \xleftrightarrow{k_5} CO_2 + H_2$ (2.18) ΔH_R = - 41.1 MJ kmol^{-1}

Methanation reaction: $CO + 3H_2 \xleftrightarrow{k_6} CH_4 + H_2O$ (2.19) ΔH_R = - 206.1 MJ kmol^{-1}

The final product gas composition is hugely dependent on the feed concentration (amount of water), temperature and reaction times. The chemical equilibrium can be attained for long reaction times and the products may be essentially limited to volatile gases (H_2, CO, CO_2, CH_4). However, this may vary depending on the reaction conditions and type of feedstocks. The analysis of the chemical thermodynamics of the above six gasification reactions reveals that low temperatures and high pressures favour the formation of CH_4, Whereas high temperatures and low pressures favour the formation of H_2 and CO [**195**]. On the other hand, when the gasifier temperatures and reaction times are not sufficient to attain chemical equilibrium, the product gas is likely to contain various amounts of light hydrocarbons such as C_2H_2 and C_2H_4, as well as heavy hydrocarbons that condense to a black, viscous liquid known as tar. Tar is an undesirable by-product of SCWG as it can block valves, in line filters and interferes with downstream conversion processes.

2.4.4 SCWG Chemistry

Organic compounds and gases are miscible in SCW, and because of that, it is possible to conduct chemistry in a single phase that would otherwise have to occur in a multiphase. There are several advantages for being able to conduct chemistry in a single phase:

- There are no inter-phase mass transfer limitations reducing the reaction rates.
- In addition, higher concentrations of reactants can be attained.

A strong dissociation of water near the critical point can generate a sufficiently high H^+ ion concentration, which enhances its ability to act as an acid catalyst to proceed without any added acid. Several studies have been conducted in order to unravel such ionic mechanisms for the conversion of biomass-derived components in supercritical water [**196, 197**]. Some findings have revealed that, indeed, near the critical point, ionic chemistry is more dominant than radical chemistry [**198, 199**]. In addition, parts of the reaction network of the decomposition of model compounds in hot compressed water have been elucidated. However, a reaction scheme provided with rate equations, useful for reactor engineering purposes, is not yet available.

2.4.5 Reaction products of SCWG

Various studies have reported on the main products of SCWG of glycerol: products gases [H_2, CO, CO_2, CH_4, and light hydrocarbons], condensate liquids [aldehydes (formaldehyde, acetaldehyde), alcohols (methanol, ethanol, allyl alcohol) and acids (formic acid, acetic acid)] and char [**200, 201**] have all been reported. These products can be accomplished in supercritical and near-supercritical water. A proposed and simplified reaction pathway for product formation is shown in Fig.2.7. These products highly depend on feedstock selection, the catalyst choice and the operating conditions.

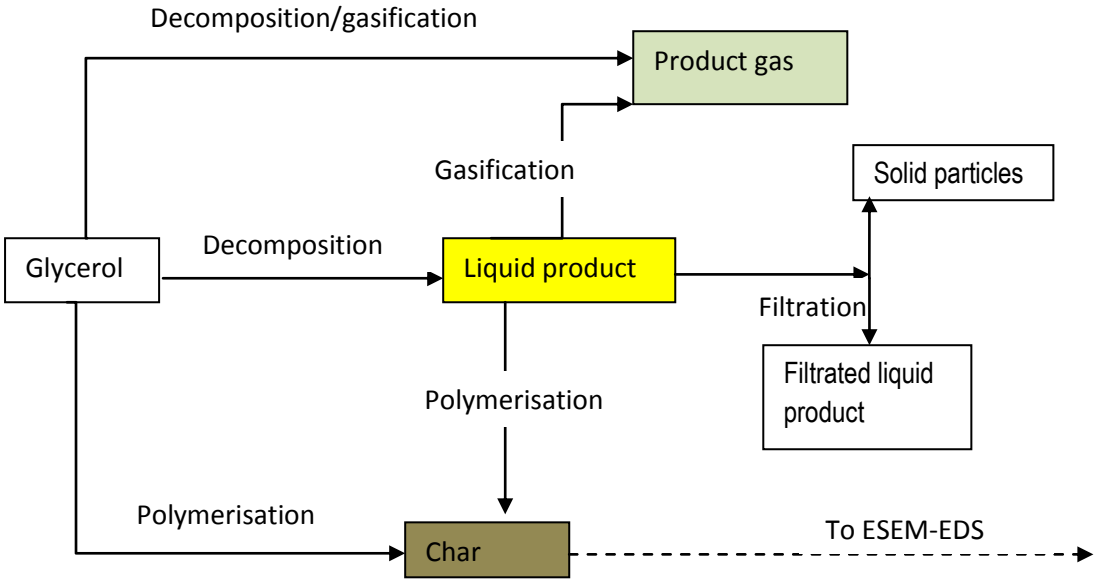

Fig.2.7. Proposed simplified pathways of products

Gas formation in SCW is promoted by the enhanced solubility of the organic compounds in the supercritical water that speeds up the reaction, leading to high gas yield. The product gas is formed from either direct decomposition of organic waste (glycerol), or indirectly via intermediates of condensate liquid products.

Aldehyde formation in SCW. In hot water, the reaction behaviour of an aldehyde is rather complex even without catalysts. When a single aldehyde is dissolved in supercritical water, self-disproportionation and disproportionation reaction occurs. In self-disproportionation, where the aldehyde reacts in and with water to produce alcohol and acid:

$$2\ R\text{-}CHO + H_2O \leftrightarrows R\text{-}CH_2OH + R\text{-}COOH \qquad (2.20)$$

Acid formation in SCW. A study has demonstrated that most organic acids (formic acid, acetic acid and acrylic acid) are formed in SCW through intermediates [**202**]. For instance, glycerol can decompose into intermediates compounds such as acetaldehyde followed by acid formation [**203**] e.g acetic acid. Aldehyde and formic acid can form alcohols with or without catalyst. The scheme is given by

$$R\text{-}CHO + HO\text{-}CHO + H_2O \rightarrow R\text{-}CH_2OH + H_2CO_3 \qquad (2.21)$$

The formation of formic acid is generated through thermal de-carbonisation of the aldehyde; carbon monoxide is generated as a decomposition product, and reacts with water to produce formic acid. However, an abundance of $H3O^+$ ions can be attained in SCW, which leads to pH decrease by a value of three units, which favours acid catalysed reactions.

Alcohols in SCW. It has been known for many years that it is possible to produce mixtures of methanol and higher alcohols from synthesis gas by alkali promotion of the methanol synthesis catalysts and appropriate modification of the reaction conditions [**204, 205**]. The economic viability of syngas

conversion is determined by capital costs and average product price. The manufacture of synthesis gas is by far the most capital-intensive part of a gas conversion plant. On the other hand, aldehydes in hot water, can also produce alcohol in excess to the acid (refer to equation 2.20). The catalysts and reaction conditions for synthesis of alcohols are reviewed in section 2.5.2.

Char formation in SCW. Char is a by-product, which constitutes a main problem of SCWG. Soluble compounds in SCW can polymerise to give char causing reactor plugging, heat exchanger fouling, catalyst deactivation, and, in particular, reducing the carbon gasification efficiency. An insight to understanding the char formation mechanism is therefore crucial in order to minimise its formation and to achieve complete conversion of the organic wastes in SCW. The char polymerisation depends strongly on reaction kinetics, process conditions (temperature, pressure, flow rates), and reactor design.

2.4.6 Design considerations of SCWG apparatus

The chemical content of the feedstock and product influences the design of SCWG equipment. Potential problems to account for during the design include slagging, fouling and corrosion of the gasifier and heat exchanger components [**206**]. For most biomass feedstocks, silicon, potassium, calcium, chlorine, sulfur and to some extent phosphorous, are the principal elements involved in the fouling of surfaces. Slagging occurs when a material is melted and then condenses on surfaces or accumulates as hard, dense particles (e.g. clinkers). Slagging also occurs when ash and other components of the reaction gases melt and condense on surfaces.

2.4.6.1 Corrosion issues

Corrosion in aqueous systems up to supercritical temperatures is determined by several solution-dependent and material-dependent factors. Solution-dependent factors are density, temperature, pH value, the electrochemical potential of the solution, and the aggressiveness of the attacking anions. Material-dependent parameters include alloy composition, surface condition, material purity, and heat treatment. Corrosion phenomena that are observed include inter-granular corrosion, pitting, general corrosion, and stress corrosion cracking [**206**]. In order to mitigate these issues, the feedstock for gasification should preferably have low sulfur content, low chlorine content, and low silica content. The molar ratio of sulfur to chlorine (S/Cl) should also be low since strong corrosion tends to occur when S/Cl is below 2 and moderate corrosion when S/Cl is 2 to 4 [**207**]. In addition, water should be demineralised and/or deionised before it is used as reaction medium for SCWG. Deionised water was used in this research work as part of an initial step toward mitigating the corrosion issues that result from the presence of alkali salt in the mains water.

2.4.6.2 Salt issues

During the last three decades, a number of studies have reported on the hydrothermal conversion of wet biomass to gaseous fuels up to pilot-scale [**208, 209, 210**]. Salt management was identified as a critical issue for the success of this technology [**211, 212**]. Water drastically changes its solvent properties near the pseudo-critical point, changing from a polar to a non-polar solvent. Thus, the solubility of salts in supercritical water is exceptionally low [**213, 214**] (refer to sub-section 2.3.1). Alkali salts, potassium in particular are responsible for fouling, corrosion and silicate formation found in biomass boilers. Salt precipitation from supercritical water was investigated initially in connection with supercritical water oxidation (SCWO) applications. Hodes and Marrone [**215**] gave a good overview on SCWO. A study has reported on the design of salt separator for the precipitation as an integral unit for the SCWG system [**216**] as shown in Fig.2.8.

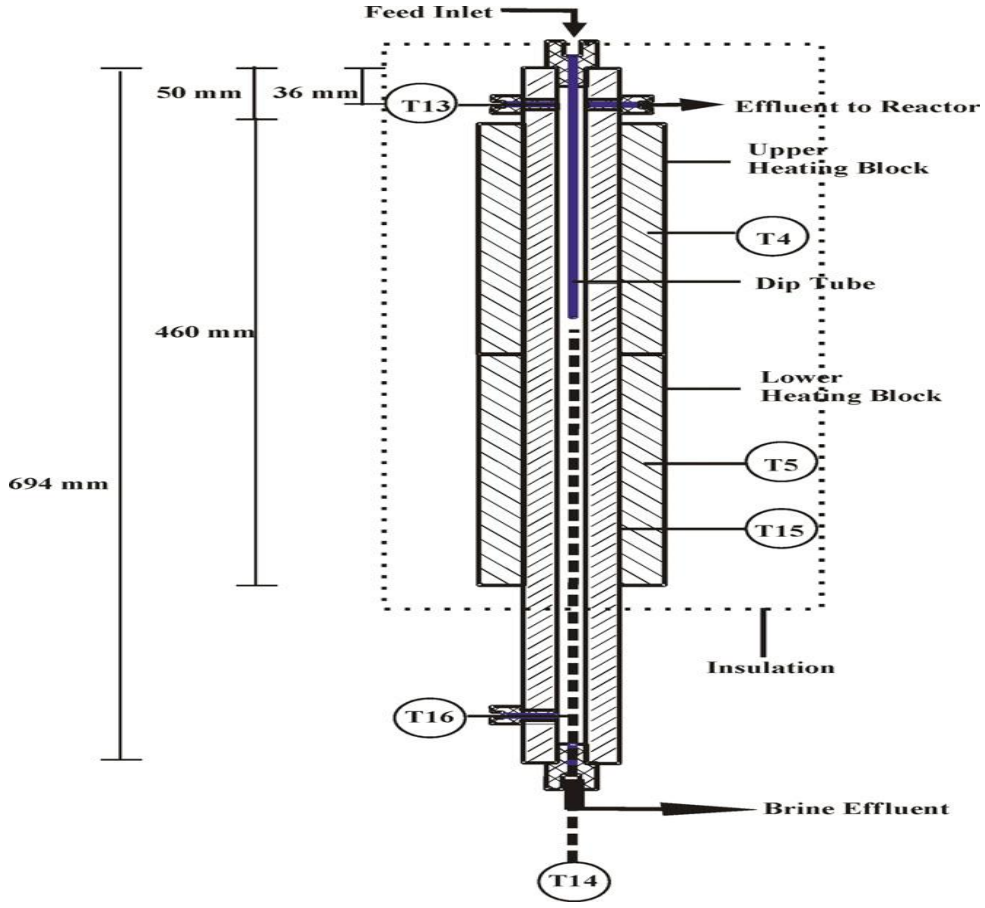

Fig.2.8. Schematic design of the supercritical water salt separator used in the continuously operated SCWG plant [**216**].

It can be noted that the design of the above salt separator vessel is similar to the MODAR reverse flow reactor built for supercritical water oxidation purposes [**217, 218**]. Using this separator in a continuous SCWG process, salts could be recovered as concentrated brine with high efficiencies between 80 and

92% [**219**] depending on the alkaline elements and operating temperature of the separator. The salt separation would proceed before the catalytic reactor because salt may act as catalyst poisons and would therefore lead to a deactivation of the catalyst inside the reactor. This arrangement would contribute to achieve a useful catalyst lifetimes. Another good aspect of salt removal is that the concentrated brine effluent could be recycled as valuable nutrients and fertilizers after further conditioning.

2.4.6.3 Reactor Designs

Reactors used. PFR and PBR are similar, except that the PBR is designed for fluid-solid heterogeneous reactions involving catalysts. The advantage of a PFR is that it is relatively easy to maintain (there are no moving parts), and high conversion per volume of the reactor can be achieved. The disadvantage of a PFR is the difficult control of temperature within the reactor. In addition, when the reaction is exothermic, hot spots can occur in a PFR. It is also essential to note that, most homogeneous liquid-phase flow reactors are CSTRs, whereas most homogeneous gas –phase flow reactors are tubular.

In order to design a suitable reactor, the obvious essential elements that have to be considered include reaction rate equation, mass balance (dependent to the type of reaction) and heat transfer. In addition, corrosion and salt removal are other issues to be considered for gasifier reactor design particularly in this case of SCWG. It is proposed that a broad strategy for reducing slagging, fouling and corrosion problems in SCWG can be adopted in a similar approach to that of biomass boilers. For instance, the utilisation of pre-treatment techniques such as washing feedstock (e.g straw) to reduce the amount of chlorine and potassium can be highly beneficial.

Temperature controls. Temperature can be used to control deposits to a certain extent, especially as a short term or intermittent solution. Slagging can be avoided by operating the gasifier in a lower temperature regime that keeps the temperature well below the flow temperature of ash formation. This is advisable, especially when catalyst is used. However, gas streams throughout the system should be maintained above the dew points of its corrosive contents. In particular, sulfur and chlorine result in low temperature corrosion if they are allowed to condense out on surfaces. Reducing temperature to control deposits also reduces the capacity and can have undesirable economic consequences.

Feedstock selection. A primary feedstock potentially contains a variable degree of elements such as chlorine and sulphur. Improved selection of feedstock could play a prominent role in mitigating the corrosion or fouling problems.

Using corrosion-resistant materials. When selecting materials for components for the reactor, downstream equipment and ancillaries, it is essential that in order to avoid corrosion high chromium stainless steels such as AC66 or hastelloys materials are used.

Moisture content is critical in combustion or gasification process. Maximum moisture content required for conventional gasification depends on the gasifier type. For conventional gasification, a downdraft fixed bed gasifiers cannot tolerate moisture contents above about 20%. Updraft fixed bed gasifiers and fluidised bed gasifiers can tolerate higher moisture contents of 50% and 65%, respectively [**220**]. Moisture content is an issue not relevant in the gasifier of the supercritical water process since there is no needed to dry the feedstock. However, a suitable gasifier for this process is still in the research and development phase, but once established promises to widen the range of possible feedstocks that can be used. Gasifiers especially for straw and other bio-fuels with high alkali and chlorine contents have been developed [**221**]. Fluidised bed gasifiers are in general better suited for these materials due to their lower operating temperatures and low moisture content.

2.4.7 Review of SCWG Catalyst

A number of homogeneous and heterogeneous catalysts have been used successfully in supercritical water and are reviewed in this section. The mechanism of reaction with a heterogeneous catalyst in SCWG is similar to Langmuir-Hinshelwood (L.H.).

2.4.7.1 Typical catalysts

There are three main groups of catalyst that could be used for thermal and hydrothermal conversion of organic wastes into hydrogen or/and syngas. Noble metal-based (Rh, Ru, Ni, Fe), non-noble metal-based (Fe_2O_3 and Fe_3O_4) and homogeneous solutions containing a dissolved catalyst, such Co, Ru, or Rh. Elliott has published a comprehensive review of the research efforts on catalytic SCWG [**222**].

Studies have reported on the addition of K_2CO_3 [**223**] or/and Na_2CO_3 [**224**] in CSCWG of glycerol for the production of hydrogen. They found that the addition of K_2CO_3 in CSCWG process could enhance the glycerol gasification efficiency and increase the H_2 yields by promoting the WGS reaction. Similarly, Na_2CO_3 also increases H_2 yield and Chemical Oxygen Demand (COD) destruction efficiency. Gasification efficiencies were up to 95.8% and 98%, and hydrogen yields could reach 4.14 and 5.08 mol/mol, respectively [**224**].

Metals are typical catalysts for SCWG because they can promote a high level of carbon conversion to gas at relatively low temperature. Several heterogeneous catalysts have been studied to promote hydrogen yield, to reduce the formation of tars and char during CSCWG reaction. Among them, a metal-based made of Ru/ ZrO_2 (1 wt% Ru) [**225**] and Ru/Al_2O_3 [**226**] and Rh [**227**] have showed

promising results. These studies have demonstrated that using Ru/ZrO_2 catalyst, the rate of glycerol conversion augmented and favoured the carbon-carbon scission reactions to form product gas, as well as acetic acid and acetaldehyde as the main primary products. Whereas carbon-carbon bond forming reactions are predominant using a Ru/Al_2O_3 catalyst. However, Ru has more catalytic activity than Rh or Pd.

The use of 12-14 wt% Ni (16-18% NiO) on an Mg or Al_2O_3 support [**228**] has been studied for syngas production. This work has indicated that Ni has the highest activity for reverse-WGS by promoting CO formation rather than CO_2, and was highly suitable for steam reforming of hydrocarbons (C_1, C_2 and C_3). A typical exit gas composition were 55 vol % H_2, 20-25 % vol CO, 16-20% CO_2, 4-8% CH_4, 1-20% C_2,1-2% C_3, and tars. H_2/CO ratio at the reformer exit was between 2.0 and 3.0 [**228**]. Other metal based catalysts were also reported and were found to favour syngas production with application to FTS. These catalysts include $NiMO/Al_2O_3$, $PtPd/ Al_2O_3$, $CoMo/ Al_2O_3$, Inconel powder and Pt-Re /C [**229, 230**].

After extensive review of the literature, no work has reported on the use of metal oxides for CSCWG of glycerol. Thus, this work has investigated the use of low cost Fe_2O_3 and Fe_3O_4 for CSCWG at temperatures up to 550 °C, to study the conversion of glycerol into gaseous products.

Gasification of organic wastes to hydrogen or syngas (CO + H_2), followed by catalytic conversion of syngas, could produce ethanol in large quantities. However, the catalytic conversion of syngas to ethanol remains challenging, and no commercial process exists as of today although the research on this topic has been ongoing for the past 90 years. Homogeneous catalytic processes are relatively more selective for ethanol via FTS and difficult to separate from SCWG products. However, the need for expensive catalyst, high operating pressure, and the tedious workup procedures involved for catalyst separation and recycling issues make these processes unattractive for commercial applications. On the other hand, the heterogeneous catalytic processes for the conversion of syngas to ethanol have suffered from low yield and poor selectivity. This is because of the slow kinetics of the initial C–C bond formation and fast chain growth of the C_2 intermediate.

2.4.7.2 The choice of the catalysts

Many factors such as suitability (stability, lifetime, and effectiveness), availability and economic (cost) affect the selection of a catalyst. Homogenous catalysts based on noble metals are devilishly difficult to separate from products, to recover and reuse. Using precious metals as heterogeneous catalyst can increase the operating cost due to their high value. The problem of reducing operating cost and ease of separation can be explored with non-noble metals-based catalyst. The choice of catalysts chosen to be investigated in this work was based on a similar consideration to the above:

- Lack of previous research work (remarkably no information available)
- Their suitability based on literature review information
- Their availability (provided by local companies, hence no transport cost)

In addition, their economy (use of low cost catalyst, which could be just as effective as an expensive catalyst). Considering the above criteria, Fe_2O_3-Cr_2O_3 and Fe_3O_4 were selected as low cost and potential effective catalysts in this project.

2.5 Commercial scale and majors research groups worldwide in SCWG

SCWG of wet organic wastes is an advanced technology, which has drawn attention of research groups across the world. However, there is remarkably only few medium to large scale pilot plants for SCWG that are being constructed and operated. The most recognisable ones are:

- Forschungszentrum Karlsruhe (FzK) in Germany, which is the largest plant, in operation since the beginning of 2003, with a design capacity of 100 Lh^{-1}, and was built to demonstrate supercritical gasification of wet residues from wine production.
- The University of Twente (Enschede, Netherlands), with a capacity of 5-30 Lh^{-1}, designed for temperatures up to 650°C and pressures of around 300 barg.
- The Wolter Prins (BTG Biomass Technology Group BV, Netherlands). BTG is a private company specialised in design, construction of bench-scale set-up of SCWG system. Pilot plant: capacity 3-30 L/h, Max. Temperature 650°C, Max pressure 350 barg, organic content 5-30 wt%

Other leading groups and institutions currently working on various aspects of SCWG technologies are:

- Tomoaki Minowa (National Institute of Advanced Industrial Science and Technology, Japan) looks into the reaction kinetics, chemical-physical thermodynamic data.
- University of Tokyo focuses on process development and economics of SCWG
- Yukihiko Matsumura (Hiroshima University, Japan)
- Michael J. Antal, Jr.; (University of Hawaii, USA)
- Doki Yamaguchi (University of Melbourne)
- Andrea Kruse (Forschungszentrum Karlsruhe, Germany)
- University of Birmingham, UK. Pilot plant: capacity up to 4.7 Lh^{-1}, Max. Temperature 600°C, Max pressure 330 barg, organic content up 40 wt% for solvent-soluble compounds.

2.6 Summary of SCWG of organic wastes

In this chapter, various properties of SCW and their benefit to SCWG of organic materials were reviewed. Many studies have reported on the behaviour of chemical reactions in the gas phase or liquid phase. Studying reactions at supercritical conditions could be based on the same techniques and concepts that are used to study reactions in solution. This chapter also discussed the concept for organic wastes processing, the feedstock selection, the processing routes, and associated technical challenges. Many routes for the conversion of organic materials or biomass into bio-based products already exist. However, the technology faces many challenges including cost reduction in order to develop the processing techniques at large scale, with marketable products. Any processing technique at a commercial scale will have to deal with a much larger range of feedstock, which means they must make use of a wider variety of processing technologies. However, gasification and pyrolysis could complement each other in an integrated process known as bio-refining.

CHAPTER 3. MATERIALS AND EXPERIMENTAL SYSTEM

3.1 Statement of facilities

The SCF research group at the University of Birmingham has comprehensive experience and various facilities, however, the SCWG project was still at an early stage when the author joined the SCF group in September 2009; in fact, no rig for SCWG process existed. In collaboration with local and international businesses, the author completed the construction and commissioning of the pilot plant for SCWG (capacity 4.71 litre/min slurry, 300 barg and up to 600°C) at the chemical engineering department. Parr Ltd-UK collaborated on testing the reactor heaters; Sentinel Ltd based in the United States of America investigated and upgraded the pre-heater controller unit; and in partnership with a local software designer, the author designed the software (Labview) to enable the process parameters to be viewed on a laptop. The School's insurer provided a safety inspection and insurance for the equipment used in the construction.

This section presents the constructed process plant for the SCWG with detailed information on the equipment selected as well as the materials used during its construction. The analysis of the resulting products and characterisation of the catalysts is also presented.

3.2 Materials

The main materials used in this work were the feedstock (pure glycerol, crude glycerol and digestate), the water for feed preparation and catalysts (iron oxide-chromium oxide and magnetite).

3.2.1 Feedstock

3.2.1.1 Pure glycerol

A model compound [Pure Glycerol (99 % purity)] purchased from Sigma Aldrich, UK was used without further purification. Glycerol (pure and crude) feed concentration was prepared in the same way by mixing a known amount of solute into a known quantity of deionised water. Glycerol ($C_3H_8O_3$)

was utterly soluble in the water even at ambient conditions. However, the mixture was agitated to speed up solubility. The solution of pure glycerol remained homogeneous, clear and transparent when dissolved in water (Refer to Fig.3.2). Because of the hygroscopic nature of glycerol, the solution was not left in open contact with air for longer than necessary in order to prevent moisture absorption that could affect the feed concentration. The solution was prepared and used immediately after the SCWG system was equilibrated (refer to sectio .4).

Fig.3.1: Chemical structure of glycerol molecule

It can be seen in Fig.3.1 that glycerol has three hydrophilic hydroxyl groups. These 3-OH groups are responsible for glycerol solubility in water and its hygroscopic nature.

3.2.1.2 Crude glycerol

Crude glycerol was obtained as by-product from biodiesel production (primary feed was vegetable oil extracted from Olea/olive plant) and was supplied from Brazil. It was characterised, and the purity was determined before use. This was determined by running a sample at different concentrations on the GC-FID. The crude glycerol was characterised to determine its chemical composition hence purity and physical properties (density and viscosity) as described in section 3.6 and 3.7. Crude glycerol was preheated to 40°C due to coagulation at room temperature (15 °C), and the solution was prepared in the same way as described in sub-section 2.5.

Fig.3.2 Image of pure (left) and crude glycerol (right)

As showed in Fig.3.2, the solution of crude glycerol was a homogeneous, but brown in colour compared to a pure glycerol that is clear and transparent. The main compositions of the crude glycerol are shown and discussed in the next chapter (refer to chapter 4).

3.2.1.3 Digestate

A sample of digestate was provided by Gleadell Agriculture, UK and was recovered as a waste residue from anaerobic digestion either by acidogenesis (if plant wastes containing fibres, grass or lignocellulosic (LC) biomass are used as feed) or by methanogenesis (if sludge from liquor is used). The main product of this process is the biogas. A sample of digestate produced by acidogenesis (Nitric acid) was characterised to determine its elemental composition by semi-quantitative analysis using Agilent series 4500 series inductively coupled plasma mass spectrometry (ICP-MS) technique, and the results are shown in appendix S.

3.2.1.4 Water

Deionised water was obtained at a temperature of 26°C from the University facilities and was used to prepare all the feed concentrations. In the ion exchange system, water is exposed to electrically charged resins that attract and bind to the salts. Removing salt elements, such as Na, Ca, K, and P in water, which contributes to mitigate salt deposition in the reactor, hence eliminating the slagging and corrosion issues.

3.2.2 Catalysts

Two catalysts were used in this work after intensive review of the literature for suitable catalysts. The first one was a blend of iron oxide-chromium oxide, which was prepared by the manufacturer. This catalyst was used to study the CSCWG of pure glycerol, and to establish the best operating conditions for hydrogen production. The second one was magnetite provided by Minelco.ltd, UK, and was used to study CSCWG of pure and crude glycerols.

3.2.2.1 Iron oxide-chromium oxide

A blend of Iron oxide-chromium oxide (model: Catal CT 54), prepared and supplied by the manufacturer (Catal Ltd) was used to promote water gas shift reaction (WGS) for the production of hydrogen. It has been suggested that iron oxide could have a high activity on organic decomposition and chromium could promote high temperature shifts (HTS) for the conversion of CO in reformate streams according to Catal Ltd. The catalyst has been fired to reduce the surface area to 58 m^2/g and

particle size [3.5 mm cylinder with 4 mm diameter]. Chromium was added to the active metals to stabilise the oxide on the surface of the iron by promoting oxidation resistance. This catalyst was reported to be capable of withstanding extended steaming without loss of mechanical strength, and it is suitable for high temperature (HT)-WGS reactions for the conversion of CO in reformate streams. Various characterisations techniques (BET, XRD and TGA) were used to characterise a range of samples before and after utilisation (Refer to section 3.7). Fig.3.3 shows the molecular structure of iron oxide-chromium oxide.

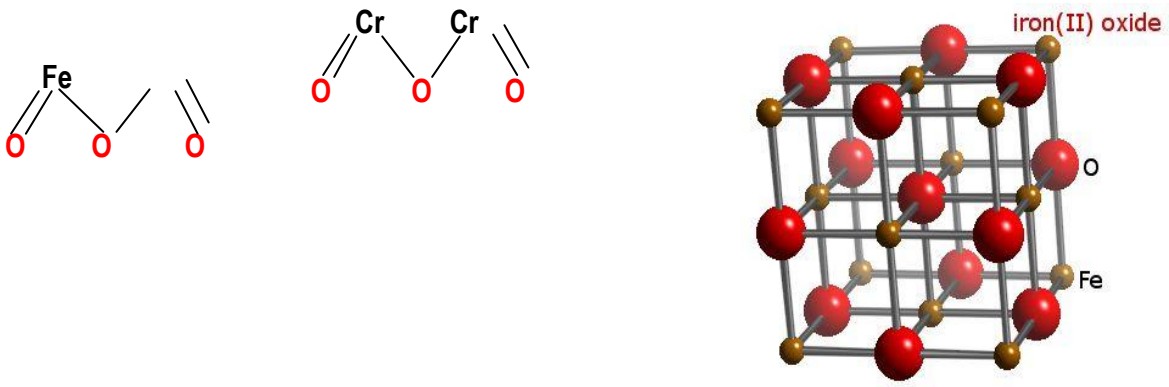

(a) Iron (II) oxide (b) Chromium (II) oxide (c) crystallographic of iron (II) oxide

Fig.3.3. Iron oxide molecular structure

It can be seen that iron (II) oxide structure is composed of Fe together with O. The chromium II oxide is composed of Cr together with O. Most iron oxides are crystalline at variable degree. The degree of structural order and the crystal size are, however, variable and depend on the conditions under which the crystals were formed. In this work, the crystalline range for the Fe_2O_3-Cr_2O_3 sample was studied by XRD analysis and showed to display a poor crystalline structure (refer to sub-section 3.7.3). It can be seen that the iron oxides are made up of close packed arrays of anions. The crystallographic arrangement is orthorhombic for Fe_2O_3 compare to cubic for magnetite.

3.2.2.2 Magnetite

Minelco Company (based in North Lincolnshire) supplied two samples of magnetite: a standard sample, d_{50}= 150 µm and crushed sample that contains variable particles sizes (d_{50}). The latest was classified by carrying out a particle size distribution (refer to appendix B). Magnetite samples were characterised by various characterisation techniques (BET, XRD and ESEM-EDS), and the results are presented in chapter 4. It has been suggested that this catalyst has the potential to promote WGS reaction due to the high content in iron and oxygen. Fe_3O_4 catalyst samples were characterised by XRD and ESEM-EDS analysis to study the crystalline range and chemical composition, respectively. (Refer to Appendix L, M, N). Fig.3.4 shows a structure of Fe_3O_4 in simplified and cubic form.

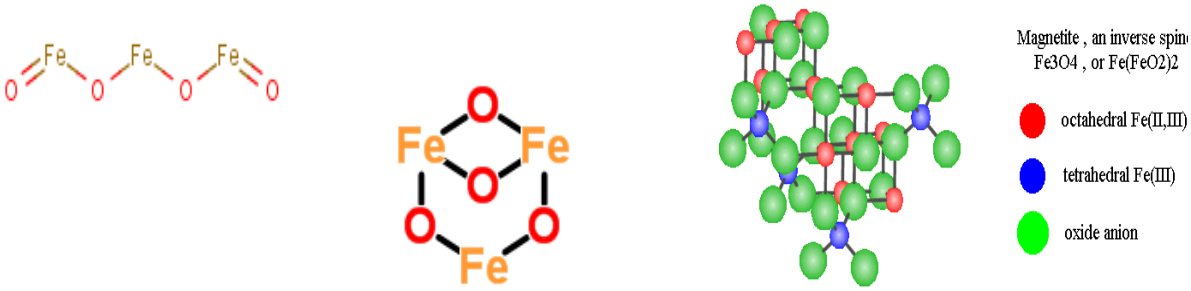

(a) Simplified structure of Fe_3O_4 (b) Cubic structure of Fe_3O_4 (c) Magnetite in an inverse spinal form

Fig.3.4. Magnetite molecular structure

It can be seen that the structure of magnetite is that of inverse spinel. The structure has a face-centred cubic unit cell based on 32 O^{2-} ions, which are regularly cubic close packed. Magnetite (Fe_3O_4) differs from most other iron oxides in that it contains both divalent and trivalent iron. The divalent iron may also be partly or fully replaced by other divalent ions (e.g. Mn^{II} to Zn^{II}). A study has reported that fitting of guest ions into the structure is assisted by the flexibility of the oxygen framework, which can expand or contract to accommodate cations that differ in size from Fe^{II} [**231**].

3.3 Equipments and SCWG process

Fig.3.5 and 3.6 show the simplified process diagram of the SCWG of organic waste/biomass process system for hydrogen production. The first is a small-scale process with one stage separation. The second is a large-scale process with large reactor and two-stage separation system. Environmental and economical benefits motivate interests in large-scale use of organic waste for energy and hydrogen production. The SCWG process consists of a number of unit operations such as high-pressure pump, heat exchanger, reactor, gas-liquid separators. All the equipments are designed to withstand a high pressure (up to 330 barg) and aqueous environment and their functionality are provided in a subsequent section.

3.3.1 Small scale process

The small-scale process for SCWG was designed to study the organic wastes processing in SCW under laboratory scale. The objective was to reduce the operating cost of the process due to the high cost of obtaining the model compound of feed. A diaphragm pump was used to transfer the feed into the reactor after it was preheated using a coil preheater. A small-scale reactor (30ml capacity) was fabricated at the University workshop, and operating temperature up to 600°C; the maximum operating

pressure was around 300 barg. A residence time of up to 27 seconds was required to achieve complete carbon conversion, depending on the feedstock concentration and operating temperature. A small coil condenser was placed downstream of the reactor, and before the small separator, which was essential for the process to achieve high thermal efficiency. A small size separator was used for the gas-liquid separation under high pressure. Its design capacity was 285 ml volume, and 150 barg. A pressure regulator was used to reduce the upstream pressure from up to 300 barg down between 40- 60 barg.

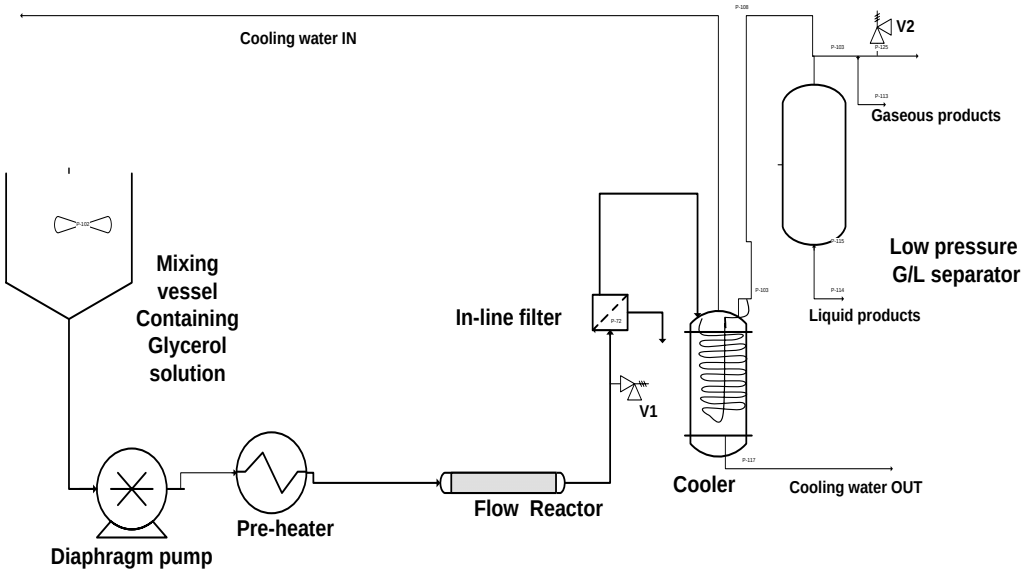

Fig.3.5. Simplified process diagram of the small-scale rig

3.3.2 Large scale process

The large-scale process for SCWG was designed to study the organic wastes processing in SCW under pilot plant size. The sample diaphragm pump described in subsection 3.3.3.1 was used to transfer the feed into the reactor after a coil preheater has preheated it. Parr Instrument Ltd supplied a large-scale flow reactor (0.96-litre capacity), operating temperature was typically between 500 to 600°C; the maximum operating pressure was around 300 barg. A tube heat exchanger was placed between the outlet streams from the reactor and inlet of the high-pressure separator. Two stage units of separator were used for the gas –liquid separation; one for high pressure up to 300 barg and the other for low pressure (up to 110 barg). The aim of the stage separation was to maximise the gas- liquid separation and thus the hydrogen–rich gas. It is expected that solubility of the individual components in the product gas will vary with temperature and pressure. A pressure regulator was used also to reduce

the upstream pressure from 250-300 barg to 40-60 barg. A process flowsheet is provided in appendix C.

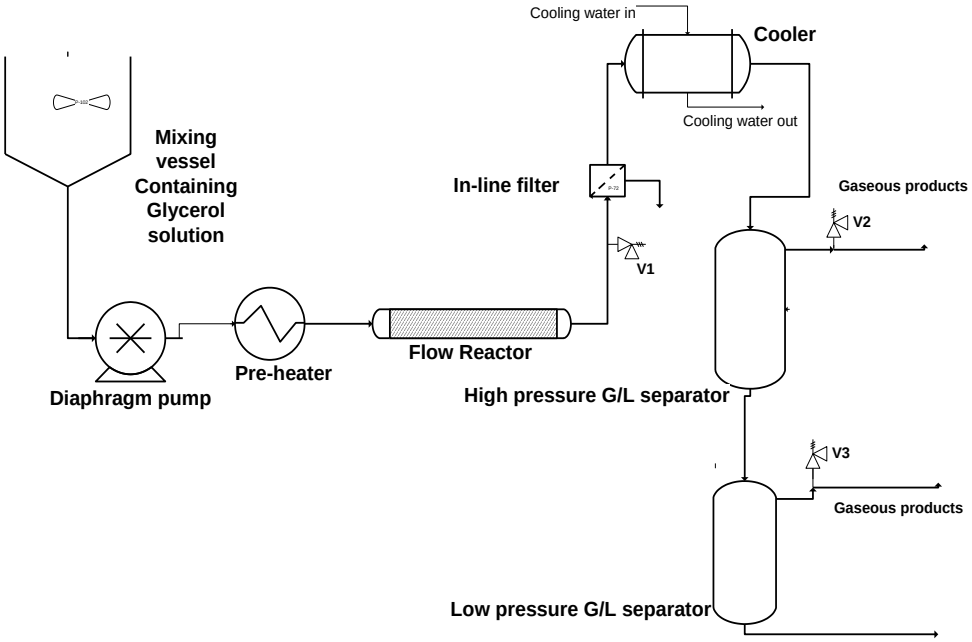

Fig.3.6. Simplified process diagram of the large-scale rig

Fig.3.7. Image of the full process after construction

(Note: separator unit in the foreground and reactor in the middle)

3.3.3 Main equipment

3.3.3.1 Diaphragm Pump

A high-pressure diaphragm pump manufactured by Lewa GmbH, serial n° 493077-010.001, Model LDC1 (Refer Fig.3.8) was used to pressurise and transfer the feed fluid into the reactor. This pump was equipped with an internal pressure relief valve (set at 330 barg) and had a maximum operating pressure of 300 barg and fluid temperature up to 20°C for a maximum flow rate capacity of 4.71 Litres/hours of water slurry. The viscosity capacity that the pump could handle was 1.04 mPa.s at STP.

Figure 3.8. High-pressure diaphragm pump

The pump was calibrated using a model compound of glycerol and water at variable concentrations and pressures (refer to section 3.6.1 and appendix D). The organic stream was fed into the reactor at a desired flow rate and pressure by setting a pump stroke length and manually adjusting the pressure regulator (up to 400 barg), accordingly to the calibration curve.

3.3.3.2 Pre-heater

An electrical heater unit shown in Fig.3.9 was used to pre-heat the feed entering the reactor. The pre-heater was purchased from Autoclave Engineers Company, (Model 401C-0524, serial number 07250430-1). The pre-heater was a coiled tube heat exchanger made in HAST-C (test pressure 10500 psi) rolled over the external surface of the block metal. The mechanism of heat transferred was by conduction from the heating block to the coiled tube through which the process feed passed.

Figure 3.9. Electrical pre-heater

Internally, the electrical heater was constructed of a high temperature heating element and was insulated using ceramic materials. An outer stainless steel shell was fitted over this portion creating a housing, which was wrapped around the vessel outside surface. Ceramic fibre insulation between the insulators and steel shell lowered the heat loss to the external surface. Three thermocouples (K type) were provided and were used to control and monitor furnace temperatures. One thermocouple was measuring the external temperature of the heating block, one the inside temperature of the furnace and the other one measuring/controlling the outer process temperature leaving the furnace. All three temperatures were monitored and controlled from a Sentinel Series Controller unit (model 40C-0578) supplied by Autoclave Engineers. The process control thermocouple was located in a Thermo well that was designed to make contact with the process media as it exits the pre-heater. The feedback from this thermocouple is routed to the PLC (Programmable Logic Controller) in the Sentinel unit. The process temperature is then compared to the target set point entered into the touch screen or the Watchtower software. The Sentinel control unit was using an industry standard PID, (Proportional Integral Derivative), type control algorithm to determine the amount of power output required from the heater to obtain the desired set point. If at any time, the process temperature exceeds the alarm limit set in the Controller the system will shut down until the alarm condition clears and is acknowledged and reset by the operator pressing the acknowledge and reset push buttons

3.3.3.3 Reactors

3.3.3.3.1 Small scale reactor

The small-scale reactor used in this work was also a flow reactor, constructed locally using a stainless steel tube 316 L (O/D =25.2 mm, wall thickness = 3.2 mm, length = 110 mm as measured; hence an ID=0.0188 mm and a volumetric capacity of 30 ml as calculated). The reactor was capped with Swagelok fittings/valves. This reactor was packed with the catalyst of choice as described in

section 3.5.3. All catalytic processes, regardless of type, involve various phenomena in addition to the desired catalytic reactions. These include: side or interfering chemical reactions, thermodynamic, physical and chemical equilibrium, heat transfer, mass transfer between phases or even within a given phase, flows of fluids (free convection or forced convection) or granular solids; these phenomena are differently affected by the operating variables and reactor size and geometry as reported by Trambouze [**232**]. Although a flow reactor does not have good temperature control, it is remarkably good for heat transfer, it has a high conversion per volume, can have large catalyst loading capacity, and has no problems with catalyst attrition, as well as its low operating cost and easy to scale-up. Furthermore, the plug flow reactor is used for fast reaction and high temperature/pressure operation, which is ideal for a supercritical fluid. The chemical reaction proceeds as the reagents travel through the reactor. The changing reaction rate creates a gradient with respect to distance traversed; at the inlet to the PFR, the rate is exceptionally high, but as the concentrations of the reagents decrease and the concentration of the product(s) increases the reaction rate slows.

3.3.3.3.2 Large scale reactor

The large-scale reactor was a flow reactor as shown in Fig.3.10 (part n° QW9478 A, manufactured by Parr Instrument Company, USA), which was constructed from Hastelloy. Hastelloy C-267 was used to provide high resistance to corrosion, pitting and cracking, which is due to high nickel content to 54 wt %). This reactor has a length of 0.96 m; inside diameter 0.025 m and outside diameter 0.050 m. The design parameters were 550°C and 345 barg for the pressure with a volume of 0.632 Litres. The reactor was fitted with bursting disc (BD) at the inlet and with a pressure relief valve (PRV) at the outlet for safety precaution.

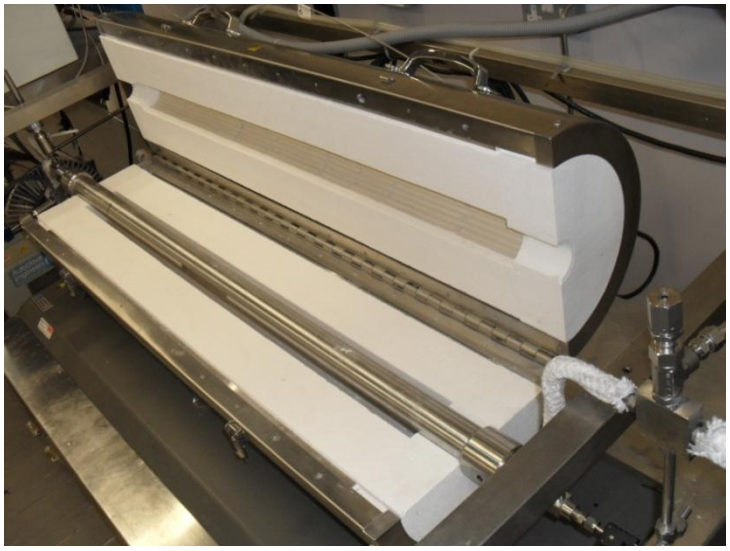

Figure 3.10. Flow reactor-large scale

3.3.3.4 Condenser

3.3.3.4.1 Small scale condenser

On the small-scale rig, the cooler was a coil type condenser, locally fabricated at the university workshop using 316L stainless steel materials. The condenser process temperature was monitored from the temperature indicator and Labview routed by two K-type thermocouples at the inlet and outlet process fluid to the condenser, which were routed through Labview (v.3.1).

3.3.3.4.2 Large scale condenser

On the large-scale rig, the condenser was a heat exchanger type provided by Autoclave Engineers (model 401C-0530, serial number 07250430-2) test pressure 8500 Psi. As shown in Fig.3.11, the external body parts and coil tubes were constructed from SA312 GRTP304L and HAST-C materials, respectively.

Fig.3.11. Condenser unit on a large-scale rig.

The condenser temperature was controlled from the process media monitoring thermocouple, located in the outlet flow of the condenser. The feedback from this thermocouple is routed to the PLC (Programmable Logic Controller) in the Sentinel unit. The process temperature is then compared to the target set point entering into the touch screen or the Watchtower software. As the process temperature or set point changes, the Controller makes appropriate adjustments to the cooling valve to bring the process temperature in-line with the operator set point. If at any time, the process temperature exceeds the alarm limit set by the operator, the controller of the system will be shut down (control valve opens 100%) until the alarm condition clears and is Acknowledged and Reset by the operator pressing the acknowledge and reset push buttons.

3.3.3.5 Separators

3.3.3.5.1 Small scale separator

On the small-scale rig, one mini-separator was used and was supplied by Swagelok –Manchester Ltd (model: DW7119). Working pressure: 100 barg, design parameters: pressure of 150 barg, 285 ml of volume, and construction materials: 304 L stainless steel. This small separator was operated in the same way as the large-scale separator described in subsection 3.3.3.5.2.

3.3.3.5.2 Large scale separator

On the large-scale rig, two separators made in SS 316 L were used for the gas /liquid separation downstream of the reactor. The first is a high pressure (330 barg max.). The second is a low pressure (110 barg max.). In the separators, the operating conditions are adjusted after the reaction in order to modify the state of the water. The high-pressure gas/liquid separator shown in Fig.3.12 was designed for 330-barg pressure at 30°C (serial n° 1069, manufactured by LAB-TEMP). The low-pressure gas/liquid separator was designed for 110 barg pressure at 30°C (serial 1069, manufactured by LAB-TEMP).

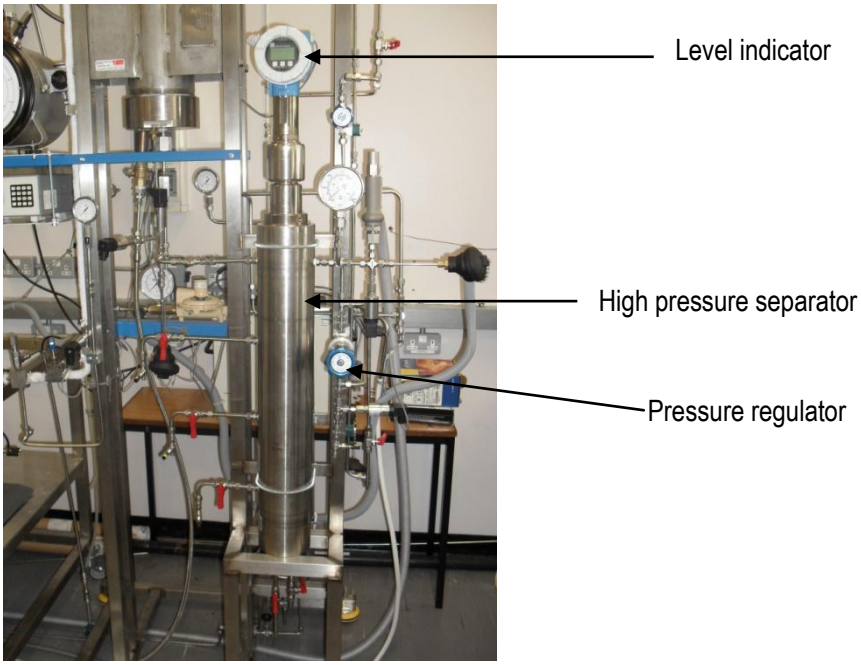

Fig.3.12. Gas/liquid separators

The high and low pressure separators were each equipped with pressure relief valves (PRV) at the inlet and outlet streams. The pressure in the system was controlled using a diaphragm-type high-pressure regulator (PR-50 Series, supplied by Hoke). Pressure was monitored using local pressure gauges, and can also be monitored from Labview V.3.1 on a laptop. The high-pressure separator has a level

indicator (level flex Model FMP40) to monitor the liquid level inside the separator. The fluid level (interface level), gravity, pressure, temperature and liquid/gas velocities were the most critical parameters that influenced gas/liquid separation. The level was controlled in order to avoid column flooding or entrainment of the liquid in the gas stream. The gas/liquid separators used in this work were gravity separators.

3.4 CSCWG rig Operations

The CSCWG experiments were carried out in the flow reactors as described in sections 3.3.3.3. The experimental rig was first flushed with water, and the pressure was increased to the desired condition. The reactor temperature was set and controlled by a Parr controller (Model 4843). The temperature of the system was measured with four Type K thermocouples with one of the thermocouples directly measuring the reactor temperature. Water was passed for 40 minutes in order to equilibrate the system before the glycerol solution was introduced at the desired flowrate and pressure via the high-pressure diaphragm pump (Lewa LCD1, Gmbh). The product stream leaving the reactor was cooled to approximately 30°C using cooling water through a coil tube heat exchanger. A pressure regulator was used to maintain the desired upstream reactor pressure and the pressure in the downstream high pressure G/L separator, where gas is separated from the condensed liquid. A second downstream low pressure separator (up to 110 barg) was used to maximise the gas–liquid separation. Gas and liquid products samples were collected after the first 5 min and subsequently, every 15 min. The standard operating and emergency procedures of the rig are provided in appendix E.

3.5 Experimental methodology

The processing of organic wastes by CSCWG has the potential to reduce the operating cost and to offer an environmentally benign method for the production of energy and platform chemicals. This is because there is no need to dry the feedstock, the use of effective catalyst and high pressure could compensate for the high temperature requirement for the reaction. Furthermore, high gas yields with low formation of by-products such as a coke can be obtained at a temperature below 550°C due to the rapid reactivity in SCW and the high solubility of the intermediate products under reaction conditions. The experimental method has consisted of two main steps. The first one described the catalyst selection and packing. The second one studied the reaction set-up and reaction conditions.

3.5.1 Catalyst: selection and loading

In order to promote gasification at a temperature between 350 - 550°C, a catalyst is needed for reforming. The criteria (suitability, effectiveness, cost and availability) for the selection of the catalyst have been explained in chapter 1. Various studies have reported that using nickel as a catalyst at temperatures higher than 740°C, there is an increase in the H_2 and CO content of the resulting gas, combined with elimination or reduction of the hydrocarbon and methane content [**233, 234, 235**]. Nickel will also work well for low temperature SCWG (550°C) by promoting reverse-water gas shift (R-WGS) reaction. However, Ni is not a cost effective catalyst due to its high cost. A low cost Fe_2O_3-Cr_2O_3 and natural Fe_3O_4 were selected for this project over other potential catalysts. The mechanical strength of these solid catalysts is one of the most decisive factors for their selection and the reliable and efficient performance of the process. It was expected that brittle fracture, which leads to the mechanical failure of the catalyst pellets, could be avoided.

3.5.2 Catalyst preparation

A co-incipient wetness impregnation method was used for Fe_2O_3-Cr_2O_3 preparation, and this was carried out by the manufacturer before it was supplied (refer to appendix F). Sample of Fe_3O_4 was used as supplied without any form of preparation.

3.5.3 Packing of the catalyst into the reactor

The reactor was packed in-house with 32.1 g of catalyst (d_{50}= 4 mm) to occupy the entire volume of the reactor bed. The integrity of the packing was validated by running stability test to evaluate the uniformity of the packing, which resulted in a first 4 hours of instability. From 5 to 9 h the stability of the packed catalyst was reached (refer to Fig.5.3). The packing procedures were as follows:

- Catalyst was weighed and its volume recorded
- A wide mouth plastic funnel was inserted into the top of the reactor
- Approximately 20 % of catalyst volume was added
- The side of the reactor was tapped with a soft hammer whilst noting the height of the catalyst from the top of the reactor (a 15 mm length of copper pipe sat on top of the catalyst in the reactor, on which a line was marked).
- The reactor side was tapped until the copper pipe stopped dropping
- Another 20% of catalyst was added, and this procedure was repeated - tapping until the pipe stopped dropping.

The above was repeated until the desired amount of catalyst was filled. A final series of taps along the reactor/catalyst length were applied.

3.6 Pre-measurements of data

A number of pre-measurements of data were carried out prior to the experiment; for instance, the pump was calibrated to measure the flow rate. The physical properties (density) and transport properties (viscosity) of glycerol were determined. In addition, the porosity and permeability of the reactor bed were measured, as well as the particle size distribution. The method used for pre-measurements is described below.

3.6.1 Pump calibration and feed flow rate measurement

The pump was calibrated with water and model compound of glycerol in the range of pressure (up to 300 barg) and flow rates (up 4.71 Lh^{-1}) suitable for the experimental conditions. Ranges of pressures were calibrated in order to predict the feed flow rate entering the reactor at the desired pressure. Prior to start-up of the pump, the liquid was filled gradually in a tube of 1000 ml capacity. The stoke length (up to 15 mm) of the pump was adjusted. The rate of flow of a controlled-volume pump is a function of the cross-sectional area of the plunger or piston, or displacement of the diaphragm; the stroke length; and the stroking speed. The pumping action is created by a reciprocating piston, and controlled by suction and discharge check valves. The rate of flow was adjusted by changing the stroke length and/or the stroking speed. The outlet valve from the pump was checked to ensure that it was opened, and the pump was started by pressing the green start button. After ensuring that there is no leak, the pressure was slowly building up until the desired pressure was reached, and was maintained using a pressure regulator. An electronic timer was used to record the time versus a volume of flow delivered. The flow rate was calculated in ml/min by ratio the volume delivered: time, and was plotted against the stroke length setting at the study pressure. The calibration graphs are showed in appendix D.

3.6.2 Density and viscosity measurement of glycerol

An empty beaker (mass m1) was used, and a known volume of fluid (3ml) was measured and filled into the beaker using a syringe of 1ml capacity. The temperature of the fluid was recorded as well as the volume occupied (v) by the solution. The total mass of the fluid + beaker was measured as m_2. The density (ρ) of the fluid was determined as:

$$\rho = \frac{m_2 - m_1}{v} \quad (3.1)$$

A Rheometer (model AR 1000) equipped with an electronic control box (TA Instrument), was used to measure the viscosity of the crude and pure glycerol using a stress driven gravity flow. The rheometer-type AR contains an electronically controlled induction motor with an air bearing support for all the

rotating parts. The drive motor was equipped with a hallow spindle, with a detachable draw rod inserted through it. The draw rod has a screw-threaded section at the bottom, which allows the geometry to be securely attached. The measurement of angular displacement was done using an optical encoder device. Temperature control was achieved in the standard configuration via a Peltier plate system (aluminium plate was used as the flowing surface). The results are presented in appendix G.

3.6.3 Porosity and permeability of the bed measurement

Measurements of porosity of the catalyst bed for different particle size of the packing material were carried out. The porosity of the reactor bed was defined as the ratio of void volume (V_{bk}-V_{gr}) of the packing material to the total volume of the bed including void volume, given as a percentage. A beaker was weighed, and a dry sample of packing material was charged into the empty beaker and re-weighed (W1). The bulk volume (V_{bk}) occupied by the materials in the beaker was recorded. A known volume (V1) of solvent (water with density of 1g/ml) was used to saturate the materials by submersing it in the beaker. The weight of the submersed materials with solvent was measured as W_2. The grain volume was determined as;

$$V_{gr} = \frac{w_2 - w_1}{\rho_{solvent}} \qquad (3.2)$$

Thus, the porosity ε can be calculated from V_{bk} and V_{gr} using equation 3.3, where Vgr is the grain volume.

$$\varepsilon = 1 - \frac{V_{gr}}{V_{bk}} \qquad (3.3)$$

The presence of the packing material in the reactor creates resistance to the reactant flow. It is more difficult for the reactant to flow in a packed bed than in an open tube. Resistance to flow in a packed bed can be defined as permeability (P^o) in units of cm^2.

$$P^\circ = \frac{d_{50}^2 * \varepsilon^2}{180(1-\varepsilon)^2} \qquad (3.4)$$

Where d_{50} is the diameter of the particle, cm and ε is the porosity of the packed bed. The results for the porosity and permeability are shown in appendix H.

3.6.4 Distribution of the catalyst particle size

In order to study how the particle size of the catalyst affects the gasification process, a range of particle size were prepared by crushing in a pestle and mortar. The particle size distributions obtained were determined by passing through a range of classification sieves. All sieves were superposed in increasing order of their sieve size, starting from a lower up to the highest size of sieve (6000 μm). A serie of 9 sieves was used in this experiment. The crushing and/or grinding operation was aimed at producing particles of a size such that after the forming operation, pores of the desired size are formed. The crushed samples of catalyst were thrown into the higher sieve size. The sieve block was secured in order to insure stability during sieving. The results of the particle size distributions for Fe_2O_3-Cr_2O_3 and Fe_3O_4 samples are showed in appendix B.

3.7 Analytical and Characterisations Techniques

The product gas and condensate liquid product were analysed by a gas chromatography techniques in order to identify and evaluate the product composition and yield from the SCWG experiment. The fresh and used catalyst samples were characterised to determine its physico-chemical properties. The analytical methods for the products and characterisation techniques for the catalyst are described below.

3.7.1 Gas chromatography

3.7.1.1 Product gas analysis: GC-TCD

An external gas standard mixture (1% H_2, 1.01 % CO, 1% CH_4, 0.99% CO_2, 1% acetylene, ethylene, 1% ethane, 1.1% propane and 96 % N_2 as balance gas) was purchased from STG Gas Ltd, and was used to calibrate the GC (Refer to appendix I), and to determine the optimum chromatographic method for the gaseous products. Preliminary runs indicated that thermal-conductivity detector (TCD) has a low sensitivity as compared to flame-ionization detector (FID) when used to detect organic compounds /hydrocarbons in the sample gas (e.g. Ethane, ethene, propane). Therefore, the two detectors were connected in series in order to optimise analytical capability of the gas sample in a single run. This approach has provided precise analysis of the gas components (H_2, CO, CO_2, CH_4, C_2H_4, C_2H_6, C_3H_8) in a single run sample. The gas analysis was conducted with an Agilent Technologies GC 6890N series equipped with a FID and a TCD. During each experimental run, samples of the exit gas and aqueous condensate were taken periodically (first at 5 min subsequently every 15 min), with up to six samples of exit gas and condensates, taken in each run. Gas samples

were taken by gastight syringes from the gas sample outlet of the gas-liquid separator using a gas sampling bag or/and gas sampling bottle. A Restek Shincarbon ST column (micropacked 100/120 mesh, 2 meter long, 1mm I/D) was used to performed the gas separation. A packed inlet and 6 port pneumatic gas sample valve equipped with 2 ml loop was used to introduce the gas sample. Helium was used as carrier gas at a flow rate of 11.3 ml/min. The oven temperature was initially held for 8 min at 40°C, and then the temperature was increased at a rate of 50°C/min up to 250°C. The detector temperature was 250°C. A gas syringe of 2.5 ml capacity was used to introduce the gas sample into the GC system via 6-port valve. The chromatogram peaks of the gas products were identified by comparing the retention time of the sample peaks with the gas external standard. The concentration of each gas component in the sample ($C_{g,i}$) was extrapolated from the following equation (Refer to the abbreviations section for nomenclature).

$$C_{g,i} = \frac{A_s}{A_{g,i}} * C_S \qquad (3.5)$$

3.7.1.2 Liquid product analysis: GC-FID

A range of liquid standards for GC analysis such as ethanol (99 % purity), methanol (99% purity), allyl alcohol (99% purity), acetaldehyde (99% purity), formaldehyde (99% purity), propionaldehyde (97% purity), acrolein 98 % purity)and 2-propanone (98% purity) were purchased from Sigma Aldrich, UK. These standards were used to identify, calibrate and to establish the analytical method for the GC – FID. 1-propanol (99 % purity) was purchased from Sigma-Aldrich, and it was used as internal standard as described below. The analytical conditions and parameters of the GC-FID are shown in table 3.1.

Components in the liquid products were quantified from an internal standard (1-propanol). A concentration of 5 mg/ml of internal standard was prepared, and 500 µl was injected into the liquid samples prior to analysis. The correction factor (ratio of the areas of component liquid standard: areas of internal standard) was plotted against five standard concentrations for each liquid standard component in order to obtain a linear calibration curve with $R^2 > 0.996$; (refer to the calibrations curves in appendix J. The concentration of component in the liquid sample $C_{L,i}$ was determined using equation 3.6:

$$C_{L,i} = (\frac{A_{L,i}}{A_s} + Y) / slope \qquad (3.6)$$

It is essential to note that all the aldehydes present in the liquid condensate have poor chromophores, and therefore, direct ultraviolet (UV) detection was not plausible. The chromatographic method and conditions for gas and liquid samples are shown in table 3.1

Table 3.1. Summary of the GC conditions for gas and liquid analysis

Parameters	Range values or maximum	Set values for GC-TCD Gas analysis	Set values for GC-FID Liquid analysis
Carrier gas type	---	Helium	Helium
Carrier gas flow rate	10-60 ml min^{-1}	12 ml/min	1.5 ml min^{-1}
Reference gas type	---	Helium	Helium
Reference gas flow rate	15-60 ml min^{-1} at 22-50 pisg		
Makeup gas type	2-3 ml min^{-1} at	Helium	Helium
Makeup gas flow rate	packed column <10 pisg	2 ml/min	
Detector gas	H_2	N/A for TCD	30 ml min^{-1}
Sample loop volume	---	2 ml	Auto injection by using auto sampler
Sample size injected	1-10 µl	1 µl	0.2 µl
Split or split less	---	Split less	Split 1:10
Column	---	ShinCarbon ST: Micro packed column, ShinCarbon used for packing is a highly stable material. 1 mm ID, length 2 m	DB-Wax 7032 capillary column, 0.25 mm ID and 0.25 µm film thickness, 30 m length
Injector temperature	---	100°C	180°C
Oven temperature	300°C (max.)	Initial temp= 40°C, at the initial time = 0 min (hold for 8 min) Rate 1= 50°C/min up to 250°C	Initial oven temperature was 35 °C, held for 5 mins, then 10 °C/min up to 230°C
Detectors type		TCD and FID	FID (max. T=250°C)
Detectors temperature	200-300°C	hooked in series TCD (max T =250°C)	
Analysis time/run time	---	32 mins	36 mins

3.7.1.3 Determination of crude glycerol purity

The purity of crude glycerol was characterised together with its density and viscosity. Crude glycerol was obtained from Federal University of Ceará in Brazil with a primary feed from Olea vegetable. Its purity was determined by injecting a sample at different concentrations on the GC-FID using the calibration methods described in section 3.7.1. Experiments were performed using pure glycerol and crude glycerol at variable conditions. A known concentration of crude glycerol was prepared similarly as for the pure glycerol and as for standard calibration. 1ml in volume of this concentration was filtered using syringe filter with 0.22 µm pore size, and was filled into a vial of 2 ml capacity. The retention time of the standard glycerol was used to identify the retention time of the crude glycerol with a margin of ± 0.5 mins. The purity of the crude glycerol was determined using the calibration and linear graphs as shown in Fig.3.13.

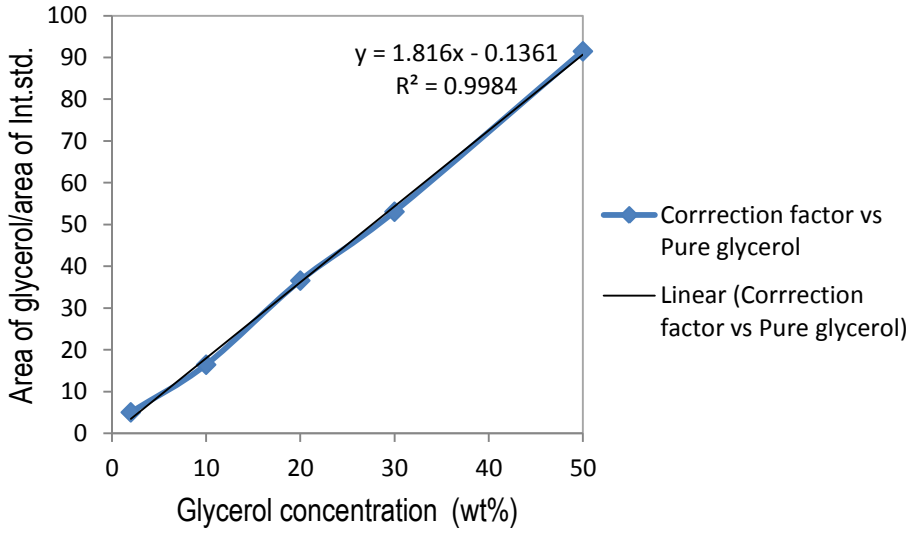

Fig.3.13. Pure glycerol calibration graph

In order to compare to a selected standard glycerol (pure glycerol) concentration, a similar concentration of crude glycerol (x'_2) with internal standard was prepared and ran to determine the peak areas. The peak areas of the glycerol in the solution was divided with the internal standard peak area to determine the correction factor (CF) on the y-axis (refer to appendix K). The actual concentration of crude glycerol (x_2) was extrapolated from the linear equation 3.7 as:

$$X_2 = \frac{CF + 0.1361}{1.816} \qquad (3.7)$$

The purity of the crude glycerol was then determined using the following equation:

$$\text{Purity of crude glycerol} = \frac{X_2 * 100\%}{0.98 * X_1} \qquad (3.8)$$

Where x_1 are a known concentration for standard glycerol with 98 purity that is similar to x'_2. The results of the crude glycerol purity are shown in table 4.1

3.7.2 Chemical oxygen demand (COD) analysis

Chemical oxygen demand (COD) was used as a measure of oxygen requirement of a sample that is susceptible to oxidation using strong chemical oxidant such as potassium dichromate, mercury II sulphate and potassium permanganate. COD was also used to measure the amount of organic compounds in water. These are indispensable measurements for understanding the pollution strength of water and waste liquid. The aim of this analysis was to evaluate the amount of organic compounds in the condensate liquid sample before and after CSCWG. Materials and experimental procedures for COD analysis are shown in appendix V.

Different concentrations of pure glycerol 0.2, 0.5, 1 and 2.5 wt% were prepared by dilution in deionised water. A pipette and syringe were used to measuring the sample amount for COD analysis. The COD of one sample was measured at the left, middle and right positions of the analytical tube. These three measurements were used to determine the average value of the COD reading and the relative standard deviation as shown in table 4.2 (Refer to section 4). The relative standard deviation was determined by running a series of three COD experiments with fresh sample of pure glycerol.

3.7.3 Catalyst characterisation

The characterisation of the catalyst was carried out to determine the physico-chemical properties and evaluate its performance; to examine catalytic activity/and deactivation. A series of characterisation techniques (XRD, XRF, ESEM, TGA, Chemisorptions and BET) were used to characterise the catalyst properties of a non-supported, heterogeneous**,** Fe_2O_3-Cr_2O_3 and natural magnetite (*Fe_3O_4*)**.**

3.7.3.1 XRD analysis

Powder XRD measurements were performed on all catalyst materials before (fresh catalyst) and after utilisation (used catalyst) in order to assess the crystalline, orientation of single crystals and phase identification of the materials. The principle of operation involved projection of light of a known spectral energy on the pellet of pigment kept at 90° to the light source and measurement of the intensity of the reflected light photo detectors. XRD analysis was carried out using a Bruker –AXS (Siemens) X-Ray Diffract meter (model D5005) with 2.2 kW sealed Cu Source equipped with a Scintillation Counter Detector, a general area detector employing the Bragg-Brentano geometry and the CuKa1 wavelength. A dry sample of the catalyst was crushed into powder in order to reduce the particle surface area for

better diffraction before XRD measurements. The powder catalyst was then loaded into the carrier plate and placed into the detector chamber.

The data were collected at scanning parameters of 15-50°; two-theta range with a step increment of 0.01° and the time for each step was 2s. The data were visualized and indexed using the Diffract plus XRD commander software. The value of the wavelength can be obtained from the formula E (eV) =1236/wavelength (nm) and the crystallite size could be determined using the Debye Scherrer method [**236**]. The results of the peak intensity for iron oxide-chromium oxide and magnetite are shown and discussed in section 4 (also, refer to appendix L).

3.7.3.2 ESEM-EDS analysis

Emission scanning electron microscopy (ESEM) (model 6650) was used to perform structural and chemical characterisation of the catalyst samples. The instrument was operated with a backscatter electron (BSE) detector. Characterisation was performed on the catalysts (fresh and used iron oxide) with a detection area of 10 mm^2, resolution of 5.9 keV to 133 keV]. This ESEM was equipped with 3 detectors:

- Secondary electron detector
- X-Ray detector for energy dispersive spectroscopy (EDS)
- Back scatter electron (BSE) detector

A silver plate was used to place the sample, which was put into the chamber tube for scanning. The SEM was operated with BSE detector at an accelerating voltage of 15 kV, and the scan was performed at different space magnification from 10 to 5000 x with a wavelength distance was of 10 μm. The vacuum pump was started and left for approximately 3 min. This was done to provide sufficient time for the vacuum pressure level to decrease to 1.3×10^{-5} mbar. Energy dispersive spectrometry (EDS) equipped with X-Ray detector was also performed to identify chemical elements and composition of the sample for a small area of interest on the sample. The ESEM-EDS results of the iron oxide and magnetite are showed and discussed in section 4 (also, refer to appendix M and N).

3.7.3.3 TGA analysis

TGA was performed on the catalyst to determine changes in weight loss as a function of temperature. This could help to determine the thermal stability, mass of impurities such as coke on the surface, oxidative stability of the catalyst used as well as the potential lifetime of the catalyst. The TGA experiment was carried out on a single furnace, model TGA701S4C (Heating temperature up to 1000°C) that improve temperature accuracy across the entire range. This instrument was operated

from a PC-controlled Windows -based operating software with compliance to 21 CFR-Part 11 for a closed analytical system. The technique was used to characterise iron oxide and magnetite respectively, which can exhibit weight loss or gain due to decomposition, oxidation or dehydration or other factors. The method was to heat the sample of the catalyst, and to determine the percent by mass of the sample. A sample of 2.106 g was measured and filled into the sample pan of 1 ml capacity, before it was placed into the TGA- furnace. Purge gas (N_2) was applied to remove corrosive off-gases. A small sample size (4mm o/d particles) was used, and the thermocouple was positioned to apply good thermal contact between the sample and the temperature sensors. Temperature of the sample was raised gradually (up to 600°C) at a heating rate of 10°C/min. The plot of weight (percentage) against temperature was obtained and is showed in section 4.4.2 (also, refer to appendix O).

3.7.3.4 BET analysis

The Brunauer-Emmett-Teller (BET) surface area analysis was used to determine the specific surface area (m^2/g) of sample materials (powders, solids and granules). This analysis was carried out on a Micromeritics instrument (Model ASAP2010) in order to investigate the catalyst properties such as the surface area, void volume, density of the solid material in the particle, pores volumes and pore size distribution. In theory, The BET method is based on adsorption of gas (N_2 at 77 K was used) on a surface of a sample and the amount of gas adsorbed at a given pressure allows the determination the surface area. N_2 adsorption isotherm was performed on sample until saturation pressure was reached and that pressure increases resulting from N_2 adsorption increases. The theory is based on the BET equations [**237**]. As follows:

$$P/n^a*(P°-P) = 1/n_{m*C} + (C-1)*P/n_m*C*P° \quad (3.9)$$

$$A_S\,(BET) = n_m*L*a_m \quad (3.10)$$

$$A_s\,(BET) = A_S\,(BET)/m \quad (3.11)$$

Where n^a is the amount adsorbed at the relative pressure P/P^o and n_m is the monolayer capacity, C is the gas concentration, A_s (BET) is the total and specific surface areas of the adsorbent (of mass m) and L is the Avogadro constant. It is expected that a higher surface area material is more likely to react faster, dissolve faster and adsorb more gas than a similar material with a lower surface area. Thus, BET analysis can help in providing a better understanding of the behaviour of the catalyst. A known amount (~0.25 g) of catalyst sample was measured and placed in the absorbing chamber, and heated slowly to 200°C for 10 h under vacuum (~50 m Torr). The sample (adsorbent) was then transferred to the adsorption unit, and the N_2 adsorption was measured at the boiling temperature of nitrogen [-195.79°C (77.36 K)]. The BET results are shown and discussed in section 4 (also, refer to appendix P).

3.7.3.5 Chemisorptions

In general during the catalytic supercritical water gasification (CSCWG) process, molecules of reactants inter-act (chemically and physically) with heterogeneous catalyst surface, and therefore, various reactions (hydrogenation, hydrocracking, reforming, polymerization and oxidation) and phenomena's such as catalyst cracking, gas adsorption and desorption on the surface of the catalyst could occur. In order to evaluate the extended impact of these phenomena, pulse chemisorptions analysis was carried out to determine catalyst properties such as the active metal surface area, percent metal dispersion and the average active particle size. Analysis was performed with a Micromeretics (AutoChem II 2920 model) series instrument that was able to perform pulse chemisorptions and temperature-programmed analysis. The instrument was equipped with a TCD detector; a furnace (rate from ambient to 1100°C), a diversion ports that allow trapping the condensates in the gas flowing from the sample before it reaches the TCD. Helium was used as carrier gas. The sample was prepared by measuring 1.04 g of the catalyst sample that was dispersed in a clean sample tube. Subsequently, the sample tube was placed into the furnace, and one thermocouple was placed into the sample tube and tightens into the furnace with a ferrule.

For the pulse chemisorptions analysis, a measured dose of reactant gas (50mLmin^{-1} of CO) was applied to the sample catalyst and the injected gas chemically reacts with each active sites. The pulse chemisorptions method was set to run with a reduction step so that Fe_2O_3 could be reduced to its metal form Fe and Cr_2O_3 to Cr as summarised on the following reduction reactions:

$$Fe_2O_3 + 3CO \rightarrow 2Fe + 3CO_2 \qquad (3.12)$$

$$Cr_2O_3 + 3CO \rightarrow 2Cr + 3CO_2 \qquad (3.13)$$

During CSCWG, heating-up organic material at high temperature (up to 600°C) will obviously produce char that could lead to carbon deposition on the catalyst surface; thus could also provide an environment for direct reduction of Fe_2O_3 to occur at the interface between iron oxide and solid carbon as shown in equation 3.14.

$$Fe_2O_3 + 3C \rightarrow 2Fe + 3CO \qquad (3.14)$$

In effect, Fe_2O_3 could be reduced to its metal form during CSCWG by either reacting with the reducing carbon (when char is formed) or CO (when gas product is formed). However, the formation of high concentration CO in the gas product will create a barrier for continuous contact between iron oxide and the reducing gas. Consequently, the reduction rate is likely to decrease as the reaction progresses. The results of chemisorptions are presented and discussed in section 4.

CHAPTER 4. PRELIMINARY RESULTS AND DISCUSSION

4.1 Introduction

This chapter presents and discusses the results of the catalyst characterisations, the purity of glycerol and the chemical oxygen demand before and after CSCWG. The objective is to provide scientific understanding of the catalyst behaviour in CSCWG processes, to evaluate the impact of glycerol purity and COD on the CSCWG process.

4.2 Determination of crude glycerol purity

As described in chapter 2, the purity of the crude glycerol was studied and the results are shown in table 4.1.

Table 4.1. The results of the purity of crude glycerol

Selected Concentration of pure glycerol (x_1)	Peak areas (Ax) of the pure glycerol	Prepared similar concentration of x_1 for crude glycerol, (x'_2)	Peak areas (As) of the crude glycerol	Internal standard	Actual Concentration of crude glycerol (x_2) $x_2 = \frac{CF + 0.1361}{1.816}$ Where CF= Ax/As	Purity of the crude glycerol= $\frac{x_2 * 100\%}{0.98 * x_1}$ (4.1)
		wt%			wt%	%
2	3230	2	1423	581	1.42	72.4
5	5250	5	4243	626	3.81	77.7
15	16933	15	12731	623	11.32	77.1

It has been mentioned in chapter 3 that crude glycerol was produced during the biodiesel production by transesterification process, and the primary feed was obtained from Olea vegetable production. Table 4.1 shows that the average purity of the crude glycerol was approximately 75 % glycerol, which is considerably lower as compared to the model compounds (98 % purity). This lower purity is due to inefficiencies during biodiesel separation of the crude glycerine, and lower reaction of the

transesterification probably attributed to the catalyst used or/and operating conditions. In effect, this low purity level of crude glycerol could significantly increase the purification cost, and therefore, the production cost of the biodiesel. The impurities were higher around 25 % contaminants such as soap, salt, methanol and water compare to model compound with less than 2% impurities. The high level of impurities could have a significant impact on the SCWG process. On the other hand, the presence of methanol was detected and quantified to be around 11 % of the crude glycerol studied (refer to appendix K), which confirmed that methanol was the alcohol of choice for the transesterification.

4.3 Chemical oxygen demand (COD) results

The COD measurement was carried out to determine the quantity of oxygen requirement to oxidize the organic matter in a liquid sample before and after SCWG reaction. This was performed under specific conditions of oxidizing agent, temperature, and time as described in section 3.7.2, and the results are presented in tables 4.2.

Table 4.2. COD analysis results;

a) COD of fresh sample of pure glycerol

Initial **c**oncentration of glycerol in the sample	Average COD-measurement	Percentage of organics in the sample	Relative standard deviation
wt%	mg/l	wt%	mg/l
0.2	1855	1.26	230
0.2	2085	1.42	156
0.5	5245	3.57	112
0.5	4985	3.39	260
1	13700	9.33	89
1	13525	9.21	175
2.5	>10000	>6.81	
2.5	>10000	>6.81	

b) COD of un-catalysed SCWG of pure glycerol

SCWG experimental conditions	Average COD-measurement	Percentage of organics in the sample	Relative standard deviation
	mg/l	wt%	mg/l
400°C, 250 barg, 27 s, feed of 15 wt% glycerol	>10001	>8.67	---
450°C, 250 barg 27 s, feed of 15 wt% glycerol	>100002	>8.67	---
500°C, 250 barg 27 s, feed of 15 wt% glycerol	8254	5.62	205
550°C, 250 barg, 27 s feed of 15 wt% glycerol	4395	3.81	15
550°C, 250 barg, 28 s, feed of 20 wt% glycerol	12870	11.16	125
550°C, 250 barg, 48 s, feed of 20 wt% glycerol	12620	10.95	155
550°C, 250 barg, 90 s, feed of 20 wt% glycerol	<85	<0.058	
500°C, 250 barg, 180 s, feed of 20 wt% glycerol	>10000	>8.67	

c) COD of CSCWG of pure glycerol over Fe_2O_3-Cr_2O_3.

SCWG experimental conditions	Average COD-measurement	Percentage of organics in the sample	Relative standard deviation
	mg/l	wt%	mg/l
500°C, 250 barg, WHSV=125 h^{-1}, 32.1 g, d_{50}=4mm feed of 30 wt% glycerol	>10000	>8.67	
500°C, 250 barg WHSV=125 h^{-1}, 32.1 g, d_{50}=4mm, feed of 20 wt% glycerol	12864	8.75	112
500°C, 250 barg WHSV=125 h^{-1}, 32.1 g, d_{50}=4mm, feed of 15 wt% glycerol	6845	4.66	88
500°C, 250 barg, WHSV=125 h^{-1}, 32.1 g, d_{50}=4mm, feed of 10 wt% glycerol	3563	2.42	97
500°C, 250 barg, WHSV=125 h^{-1}, 32.1 g, d_{50}=4mm, feed of 5 wt% glycerol	< 85	<0.057	
550°C, 250 barg, WHSV=125 h^{-1}, 32.1 g, d_{50}=4mm, feed of 2 wt% glycerol	< 38	<0.025	

d) COD of CSCWG of pure glycerol over Fe_2O_3-Cr_2O_3

SCWG experimental conditions	Average COD-measurement	Percentage of organics in the sample	Relative standard deviation
	mg/l	wt%	mg/l
500°C, 150 barg, 27 s, feed of 10 wt% glycerol	11500	9.97	60
500°C, 200 barg 27 s, feed of 10 wt% glycerol	11545	10.01	10
500°C, 250 barg 27 s, feed of 10 wt% glycerol	11645	10.10	50
500°C, 270 barg, 27 s feed of 10 wt% glycerol	7275	6.31	15

e) COD of CSCWG of pure glycerol over Fe_2O_3-Cr_2O_3

SCWG experimental conditions	Average COD-measurement	Percentage of organics in the sample	Relative standard deviation
	mg/l	wt%	mg/l
500°C, 270 barg, WHSV=125 h^{-1}, feed of 15 wt% glycerol, catalyst:10.1 g, d_{50}= 4 mm	2145	1.24	20
550°C, 250 barg WHSV=125 h^{-1}, feed of 15 wt% glycerol, catalyst:10.1 g, d_{50}= 4 mm	<30	<0.017	
450°C, 250 barg WHSV=125 h^{-1}, feed of 15 wt% glycerol, catalyst:5 g, d_{50}= 4 mm	8845	5.11	35
500°C, 250 barg, WHSV=125 h^{-1}, feed of 15 wt% glycerol, catalyst: 5 g, d_{50}= 4 mm	2880	1.66	110

f) COD of CSCWG of pure glycerol over Fe_2O_3-Cr_2O_3

SCWG experimental conditions	Average COD-measurement	Percentage of organics in the sample	Relative standard deviation
	mg/l	wt%	mg/l
500°C, 150 barg, WHSV=125 h^{-1}, 15 wt% glycerol, catalyst:10.1 g, d_{50}= 4 mm	11500	9.97	60
500°C, 200 barg WHSV=125 h^{-1}, 15 wt% glycerol, catalyst:10.1 g, d_{50}= 4 mm	11545	10.01	10
500°C, 250 barg WHSV=125 h^{-1}, 15 wt% glycerol, catalyst:10.1 g, d_{50}= 4 mm	11645	10.10	50
500°C, 270 barg, WHSV=125 h^{-1}, 15 wt% glycerol, catalyst:10.1 g, d_{50}= 4 mm	7275	6.31	15

g) COD of the liquid products from CSCWG of crude glycerol over Fe_3O_4

CSCWG experimental conditions	Average COD-measurement	Percentage of organics in the sample	Relative standard deviation
	mgL^{-1}	wt%	mgL^{-1}
550°C, 250 barg, **WHSV**=125 h^{-1}, feed of 15 wt% glycerol, catalyst:10.1 g, d_{50}= 4 mm	1315	0.89	27
500°C, 250 barg **WHSV**=125 h^{-1}, feed of 15 wt% glycerol, catalyst:10.1 g, d_{50}= 4 mm	1398	0.95	69
550°C, 250 barg, **WHSV**=125 h^{-1} feed of 15 wt% glycerol, catalyst:10.1 g, d_{50}= 4 mm	1092	0.74	55
550°C, 250 barg, $\mathbf{WHSV = 125\ h^{-1}}$, feed of 5 wt% glycerol, catalyst: 10.1 g, d_{50}= 4 mm	115	0.11	16

It can be seen that the results for the measurement of organic matter in the sample by COD test were significantly variable depending on the process conditions for SCWG such as the temperature; pressure feed concentration effect, residence time and catalyst loading effects. The maximum standard deviation per test was up to 260 mg/L COD, with accuracy as percent relative error of ± 1.7%.

The results reveal that the maximum glycerol concentration that can be directly measured from this method was 1 wt% glycerol (standard sample) for a maximum COD value of 14150 mg/l. Above 2.5 wt% glycerol, the COD value was higher than 10000 mg/l of the test tube used, and sample dilution was necessary in this case. At 0.2 wt% glycerol standard concentration, the COD was 1855 mg/l suggesting that the minimum glycerol concentration that could be meassured was well below 0.2 wt%. The results in table 4.2 reveal that change of pressure during CSCWG runs has negligible effect of the COD as the average COD readings were approximately 11500 mg/l for each sample, representing an average of 10 % organic in the sample. However, when the operating pressure was 270 barg and T= 500°C, the organic in the liquid sample drops about 6.3 %, which suggested an improved reactivity of the feed.

Residence time variation between 28 to 48 seconds also has no significant effect on the COD concentration. Average values were consistently around 12800 mg/l. However, temperature variation during CSCWG has demonstrated a significant impact on the COD measurement; for instance COD

readings were >10000 mg/l, for a liquid sample resulting from CSCWG at a temperature between 400-450°C, which demonstrated that a significant amount of organic compounds was presented in the sample at low temperature due to poor gasification. On the other hand, when process temperature was 550°C; the COD result was around 4395 mg/l, which indicated that many organic compounds were destroyed during CSCWG experiment. An initial glycerol feed concentration that was fed into the CSCWG system appears to have a considerable impact on the COD value. Average readings were 11645, 12745, >10000 for initial glycerol feed concentration in CSCWG of 10, 20 and 30% wt glycerol, respectively. This was due to polymerisation reactions at increasing feed concentration, which resulted into tar formation. It can be seen also that when magnetite catalyst was used for the CSCWG, the amount of COD were lower (average 1268 mg/l), representing less than 1% organic in the condensate liquid sample. This indicated that the rate of gasification was higher resulting to increase catalytic activity compared to the same conditions over iron oxide-chromium catalyst.

4.4 Catalyst characterisations

4.4.1 BET results

N_2 at 77 K adsorption isotherms for used and fresh samples are shown in Figs. 4.1 and 4.2. It can be noticed that increased pressure results in an increase N_2 adsorption confirming the fact that, the rate of absorption or desorption was temperature or/and pressure dependent (refer to appendix O). Also, the adsorption-desorption process was reversible up to a pressure of about 600 mmHg pressure. At the saturation pressure of 746 mmHg, the desorption branches decline abruptly for relative pressures between 600 to 700 mmHg, which manifests itself in the presence of more or less pronounced hysteresis shape. Summary of the BET report for iron oxide-chromium oxide and magnetite is shown in table 4.3.

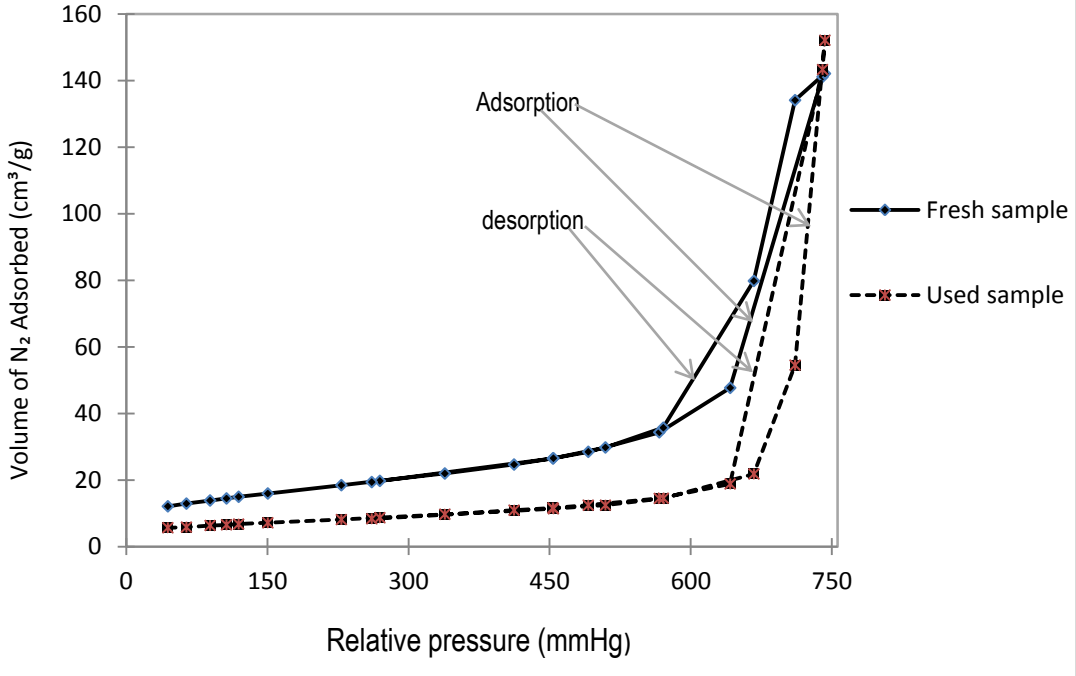

Fig 4.1. BET volume of N_2 adsorbed on Fe_2O_3-Cr_2O_3 versus relative pressure

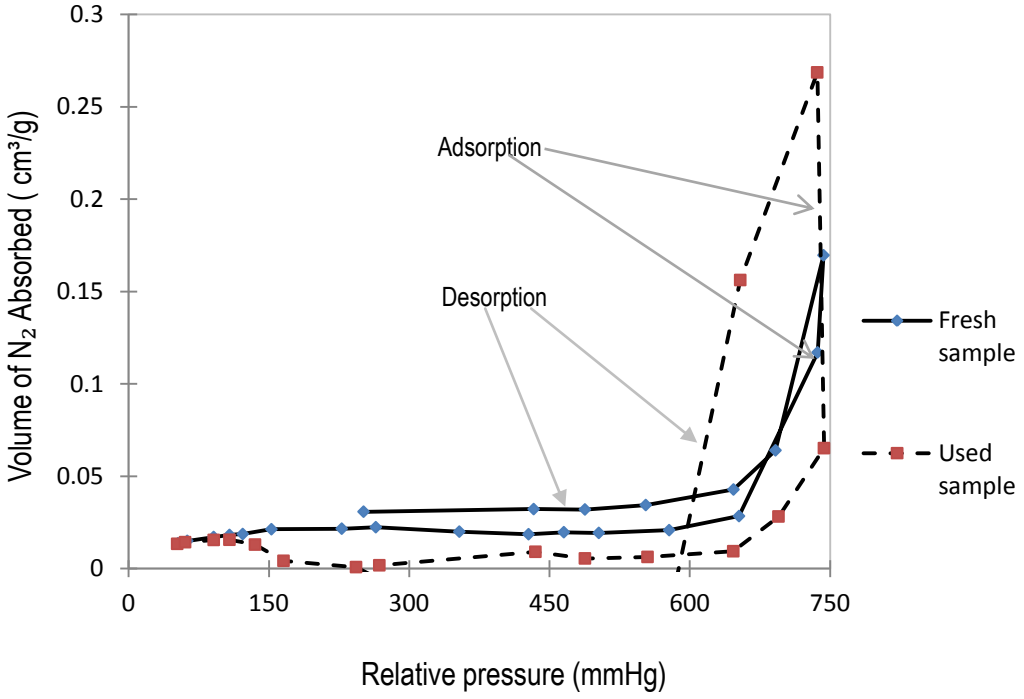

Fig 4.2. BET volume of N_2 adsorbed on *Fe_3O_4* versus relative pressure

Table 4.3. Summary of the BET report for iron oxide-chromium

	Unit	F1_Fresh_1	U1_Used_1 (172 h)	Fresh	Used (9 h)
Sample name		Iron oxide	Iron oxide	Magnetite	Magnetite
Sample weight	g	2.21	2.19	2.46	2.49
Sample particle size	µm O/D	4000	4000	150	150
Area					
BET Surface Area	m^2g^{-1}	58.11	25.83	0.0496	0.0356
Langmuir Surface Area	m^2g^{-1}	80.38	35.76	0.0665	0.0681
Micro pore Area	m^2g^{-1}	0.03	2.06	0.0645	0.0151
External Surface Area	m^2g^{-1}	58.08	23.77	0.0149	0.0507
Volume					
Single Point Adsorption micropore	cm^3g^{-1}	0.21	0.23	0.000701	0.000123
Micro pore volume	cm^3g^{-1}	0.00063	0.0007	0.000031	0.000012
Pore size					
Adsorption average pore size (4V/Å by BET)	Å	151.32Å	364.37Å	565.3034Å	138.5029Å

It can be seen in table 4.3 that BET surface area of the fresh Fe_2O_3-Cr_2O_3 was 58.1 m^2g^{-1}, and was reduced to 25.8 m^2g^{-1} in the used sample (172 h). This significant decrease may have resulted from sintering of metals and erosion under SCW conditions as evidenced by fragment deposition on the used sample (refer to Fig 4.6) after ESEM analysis. It has been suggested that surface area is one of the principal factors that contribute to govern the catalyst activity [**238**]. Thus, the significant reduction of the surface area has resulted in a reduction of catalyst activity as evidenced by lower yield of the product gas. It is suggested that sintering of the metals may have been promoted by exothermic reactions; for instance, coke reaction with SCW can form carbon monoxide and hydrogen or methanation reaction; these reactions produce heat, which may raise the temperature of the catalyst inside the bed and result into sintering. On the other hand, gas-solid reactions can play a positive and significant role for coke removal on the catalyst. In addition, a reduction of the BET surface area has contributed to lowering the adsorption abilities of the materials, which might be the main reason of the lower N_2 adsorption volume of the used sample as shown in Fig.4.2. For a fresh sample, BET surface area is higher, resulting in a high adsorption on the surface. These results are consistent with the

theory that states that " as material reacts with its surroundings via its surface, a higher surface area material is more likely to react faster, dissolve faster and adsorb more gas than a similar material with a lower surface area" [**239**]. In addition, BET surface area reduction was observed when fresh and used magnetite were analysed. Surface areas were reduced from 0.049 to 0.035 m^2g^{-1} for magnetite (d_{50} = 0.15 mm) for fresh and used sample (9 hrs on-stream), respectively. This was attributed also to the effect of SCW conditions, which may have resulted in metal erosion. No evidence of sintering was observed at this stage, probably due to reduce exposure on-stream of the used sample.

A significant increase in the micropore area from 0.03 to 2.06 m^2g^{-1} of the fresh and used iron oxide (172 h) may have resulted from the formation of new micropores at the surface of the catalyst. SCW has the power to act as a strong oxidant, therefore, could promote higher reactivity and diffusion rate of the gases on the catalyst, resulting in the formation of pores. On the other hand, the presence of impurities and coke on the surface of the catalyst would concomitantly reduce the micropore area. Although, nitrogen adsorption is a standard and most commonly used method of evaluating surface area and porosity [**238, 239**], the adsorption-desorption behaviour of nitrogen at 77 K in the pore size range explored in this experimental study is quite exceptional since the isotherms are reversible for pores of the size up to about 4 nm [**240, 241**]. This was probably due to char formation as evidenced by the presence of char in the chemical composition of the used sample after ESEM-EDS analysis (refer to appendix N). However, the micropore area was decreased from 0.064 to 0.015 m^2g^{-1} of the fresh and used magnetite (0.15 mm particle size). This is attributed to coke deposition on the catalyst surface, which may have resulted in covering of the active metals surface sites. Similarly, when a large particle of 1 mm magnetite was analysed, the micropore area increased significantly from 0.1016 to 0.6178 m^2g^{-1} for the fresh and used samples, respectively. This is attributed also to the formation of new micropore within the surface of the catalyst. The quantity and the size of the micropores area may have been influenced by the reaction conditions of the used magnetite. The slight increase in the total nanopore volume of the fresh and used samples of iron oxide (0.21 and 0.23 cm^3g^{-1}, respectively) and the minor change to the micropore volume (0.0006 and 0.007 cm^3g^{-1}, respectively) suggest that pore blockage and filling from coke deposition was negligible. Similarly, the micropore volume also increased with fresh and used magnetite (0.15 mm particle size) from 0.000061 to 0.000285 cm^3g^{-1}, respectively. This also is attributed to modification of the pore structure for the used sample due to the effect of SCW, as evidenced by the formation of a large volume of meso- and macropores.

It can be seen also that micropore volume decreased from 0.000013 to 0.000012 cm^3g^{-1} for the fresh and used magnetite of 1 mm particle size, respectively. This is also attributed to pore blockage by filling from coke deposition. The quantity of coke formation is dependent on the operating conditions such a feed concentration and temperature at which the catalyst was exposed.

4.4.2 TGA results

The TGA provides a graph of mass loss versus temperature over the range of 25 to 600°C as shown in Fig.4.3. The graph shows that temperature increases with the weight loss of the sample. This is because, high temperature can speed the physical change of the sample, leading to a solid-state transformation of the used sample. The loss of weight of the catalyst is possibly by crystallization, decomposition, reduction, evaporation of moisture. Fig 4.3 shows the profile of weight losses or gain of the iron oxide-chromium oxide and magnetite versus heating temperatures, respectively (A summary of the TGA results is shown in appendix O). It is expected that weight loss would increase as the temperature increases.

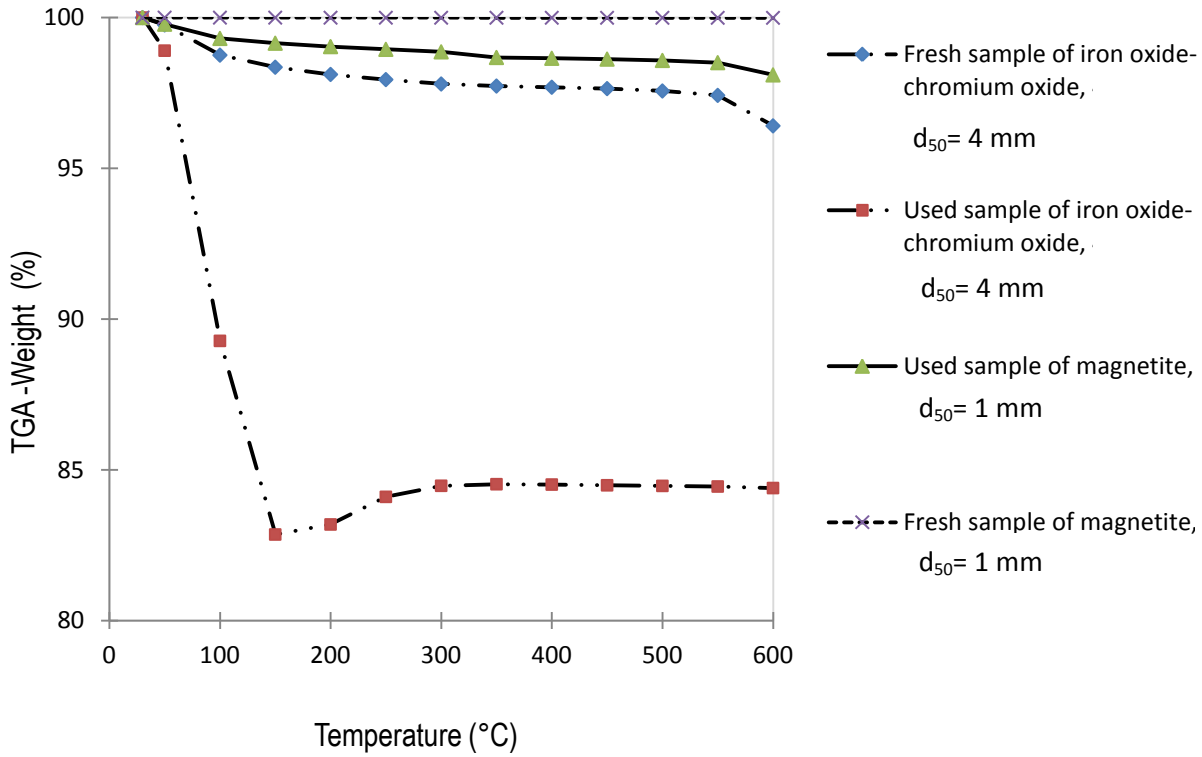

Fig 4.3. Temperature vs weight% of sample for iron oxide-chromium oxide and magnetite

Note: Used samples of iron oxide-chromium oxide and magnetite after 172 h and 9 h time-onstream, respectively.

It can be seen in Fig.4.3 that significant weight loss has occurred at a temperature around the boiling point of water for the used iron oxide-chromium (d_{50}=4 mm) as a result of moisture evaporation. Small decreases were observed for the other samples (fresh of iron oxide-chromium oxide, d_{50}= 4 mm and used magnetite, d_{50}= 1 mm). Likewise, when temperature increases above 150°C, the weight loss

of the iron oxide-chromium oxide (fresh and used sample) also increased, but at a slower rate (Fig.4.3). This was attributed to solid-state transformation of the sample due to change in the kinetic parameters. The weight lost of the iron oxide was probably due to crystallization, or/and decomposition or/and reduction. On the other hand, no sign of moisture evaporation was observed on the magnetite sample, which confirmed that the sample was well dried. At temperature above 150°C for fresh magnetite, the weight loss did not change, probably due to the high thermal resistance of the magnetite under conditions studied when compared to iron oxide-chromium oxide. However, for used magnetite and fresh iron oxide-chromium oxide, a small decrease was seen because of residual carbon.

4.4.3 XRD results

The XRD was performed on the catalysts for the identification of crystalline phases and the results for iron oxide-chromium oxide and magnetite are shown in Fig.4.4 and 4.5, respectively. It is suggested that variations of ratios between lines would indicate the order of imperfections along certain crystallographic directions or spontaneous orientation of the crystallites in the sample holder.

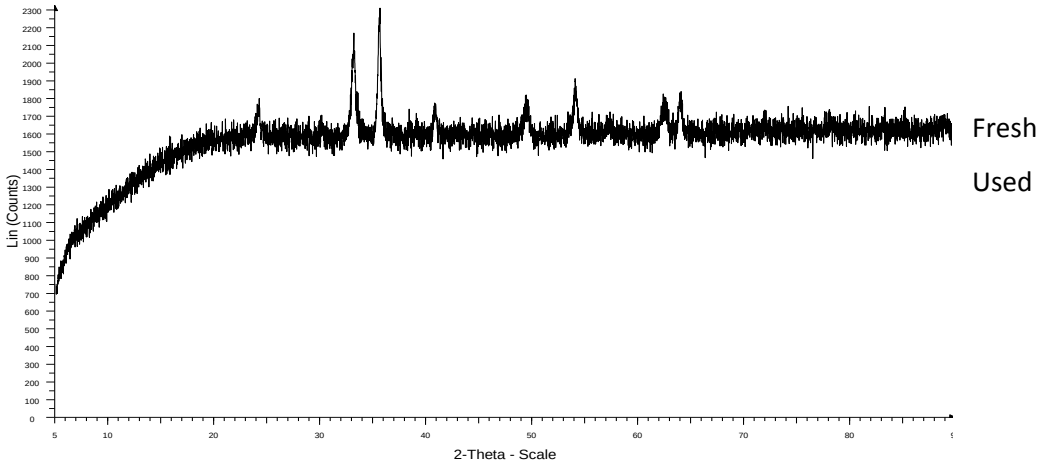

Fig. 4.4. XRD profile of the fresh and used (after 172 h on-stream) sample of iron-chromium oxide

Note: index of the peaks are given in appendix J

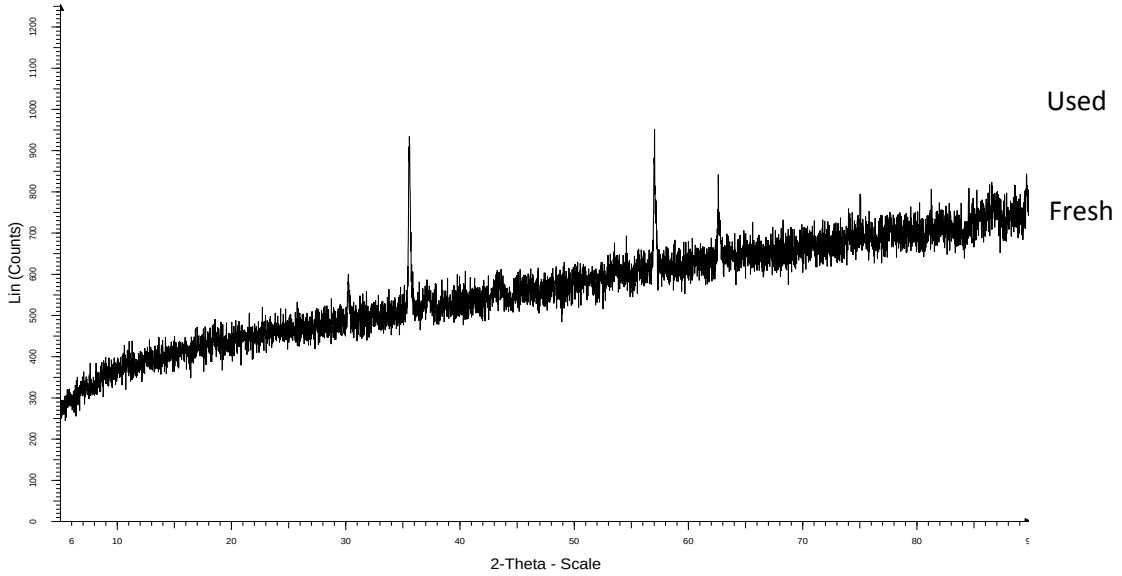

Fig. 4.5. XRD profile of the fresh and used (after 9 h on-stream) sample of magnetite

Note: index of the peaks are given in appendix J

It can be seen in Fig 4.4 and 4.5 that the X-ray diffraction patterns have consistent background variation, and the presence of the main diffraction peaks with variable intensity and height. This indicated a poor crystalline structure on both iron oxide and magnetite catalysts. The high level of background noise was due to iron content in the sample that fluoresces in the copper of X-radiation used. In addition, it can be seen that additional diffraction peaks had emerged at a different location when a used sample of iron oxide or magnetite were analysed, which suggested a possible phase change as a consequence of the SCW. However, due to the metal composition in the sample such as Cr and Fe, which have similar X-ray scattering, their discriminatation from Rietveld analysis were going to be impossible. Thus, Reitveld analysis was not performed. The aim of Rietveld analysis would have been to determine any phase composition change due to exposure in SCW conditions.

4.4.4 ESEM results

An ESEM was used to scan the surface of the sample catalysts with a finely focused electron beam to produce an image from the beam-specimen interactions detected by X-ray detector. This analysis was followed by the chemical composition determination in the sample by EDS at low vacuum mode, equipped with a backscattered detector. The ESEM results are shown on Fig.4.6 (a, b, c, d), and the associated EDS results are shown in appendix M.

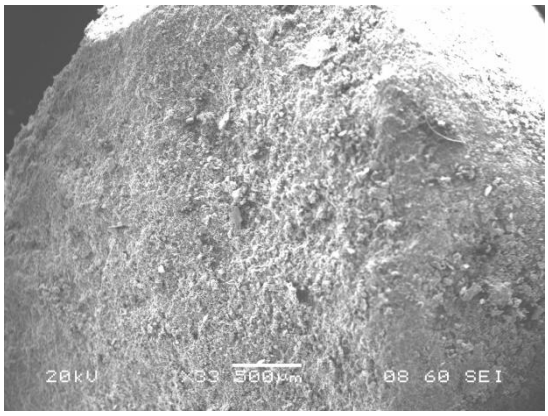

(a) Fresh sample of magnetite

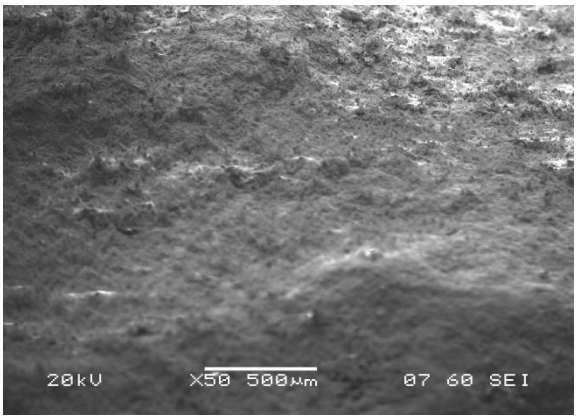

(b) Used (after 9 hrs on-stream) sample of Magnetite

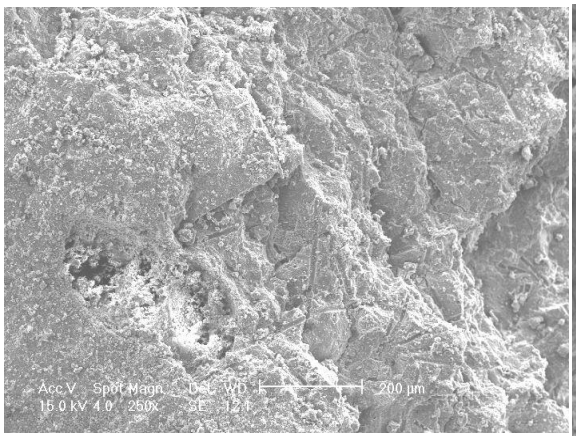

(c) Fresh sample of iron oxide-chromium oxide

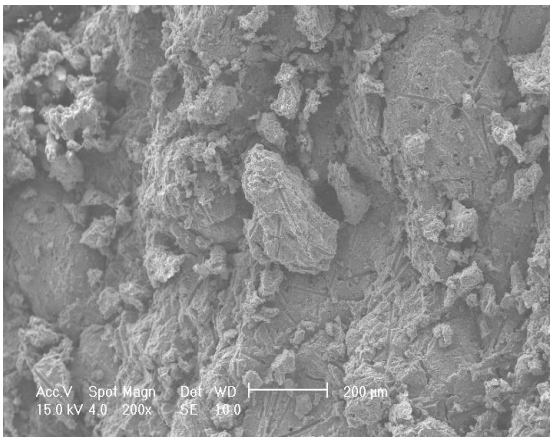

(d) Used (after 172 hrs on-stream) sample of iron oxide-chromium oxide

Figs. 4.6 a, b, c and show the ESEM images for structure analysis of Fe_2O_3+Cr_2O_3 catalyst for fresh and used samples.

Note that a and c images are at the same scale of 200 µm and c, d images for Fe_3O_4 are at the same scale of 500 µm.

It can be seen on Figs.4.6 (a, c) that the surface analysis of fresh samples of iron oxide and magnetite were different; score marks were presented on the fresh and used sample of iron oxide, which were

attributed to the method of preparation. A pellet of iron oxide was crushed to pass a 200 microns sieve, before mixing with 1% graphite, in order to obtain a final pellet. However, significant change on the structure was observed on the used iron oxide as evidenced by small fragment deposition on its surface. This was attributed to sintering of metals due to SCW conditions. On the other hand, no substantial change was observed on the used magnetite, probably because the sample was exposed on stream for a shorter time 9 h when compared to 172 h for used iron oxide. In addition, the surface of both catalyst samples exhibit some degree of porosity, which were confirmed by the range of their pore sizes by BET analysis (refer to table 4.4).

4.4.5 Chemisorptions

For the pulse chemisorptions analysis, a known dose of the adsorbing/reactant gas, CO (50 ml/min) was applied to the sample catalyst of 1.04 g iron oxide-chromium oxide (d_{50}=1-1.7mm) as measured, and the injected gas chemically reacts with the available active sites on the catalyst sample. The peak areas of the adsorbing gas (CO) as a function of time vs signal for fresh and used sample of Fe_2O_3-Cr_2O_3, respectively are shown in appendix Q. Other parameters such metal dispersion and surface area are presented in table 4.4.

Table 4.4. Result of CO adsorption on Fe_2O_3-Cr_2O_3 catalyst

Parameters	Values	Values
	Fresh of Fe_2O_3-Cr_2O_3	Used of Fe_2O_3-Cr_2O_3
Active Loop Volume at 110.5°C	0.38370 ml STP	0.38368 ml STP
Cumulative Volume	0.034475 mLg^{-1} STP	0.02726 mLg^{-1} STP
Metal Dispersion	12.83 (%)	9.7 (%)
Metallic Surface Area	0.6106 m^2g^{-1} sample	0.0475 m^2g^{-1} sample
Metallic Surface Area	0.8755 m^2g^{-1} metal	0.0681 m^2g^{-1} metal
Active Particle Diameter	785.9048 nm	11303.4177 nm

It can be seen that 0.34475 mLg^{-1} at STP was the cumulative volume of CO adsorbed on 1.04 g sample catalyst of Fe_2O_3-Cr_2O_3. This study has indicated that metal dispersion was lower; about 12.23 % possibly because of the large pore size of the iron particle or because of the low surface area. Metallic surface area, which represents the available surface area of absorbing material on the sample has a lower value about 0.8613 m^2g^{-1} metals and has reduced to 0.6008 m^2g^{-1} for fresh and used sample, respectively. This was attributed to large metal particles size that has resulted in poor metal

dispersion. It is suggested that high composition of Fe-Cr (91-9 % wt, respectively) content may have contributed to poor metal dispersion and smaller surface area, which have contributed to reduce the catalytic performance. Furthermore, the sample Fe-Cr catalyst was not supported; therefore, most of the active sites of the iron oxide could have been covered with chromium oxide, hence poor metal dispersion. As expected, the metal dispersion on the used sample was lower (0.0097 %) as compared to the fresh sample (0.1288 %). This is because used sample catalyst has undergone possible alteration of its properties or transformation under the effect of heat. The main causes of these alterations could be attributed to three factors: (i) Mechanical due to stress suffered by the catalyst particles such as crushing, attrition, abrasion or erosion. (ii) Chemical by poisoning because of chemisorptions of reaction products or by coke formation on the active sites. (iii)The formation of deposits on the catalyst, which may have occurred by simple deposition (fouling) such as char or catalytic or thermal transformation of feed components (coking). Furthermore, a mechanical or physical and/or chemical alteration could consequently lead to more or less fast loss in activity, which has led to reduce selectivity towards H_2 formation.

Table 4.4 also shows that metallic surface area of the used sample was also significantly lower (0.0475 m²/g sample) as compared to 0.6106 m²/g sample for the fresh sample. This reduction in metallic surface area is attributed to thermal deactivation through sintering or to loss of active material by vaporization or mechanical deactivation through attrition or/and erosion, which contribute to catalyst deactivation. At high temperatures, catalysts may suffer from the loss of the active phase through volatilization. Although, metal loss through direct volatilization is an insignificant route of the catalyst deactivation, it is more likely that, large amounts of catalytic materials (oxides of Fe-Cr) metal can be transported to either substrate where they can react or into the gas phase where they are lost in the effluent gas stream. Other possible cause of catalyst deactivation may be because of coke formation; the formation of coke is likely to cover or/and fill the active surface sites leading to decrease in the active surface area. (Refer to subsection 3.4.1 for BET surface area measurement).

4.5 Summary of the preliminary results

There is considerable interest for investigating the catalyst properties by various characterisation techniques including XRD, ESEM-EDS, BET and TGA. Each technique provides specific information on the catalyst such a surface structure (amorphous or crystalline), porosity, composition, thermal strength, metal dispersion and BET surface area. Catalyst characterisations provide opportunities to predict and maintain catalyst activity, as well as accelerating its regeneration and extending the lifetime. The X-ray diffraction patterns for Fe_2O_3-Cr_2O_3 and Fe_3O_4 indicated a poor crystalline structure. The surface analysis by ESEM exhibits some degree of porosity for both iron oxide and magnetite. Score marks

were observed on fresh and used sample of the Fe_2O_3-Cr_2O_3, which was attributed to the method of preparation. Sign of fragment deposition was observed on the used sample of Fe_2O_3-Cr_2O_3, which may have resulted from sintering of the metals. BET surface area was influenced by the size of particle and was reduced when it was exposing on stream. The level of reduction was also dependent to the time on-stream and the catalyst selection. BET surface area of the Fe_2O_3-Cr_2O_3 (d_{50} = 4 mm) was reduced from 58.11 m^2g^{-1} to 25.82 m^2g^{-1} for fresh and used sample (172 h), respectively and for the magnetite (0.15 mm particle size) from 0.049 to 0.035 m^2g^{-1} for fresh and used magnetite, respectively. The purity of glycerol was determined to be around 75 wt% of the crude glycerol, with about 11 wt% of methanol. COD test on the liquid sample of the CSCWG was found to be lowered (~11 wt %), depending on the operating conditions of the CSCWG process. No significant degradation due to thermal effect alone for the fresh sample of iron oxide-chromium oxide and magnetite catalysts were observed. These analyses have demonstrated the potential strength and suitability of Fe_2O_3-Cr_2O_3 and Fe_3O_4 for CSCWG process.

CHAPTER 5. SCWG OF PURE GLYCEROL

5.1. Introduction to SCWG of pure glycerol

The world continues to explore alternative source of energy and chemicals in order to reduce dependency on fossils fuels and to ensure the security of energy supply. Biodiesel production could play a significant role in this process. Large amounts of glycerol are obtained as waste products from biodiesel production, with about 1 kg of glycerol produced for every 10 kg of biodiesel. In 2009, the biodiesel product from the European Union and United States reached a massive share of 9 and 2.7 million tons respectively, from a total of 16 million tons worldwide. Hence, 1.6 million tons of glycerol were produced, therefore, as an obligatory by-product [**242**]. Glycerol can be used as an ingredient in various fields, for example, in the food industry as humectants, solvents and sweeteners, and also in the medical, pharmaceutical and cosmetic industries, but the demand for glycerol in these processes is limited. Raw glycerol obtained from biodiesel production contains impurities, and its purification process will, therefore, be costly due to the requirement of separation units, which require energy input. However, crude glycerol is widely available and cheap and offers new opportunities for chemistry and energy use [**243, 244**].

Catalytic supercritical water gasification (CSCWG) is a promising route in which organic matter can be efficiently decomposed to produce a mixture of gases and value-added liquid products depending on the process conditions [**245**]. The gas mixture can contain hydrogen, carbon monoxide, carbon dioxide, methane, ethylene, and the liquid fraction, can contain value added products (e.g. Acetaldehyde, acetic acid, acetone, methanol and ethanol); char can also be obtained [**246, 247**]. Water, above its critical point [≥221 barg, ≥374°C], has low relative permittivity (6 compared to 80 at ambient), high ionic product (10^{-11} as compared to 10^{-14} for subcritical) [**248**], which can be manipulated by changing pressure and temperature. These properties offer a number of advantages for organic material, such as enhanced capability to dissolve non-polar compounds, high reactivity and the ability to act as an acid/base catalyst.

The review of the literature has reported on the production of hydrogen and/or syngas by supercritical water processing of crude glycerol solutions [**249-253**]. The selectivity of the process toward either H_2 or syngas (H_2 + CO), or CH_4 can to some extent be steered by tuning the process conditions and by catalyst selection [**254, 255**]. A number of studies have demonstrated that hydrogen yield can be

promoted while reducing the formation of tars and char over the utilisation of heterogeneous catalysts such as Ru and Ni [**256, 257**] in a CSCWG process. However, the aim of this work is to combine the utilisation of an effective and low cost catalyst (iron oxide based) at temperatures up to 550°C, to attain conversion of glycerol to gaseous products. Under less severe conditions, conversion of glycerol to value added liquid products could be expected. This section reported on the effects of operating conditions (temperature, pressure, feed concentration, WHSV and time online) and the effects of catalyst parameters (loading and particle size) on the yields of product gas and condensate liquid products. This section also aims to establish the best operating conditions for processing glycerol using SCW for the production of hydrogen and a desired mixture of H_2: CO (2:1 ratio) that is suitable as feedstock for FTS process.

5.2 Preliminary Considerations

Before studying the CSCWG of pure glycerol, a series of experiments were carried out to assess the non-catalytic processing of glycerol in SCW under the influence of temperature and the reproducibility of the non-CSCWG within the experimental errors margin. These experiments were performed as a foundation in order to compare the impact of non-catalytic and the catalytic on the SCWG process.

In the process of non-CSCWG processing, glycerol under the influence of temperature decomposes to produce hydrogen, carbon dioxide and water vapour according to the equation 5.1, which means that the WGS reaction consumed much of the CO to produce CO_2. It can be noted that the overall chemical reaction represented in equation 5.1 does not account for char and hydrocarbons formation, and that the decomposition takes place in the preheating unit and in the flow reactor where SCW reforming reaction are occuring. However, it is expected that char and volatile hydrocarbons would formed a part of the decomposition products from the reaction during the experiments.

$$C_3H_8O_3 + 4H_2O \rightarrow 7H_2 + 3CO_2 + H_2O \qquad (5.1)$$

5.2.1 Ascertain experimental errors on the non-catalytic SCWG of pure glycerol

The experimental errors for the non-CSCWG of pure glycerol were evaluated by running three experiments at the same conditions as shown in table 5.1. Gas samples were collected as described in the experimental section 3.4 (after 5 min feed injection and subsequently every 15 min). All gas samples were analysed as also described in section 3.7. The experimental conditions and the cumulative value of the gas composition over time and its margin of error are shown. The actual

experimental error margin was evaluated by calculating the errors produced in the gas composition from repeating an experiment several times (three times minimum) on different days. The maximum error margins obtained were up to ±10.8 of the gas composition.

Table 5.1. Operating conditions and results for the ascertains experimental errors for the *Non-CSCWG of pure glycerol, feed concentration = 15 wt% of pure glycerol, pressure=250 barg, temperature=550°C, Flow rate =65 ml/min, τ = 27 s, no catalyst, small reactor.*

Experiment number	Run_E75	Run_E76	Run_E77	Average value after 3 runs	Relative error margin (mole %)
Cumulative gas composition (mole %)					
H_2	24.49	25.43	24.98	24.97	± *0.48*
CO	9.82	6.12	5.77	7.24	± *2.58*
CO_2	8.20	9.04	6.23	7.83	± *1.21*
CH_4	5.61	10.09	24.18	13.29	±*10.8*
C_2H_4	51.85	48.78	38.81	46.48	±*7.67*
Syngas	34.31	31.55	30.75	32.21	±*3.06*
Products gas yield (wt %)	83.5	80.64	89.42	84.52	± *4.99*
Char yield (wt %)	0.49	0.58	0.31	0.46	± *0.14*
Glycerol conversion (%)	73.30	67.39	78.61	73.10	±*11.22*

It can be seen in table 5.1 that the maximum error margin for the gas composition was observed for the hydrocarbons; CH_4 and C_2H_4, ±10.8 and ±7.6 mole% errors, respectively. This is attributed to poor thermal cracking of hydrocarbons, which may be due to feed concentration range and the absence of catalyst. The high yield of hydrocarbons and the presence of unconverted glycerol in the liquid sample

are evidence of incomplete conversion of the feed. This indicated that a catalyst is needed in order to increase reaction rate enhanced gas yields with better yield to hydrogen, and to promote catalytic cracking at the reported conditions. However, the catalytic effect of the reactor wall (made of 316L-SS) cannot be disregarded, as evidenced by high rate of product gas (~84 wt %). The results have demonstrated that hydrocarbon formations were the prominent gas products, which cannot be neglected as initially assumed (refer to equation 5.1). Light hydrocarbons formed part of the decomposition products of the glycerol in SCW.

5.2.2 **Effect of temperature on the non-catalytic SCWG of pure glycerol**

The aim was to assess the influence of gasification temperature on product gas composition and yield. In order to determine the conversion of glycerol at the reported conditions (15 wt% glycerol, 250 barg, residence time =27 s), four different heating temperatures (400, 450, 500, 550°C) were performed in the small reactor after preheating at 500°C. These conditions were chosen based on the maximum operation conditions of the rig, the lowest residence that was possible to deliver at the chosen feed concentration, and a moderate concentration that is less likely to complicate the reaction rate due to polymerisation. After reaction, the products stream was cooled to about 30°C using mains water. Gas and liquid samples were each collected after 5 min and subsequently every 15 min at pressure between 40-60 barg. Analysis of the samples showed the presence of a fraction of unconverted glycerol in the liquid stream, and its quantity was dependent on the reaction temperature. The results are shown in Figs.5.1 and 5.2.

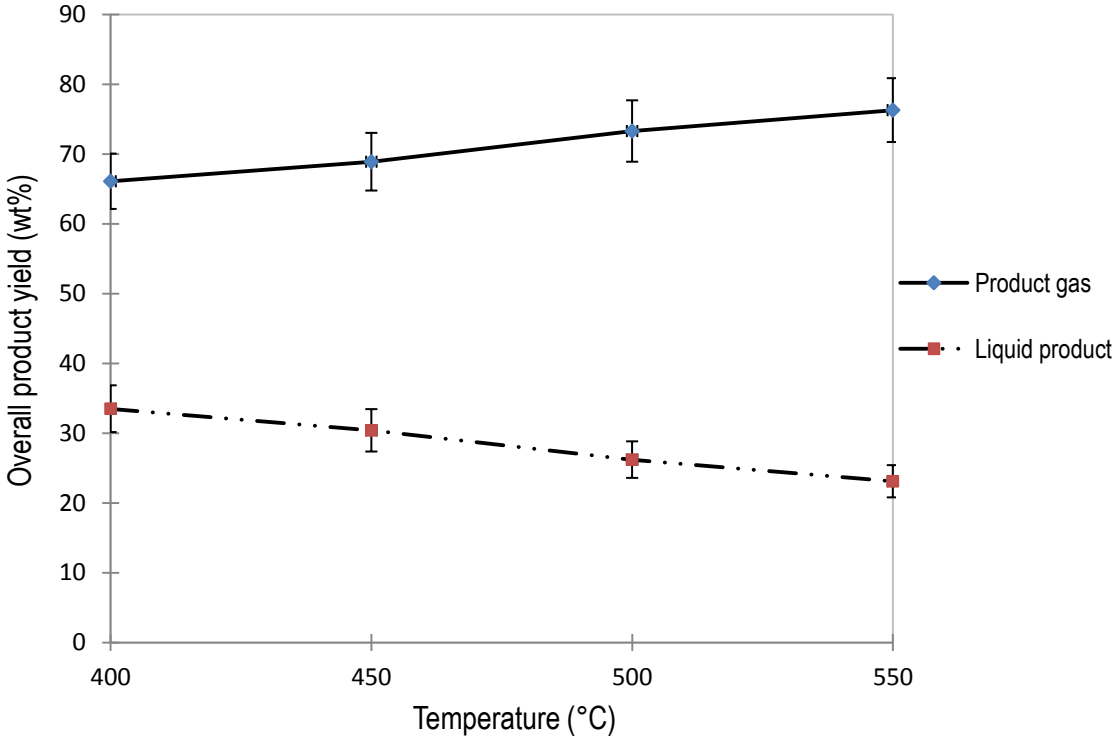

Fig.5.1. Gas and liquid product yields for non-catalytic SCWG of 15 wt% glycerol.
Small reactor, P=250 barg at F=65ml/min, τ = 27 s

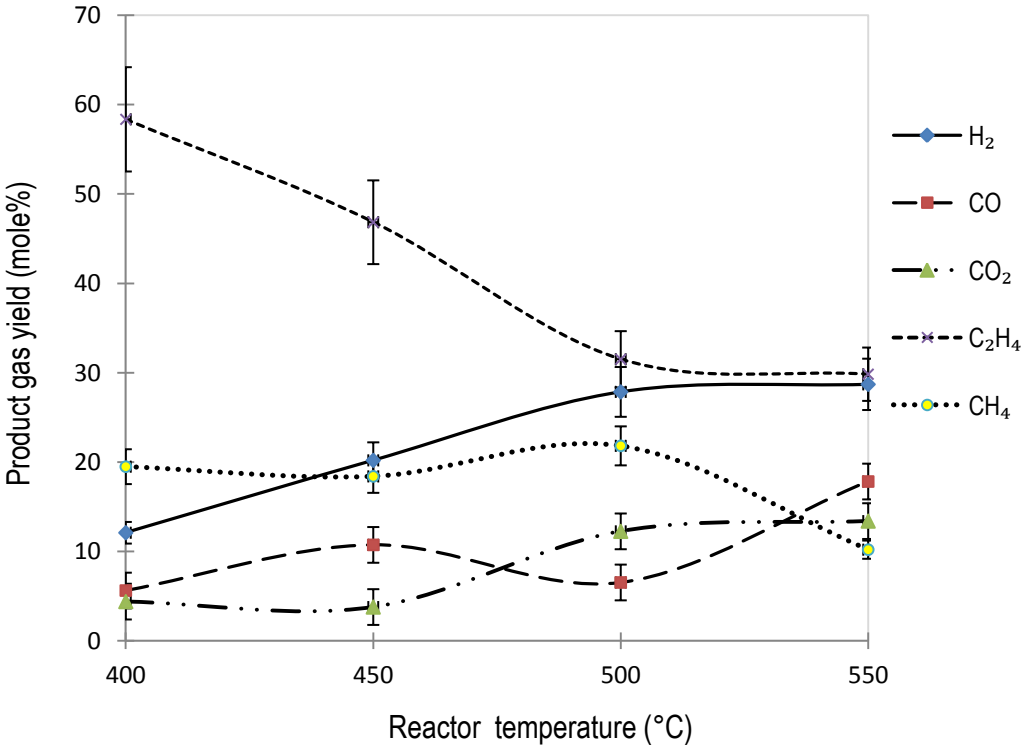

Fig.5.2: Gaseous products identified from the non-catalytic SCWG of 15 wt% glycerol.
Small reactor, P=250 barg at F=65ml/min, τ = 27 s

As expected, temperature has an influence on the product gas yield and composition. The overall gas product increased with temperature from 67 to 76 wt% at 400 to 550°C, respectively (Fig. 5.1). This is attributed to improving thermal effects, which contributed to the degradation of glycerol into gaseous products. The low value of COD analysis of the liquid sample is evidence of decomposition and less organic in the sample (4395 mg/l at 550°C compare to 8254 at 500°C). The amount of organic compounds in the liquid sample decreased from 5.6 to 3.8 wt%, with increased temperature (refer to table 4.7-chapter 4). The formation of a mixture of gases: H_2, CO, CO_2, CH_4 and C_2H_4 (refer to Fig.4.2) resulted from the variety of reactions that occur in this process; e.g. WGS, methanation and hydrolysis. It can be seen that when the temperature increased from 400 to 550°C, the H_2 and CO_2 yield increased from 13 to 28 mole% and 4 to 14 mole%, respectively. The CO yield increased from 6 to 14 mole% over the same temperature range. This would imply that besides the WGS reaction, other reactions such as char reforming ($C+H_2O \rightarrow CO+H_2$), or/and hydrocarbon cracking at high temperature, may be contributing to the increasing CO and H_2 yields.

CH_4 yield is 19 mole% at 400°C, but declines to 10 mole% at 550°C. This indicated that CH_4 formation was favoured at a lower temperature, while high temperature can promote methane reforming in SCW conditions. Similarly, ethylene yield declines from 58 to 31 mole%, which would have resulted from cracking under increasing temperature. The catalytic effect of the stainless steel reactor should, however, not be disregarded [**258**].

5.3 CSCWG of pure glycerol over Fe_2O_3-Cr_2O_3 Catalyst

Section 5.2.2 has demonstrated that non-CSCWG of pure glycerol under 550°C can be accomplished at a reduced gasification rate (up to 89 wt% product gas), accompanied by lower organic compounds (<3.8 wt%) in the liquid product as evidenced by the COD analysis (4395 mgL^{-1}). In comparison, a series of tests were undertaken using an Fe_2O_3-Cr_2O_3 catalyst as described in section 3.2. Initially, a series of experiments were performed to evaluate the stability of the catalyst in the reactor bed. A total amount of 32.1 g of Fe_2O_3-Cr_2O_3 catalyst (d_{50}= 4 mm) was packed in-house in the gasifier bed to fill the full reactor bed (refer to chapter 3). The integrity of the packing was validated by assessing the catalyst stability as described in section 5.3.1, which resulted in an initial period of instability followed by relative stability. This latest indicated a relative uniformity of the packing at this stage. Each experiment was carried out in the same way as described in sections 3.4 and 3.5. All gas samples were analysed according to the method described in section 3.7 to assess any variation of the product gas yield.

5.3.1 **Assessment of the catalyst stability**

Preliminary experiments were developed to assess the stability of the catalyst, the experimental conditions and the analytical procedure by running five experiments at the same conditions. During this work, glycerol conversion and the composition of the gas products were monitored for extended periods, in order to determine changes in the activity of the catalyst and product selectivity. In general, the catalyst had an initial period in which significant changes in gas composition were observed (runs 1 to 4), but reached steady-state and showed stable activity after 5 runs of average 2 hours each (runs 5, 6, 7 and 9) as shown in Fig 5.3. This relative stability is attributed to the completion of the metal oxide reduction phase or/and pre-treatment by removal of impurities on the catalyst that contributed to expose the active sites of the catalyst, and therefore favoured high diffusion of reactants.

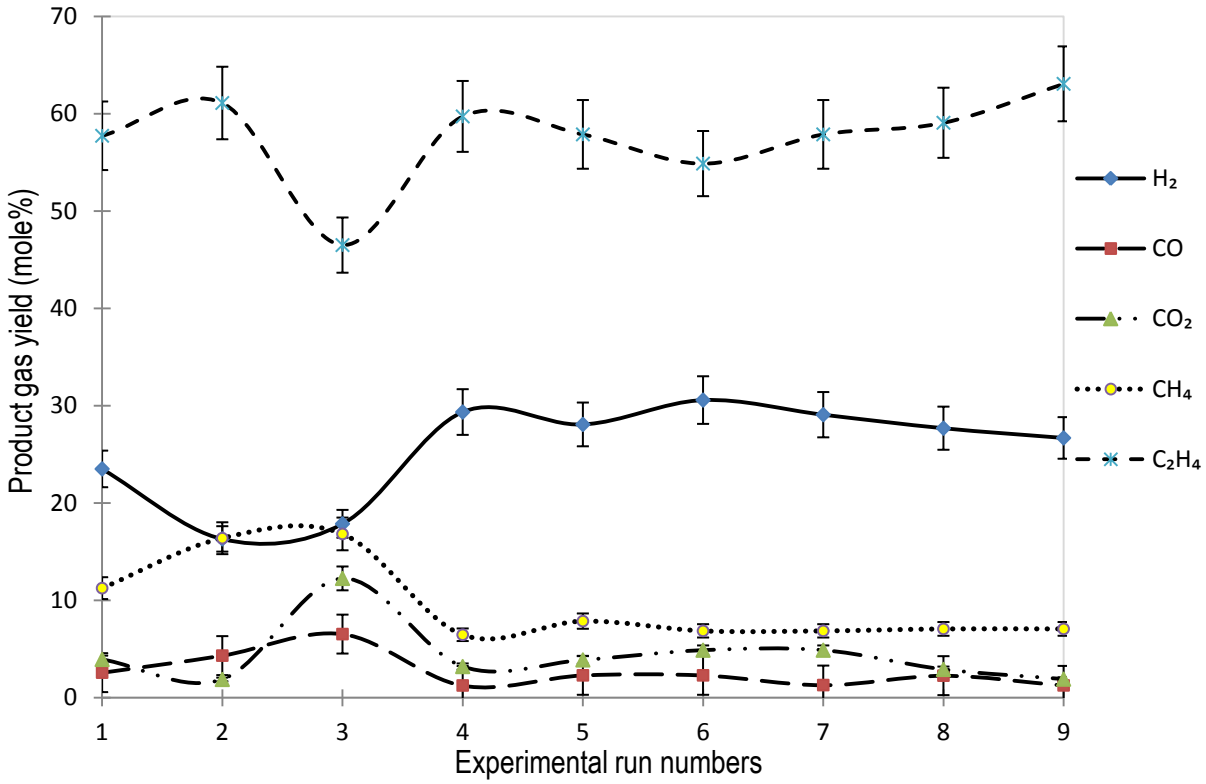

Fig.5.3. Catalyst stability assessment;

Small reactor, 20 wt% glycerol, 500°C and 250 barg, WHSV=125 h^{-1}, Fe_2O_3-Cr_2O_3 (d_{50}= 4mm), 32.1g

It can be observed in Fig.5.3 that the yield of the individual gas component was relatively constant from run 5 to 9, which indicated that the activity of the catalyst was relatively stable.

CSCWG of glycerol was carried out to study the effects of process parameters on liquid, gas and char yields, as well as the product gas composition and total gas production. The main products of the CSCWG of pure glycerol over [85 wt% Fe_2O_3 + 15 wt% Cr_2O_3] catalyst were identified as a mixture of hydrogen, carbon monoxide, carbon dioxide, methane, ethylene methanol, ethanol and allyl alcohols, formaldehyde, acetaldehyde, propionaldehyde, allyl aldehyde, valeryaldehyde and char as identified in the product gas and liquid samples. This is similar to previous studies (pressure up to 300 barg and Temperature up to 550°C) that have indicated that glycerol can decompose into carbon monoxide, carbon dioxide, methane, ethylene, acetaldehyde, acetic acid, acetone, methanol, acrolein, ethanol, water and char [**259, 260, 261**] over Ru/ZrO_2, Ru/Al_2O_3 and Ni/Al_2O_3 catalysts, respectively. As high as 98 % glycerol conversion was achieved at temperature up to 500°C.

5.3.2 **Ascertain of experimental errors**

Following the catalyst stability experiments, which has showed a relative stability for up to 9 h of operation, the experimental errors for the CSCWG of pure glycerol over Fe_2O_3-Cr_2O_3 catalyst were evaluated by running 3 experiments at the same conditions. Gas samples were collected in the same way as described in the section 3 (after 5 min feed injection and subsequently every 15 min). The experimental conditions and the cumulative value of the gas composition over run time and its margin of error are shown in table 5.2. The relative experimental error margin was evaluated by calculating the errors produced in the gas composition from repeating an experiment several times (3 times minimum) on different days. The maximum error margins obtained were up to ±7.1 of the gas composition.

Table 5.2. Operating conditions and results for the ascertain experimental errors for the CSCWG of pure glycerol over Fe_2O_3-Cr_2O_3*: Feed concentration = 5 wt% of pure glycerol, pressure=250 barg, temperature=550°C, Flow rate =65 ml/min, WHSV= 390 h^{-1}, catalyst loading=10.2 g, d_{50} =3.5 mm cylinder with 4 mm diameter, small reactor*

Experiment number	Run_E82	Run_E83	Run_E84	Average value after 3 runs	Relative error
Cumulative gas composition (mole %)					mole%
H_2	38.07	35.12	30.93	34.70	± *3.37*
CO	4.81	4.87	3.51	4.39	± *0.88*
CO_2	4.47	4.77	5.16	4.8	± *0.36*
CH_4	29.79	35.72	43.31	36.27	±*7.1*
C_2H_4	22.82	19.5	17.07	19.79	±*3.02*
Syngas	42.88	39.99	34.44	39.09	*4.25*
Products gas yield (wt %)	78.76	92.76	88.19	86.57	± *6.19*
Liquid products yield (wt %)	20.06	6.84	11.15	13.03	± *7.03*
Char yield (wt %)	0.64	0.21	0.35	0.41	± *0.19*
Glycerol conversion (%)	96.9	96.39	98.61	97.30	±*1.31*

It can be seen in table 5.2 that CH_4 yield showed the maximum error margin for the gas composition (±7.1). Without any doubt, the results indicated the use of Fe_2O_3-Cr_2O_3 had a positive influence on the gasification chemistry by increasing the overall product yield with high selectivity toward hydrogen compared to non-CSCWG process (24-26 mole% H_2, 80-83 wt% product gas). In

addition, low yield of hydrocarbons in the liquid products is evidence of catalytic cracking. As expected, evidence of char formation was observed on the catalyst after ESEM-EDS analysis; Carbon value in the fresh sample increased from 4.57 to 7.19 wt%, hence a cumulative of 2.62 wt% (refer to appendix N). In addition, the presence of dark colour on the reactor wall was observed also. The low margin error of the products is attributed to a combination of improved operating conditions and the presence of the catalyst. The low margin error provides an indication of the reliability of the experimental results.

5.3.3 **Effect of operating conditions on gas products for CSCWG of pure glycerol**

In order to determine the effect of operating conditions on the product gas yields for the CSCWG of pure glycerol over Fe_2O_3-Cr_2O_3, a series of experiments were performed. The effect of WHSV, pressure, temperature, feed concentration and online time were studied each by varying one parameter while keeping the others constant. Each experiment was carried out in a similar way as described in section 5.2.1. The product gas was analysed as described in section 3.7, and the results are shown in Figs.5.4, 5.5, 5.6, 5.7, 5.8 and 5.9.

5.3.3.1 **Weight hourly space velocity (WHSV)**

The effect of WHSV was studied by varying this parameter between 19 to 125 h^{-1}, and results are shown in Figs.5.4 and 5.5. The product gas analysis at the reported conditions shows that the main products were H_2, CO, CO_2, CH_4, and C_2H_4. The effect of WHSV appears to increase the selectivity toward H_2 and CO yields as shown in Fig.5.4. However, the overall gas product did not increase considerably, which suggested that the gasification could be less dependent on WHSV. Note that Fig.5.4 has a log y-axis for clarity.

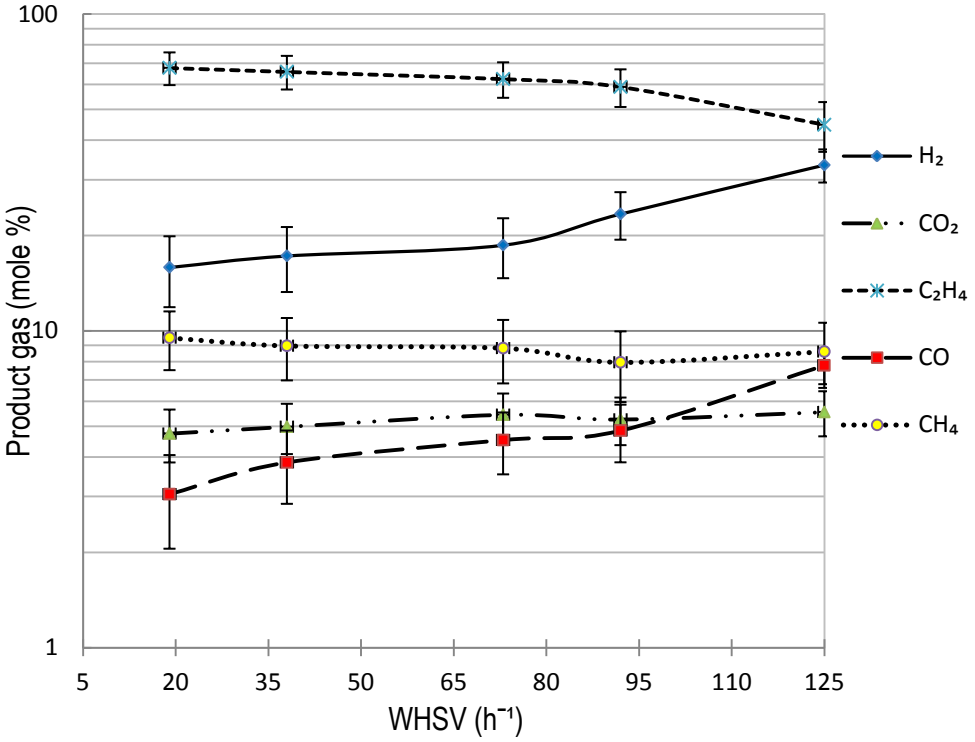

Fig.5.4. Effect of WHSV on CSCWG of 20 wt% glycerol

Small reactor, T=500°C and P=250 barg.

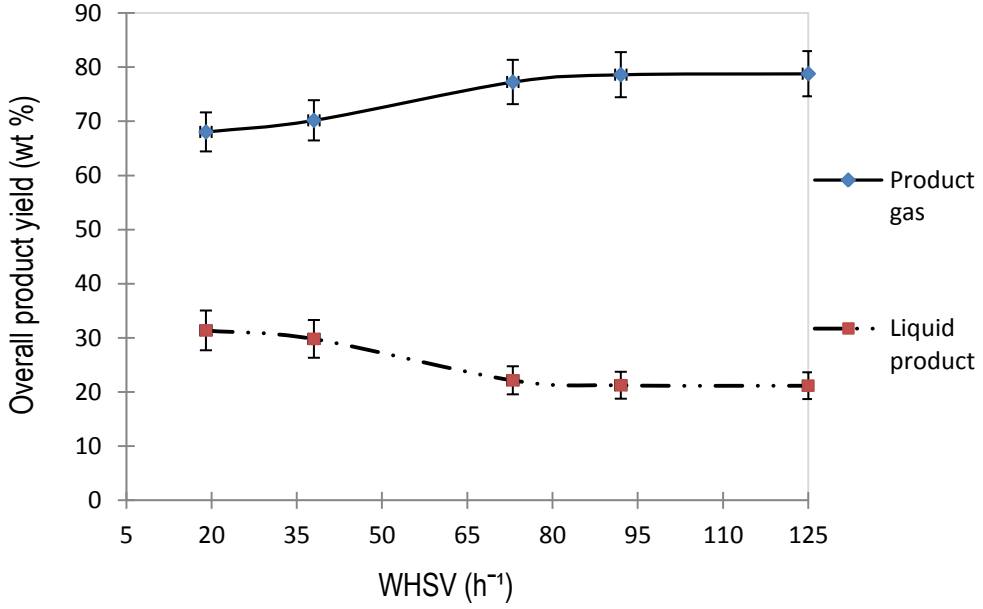

Fig.5.5. Effect of WHSV on CSCWG of 20 wt% glycerol

Small reactor, T=500°C and P=250 barg. Note gas and liquid yields do not equal to 100 % as char formed part of the overall product

5.3.3.2 System pressure

The effect of pressure was studied between 170 to 270 barg (below and above the critical pressure of water) and was found to have a small effect on the gas composition (H_2, CO, CO_2, CH_4, C_2H_4) and yield in the subcritical region (<221 barg), except for H_2 and C_2H_4 as shown on Fig.5.6. A positive pressure effect was noticeable in the supercritical region, which resulted in the increasing yields of H_2, CO and CO_2 coupled with a slight decrease in the hydrocarbons.

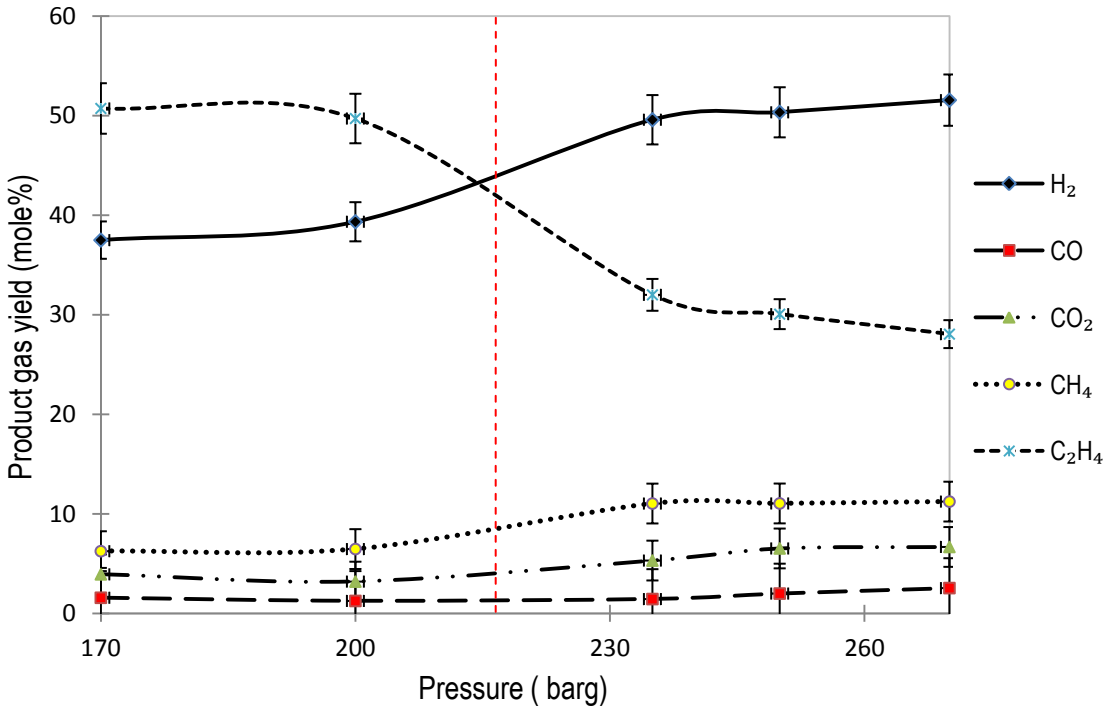

Fig.5.6. Effect of pressure on gas product yield for 10 wt% glycerol

Small reactor, 500°C, 250 barg, WHSV=125 h^{-1}

Vertical dotted red line indicates supercritical conditions at 221 barg

At subcritical conditions, H_2 yield increases with pressure from 37 to 52 mole %, while CO yield remains relatively constant at 2 mole %. The increases in H_2 and CO_2 yields with increasing pressure are attributed to the promotion of the WGS reaction. However, unidentified side reactions could occur also, as evidenced by the increase of CO yield in the supercritical region, which became noticeable under the influence of high pressure. The ionic product of water increases with increasing pressure, therefore, the hydrolysis reaction that plays a significant role in CSCWG also increases. CO_2 yield increases from 4 to 7 mole % when the pressure crossed the supercritical water region, which further indicates that the WGS reaction is favoured, an observation similar to other research findings [**264**]. The process can be operated at an optimal pressure to enhance the gas selectivity in order to either maximise H_2, CH_4 or syngas yields.

Methane yield was relatively low (~ 6 mole %) in subcritical conditions, but it increased slowly to 11 mole % in the critical regions, whereas ethylene yield was 51 mole % at low pressure (170 barg) and decreases sharply to 28 mole % at 270 barg, which may indicate its reformation under supercritical water conditions. It has been reported that using a suitable metal based catalyst and moderate temperature (<500°C) and pressure (>71 barg), ethylene can be reformed into ethanol [**265, 266, 267**] as shown in equation (5.2). Evidence of increasing ethanol yield in liquid samples was observed (refer to Fig.5.17).

$$C_2H_4 + H_2O \xleftarrow{\text{Pressure} < 71\ bar,\ \ 300 < T < 500°C,\ \text{Metal based catalysts}} C_2H_5OH \qquad (5.2)$$

In addition, the COD analysis of the liquid product has confirmed little effect of organic degradation over the pressure range. The percentage of organic in the liquid sample remained relatively stable between 9.97 to 10.1 wt%, from increasing the pressure from 170 to 250 barg, respectively. However, this value decreased significantly to 6.6 wt% when the pressure was increased to 270 barg (refer to table 4.3). This is attributed to the improved gasification rate as a result of high reactivity, enhanced by the solubility of reactants and products.

5.3.3.3 **Reactor temperature**

The influence of the reactor temperature was studied between 400 to 550°C in order to maximise the overall product gas, and to evaluate individual components such as hydrogen, syngas and methane yields. The trends of these yields are shown in Figs. 5.7 and 5.8.

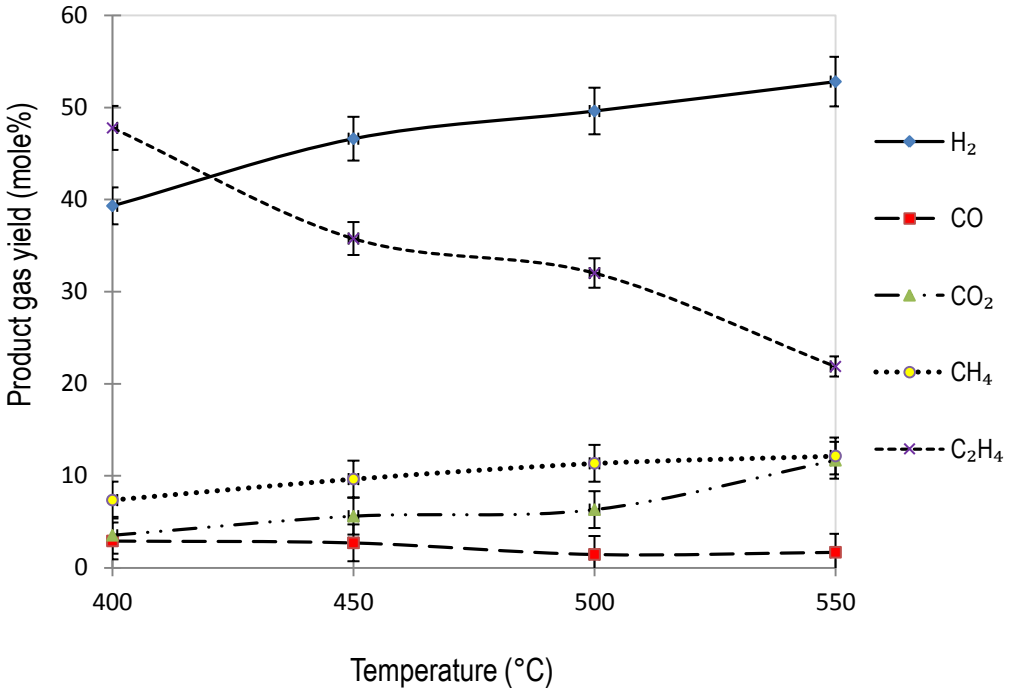

Fig.5.7. Effect of temperature on gas products yield for 10 wt% glycerol

Small reactor, *235 barg, WHSV=125 h^{-1}*

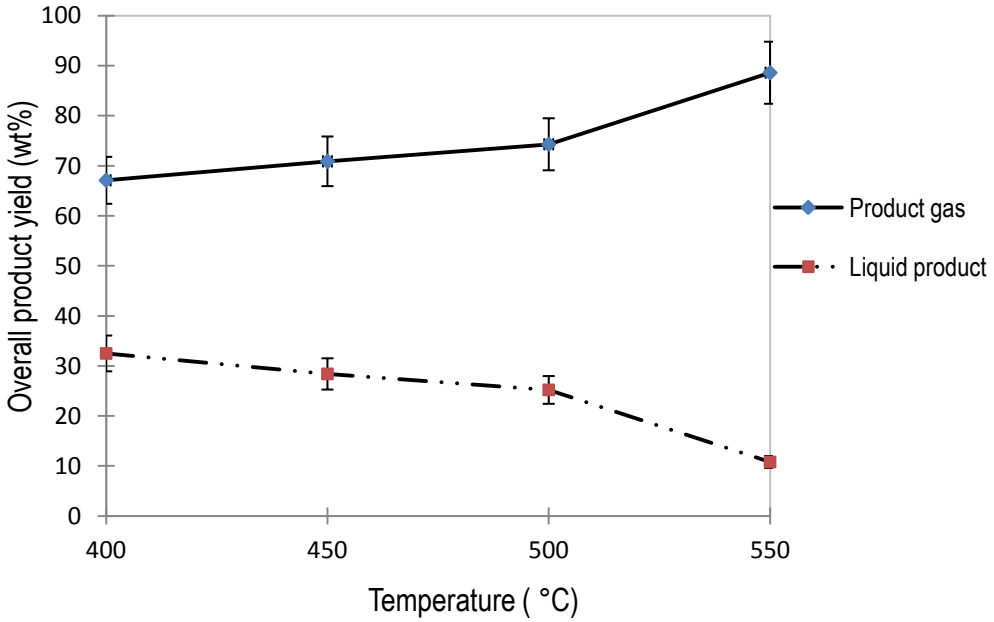

Fig.5.8. Effect of temperature on gas-liquid product yields for 10 wt% glycerol

Small reactor, 235 barg, WHSV=125 h^{-1}.

Note gas and liquid yields do not equal to 100 % as char formed part of the overall product

The influence of reactor temperature between 400 to 550°C was studied to evaluate gas yields, and to maximise the overall gaseous product. The results are shown on Figs.5.7 and 5.8.

It can be seen in Fig.5.7 that H_2 yield increases at a low rate from 39 to 53 mole %, while CO_2 yield is initially low (4 mole %) at 400°C, but increases to 12 mole % at 550°C, which may be attributed to the activity of the WGS reaction. Ethylene decreases from 48 to 22 mole% when temperature increases from 400 to 550°C, respectively. This can be is attributed to thermal cracking at higher temperature. On the other hand, methane yield is low (8 mole %) at 400°C, but increases slightly to 12 mole % at 550°C. This could be due to the effects of side reaction, such as methanation and cracking of C_2H_4. Loss of catalyst activity would favour side reactions, such as methanation ($3H_2 + CO \rightarrow CH_4 + H_2O$) and polymerisation of ethylene to form coke. After 172 hours on-stream a dark/black colour material deposited on the inside of the reactor wall was identified as coke by ESEM-EDS analysis; the fresh and used samples, gave carbon dry catalyst weights of 4.5 and 7.2 wt%, respectively; representing 2.7 wt% carbon (refer to appendix N). The accumulation of carbon on the catalyst surface could contribute to the consumption of hydrogen through gas-solid reactions i.e. $C + 2H_2 \rightarrow CH_4$ (ΔH_R = -74.8 kJ mol^{-1}). This reaction is exothermic and consequently, temperature has a negligible effect on its formation. Some researchers have reported that methane selectivity could be 40 to 60 mole % for supported Fe [**267**], and as high as 95 mole % when the temperature is between 350 to 550°C [**267, 268**]. Other studies have revealed that low temperature and high pressure favour the formation of CH_4, but reduce the decomposition reaction rate of glycerol [**269, 270**] over Ni and Ru catalysts. In contrast, high temperature (associated with a low pressure regime) favoured the formation of H_2 and CO. In light of this, and the results shown in Figs 5.7 and 5.8, the hydrocarbon yield can be attributed to the catalyst choice, catalyst activity and reaction conditions (particularly temperature) in the CSCWG of glycerol.

At 400°C, syngas (H_2:CO) yield was ~42 mole % and increased to 55 mole % at 550°C. Syngas yield was high because of improved H_2 yield and as a result, H_2:CO ratio increased from 13:1 at 400°C to 26:1 at 550 °C. Water in the CSCWG process would have promoted the WGS reaction (ΔH_R = +41.0 kJ mol^{-1}) and decreased CO concentration. The reverse-WGS ($CO_2 + H_2 \rightarrow CO+H_2O$; though this is less thermodynamically favoured at higher temperature ΔH_R = - 41.0 kJ mol^{-1}) and/or C(s) + $CO_2 \rightarrow 2CO$ may have contributed in CO formation as suggested in other findings [**271, 272**], where Fe/Cu and Ru/Ni catalysts were used. These types of side reactions are known to occur if the catalyst lost its activity. Fig.5.8 shows that the overall gas yield increases from 67 wt% at 400°C to 89 wt% at 550°C; meanwhile the liquid product decreased from 35 wt% to 10 wt%, respectively. It is worth noting that gas yields are higher than those obtained without Fe_2O_3+Cr_2O_3 catalyst (refer to Fig.5.1). The increase of gas yield is due to catalytic cracking and thermal cracking of glycerol and liquid products as the temperature increased. At 550°C, complete conversion of glycerol was achieved as evident by the

absence of glycerol in the analysed liquid sample, whereas 49 wt% of unconverted glycerol was present in the sample at 400°C. The COD analysis of the liquid sample at 500°C gave a measurement of 2395 mg/l COD, representing 1.6 wt % of glycerol in the sample. It should be noted that continued operation at ≤ 400°C for feed concentrations greater than 50 wt% glycerol, resulted in plugging of the reactor as a result of coke formation. This problem, however, could be alleviated by raising the temperature above 500°C. It has been suggested that at lower temperatures the reaction rates for coke formation are higher than the rates of reforming and carbon gasification [**273, 274**]. At temperatures, <450°C lower gas yields were obtained due to poor conversion of reactants and the reduced role of the WGS reaction. Other works have revealed that low temperature could also result in a less clean product gas, which is likely to contain various amounts of light hydrocarbons, such as C_2H_2 and C_2H_4, as well as heavy hydrocarbons, the latter condense to form tar [**275, 276**]. This is also true in this work with the exception of C_2H_2, which was not observed. Tar is obviously an undesirable by-product of CSCWG as it can block valves, in-line filters and interfere with conversion processes.

5.3.3.4 **Effect of glycerol concentration**

Feed concentration is a key parameter for the economical evaluation of the gasification process. It is essential to use only the necessary amount of feed in order to achieve optimum yields. The effect of glycerol feed concentration was studied from 2 to 30 wt% at WHSV=125 h^{-1}, 235 bar and 500°C as shown in Figs.5.9 and 5.10.

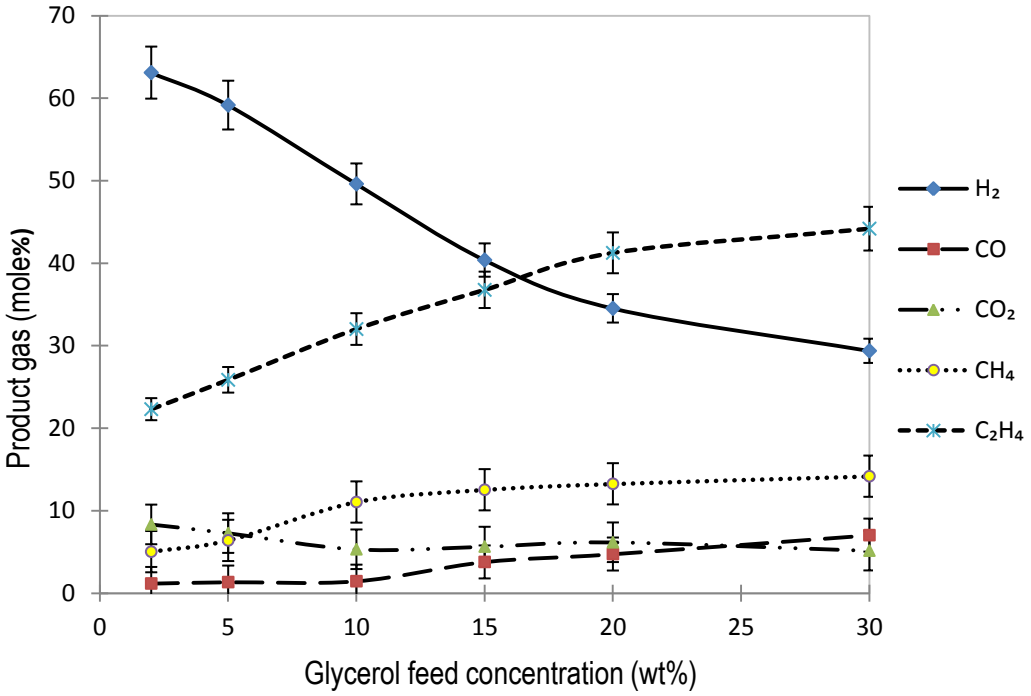

Fig.5.9. Effect of glycerol feed concentration on gaseous products

Small reactor, 500ºC, 235 barg and WHSV=125 h^{-1}

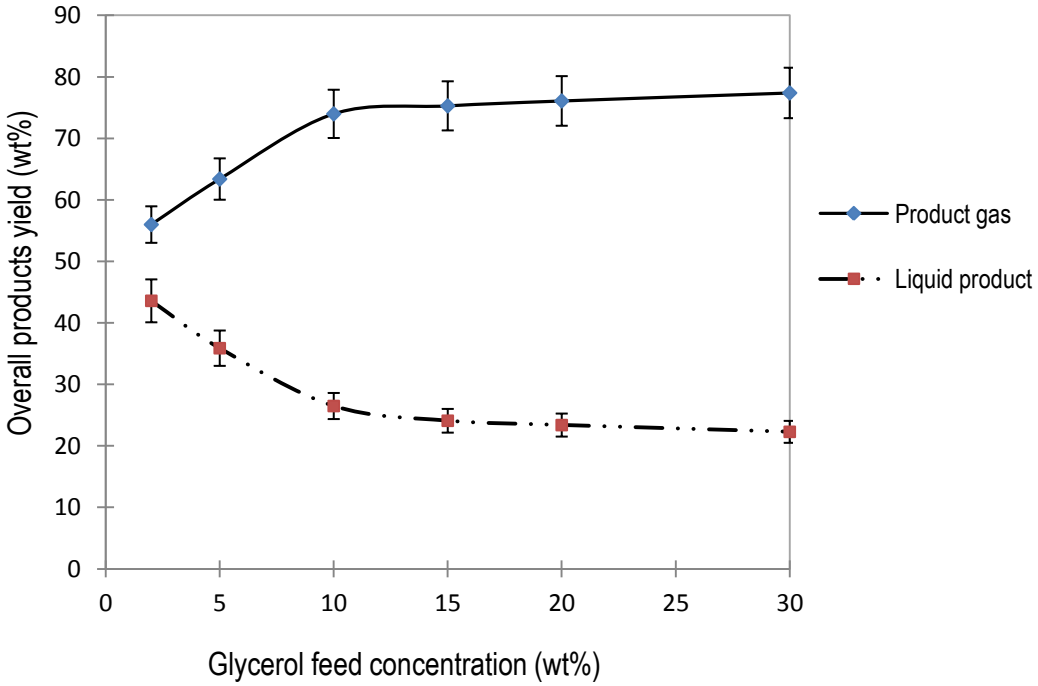

Fig.5.10. Effect of glycerol concentration on gas-liquid product yields

Small reactor, 500 °C, 235 barg and WHSV=125 h^{-1}.

Note gas and liquid yields do not equal to 100 % as char formed part of the overall product

It can be seen in Fig.5.9 that increasing feed concentration from 2 to 30 wt%, results in decreasing H_2 yield from 62 to 24 mole%. CO_2 also decreases while CO yield increases over the same range of feed concentration, which may point to the reduced role of the WGS due to high carbon to water feed concentration [**277**]. This would give less water to promote H_2 formation and also char reforming is likely to increase ($C_{(S)}$ + $CO_2 \rightarrow$ 2CO [**278, 279**]). Syngas decreased from 64 to 33 mole% with increased glycerol feedstock concentration. This is largely due to decreasing H_2 yield, which affected H_2:CO ratios. As a result, the ratio decreased significantly with increased glycerol concentration from 41:1 to 6:1 and to 3:1 for 2, 15 and 30 wt%, respectively. It has been reported that lowering the feed wt% enhances the gasification process by efficient heat transfer (due to improved thermal properties) and by distributing the reactant uniformly throughout the reactor bed [**280**]. The lower wt% of organic in the liquid sample after COD analysis gave further evidence of the improved gasification rate at low feed concentration. The COD measurement of the liquid product from the CSCWG of glycerol at the reported conditions has decreased significantly from 12864 to less than <38 mg/l for an initial feed concentration of 20 to 2 wt %, respectively (refer to table 4.2).

Methane and ethylene yields increased from 5 to 14 mole % and 23 to 44 mole %, respectively over the same range of feed concentration. At high concentrations, the reactants would flood the catalyst active sites and affect the gasification to the highest gas products. The carbon balance showed that complete conversion of glycerol to gaseous and liquid products was realised even for the highest feed concentrations tested (30 wt% glycerol) at 550°C using the reported catalyst. Fig.5.10 shows that the liquid product decreases from 44 to 22 wt% when glycerol feed concentrations increases from 2 to 30 wt%, respectively. Conversely, the gas yield increased significantly from 55 to 77 wt% in the same range. This is due to the increasing reactions that contributed to increase in light hydrocarbon and CO yields. The polymerisation of the reaction at high feed concentration has contributed to the increased formation of hydrocarbons (methane and ethylene), and therefore to the formation of higher product gases.

5.3.3.5 **Effect of time online on the gas yield**

The effect of time online was studied by monitoring the gas product yield for up to 10 hours to provide valuable data about catalyst stability. It can be noted that this series of experiments is similar to that of catalyst stability. The results of the effect of online time are shown in Fig.5.11.

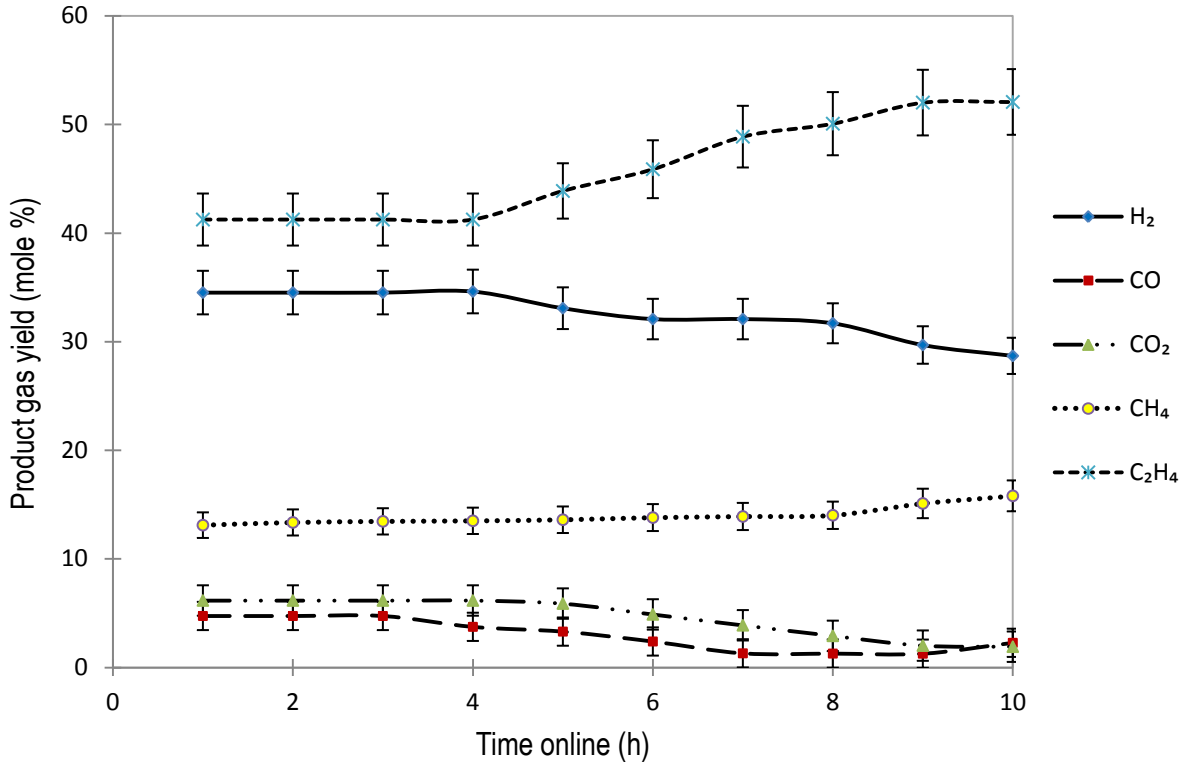

Fig.5.11. Effect of time online on gas product yield for 20 wt% glycerol;

Small reactor, 500°C, 235 barg and WHSV=125 h^{-1}

The effect of time online was studied by monitoring the gas product yield for up to 10 hours to provide important data about catalyst stability. It can be seen in Fig.5.11 that hydrocarbon yields increased with time online; methane and ethylene yield increased slowly from 13 to 16 mole % and 41 to 52 mole%, respectively. The increase in methane may have resulted from gas-solid reactions that would be occurring ($C + 2H_2 \rightarrow CH_4$) due to char formation. On the other hand, CO remains stable during the first 3 hours; they then both decrease sharply thereon from 34 to 28 mole % for H_2, and from 5 to 2 mole % for CO. This could also be due to a decrease of active sites resulting from the deposition of coke on the catalyst particles or thermal transformation of the catalyst as evidenced by deposition of fragments on the catalyst surface (refer to Fig.4.6). Carbon monoxide and hydrogen can also produce methane through methanation side reactions: $CO + 3H_2 \rightarrow CH_4 + H_2O$ and $CO_2 + 4H_2 \rightarrow CH_4 + 2H_2O$ and may contribute for the low H_2 yield. Both of these reactions are exothermic and are favoured by lower temperature as compared to steam reforming of methane (SRM), which would occur at high temperature (700 to 800°C). Evidence of char formation was revealed also by ESEM-EDS analysis of the fresh and used sample after 9 hours on-stream, which gave carbon dry catalyst weight percentages of 5.2 and 5.5 wt%, respectively; representing an accumulation of 0.3 wt% (±1%) of char. However as seen in section 5.3.3.3, temperature is a salient parameter for char formation.

5.3.4 **Effect of catalyst parameters on gaseous products**

To study the influence of catalyst parameters on the product gas, two series of experiments were carried out to assess the impact of Fe_2O_3-Cr_2O_3 loading and particle size on the CSCWG process. In the first series of experiments, various masses of catalyst were loaded into the reactor in the same way as described in section 5.2.3, which were maintained stable in the reactor bed using two sections of mesh and steel spring (refer to section 5.3.2.1). All experiments were performed in the similar ways as described in section 3.5.2. The operating conditions were kept constant while varying only the catalyst loading. In the second series of experiments, various particle sizes of Fe_2O_3-Cr_2O_3 were studied to determine the influence of particle size change on the product gas yield. The best catalyst loading (10.2 g, d_{50} = 4 mm) determined in section 5.2.4.1 was used in conjunction with the optimum operating conditions (P=250 barg, T=550°C, WHSV= 125 h^{-1}, 15 wt% glycerol) determined in section 5.2.4. Only the particle size of the catalyst was varied, and its size distributions are shown in appendix B. The product gas of both series of experiments were analysed and the results are discussed in section 5.3.4.1 and 5.3.4.2.

5.3.4.1 **Effect of Fe_2O_3-Cr_2O_3 catalyst loading**

Experiments to study the effect of catalyst loading were carried out in the same PBR as reported in section 3. Fresh samples of Fe_2O_3-Cr_2O_3 loading were varied as follows: 5, 11, 22 and 32.1 g. The bed for the catalyst loading was created using two sections of mesh (50 µm pores size) that was cut to accommodate the inner diameter of the reactor (ID=21 mm) at both ends. The catalyst was weighed, placed inside two portions of mesh, and these were kept stable, with a supporting steel-spring that has an outside diameter equivalent the inner diameter of the reactor. The mesh and steel-spring were initially tested, and were shown to have no effect on the gas composition and yield. The results are summarised in Fig.5.12 and table 5.3.

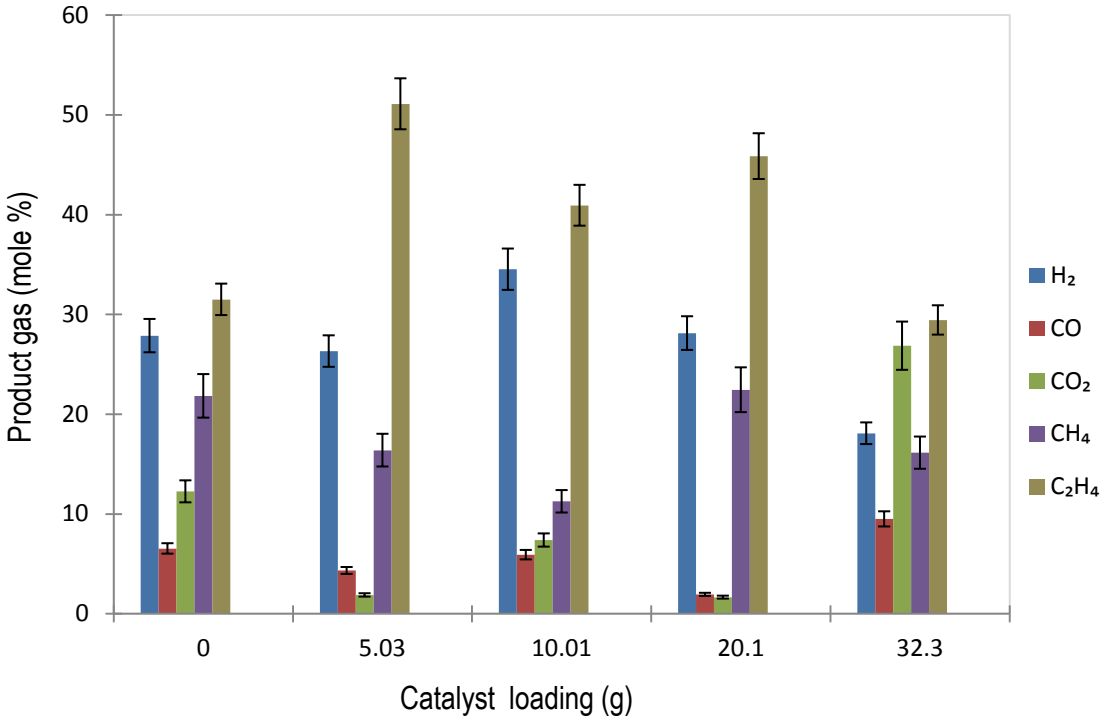

Fig.5.12. Product Gas composition for the CSCWG of 15 wt% pure glycerol.

Small reactor, T= 500°C, P=250 barg, catalyst loading=10 g, WHSV=125 h^{-1}, *for variable loading of the catalyst (d_{50} of 3.5 mm cylinder with 4 mm diameter).*

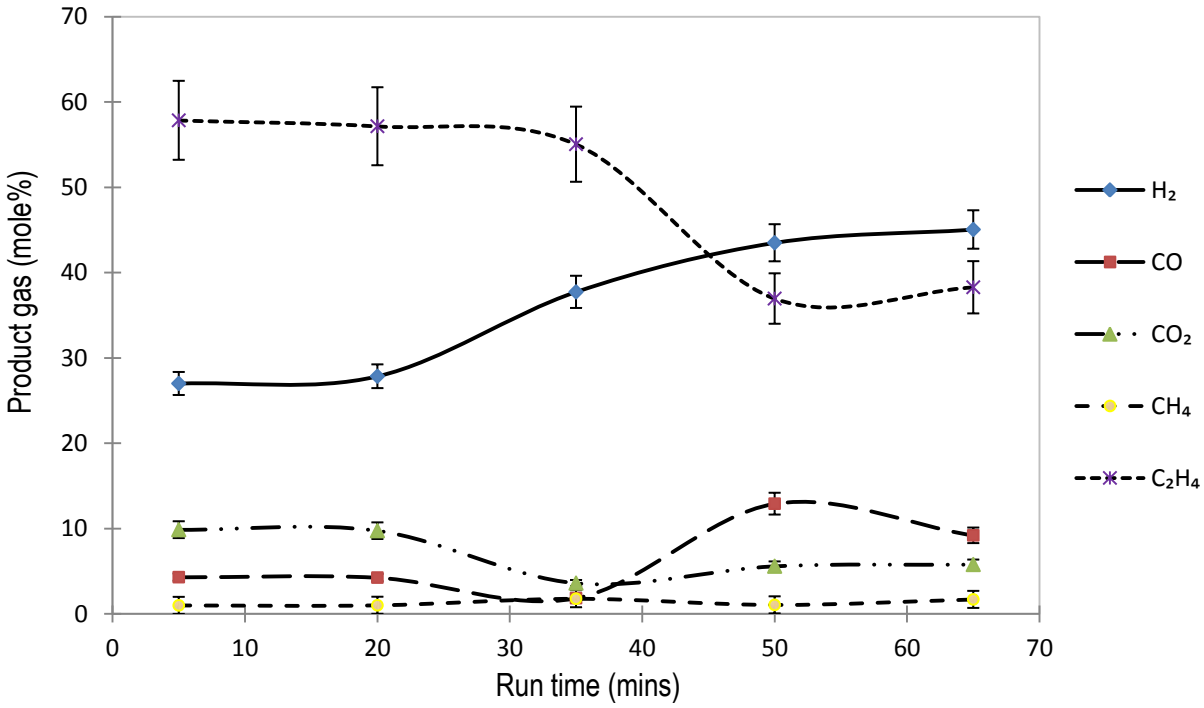

Fig.5.13. Gas composition along time-on-stream of the catalyst for CSCWG (E36)

Small reactor, 15 wt% pure glycerol, 10.1 g iron oxide, P=250 barg, T=500°C, WHSV=125 h^{-1}

Table 5.3. Product distribution at the exit of the CSCWG for variables loading and uniform d_{50} *of 3.5 mm cylinder with 4 mm diameter,* s*mall reactor, 15 wt% pure glycerol, 10.1 g iron oxide, P=250 barg, T=500°C, WHSV=125 h^{-1}*

Experiment number	*E44*	*E32*	*E36*	*E40*	*E42*
Catalyst loading	0	5.0	10.1	20.1	32.3
Cumulative gas composition (mole %)					
H_2	27.8	26.3	34.5	28.1	18.1
CO	6.5	4.3	5.9	1.9	9.4
CO_2	12.2	1.8	7.3	0.6	26.8
CH_4	21.8	16.3	1.2	23.4	16.1
C_2H_4	31.5	51.0	50.9	45.8	29.4
Syngas	34.3	30.6	40.4	30.0	27.5
Gas products yield (wt %)	71.1	82.2	81.7	77.3	82.8
Liquid yield (wt %)	28.1	17.3	17.6	21.9	16.6
Char yield (wt %)	0.8	0.5	0.5	0.6	0.5
Glycerol conversion (%)	49.7	91.9	99.8	73.7	61.7

It can be seen in Fig.5.12 and table 5.3 that increasing the amount of catalyst from 0 to 10.01 g loading; CH_4 decreases, C_2H_4 increased and H_2 yield increased. On the other hand, when the amount of catalyst was increased from 10.1 to 32.1 g, C_2H_4 decreases along with H_2 yield. Also, it can be observed in table 5.3 that the product gas yield increased from 71 wt% to above 82 wt% for non-CSCWG and CSCWG, respectively, which suggested that Fe_2O_3-Cr_2O_3 catalyst has a positive effect toward SCWG overall. However, the degree of activity and selectivity toward hydrogen were variable as

a function of the amount of catalyst loaded. This is because, at a given metal catalyst loading; the number of active sites in a catalyst is a function of the metal dispersion, which is defined as the fraction of the total atoms of the active element that is exposed at the surface. The dispersion is, in turn, inversely proportional to the crystallite size [**281**]. In the case of Fe_2O_3-Cr_2O_3 catalyst, the metal dispersion was below 12 % as measured by Micromeritics (AutoChem II 2920 model), corresponding to an average crystallite size of about 4 nm. Another factor that could contribute to low iron dispersion was the high metals loading (85 wt%) on the sample catalyst. It should be noted that the catalyst used in this work has no support, which suggested that the influence of the support surface area parameter that occurred by interactions with reactants have not contributed to catalytic performance. The high yield of methane obtained from large Fe_2O_3-Cr_2O_3 loadings could be attributed to increase of sensitivity in crystalline size, which may have favoured methanation reaction. The product gas yield of the CSCWG was higher when compared to non-CSCWG. This may have resulted from a high reaction rate driven by lower activation energy. However, the limiting factors for the reaction rate would be the combination of catalyst loading and its activity. In addition, other parameters such as the diffusion of glycerol solution on the surface of the catalyst particle and the diffusion of gaseous products from the surface would have also influenced the rates of reactions. In this case, the diffusion rate would have been dependent on many factors, such as the large catalyst d_{50} (3.5 mm cylinder with 4 mm diameter), the concentration of the reactants, and the operating temperature inside the reactor bed and char formation on the surface of the catalyst due to polymerisation reactions.

It can be observed in table 5.3 that the product gas yield has not increased with higher catalyst loading. This is because the amount of catalyst alone could not result to increase the reaction rate. Other factors such as catalyst stability, possibly reactor bed porosity and particle movement under high pressure may have contributed to the change observed on the product gas yield over catalyst loading. However, catalyst loading plays a pivotal role on selectivity toward hydrogen and hydrocarbons. A high yield of hydrogen (36 mole%) was observed at 10.1 g catalyst loading, which suggested that activity of catalyst was higher due to increasing access of reactant on the active sites of the catalyst. On the other hand, ethylene and methane yields were high (46 and 23 mole% respectively) with an increase of catalyst loading to 20.1g, and could be attributed to decreasing in gasification efficiency, hence low catalytic cracking of hydrocarbons resulting from difficulties of accessing the active sites of the catalyst.

Fig.5.13 shows that H_2 content and the overall gas composition varies with run time due to the catalyst activity and thermal cracking. Hydrogen increased from 28 to 46 mole% with run times from 5 to 65 min. Concomitantly, ethylene decreased over the same time from 58 to 48 mole%. This is due to catalyst activity that contributed to increase hydrogen yield as a result of catalytic cracking of

hydrocarbons (ethylene). The WGS reaction would have had a significant role between the first 5 to 20 mins, as evidence by high yield of CO_2 (10 mole %) and H_2. Thereafter, WGS reaction decreased due to increasing influence of other reactions such as hydrocarbon cracking. After 65 min, it can be mentioned that the catalyst showed no sign of deactivation as evidenced by the similarity of the surface structure (refer to appendix M), and high yield of H_2 (> 46 mole%) and product gas. This indicated that the lifetime of Fe_2O_3-Cr_2O_3 was well above 65 min in SCWG.

5.3.4.2 **Effect of Fe_2O_3-Cr_2O_3 particle sizes**

In order to determine the effect of the catalyst particle size diameter. A series of experiments using d_{50} with diameters between 0.125 and 6 mm at 500°C were performed. These particles were obtained by crushing and sieving until different size intervals were obtained as reported in chapter 3 (refer to appendix B for size distribution). The study also aimed to determine if the internal diffusion played a role in the CSCWG reaction. The main product gas distribution and the overall products are in table 5.4.

Table 5.4. Product distribution at the exit of the catalytic reformer for several *d_{50} of the catalyst in a small reactor, Feed=15 wt% pure glycerol, T= 500°C, P=250 barg, catalyst loading=10 g and WHSV= 125 h^{-1}.*

Catalyst; d_{50} (mm)	0.1	0.5	1	4	6	6
Cumulative gas composition (mole %)						
H_2	21.1	28.5	32.8	33.5	38.1	42.0
CO	4.2	3.2	8.0	5.7	6.3	6.3
CO_2	10.1	11.6	19.8	17.1	15.7	11.7
CH_4	34.5	30.1	18.3	18.2	10.3	10.9
C_2H_4	29.1	26.7	21.1	25.4	29.6	29.1
Syngas	25.3	31.7	40.8	39.2	44.4	48.3
Gas products yield (wt %)	80.4	71.8	79.1	81.7	73.9	79.1
Liquid yield (wt %)	18.9	27.3	20.2	17.6	25.2	19.4
Char yield (wt %)	0.5	0.8	0.6	0.5	0.7	0.6
Glycerol conversion (%)	99.1	79.8	85.5	99.8	93.9	90.2

Fig.5.14. shows the effect of particle diameter of Fe_2O_3-Cr_2O_3 on the amount of gas produced. The amount of gas produced increased from 71.8 to 81.7 wt% when d_{50} increased from 0.5 to 4 mm. This is due to the decrease in the porosity of the reactor bed from 35 to 27%, respectively as the particle diameter decreases, coupled with an increase in permeability from 4.02 $*10^{-6}$ to 1.21 $*10^{-4}$ cm^2, respectively. The reduction in the particle diameter of the packing offers resistance to the flow of the reactant, which can be defined as permeability. The porosity and permeability of the packed bed for the different d_{50} of the packing materials is given in Appendix H.

The experimental results of the effect of d_{50} on product gas yield are given in Table 5.4 and Fig.5.14, and it can be expected that a given amount of reactant in contact with the same amount of catalyst surface, for the same length of time may bring the same degree of decomposition. If the surface of the catalyst was the factor affecting the amount of reaction, then catalysts of different sizes would give the same amount of reaction at the same values of *R/A,* where *R* is the rate of feed and (*A)* external surface area. However, this cannot be a reliable assumption and little information is available to support this hypothesis. In effect, the reaction rate in a catalytic environment is more likely to be affected by the active sites of the catalyst rather than the external surface area of the catalyst. It has been demonstrated that where the surface area of the catalyst is readily measurable, the activity is roughly proportional to the contact area [**282**]. On the other hand, for irregular particle sizes, which are most widely used in industry, it seems also reasonable to expect that the increase in catalytic activity might be a function of the increase in the external surface area. However, the effect of catalyst support on the catalyst activity cannot be neglected.

It can be observed in table 5.4 that when d_{50} was reduced from 0.5 mm to 0.125 mm, the product gas yield was increased from 71.8 to 80.4 wt%, respectively. Liquid product yield concurrently decreased from 28.1 to 19.5 wt%. In addition, char products increased slightly from 0.5 to 0.8 wt%. This is due to the porosity of reactor bed, which decreased from 0.47 to 0.39, and improved contact points between the particle and reactant in the reactor bed.

It can also be observed in table 5.4 that gas yield increased from 71.8 to 79.1 and 81.7 wt% when d_{50} was increased from 0.5 to 1 and to 4 mm, respectively. Concurrently, the liquid product decreased in the same range of particle size from 27.3 to 20.2 to 17.6 wt%. This result is probably due to the increase of metal dispersion that contributes to improve the catalyst activity and possibly to the increase in diffusion rate of feed on the surface of catalyst that contributed to improve the reaction of feed for better conversion; therefore improving the gasification yield. Furthermore, increased metal dispersion would potentially contribute to improve the thermal conductivity of the catalyst; hence, better heat transfer between reactants and surface of the catalyst. However, when d_{50} was increased from 4

to 6 mm, the gas yield decreased slightly from 81.7 to 79.1 wt%, which suggested that d_{50} > 4 mm was not controlling the diffusion. Thus, it has no driving force on the reactions. The effect of particle diameter of iron oxide on the composition of product gas was studied and the results are shown in Fig.5.14.

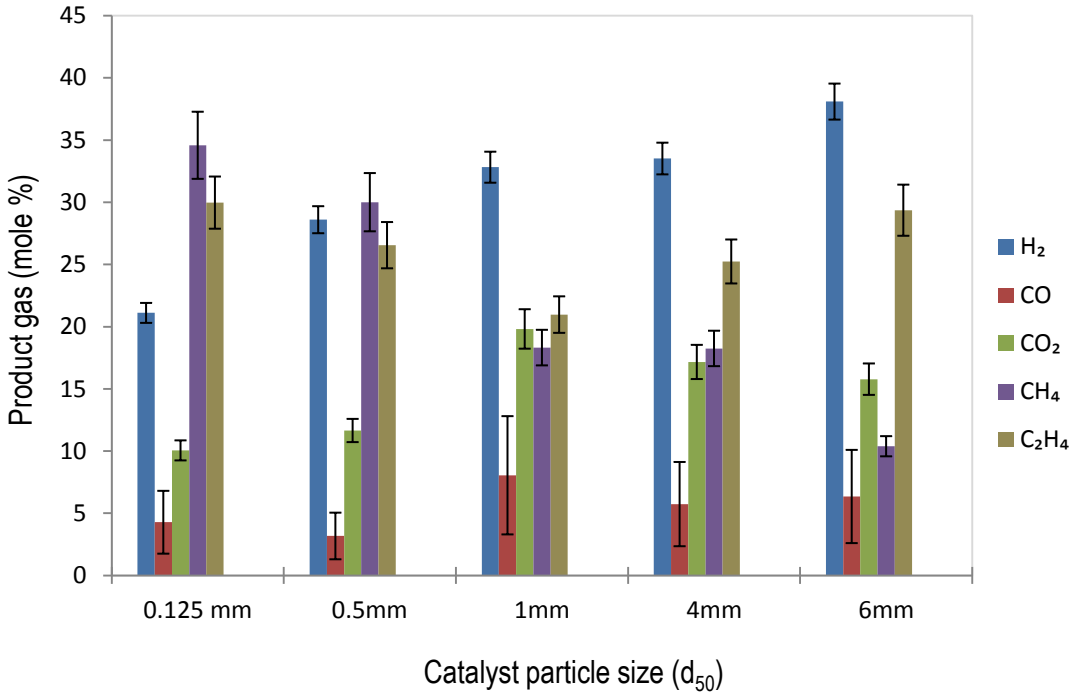

Fig.5.14. Product gas composition for the CSCWG of 15 wt% pure glycerol over Fe_2O_3-Cr_2O_3

Small reactor, T= 500°C, P=250 barg, catalyst loading=10g, WHSV= 125 h^{-1}, variable d_{50} of the catalyst

It can be seen that hydrogen yield increased from 21 to 37 mole% with the increasing d_{50} from 0.125 to 6 mm, respectively. Concomitantly, CO_2 increased from 10 to 29 mole %, before decreasing slowly to 16 mole%, with increasing d_{50} from 0.125 to 1 to 6 mm, respectively. This is probably due to the increasing role of WGS reaction with increasing d_{50} from 0.125 to 1 mm. Above 1mm, the role of WGS reaction decreases with reducing CO_2 formation coupled with increased ethylene yield, which probably indicated the dominance of side reactions such as hydrogenation of methane for ethylene formation. Furthermore, the increase of hydrogen coupled with the decrease of methane yield with increasing particle size could also be attributed to methane cracking or/and methane reforming ($CH_4 \leftrightarrow C + H_2$) into gaseous and coke under the influence of d_{50}. On the other hand, ethylene also decreases slightly from 30 to 21 mole%, which is attributed to increase of d_{50} from 0.125 to 1 mm, respectively. When d_{50} was increased from 1 mm to 6 mm, ethylene increases from 21 to 29 mole%, respectively. This fact of decreasing hydrocarbon yields coupled with high product gas yield would indicate a diffusion control between $1 < d_{50} < 4$ mm approximately.

Syngas yield increased moderately from 24 to 43 mole% with an increase of d_{50} from 0.125 to 6 mm, respectively. This is due to the high proportion of hydrogen in the gas products. The increase in catalyst particle diameter appears not to affect the CO yield, which remains low at 8 mole%, with 1 mm particle size. CO decreased from 8 to 6 mole% when d_{50} increased from 1 to 6 mm, respectively, which is partly attributed to a small role of WGS reaction that consumed CO for the production of H_2 ($CO + H_2O \leftrightarrow H_2 + CO_2$); Large particle size seems to have contributed significantly to the methane cracking into hydrogen and char; hence high hydrogen yield.

5.3.5 **Effect of process parameters on liquid products for CSCWG of pure glycerol**

This section evaluates the influence of WHSV, pressure, temperature and feed concentration on the liquid products formation from the CSCWG of pure glycerol over Fe_2O_3-Cr_2O_3.

Liquid product analysis showed that the main consistent condensable liquid products were significant amounts of methanol, allyl alcohol, formaldehyde, and depending on the conditions, low yields of acrolein acetaldehyde and propionaldehyde. These products were found also in other studies [**283, 284**]. The wide variety of products reflects the complexity of the reaction mechanisms involved in the hydrothermal decomposition of glycerol, which can be summarised in the coexistence of competing ionic and free radical pathways [**284**]. Most of these liquid products were formed in subcritical and supercritical conditions.

5.3.5.1 **Influence of WHSV**

The influence of WHSV on the liquid products was studied, by running a series of CSCWG experiments in a small reactor where the feed flow rate was varied while keeping constant the amount of catalyst loading at 32.1 g (d_{50} = 4 mm), at a reaction temperature of 500°C, feed concentration of 20 wt% and pressure of 250 barg. Fig.5.15 shows the results of WHSV variation from 19 to 125 h^{-1}.

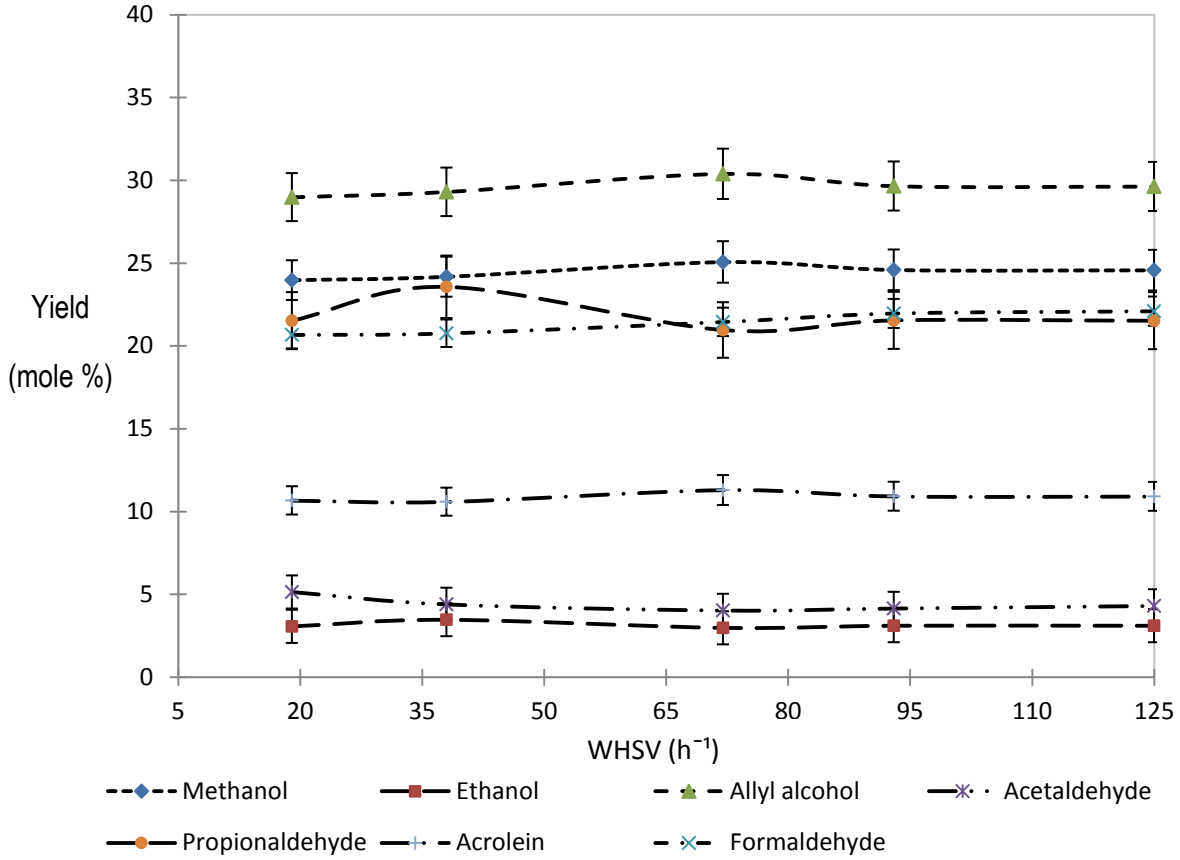

Fig.5.15. Influence of WHSV on the liquid products;

Small reactor, *20 wt% glycerol at T=500°C and P=250 barg*

It can be seen that the distribution of most of these products varies insignificantly over the WHSV. Allyl alcohol, methanol and formaldehyde; are the dominant carbon-liquid products, and were in the range of 28 - 29 mole%, 23 - 24 mole% and 20 - 23 mole%, respectively. For the WHSVs reported the distribution indicates that their formation might result from both primary and secondary reactions. An ionic pathway, which is favoured at increasing water density; (enhances with high pressure at constant temperature) is the likely route of their formation. Acetaldehyde and propionaldehyde yields were also stable in the range of 5 to 4 mole % and 23 to 21 mole% for WSHVs from 36 to 78 h^{-1}, respectively. This indicated a possible conversion into secondary products by free radical pathways favoured at low densities. This is because the reduced effect of hydrogen bonding that decreased with a decrease in the density of water in a SC is responsible for the change in solubility properties in SCW. It has been reported that allyl-OH is formed only by free radical mechanism while acetaldehyde and acrolein are formed by ionic or/and free radical reaction **[285].** This work suggests an ionic pathway is also of consideration for allyl alcohol formation at the reported conditions. The slight increase of methanol with

WHSV is regarded as a primary product and as an intermediate in the higher alcohol synthesis, since the ratio of methanol to higher alcohols increases with increasing WHSV.

The influence of Fe_2O_3-Cr_2O_3 catalyst on the distribution of liquid products appears to be minor. This is because their mechanisms of formation were more dependent on the temperature and pressure.

5.3.5.2 **Influence of system pressure**

The influence of system pressure was studied by running a series of experiments in a small reactor where only the pressure was varied between 150 to 250 barg while keeping constant the temperature at 500°C, feed concentration at 10 wt% and WHSV at 125 h^{-1}. Fig.5.16 shows the results of pressure variation.

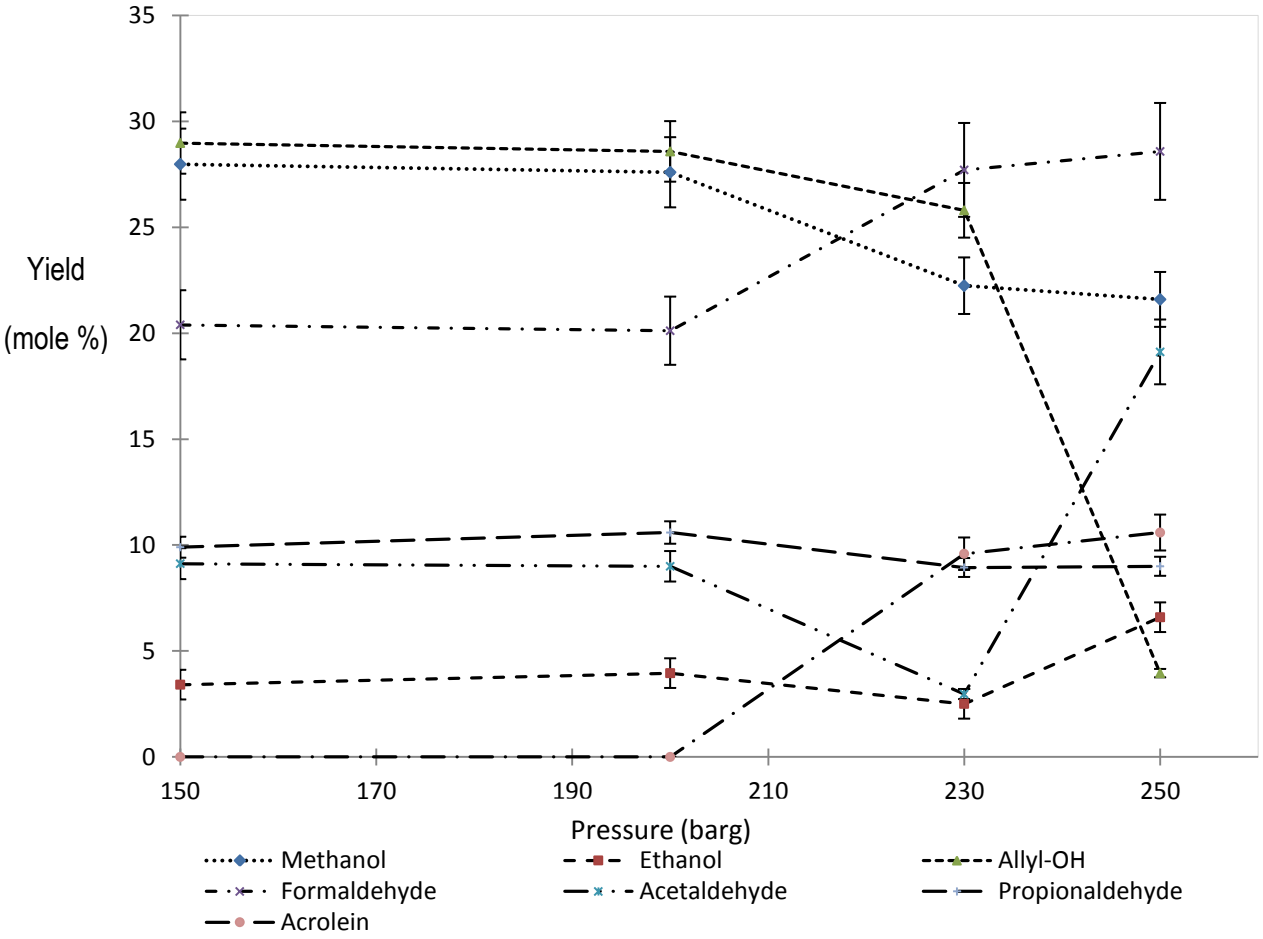

Fig.5.16. Influence of pressure on the liquid products yield

Small reactor, 10 wt% glycerol at 500°C, 250 barg, WHSV=125 h^{-1};

Vertical dotted red line indicates supercritical conditions at 221 barg

It is evident that the pressure plays a significant role on the formation of liquid products above the supercritical point (represented by the red dot line). Most of the products tend to increase, which indicated that these products might be formed largely by ionic reaction pathways due to the increased ionic product in SCW region as reported by other studies [**284, 285**]. However, methanol, allyl-OH and propionaldehyde decreased when the pressure was above 235 barg. This might point to the influence of other factors such as density change and activation energy that contributed to promote other reaction pathways and selectivity of the chemical reaction and products. For instance, the reduction yield of methanol was coupled with increasing yield of hydrogen (refer to Fig. 5.6), which indicated a possible dehydrogenation of methanol into hydrogen and carbon oxides according to equations $2H_2 + CO \Leftrightarrow CH_3OH$ and $3H_2 + CO_2 \Leftrightarrow CH_3OH + H_2O$. In addition, methanol and allyl-OH have decreased with pressure in the SC region; coupled with increased yield of aldehydes (acetaldehyde and formaldehyde). This indicated a possible reforming by SCWO of these alcohols into aldehydes.

On the other hand, a number of studies have reported that a mixture of methanol and higher alcohols can be produced from synthesis gas by alkali promotion, and by appropriate modification of the reaction conditions [**286**]. The most suitable catalysts being Rh-based and modified FT-synthesis catalysts based on Co (operating at 20-50 barg and 250- 350°C), Fe (15-30 barg and 200-300 °C), and Ru (40 - 60 barg and 220-290°C) [**287, 288, 289**] metals supported on SiO_2 or Al_2O_3. The use of Fe_2O_3-Cr_2O_3 catalyst may have favoured the formation of alcohols especially, methanol in sub-critical regions. The role of high pressure on the increasing yield of ethanol may be attributed to the catalyst productivity, which is also a function of the process pressure (increasing the process pressure can compensate for the loss in activity). Another route to alcohol formation is from the protonation of glycerol at the primary O-atom leading to the formation of methanol and formaldehyde under SCW conditions [**290**].

It can be seen also that the dehydration of glycerol into acrolein at the reported conditions appeared sensitive to pressure in supercritical conditions. This might be because of the variation of proton concentration with respect to the pressure in SCW. Acrolein appeared unstable in this condition because of the faster rate of glycerol decomposition under the thermal and catalytic influence.

5.3.5.3 **Influence of reactor temperature**

The change of the water properties with increasing temperature leads to a change of reaction pathways from ionic to free radical. The influence of reaction temperature on the liquid products was studied by varying heating temperature from 400 to 550°C while keeping the other operating conditions constant; 10 wt% glycerol, 235 barg and 125 h^{-1} of WHSV. The results of temperature effect are shown in Fig.5.17.

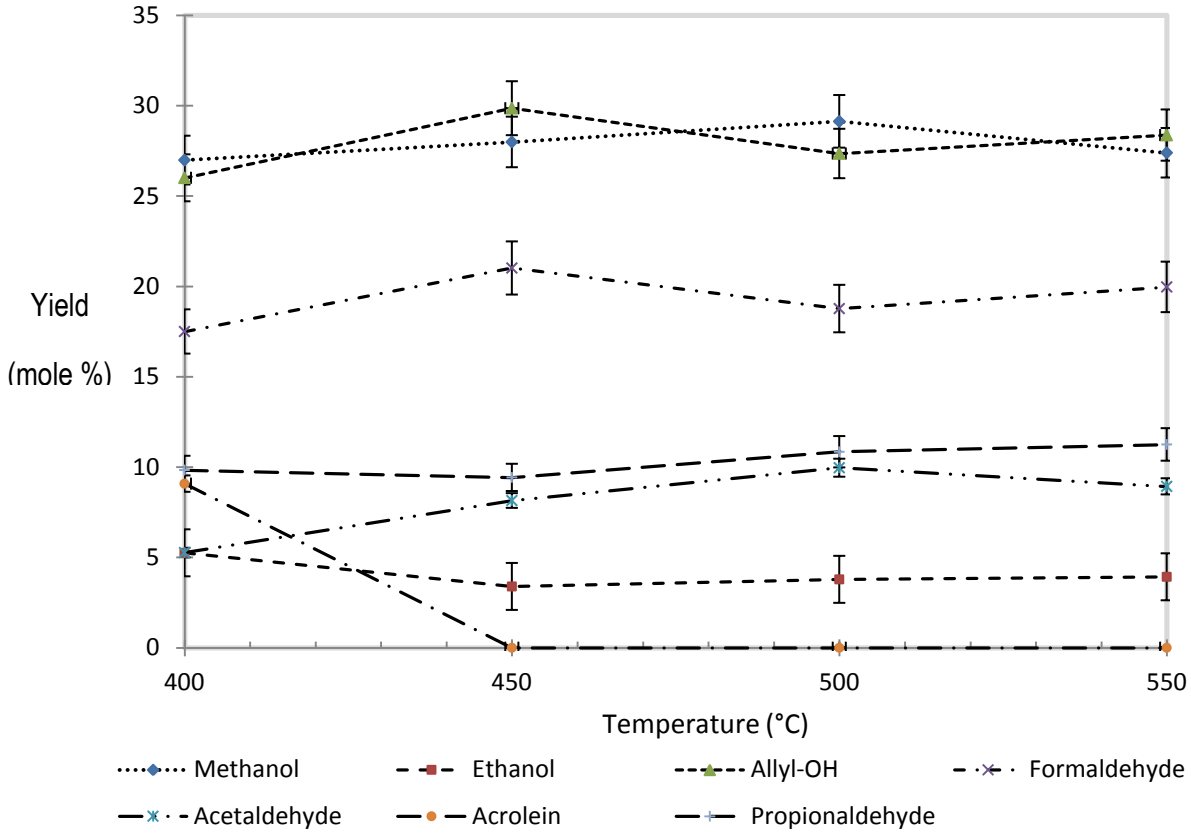

Fig.5.17. Influence of temperature on the liquid products of the CSCWG;

Small reactor, 10 wt% glycerol, 235 barg, WHSV=125 h^{-1}

The change of the water properties with increasing temperature leads to a change of reaction pathways from ionic to free radical. Formaldehyde, allyl-OH, methanol and acetaldehyde increased with temperature, which possibly indicates that their formations are dominated by free radical mechanism [**291**], due to the decrease in their density resulting from an increasing temperature at constant high pressure, which enhances the solubility and phase condition of the component involved. For instance, and by neglecting any other components in the mixture, the density of methanol at 235 barg decreases from 626 kg m^{-3} to 268 kg m^{-3} at 200 to 345°C, respectively [**292**]. Above 450°C, ethanol yield was low (4 mole %) and remained unchanged with increasing temperature, whereas propionaldehyde decreases significantly and almost ceases. This indicates that they might be formed as by-product from secondary reaction or have been destroyed at high temperature. Researchers have demonstrated that, if a suitable acid based catalyst is used, glycerol could degrade into a high yield of acrolein [**293, 294**] by simply dehydration. On the other hand, when T> 450°C, the yield of acrolein is low and nearly ceases when compared to the subcritical region; this could indicate a switch in the reaction mechanism or its rapid degradation into secondary products such allyl-OH, propanol, acrylic acid, propionic acid

[**295**]. Moreover, the decrease acrolein at high temperature (>450°C) was coupled with an increase in methane yield (refer to our earlier work), which could be attributed to a possible reforming of acrolein as postulated also in the literature [**296**]. It can be seen that acetaldehyde increased from 5 to 9 mole% with temperature from 400 to 550°C, respectively. This is coupled with low yield of ethanol and high yield of hydrogen (see ref. 50), indicating a possible dehydrogenation of ethanol to acetaldehyde according to reaction; $C_2H_5OH \rightarrow CH_3CHO + H_2$.

5.3.5.4 **Influence of feed concentration**

Section 5.2.3 has demonstrated that the feed concentration is a crucial parameter of the SCWG process. The influence of feed concentration on the liquid product was studied by varying feed concentration from 2 to 30 wt% glycerol solutions while keeping other parameters constant, and the results are shown in Fig.5.18.

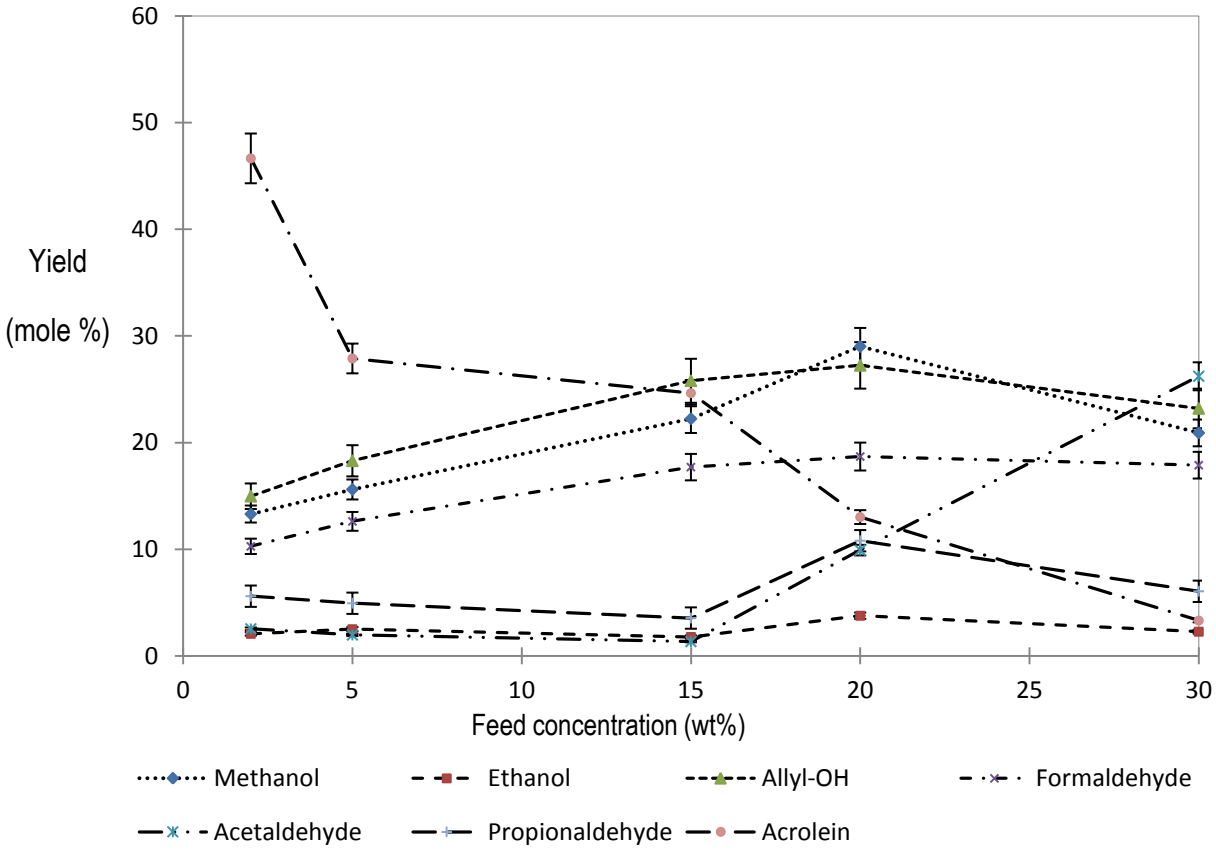

Fig.5.18. Influence of glycerol concentration on the liquid product formation

Small reactor, P=235 barg, T=500°C, WHSV= 125 h^{-1}

It can be seen that methanol, allyl-alcohol, and formaldehyde increased from approximately 13 to 29 mole%, 14 to 26 mole%, and 11 to 17 mole%, respectively when the glycerol concentration increases from 2 to 20 wt%. This could be attributed to improve mass transfer between water-soluble liquid-gas phases. The formation of formaldehyde could have resulted from the incomplete gasification reaction of carbon-containing materials as evidenced by the remaining amount of un-reacted glycerol, which was found to be 16.6% for a 30 wt% glycerol feed concentration. However, at high feed concentrations (> 20 wt% glycerol) the yields of formaldehyde, methanol and allyl-alcohol decreased as the mass per unit of volume of the solution (density) increases with increasing of glycerol concentration and ionic pathways are more dominant, and flooding of the catalyst is much more likely to occur. On the other hand, acrolein decreased significantly from 47 to 3.5 mole% when the concentration was increased from 2 to 30 wt %, which suggested possible rapid decomposition into secondary products such as allyl-alcohol, propanol, acrylic acid, propionic acid and CO_2 as reported [**297**]. As noted earlier, the decrease of acrolein was coupled with an increase in methane yield (refer to Fig.5.9), which may be attributed to its reforming as also postulated in the literature [**297, 298**]. It can be noted that unconverted glycerol in the liquid effluent determined by COD test was high with up to 31 % at high feed concentration of 30 wt %. The distribution and moderate yield of liquid products indicated that a glycerol may have been converted directly into liquid products, as well as being reformed into gas at high concentration. At high feed concentration, glycerol polymerised primarily into liquid component or/and char. Evidence of char formation was revealed also by ESEM-EDS analysis of the fresh and used sample after 9 hours on-stream, which gave carbon dry catalyst weight percentages of 5.2 and 5.5 wt%, respectively; representing an accumulation of 0.3 wt% of char (± 6% margin errors). Coke can be formed from direct polymerisation of glycerol reaction. However, coke was also formed from intermediates liquid product polymerisation such as acetaldehyde [**285**], and probably acrolein. Char or coke also contributed to lost of catalytic activity, which favoured many side reactions, more polymerisation of hydrocarbons (methane, ethylene), polymerization of glycerol or/and of liquid product. After 172 hours on-stream a dark/black colour material deposited on the inside of the reactor wall was identified as coke by ESEM-EDS analysis. Fresh and used samples, gave carbon dry catalyst weights of 4.5 and 7.2 wt%, respectively; representing 2.7 wt% carbon. The accumulation of carbon on the catalyst surface could contribute to poor catalytic performance towards liquid product reforming. Instead, gas-solid reaction such hydrogenation of coke to form methane could be favoured as evidenced in our earlier paper.

5.3.6 Effect of catalyst parameters on liquid products

The influence of catalyst parameters on the liquid products was studied in a small reactor using the experimental conditions and method as reported in section 5.3.4. Fe_2O_3-Cr_2O_3 loading and particle size were varied in each series of experiments. The analysed liquid products are shown in section 5.3.6.1 and 5.3.6.2 for the influence of catalyst loading and particle size on the liquid products, respectively.

5.3.6.1 Effect of Fe_2O_3-Cr_2O_3 catalyst loading on liquid products

The influence of Fe_2O_3-Cr_2O_3 loading and particle size parameters on the liquid products was studied. Fe_2O_3-Cr_2O_3 loading was varied from 5 to 32.1 g with d_{50} = 4 mm, Fe_2O_3-Cr_2O_3, and the results are shown in Fig.5.19.

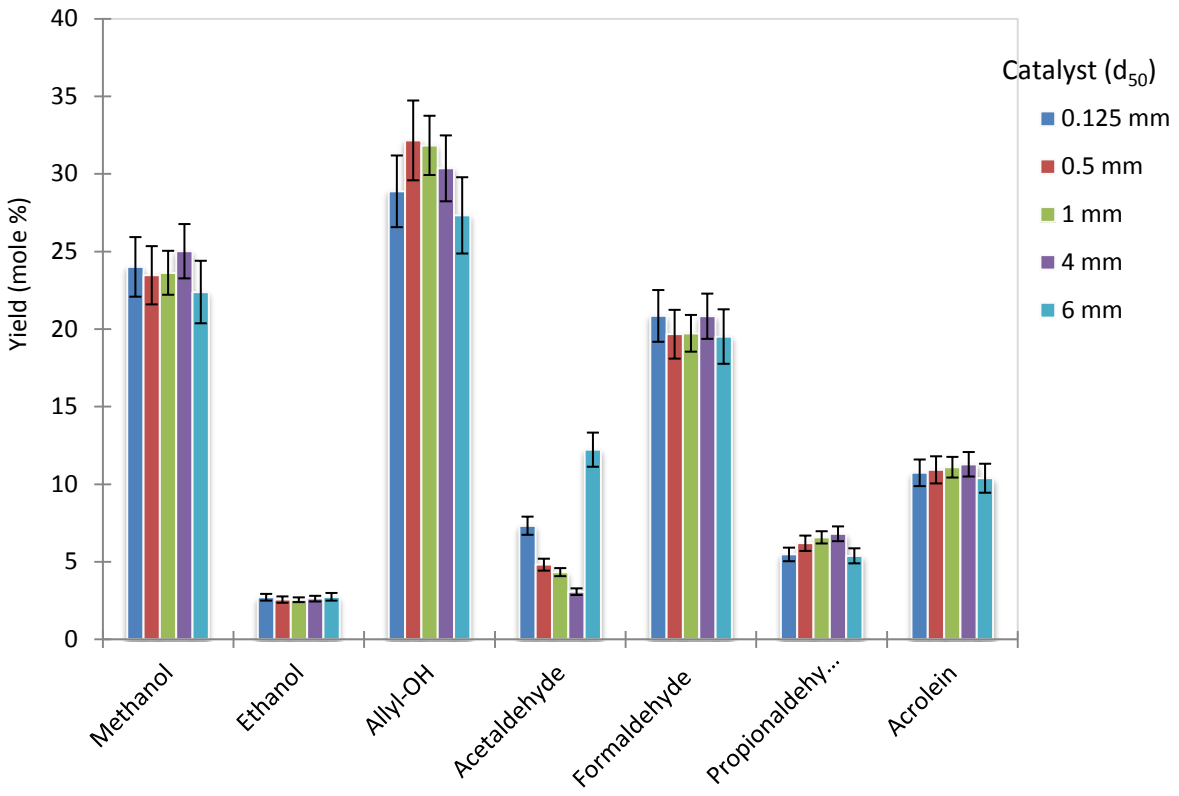

Fig. 5.19. Influence of d_{50}, Fe_2O_3-Cr_2O_3 on the liquid products yield;
Small reactor, 15 wt% pure glycerol, T=500°C, P=250 barg, WHSV=125 h^{-1}

The data in Fig.5.19 showed that Fe_2O_3-Cr_2O_3 loading has little effect on the liquid product composition and yield, which indicated that their formations were independent to catalyst loading. It is known that at a temperature above 290°C, glycerol degrades with or without catalyst into a mixture of product gas and condensable liquid products.

Methanol, allyl-alcohol and formaldehyde remain prominent in the liquid sample, which indicated their yields from the degradation of glycerol are influenced by the operating conditions such as high pressure and high temperature. The same liquid components were identified with similar compositions when the liquid samples of the non-catalytic SCWG of glycerol were analysed, which confirmed that Fe_2O_3-Cr_2O_3 did not influence the liquid product formation. It should be noted that the catalyst used in this work has no support and may have affected catalytic performance. Limiting factors for product yield would be the combination of catalyst loading and its activity. In addition, other parameters such as the diffusion of glycerol on the surface of the catalyst particle and the diffusion of gaseous products from the surface would have also influenced the rates of reaction and yield. In this case, the diffusion rate would have been dependent on many factors, such as the large catalyst particle size (4 mm Ø), the concentration of the reactants, the operating temperature inside the reactor bed and char formation on the surface of the catalyst caused from polymerisation reactions.

5.3.6.2 **Effect of Fe_2O_3-Cr_2O_3 particle sizes on liquid products**

In order to determine the effect of the catalyst particle size, a series of experiments was conducted in a small reactor using Fe_2O_3-Cr_2O_3 catalyst. Four different particle sizes (d_{50}) were selected between 0.1 and 6 mm while the operating parameters were kept constant; the results are showed in Fig.5.20

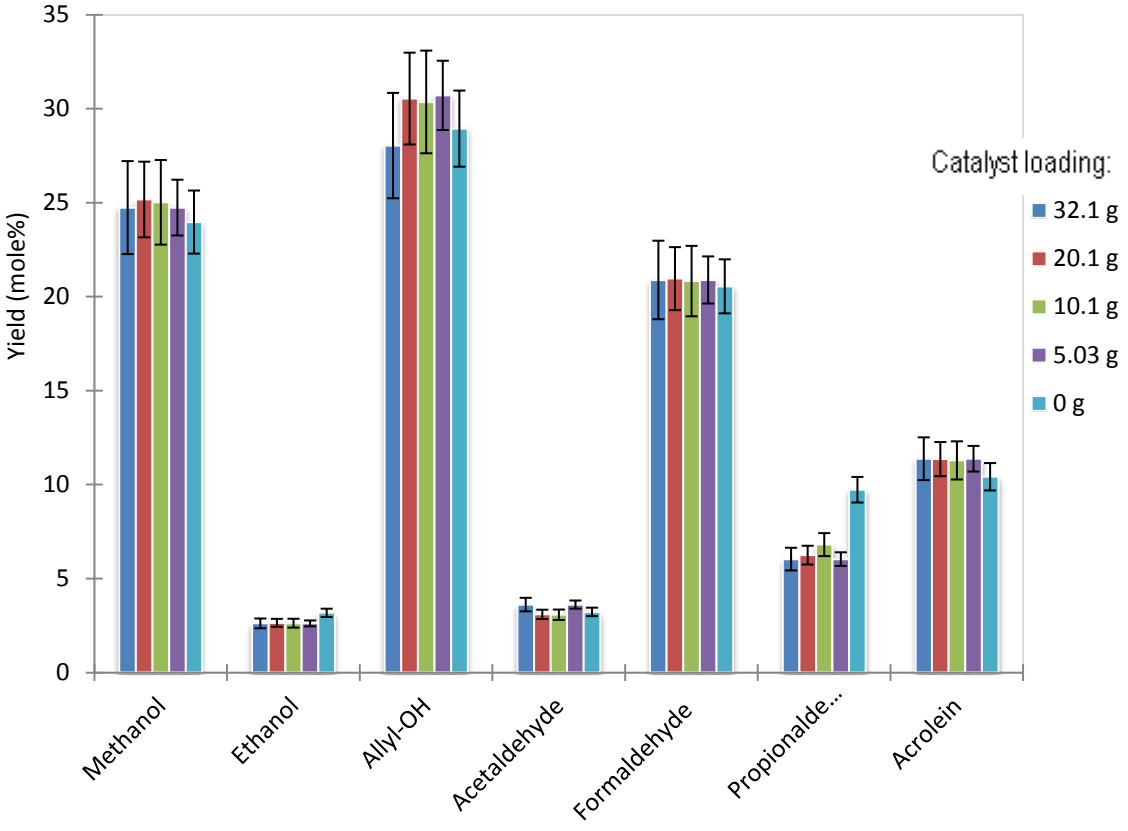

Fig. 5.20. Influence Fe_2O_3-Cr_2O_3 loading on the liquid products yield

Small reactor, 10.1 g of catalyst (d_{50}= 4mm), 15 wt% pure glycerol, T=500°C, P=250 barg, WHSV=125 h^{-1}

Allyl alcohol, methanol, formaldehyde and acrolein remained the main components in the liquid sample regardless of particle size; with yields above 10 mole% of the overall carbon-liquid product. Only small amounts of ethanol, acetaldehyde, and propionaldehyde were quantified in the liquid samples. This observation is consistent with the effect of catalyst loading. It can be concluded that Fe_2O_3-Cr_2O_3 particle size has an insignificant effect on liquid product formation in CSCWG at the reported conditions. Without catalyst, glycerol can decompose in SCW into the majority of the reported liquid products by ionic pathways or/and free radical pathways. The pH of the liquid product samples was measured, and it ranged between 4.7 to 5.1, due to the presence of organic acids such as formic and acetic acids. When d_{50} was reduced from 0.5 mm to 0.125 mm, the product gas yield was increased from 71.8 to 80.4 wt%, respectively. The overall, liquid product yield concomitantly decreased from 28.1 to 19.5 wt%. In addition, char products increased slightly from 0.5 to 0.8 wt%. This can be explained in terms of the porosity of reactor bed, which decreased from 0.47 to 0.39, and improved contact from increased tortuosity between the particle and reactant in the reactor bed leading to enhanced reforming. The overall, liquid product decreased in the same range of particle

size from 27.3 to 20.2 to 17.6 wt% while gas yield increased from 71.8 to 79.1 and 81.7 wt% when d_{50} was increased from 0.5 to 1 and to 4 mm, respectively. This result is probably due to the increase of metal dispersion that contributes to improve the catalyst activity and possibly to the increased in diffusion rate of feed on the surface of catalyst that contributed to improve the reaction of feed for better conversion; therefore improving the gasification yield.

5.4 Summary of pure glycerol over Fe_2O_3-Cr_2O_3 Catalyst

The degradation of glycerol was studied under sub and supercritical water conditions (170-250 barg and 400-550°C) using an Fe_2O_3-Cr_2O_3 (85:15 wt %) catalyst and a run time of up to 80 min. Pure glycerol was converted (up to 98% conversion) at temperature of 500°C into gaseous products largely containing hydrogen, methane and ethylene. In comparison to other gasification process, the gaseous product was relatively clean with only five components in the composition (H_2, CO, CO_2, CH_4 and C_2H_4) with low traces of char (< 2.7 wt %) on the overall products). In addition, other products of glycerol degradation were acetaldehyde, acrolein, allyl alcohol, and other un-identified products. The yields of acrolein, acetaldehyde, and allyl alcohol were as high as 11.2, 13.4, and 33.5 mole %, respectively. Complete conversion (100 mole %) of glycerol was achieved at 550°C as indicated by no trace of glycerol in the liquid sample analysis. Temperature, WHSV, and glycerol feed concentration appeared to have had an effect on the gaseous product yield. A temperature of 550°C is needed to achieve high gasification efficiency for up to 30 % wt glycerol concentration. However, pressure was found to have little effect on the gas composition and yield, except for H_2 and CO_2 by promoting WGS reaction.

The hydrogen and syngas yields were up to 60.1 and 61.4 mole% respectively, with a minimum mole ratio H_2: CO of ~3:1 largely attributed to high yield of H_2. Alternatively, the gaseous product obtained was richer in hydrocarbons: methane (14 mole %) and ethylene (69 mole %) and could be used as fuel gas with medium heating value for producing electricity through a turbine or SOFC or reforming to syngas. The Fe_2O_3-Cr_2O_3 catalyst exhibited potent stability after 9 h of operation, but was not selective at promoting the production 2:1 ratio of H_2: CO at the reported conditions. 2:1 ratio of H_2: CO is the desired syngas composition for FTS into mixed alcohols. The wide variety of products reflects the complexity of the reaction mechanisms involved in the hydrothermal decomposition of glycerol, which can be summarised in the coexistence of competing ionic and free radical pathways. In summary, the results have demonstrated also that:

- Without a catalyst complete glycerol conversion is not possible;

- Glycerol conversion increases at a higher operating temperature and decreases as the content of the feedstock increases.
- With the presence of Fe_2O_3-Cr_2O_3 catalyst, complete glycerol conversion can be achieved, even at a relatively high feedstock of up to 15 wt% at 550°C. The increasing of feed concentration above 20 wt% resulted in higher hydrocarbons yield (methane and ethylene) due to poor thermal and catalytic cracking.
- Evidence of Fe_2O_3-Cr_2O_3 physical transformation was observed after 172 hours on-stream with the presence of fragment particles on the surface, which is attributed to sintering of the metals. This has contributed significantly to loss of catalytic performance by reducing hydrogen and product gas yields.

CHAPTER 6. CSCWG OF CRUDE GLYCEROL

6.1 Introduction to CSCWG of crude glycerol

The previous chapter (5) established the optimal conditions for the decomposition of glycerol by the SCWG process. Various process parameters (WHSV, pressure, temperature, feed composition and time on stream) and catalytic parameters (catalyst loading and particle size) were studied and a summary highlights of the results are detailed in section 6.2. A study has reported that most organic wastes can be converted into useful biofuels and bio-chemicals by several routes including fractionation, liquefaction, pyrolysis, hydrolysis, fermentation, and gasification [**299**]. This chapter reports the utilisation of a crude glycerol generated as by-product during biodiesel manufacturing process as a feedstock for the CSCWG. Its availability, chemical functionality and low cost are the main advantages that make crude glycerol an attractive starting material for many processes. Crude glycerol can contain salt (KOH), sulphur, methanol and water content. However, in spite of this, the crude glycerol gasification in SCW has the potential to exhibit a positive impact on the biodiesel process. The first part of this study attempts to increase gas yields with a focus on hydrogen and syngas from the CSCWG of crude glycerol over Fe_2O_3-Cr_2O_3 catalyst. The second part discusses the use of Fe_3O_4 as an alternative catalyst at the reported best conditions. In the third section, the utilisation of pure glycerol and crude glycerol as feedstock in CSCWG are compared. Finally, the impact of Fe_2O_3-Cr_2O_3 and Fe_3O_4 catalysts on the CSCWG are evaluated.

6.2 Background experiments for best conditions determination

After studying various parameters for SCWG, the results have revealed the optimal experimental and reaction conditions for the production of higher yields of hydrogen and product gas (refer to section 5). As mentioned in the experimental methods, a PBR was formed by loading 32.1 g of Fe_2O_3-Cr_2O_3 catalyst (d_{50} = 4 mm) in 30 ml reactor. A series of experiments were carried out to assess the effect of the catalyst (refer to section 5). After an intensive review of the literature, it appears that no previous work has reported on the utilisation of low cost of iron oxide-chromium oxide or/and magnetite as catalysts for CSCWG. Some studies have reported on the utilisation of metals such as Rh, Zn, and Ni [**300, 301, 302, 303**] for the CSCWG of biomass. However, these metals are expensive, and are used

primarily to promote activity toward hydrogen, compared to the utilisation of cheap catalysts like Fe_2O_3-Cr_2O_3 or/and natural Fe_3O_4, which have the potential to increase the overall product gas yield.
In chapter (5), the effect of temperature, pressure, feed concentration, WHSV and the effect of time on stream were examined in a series of experiments at variable parameters, using inexpensive catalyst (Fe_2O_3-Cr_2O_3) and the best conditions for hydrogen and syngas- rich gas are summarised in tables 6.1 and 6.6, respectively.

6.3 CSCWG of crude glycerol over Fe_2O_3/Cr_2O_3 Catalyst for H_2 production

A summary of the best conditions for H_2-rich gas production is shown in table 6.1. The parameter range of study was limited by the maximum operational value for some of the process equipments (reactor temperature: 550°C max, pump flow capacity: 4.71 Lh^{-1} for water, at 20 °C, viscosity: 1.04 mPa.s max), and for practical constraints (e.g. feed concentration above 30 wt% was plugging the pressure regulator due to tar formation).

Table 6.1. Summary of the best conditions for H_2-rich gas production from a small reactor

Parameters	units	Range of study	Best conditions for H_2 –rich gas
Feed used:		pure glycerol	
Feed concentration	wt%	2 to 30	2-5
Pressure	barg	170 to 270	250
Temperature	°C	350 to 550	550
WHSV	h^{-1}	19 to 125	125
Catalyst selection:		Fe_2O_3/Cr_2O_3	
Particle size	mm	0.1 to 6	4
Loading	g	0 to 32 g	10.2
Bed porosity	fraction	0.2	0.2

6.3.1 Ascertaination of experimental errors

The experimental errors for CSCWG of crude glycerol over Fe_2O_3/Cr_2O_3 catalyst were evaluated by running three experiments at the same conditions as shown in table 6.2. Gas samples were collected in the same manner as described in the experimental section 3.7 (after 5 min of and thereafter every 15 min). The experimental conditions and the cumulative value of the gas composition over run time and the margin of error are shown in table 6.2. The experimental error was evaluated by calculating the

errors produced in the gas composition from repeating an experiment several times (3 times minimum) on different days.

Table 6.2. Summary of the experimental errors determination.

In a small reactor, f*eed concentration was 5 wt% crude glycerol, system pressure, 250 barg, temperature: 550 °C, WHSV: 125 h^{-1}, catalyst: Fe_2O_3-Cr_2O_3, d_{50} of 3.5 mm cylinder with 4 mm diameter, loading: 10.2 and $\varepsilon = 0.2$*

	Run_E79	Run_E80	Run_E81	Average value after 3 runs	Relative error margin
Cumulative gas composition (mole %)					
H_2	39.2	41.9	41.7	40.9	± *1.68*
CO	5.7	1.9	2.1	3.3	± *2.49*
CO_2	8.7	4.5	5.5	6.2	± *2.46*
CH_4	19.4	20.6	20.6	20.2	± *0.77*
C_2H_4	22.8	19.6	19.6	20.7	± *2.09*
C_2H_6	0.5	0.8	0.8	0.7	± *0.24*
C_3H_8	3.3	10.3	10.2	7.9	± *4.61*
Syngas	44.9	43.8	43.8	44.2	±*2.08*
Products gas yield (wt %)	89.0	85.8	88.1	87.6	± *1.87*
Liquid products yield (wt %)	10.6	14.6	11.4	11.9	± *2.72*
Char yield (wt %)	0.3	0.4	0.3	0.3	± *0.06*
Glycerol conversion (%)	86.9	90.5	89.3	88.9	±2.00

The maximum error margins obtained were up to 4.61 for C_3H_8 yield. Its formation may result from side reaction such as aqueous reforming of glycerol over the metal catalyst by free radical pathways [**304**]. However, due to the complex composition of glycerol such as free fatty acids, unidentified side reactions may have contributed to the product gas formation. The experimental errors are acceptable. However, it can be suggested that the uncertainty of the experimental errors is largely attributed to the activity of the catalyst. Many other factors affect the activity of the catalyst such as temperature, pressure, method of preparation, particle size, and shape of packing. However, the challenge is to keep the entire variable constant while one of them is being studied.

6.3.2 Influence of Fe_2O_3/Cr_2O_3 CSCWG of crude glycerol for H_2 and product gas

Crude glycerol composition can contain methanol, inorganic (Ca, K, Mn and S), water, fat, ash and other compounds depending on the primary feedstock [**305**]. This variation in composition could play a role in the gasification reaction; heavy molecules of fat could be poorly gasified, whereas methanol has the potential to enhance the gasification rate. Section 5 has demonstrated that the hydrogen content in the gaseous product stream can be increased by the lowering the feed concentration. The goal of using crude glycerol was to study the CSCWG reaction on real organic wastes to give a product gas. Four experiments were performed under the best hydrogen conditions reported in section 5.2 and table 6.1. Table 6.3 summarises the operating conditions and the product yield results for CSCWG of crude glycerol over iron oxide catalysts at 550°C.

Table 6.3. Influence of Fe_2O_3-Cr_2O_3 on CSCWG of crude glycerol for hydrogen production from a small reactor.

Experimental conditions	5 wt% crude glycerol 550°C, 250 barg, 125 h^{-1}, $\boldsymbol{\varepsilon = 0.4}$, d_{50}=2mm, 10.1g	5 wt% crude glycerol 550°C, 250 barg, 125 h^{-1}, $\boldsymbol{\varepsilon = 0.6}$, d_{50}=2mm, 10.1g	5wt% crude glycerol 550°C, 250 barg, 125 h^{-1}, $\boldsymbol{\varepsilon = 0.6}$, d_{50}=2mm, 10.1g	5 wt% crude glycerol 550°C, 250 barg, 125 h^{-1}, $\boldsymbol{\varepsilon = 0.4}$, d_{50}=2mm, 10.1g
Gas composition (mole %)				
H_2	57.4	37.8	35.8	48.9
CO	3.04	7.9	4.5	6.1
CO_2	12.7	17.9	9.6	7.6
CH_4	5.1	17.2	13.3	5.7
C_2H_4	12.1	9.5	23.9	22.5
C_2H_6	3.7	2.0	1.4	3.7
C_3H_8	5.7	7.3	11.2	5.1
Syngas	60.4	45.7	40.3	55.0
Products gas yield (wt %)	72.5	74.0	62.7	82.1
Liquid products yield (wt %)	26.6	25.1	36.1	17.3
Char yield (wt %)	0.8	0.7	1.1	0.5
Glycerol conversion (%)	95.6	98.9	85.4	96.4

On run E56, hydrogen yield reached 57.4 mole %, due to the optimal reaction conditions such as high temperature (550°C); low feed concentration (5 Wt %), high pressure (250 barg), optimal catalyst

loading (10.1 g) and catalyst particle size (refer to section 6.2). On the other hand, CO yield was smaller (3 mole %), coupled with a lower yield of methane (5.1 mole %) and a high yield of CO_2 (12.2 mole %). This suggested that aqueous-phase reforming of methane ($CH_4 + H_2O \rightarrow CO + 3H_2$) and water gas shift reaction ($CO + H_2O \rightarrow CO_2 + H_2$) were the main contributors to the high yield of H_2 and low yield of CO. As expected, WGS and H/C's cracking by thermal or/and catalytic effect favoured the formation of hydrogen as explained in chapter 5.

On the other hand, run E54 showed that char and hydrogen yields were lower 0.78 mole % and 37.8 mole%, respectively, and coupled with a higher yield of methane (17.26 mole %) and CO_2 (17.92 mole %). This is attributed to the increase gas-solid reactions such as $C_{(S)} + 2H_2O \rightarrow CH_4 + CO_2$, which resulted from carbon-SCW reforming. In general, gas-solid reactions could be promoted by high temperature (>700°C), but this was not the case (maximum temperature 550°C), which indicated that SCW may play a significant role on char gasification. Black deposits on the inner of the reactor and the darkness/carbonisation of the used catalyst, compared with a brown colour of the fresh catalyst were evidence of char formation (0.7 g). The ESEM analysis confirmed the identification of a trace amount of coke (C) on the chemical composition of the used catalyst. However, other factors such as reactant and char interaction with catalyst surface might have contributed to promote gas-solid reactions. High yield of CO (7.9 mole %), coupled with low yield of hydrogen (37.8 mole %) have supported the argument that secondary reactions may have played a prominent role at the expense of WGS.

The product analysis has showed that on runs E56 and E54 the respective product gas yields were 72.5 and 74.1 wt%. A significant yield of liquid products (26.6 and 25.1 mole%, respectively) compared to run E59b were obtained. The yield of product gas at the report conditions may be attributed to the crude glycerol feed composition used, which contains various impurities and other organic materials, such as fatty component that poorly gasified in aqueous conditions. In effect, those unconverted or non-gasified impurities could accumulate on the catalyst pores, blocking access of reactant on the catalyst active surface, resulting in loss of catalyst activity. The discrepancy of the hydrogen yield obtained at the similar experimental conditions (refer to E54, E55 and E56) suggested that pores filling and blocking with reactants was contributing on the catalyst lost of activity. On the other hand, the ESEM analysis showed that no structure transformation of catalyst at this stage. This is probably because of the limited time on-stream (only 6 h) in SCW. It can also be seen in Fig.6.7 (a and c) that the structure of fresh and used Fe_2O_3/Cr_2O_3 were similar as evidenced by lack of fragmentation, and no signs of sintering (refer to Fig.6.7).

The gas product yield was higher (82.1 wt %) on run E59b than on run E54 and E56. This may be due to increasing of bed porosity (void fraction) from 0.47 to 0.65, which contributed to increase external

mass transfer of the reactants on the surface of the catalyst. In other terms, the increase of product gas can be attributed to the drop of the volume of catalyst from 53 % to 35 % of the reactor volume.

Gaseous products formation: At the reported SCW conditions, glycerol decomposes under the thermal and catalytic effects as expected. A molecule of glycerol decomposes and absorbed on the metal crystallite sites while water is dissociated into H^+ and OH^-, and are also absorbed on the metals sites. Hydrogen could be produced either by dehydrogenation from the dissociated molecule or/and from the reaction of OH with the molecule of glycerol. The product gas may be formed primarily by free radical reactions, which are influenced by the increased temperature. High pressure can decrease their formations by free radical reactions [**306**]. Nevertheless, high pressure (refer to section 5.3.3.2) has been shown to promote WGS reaction to give high yields of hydrogen. The results have demonstrated that gaseous products were the leading products of glycerol decomposition at the conditions test, compared to liquid and char. This indicates that CSCWG over Fe_2O_3/Cr_2O_3 may be an effective route for the crude glycerol decomposition into gaseous products.

6.3.3 Influence of Fe_2O_3/Cr_2O_3 on CSCWG of crude glycerol for syngas production

As reported in the previous chapter 5, a large particle size ($d_{50} > 2$ mm) Fe_2O_3-Cr_2O_3 would have also contributed to the gas and hydrogen yields. However, size alone could not be solely responsible for the degree of catalyst activity. Other factors such as the catalyst was not supported, the porosity of the reactor bed or/and particle fluidization could have influenced the catalytic performance. In addition, when the product gas sample was left overnight in the separator, a spike change of the hydrogen yield was observed, after gas sample analysis (details are provided in appendix R). This is attributed to the improved settling of the gas-liquid phases in the separator (turbulence is reduced significantly over time after stopping the experiment, which enhances the separation).

Table 6.4 shows the experimental conditions and the products (gas, liquid and char) yield results for the CSCWG of crude glycerol using Fe_2O_3/Cr_2O_3 catalysts for the production of a target 2:1ratio of H_2: CO. To improve the syngas content, the feed concentration of glycerol: water ratio was increased to 15:85 (refer to effect of feed concentration on sub-section 5.3.3.4). This was to increase the carbon contribution on product formation while maintaining a high level of hydrogen in the product. Chapter 5 established the best operating conditions for producing syngas over Fe_2O_3-Cr_2O_3 catalyst. Similar operating conditions are used for the CSCWG of crude glycerol as shown in Table 6.4.

Table 6.4. Influence of iron oxide on CSCWG of crude glycerol for syngas production *over Fe_2O_3-Cr_2O_3*

Experimental conditions	15 wt% crude glycerol 500°C, 210 barg, 125 h^{-1}, $\boldsymbol{\varepsilon = 0.6}$, d_{50}= 6 mm, 10.1g	15 wt% crude glycerol 550°C, 250 barg, 125 h^{-1}, $\boldsymbol{\varepsilon = 0.6}$, d_{50}= 6 mm, 10.1g	15 wt% crude glycerol 500°C, 250 barg, 125 h^{-1}, $\boldsymbol{\varepsilon = 0.6}$, d_{50}=6 mm, 10.1g
Gas composition (mole %)			
H_2	22.6	42.1	37.8
CO	7.1	6.3	7.2
CO_2	7.7	11.7	14.4
CH_4	16.8	10.3	9.3
C_2H_4	21.5	13.0	17.5
C_2H_6	9.9	3.2	1.5
C_3H_8	15.1	13.1	11.5
Syngas	28.7	48.4	45.0
Product gas yield (wt %)	73.3	78.5	67.7
Liquid products yield (wt %)	25.6	20.9	30.8
Char yield (wt %)	1.1	0.6	1.5
Conversion efficiency (CE) %	73.7	84.3	75.2

Table 6.4 shows that increasing the feed concentration to 15 wt% gave an increase CO yield of ~7.2 mole% as compared to Table 6.2. At higher feed concentration, polymerisation reactions have increased. The catalytic and thermal cracking of hydrocarbons and char, which could contribute to increase the syngas yield may have been lowered, due to the choice of catalyst and the influence of the temperature range.

It can be seen in Table 6.4 that a minimum of 3:1 ratio of H_2:CO was obtained on run E60, but with low yield of syngas of 28.6 mole%. This is attributed to low pressure (210 barg) that would have contributed little to hydrogen formation as compared to high pressure over 250 barg (SCW). On the other hand, the H_2:CO ratio increases to 6:1 on run E61 with an increase yield of syngas (48.3 mole %), due to the increasing hydrogen content at higher pressure.

Syngas yield remains lower on all three runs (E60, E61 and E62) compared to table 6.4. However, the lower yield of syngas was compensated with reduce ratio (3:1) of H_2:CO. This was due to two factors:

(i) the operating temperature up 550°C only; the literature review has indicated that a high temperature (>700-800°C) could be used to increase CO yield in SCWG. Potential pathways to increase syngas yield lies in thermal or/and catalytic reforming of hydrocarbons. (ii) The activity of catalyst was not able to compensate at lower temperatures studied. The catalyst has shown little evidence of deactivation at the early stages (cumulative of 9 h on-stream) of the tests (Refer to Appendix M). i.e. as a result of low COD conversion and low recovery of carbon gases. These results indicated that temperature and pressure alone at the experimental conditions studied have not significantly improved the syngas yield. The feed concentration is also a valuable parameter for the production of syngas by SCWG as explained in section 5.3.3. High glycerol feed concentration above 15 wt% contributes to increased CO yield but at the expense of hydrogen yield. However, it was not possible to complete a successful run at high feed concentration >30 wt% with crude glycerol due to ongoing blockage on the pressure regulator and fittings, as a result of high viscous condensate liquid products.

On the other hand, selection of a more effective catalyst would have an important role if high yield of syngas with a 2:1 ratio is required. These results have demonstrated that the selection of the catalyst Fe_2O_3/Cr_2O_3 and the experimental conditions (reaction temperature<550°C) were not sufficient for the production of high yield of syngas with 2:1 ratio of H_2:CO due to the low yield of CO.

6.3.4 Influence of run time on gaseous products of the crude glycerol over Fe_2O_3/Cr_2O_3

The influence of run time on the gas product yield was studied by running each experiment for a minimum of 65 min. The glycerol feed was introduced into the small reactor at the desired operating conditions. Gas sample was collected after the first five, and subsequently after every 15 min (refer to the experimental procedure on chapter 3). Fig 6.1 shows the influence on run time on the gaseous product formations and yields.

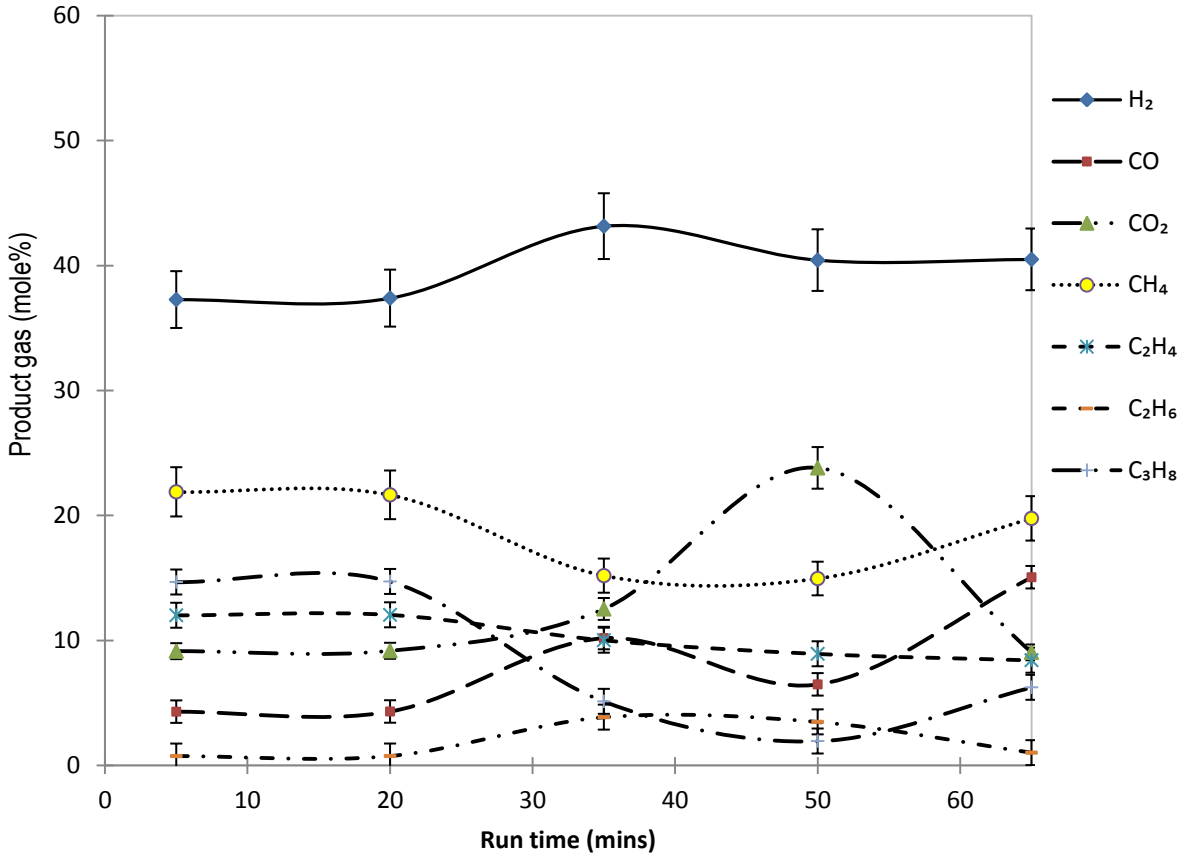

Fig 6.1. Product gas as a function of run time, run_ E54;

Small reactor, feed: 5 wt% crude glycerol, system pressure: 250 barg, Temperature: 550 °C, WHSV: 125 h^{-1}, catalyst type: Fe_2O_3-Cr_2O_3, catalyst loading: 10.1 g. d_{50}=2 mm,

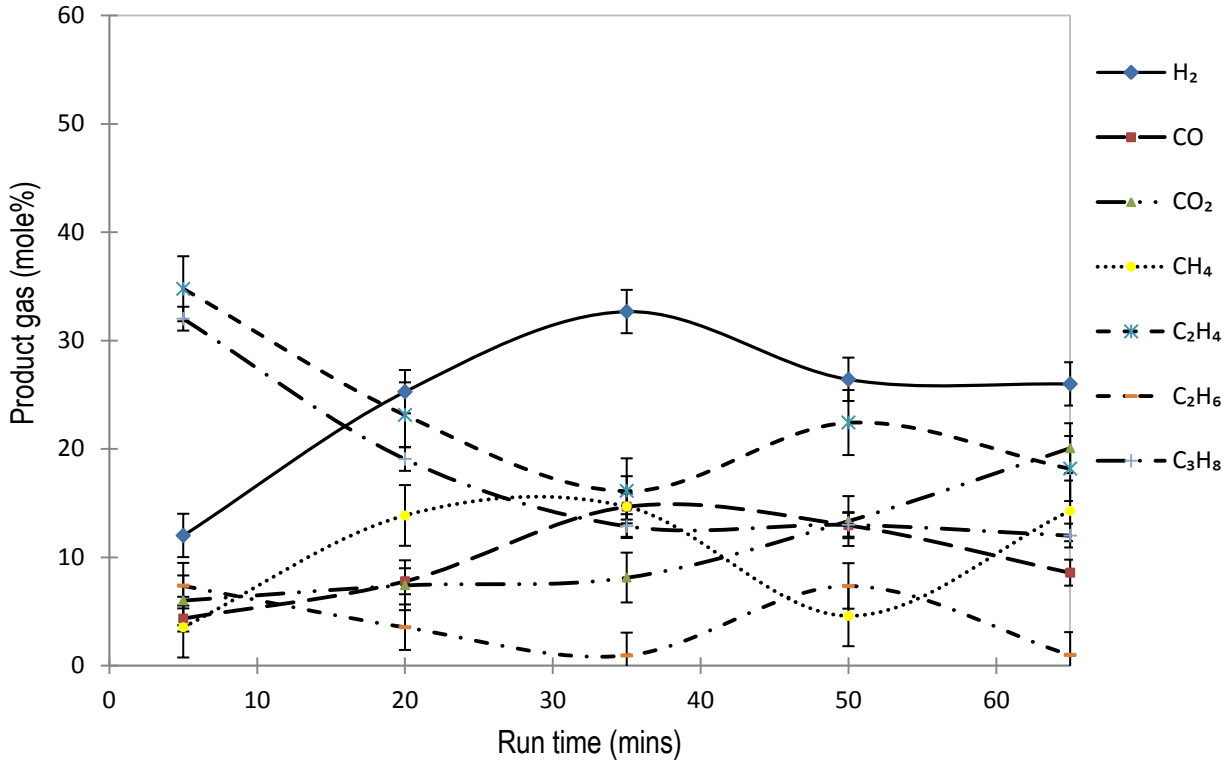

Fig 6.2. Product gas as a function of run time, run_ E60;

Small reactor, feed: 15 wt% crude glycerol, system pressure: 210 barg, Temperature: 500 °C, WHSV: 125 h^{-1}, catalyst type: Fe_2O_3-Cr_2O_3, d_{50}= 6 mm, catalyst Loading: 10.1 g.

It can be seen that the yield of each gaseous compounds does not increase linearly with run time, which indicates that their relative yields are dependent on the run time and activity of the catalyst. Hydrogen formation in CSCWG appears to be more complex than anticipated and cannot be fully summarised in this work. Further investigations may be needed (see suggestions for future work in section 7). However, the reaction mechanisms that should be considered for hydrogen formation include hydrolysis, pyrolysis, isomerisation, dehydration, condensation of liquid products, and SCW reforming reactions [**307, 308**]. Other factors such as the porosity of reactor bed, which influences the mass transfer, may have played a pivotal role on the product gas formation.

Fig 6.1 and Fig 6.2 showed that hydrogen, methane and ethylene yields changed significantly with run time. This was due to gas-phase side reactions such as the hydrogenation of ethylene to produce ethane (ethanation) or methane reforming in SCW. It can be observed in Fig.6.2 that when hydrogen yield decreases with run time, there is a simultaneous increase in methane or/and ethylene. In contrast, when hydrogen yield increases with run time, the methane or ethylene yields decreased. This

may have occurred due to mass transfer issues; inconsistent interaction of reactants and catalyst surface with run time, which can be attributed to adsorption and desorption of reactants and products on the catalyst sites.

6.3.5 Liquid products from the CSCWG of crude glycerol over Fe_2O_3/Cr_2O_3

The liquid products from the CSCWG of crude glycerol over Fe_2O_3/Cr_2O_3 were also analysed. The investigation was carried out consistently using the same equipment and analytical methods described in chapter 3. It can be observed in Fig.6.3 that the crude glycerol changed colour with run time under SCW conditions, compared to pure glycerol (which is clear and homogeneous but not shown here).

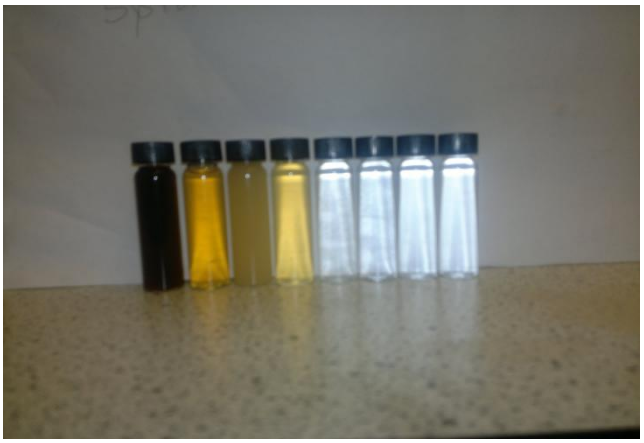

Fig.6.3. Liquid products samples appearance

(From left to the right: crude glycerol before gasification, a dilute 5 wt% crude glycerol/deionised water solution, subsequent liquid samples after gasification at 5, 20, 35, 50, 65 and 80 mins).

Small reactor, T=550°C, P=250 barg, WHSV=125 h^{-1}

It is evident that the initial sample of the crude glycerol at the reported concentration was dark/brown, and then it became progressively clear and transparent solution as the gasification progressed. This is due to an initial slow reaction rate (low catalytic activity) of glycerol decomposition, which led to its polymerisation. Subsequently, this initial slow reaction is followed by progressive gasification (high activity) in the reactor giving a variable degree of reactant conversion as a function of run time. In contrast, pure glycerol is transparent initially, and it remains clear and homogeneous during and after gasification in SCW. Table 6.5 summarises the liquid products identified and quantified from different samples.

Table 6.5. Liquid products summary for the CSCWG of crude glycerol over Fe_2O_3-Cr_2O_3

Small reactor, T=550°C, P=250 barg, WHSV=125 h^{-1}

Experiments	Run E54	Run E55	Run E56	Run E59	Run E60	Run 61	Units
Liquid products							mole%
Formaldehyde	19.81	20.28	20.17	19.23	20.89	17.33	
Acetaldehyde	6.26	6.78	6.65	11.44	4.22	18.87	
Propionaldehyde	6.31	5.78	6.34	5.49	6.57	4.96	
Acrolein	10.68	10.87	10.83	10.31	11.03	9.25	
Valeryaldehyde	4.08	5.52	3.99	3.96	3.51	3.87	
Methanol	25.44	24.61	24.72	23.48	24.11	22.64	
Ethanol	2.53	2.58	2.81	2.43	2.79	2.58	
Allyl alcohol	28.92	29.01	28.44	27.27	30.2	24.29	
Glycerol Converted	90.4	85.4	95.6	96.4	73.7	84.3	%

Note that the product gas and liquid product were considered for the calculation of percentage conversion of glycerol; the peak area of the glycerol in each liquid sample was used to determine the concentration and amount of glycerol in the sample. The concentration value was divided by the input amount of glycerol in the feed, which was based on the peak area of the feed concentration being studied.

In addition to the condensable liquid products reported in Table 6.4, the intermediate products of crude glycerol decomposition and/or polymerization were a complex mixture, which included a small amount of unknown/unconverted organic materials. The undesirable impurities such as metals and fat presented in the feed were difficult to gasify, which resulted in a much lower conversion of crude glycerol at 550°C. The experimental results indicated that conversion of crude glycerol was 91 % at 550°C, whereas complete conversion was reached when pure glycerol was used at a similar feed concentration.

Chapter 5 also demonstrated that glycerol decomposes to gaseous products (H_2, CO, CO_2, CH_4, and C_2H_4), liquid products (methanol, ethanol, allyl-OH, acrolein, acetaldehyde, formaldehyde and propionaldehyde) and char. This product composition is similar to that reported by references **309** and **310** with the exception of allyl alcohol and propionaldehyde that were also identified in the liquids products.

Liquid Products formation: The presence of condensable liquid products in SCW, point to their formation either by free radical reaction or/and ionic pathways under the influence of pressure less than SC condition and temperature. Section 2 has indicated that high temperatures (>374°C) or/and lower pressures (<221 barg) tend to favour the radical reaction pathway of product formation, whereas high pressures (>221barg) and/or lower temperatures favour product formation by ionic reactions routes in SCW.

A study has demonstrated that various metal catalysts including iron oxide based ones can be used, to influence methanol and oxides reaction at >250°C to produce formaldehyde according to the chemical equation: $CH_3OH + 2O^- \rightarrow H_2CO + H_2O$. At room temperature, formaldehyde is a gas; however, it is readily soluble in water [**311**]. The formation of formaldehyde easily results from the incomplete combustion of carbon-containing materials, as evidenced by the remaining amount of un-reacted glycerol; 145 g (representing 16.6% of the total input of 875 g) identified in the liquid product analysis. In addition, formaldehyde can thermally decompose into H_2 and CO in the absence of O_2 in supercritical water, according to reaction; $HCOH \rightarrow CO + H_2$ [**312**]. A high yield of hydrogen and a relatively low yield of formaldehyde are evidence of this type of secondary reaction.

Acetaldehyde could dissociate to produce methane and CO following the reaction:

$$CH_3CHO \rightarrow CH_4 + CO \quad (5.3),$$

Whereas low yield of ethanol accompanied by the high yield of ethylene could indicate a possible oxygenation to make formaldehyde or dehydrogenation to acetaldehyde following equation 5.4;

$$C_2H_5OH \rightarrow CH_3CHO + H_2 \quad (5.4)$$

On the other hand, ethanol proved to be kinetically stable in SCW. Dehydration to form ethylene occurs at a significant rate only at elevated temperatures [**313**].

Another study has reported that hydrogen can be obtained directly from the methanol by partial oxidation with the available oxide, decomposition or reforming in SCW [**314**]. However, methanol formation could occur via direct hydrogenation of CO, but at a much slower rate [**315**] following the reactions below.

$2H_2 + CO \Leftrightarrow CH_3OH$, (5.5) or from synthesis gas proceeding via the water gas-shift reaction

$CO + H_2O \Leftrightarrow H_2 + CO_2$ (5.6) Water-gas-shift

$3H_2 + CO_2 \Leftrightarrow CH_3OH + H_2O$ (5.7) Hydrogenation of carbon dioxide

6.4 CSCWG of crude glycerol over Fe_3O_4 for H_2 and syngas production

A summary of the best conditions (refer to section 5.2) for syngas production is shown in table 6.6. The parameter range of study was limited by the maximum operational value for some of the process equipments (reactor temperature: 550°C max), catalytic parameter (d_{50}= *6 mm* max) and for practical raison (e.g. feed concentration above 30 wt% was plugging the pressure regulator due to tar formation).

Table 6.6. Summary of the best conditions for syngas production over Fe_2O_3-Cr_2O_3 in a small reactor

Parameters	units	Range of study	Best conditions for syngas
Feed used		pure glycerol	
Feed concentration	wt%	2 to 30	15
Pressure	barg	170 to 270	250
Temperature	°C	350 to 550	550
WHSV	h^{-1}	17 to 125	125
Catalyst selection:		Fe_2O_3-Cr_2O_3	
Particle size (d_{50})	mm	0.1 to 6	6
Loading	g	0 to 32 g	10.1
Bed porosity	fraction	0.6	0.6

6.4.1 Ascertaination of experimental errors

The experimental errors for CSCWG of crude glycerol over Fe_3O_4 were evaluated by running 3 experiments at the same conditions as shown in table 6.7. Gas samples were collected in the same way as described in the experimental section 3 (after 5 min and subsequently every 15 min). The experimental conditions and the cumulative value of the gas composition over run time and their margins of error are shown in Table 6.7. The experimental error was evaluated by calculating the errors in the gas composition from repeating an experiment several times (3 times minimum) on different days.

Table 6.7. CSCWG of crude glycerol over Fe_3O_4

Small reactor, feed: 5 wt% crude glycerol, system pressure: 250 barg, temperature:550°C, WHSV: 125 h^{-1}, catalyst:Fe_3O_4, d_{50}=2 mm, catalyst loading:10.1 g, and ε =0.5.

Experimental number	Run E71	Run E72	Run E73	Average value after 3 runs	Relative error (mole %)
Cumulative gas composition (mole %)					
H_2	49.8	52.9	57.1	53.3	±*3.82*
CO	4.2	5.6	3.1	4.3	±*1.20*
CO_2	4.6	19.1	5.9	9.9	±*9.01*
CH_4	2.1	3.7	14.3	6.7	±*7.58*
C_2H_4	26.9	12.7	10.9	16.8	±*10.58*
C_2H_6	2.0	1.1	0.7	1.2	±*0.70*
C_3H_8	10.0	4.6	7.6	7.4	±*2.56*
Syngas	54.0	58.5	60.2	57.6	±*2.51*
Products gas yield (wt %)	81.7	89.3	90.6	87.2	± *5.55*
Liquid products yield (wt %)	17.7	10.3	9.1	12.3	± *3.31*
Char yield (wt %)	0.6	0.4	0.3	0.5	±*0.24*
Glycerol conversion (%)	98.8	99.1	99.8	99.2	±0.43

It can be seen that the maximum error obtained were up to ±10 of the gas composition. The maximum error bound was observed for CO_2 and C_2H_4 with values of 9 and 10 mole%, respectively. This indicated that side reactions involving CO_2 or/and C_2H_4 were highly contributing to the product gas formation and their relative yield. The mechanism of gaseous products formation could be more complex as suggested by free radical pathways. Many other factors affect the activity of the catalyst such as temperature, pressure, method of preparation, particle size, and shape of packing as discussed in sections 5.3.3 and 5.3.4. Catalyst activity was changing with run time as reflected by the fluctuation/variation in the peak profile similar to Fig.6.2. Catalyst performance can be extremely difficult to control or to predict. This is probably the main reason of the error margin of up to ±10 mole%, which is however acceptable.

6.4.2 Influence of Fe_3O_4 Catalyst on CSCWG of crude glycerol for hydrogen production

The CSCWG of crude glycerol for hydrogen production over variable particle sizes of Fe_3O_4 was studied. All runs were carried out at the same temperature and pressure. Feed concentrations (5 wt %) and catalyst loading (10.2 g) were the same for runs E68 and E74. The gasification experiments and analysis of products were carried out in a similar way as described in section 3. The reaction conditions and results are summarised in table 6.8.

Table 6.8. Influence of magnetite on CSCWG of crude glycerol for hydrogen production over Fe_3O_4.

Experimental conditions	15 wt% crude glycerol 550°C, 250 barg, 35.7 h^{-1}, $\boldsymbol{\varepsilon = 0.2}$, d_{50}= 0.15 mm, 83 g	5 wt% crude glycerol 550°C, 250 barg, 125 h^{-1}, $\boldsymbol{\varepsilon = 0.5}$, d_{50}= 2 mm, 10.2 g	5 wt% crude glycerol 550°C, 250 barg, 125 h^{-1}, $\boldsymbol{\varepsilon = 0.5}$, d_{50}= 4 mm, 10.2 g
Gas composition (mole %)			
H_2	54.7	49.1	61.9
CO	3.3	5.0	6.5
CO_2	23.2	11.9	16.2
CH_4	5.1	19.1	3.3
C_2H_4	8.1	7.3	7.5
C_2H_6	2.8	3.6	0.6
C_3H_8	2.5	3.6	3.7
Syngas	58.0	54.1	68.4
Products gas yield (wt %)	90.1	91.8	91.9
Liquid products yield (wt %)	9.7	8.1	8.10
Char yield (wt %)	0.3	0.2	0.2
Glycerol conversion (%)	90.2	92.0	99.9

It can be seen in table 6.8 shows that hydrogen yields were higher; 54.7 and 61.9 mole% for runs 63 and 74, respectively, than those in run E68 (49 mole%). This is attributed to the difference in catalyst d_{50} (0.15 and 4 mm diameter for run 68 and 74, respectively); given that the bed porosity was similar (0.56), and the other experimental conditions were kept the same. The large particle size (d_{50}= 4 mm) has resulted in high gas yield coupled with better hydrogen formation, which can be attributed to better metal dispersion on the large particle size of the catalyst. High hydrogen yield, coupled with improved

CO_2 yield indicated that WGS reaction may be occurring prominently over undesired reactions such as char hydrogenation for methane formation. In fact, Table 6.8 shows that high yield of hydrogen was coupled with low yield of methane on runs E63 and E74, which indicated that methane reforming following the reaction $CH_4 \rightarrow C + 2H_2$ has occurred. On the other hand, CO yield remains low in all three runs, which also indicated that neither the temperature (550°C)studied nor the Fe_3O_4 catalyst choice was able to promote high yield of CO formation. However, low yield of CO may be also attributed to carbon deposition that has occurred within a Boudouard reaction ($2\ CO \leftrightarrow C + CO_2$). A relative high yield (2.7 wt% dry) of identified carbon on the used catalyst sample by ESEM analysis is evidence of char formation and deposition on the catalyst. Un-gasified char deposition on the catalyst contributes to its loss of activity and degradation due to mass transport limitations as mentioned in section 5. However, the lower value of COD (<1395 mg/l) in the liquid sample is evidence that the catalyst was still active. Light hydrocarbons (CH_4, C_2H_4, C_2H_6 and C_3H_8) were identified in the product gas stream, but their respective yield remains lower in each run, compared when crude glycerol was used over the proprietary Fe_2O_3/Cr_2O_3 catalyst (refer to table 5.2). This is clear evidence of catalytic cracking of H/C's' over Fe_3O_4 that contributes to the high yield of hydrogen formation. Little structure change was observed at the early stage of magnetite (6 h on stream); there was evidence of fragmentation into small particles (refer to Fig.6.7) are signs of this minor transformation after 9 h on-stream. Continuous exposure in SCW for longer hours could lead to severe degradation due to thermal or/and SCW effects. However, the time at which this catalyst may deactivate cannot be fully established at this stage due to the shorter exposure time on stream (9 h only).

6.4.3 Influence of *Fe_3O_4* Catalyst on CSCWG of crude glycerol for syngas production

In this section, low feed concentration (5 wt% crude glycerol) was maintained as well as catalysts selection (magnetite). However, catalyst parameters such as maximum loading, particle size were varied in order to evaluate their impact on the syngas content (2:1 ratio, H_2: CO was desirable for reason explained in section 2) for the crude glycerol CSCWG over Fe_3O_4. A series of experiments were performed in the same way as described in section 3 (refer to section 3.5) over the Fe_3O_4; (refer to section 3 for the particle size distribution of Fe_3O_4). The operating conditions and results for CSCWG of crude glycerol over Fe_3O_4 for syngas production are summarised in table 6.9.

Table 6.9. Influence of magnetite on CSCWG of crude glycerol for syngas production over Fe_3O_4.

Experimental conditions	5 wt% crude glycerol 550°C, 250 barg, 47 h^{-1}, $\boldsymbol{\varepsilon = 0.2}$, d_{50}= 0.15 mm, 83 g	5 wt% crude glycerol 550°C, 250 barg, 125 h^{-1}, $\boldsymbol{\varepsilon = 0.5}$, d_{50}= 4 mm, 32.1 g	5 wt% crude glycerol 550°C, 250 barg, 125 h^{-1}, $\boldsymbol{\varepsilon = 0.5}$, d_{50}= 4 mm, 32.1 g
Cumulative gas composition (mole %)			
H_2	42.4	40.8	38.1
CO	5.5	3.4	4.8
CO_2	7.4	8.5	2.2
CH_4	3.5	9.8	20.7
C_2H_4	30.3	22.8	23.1
C_2H_6	2.9	1.4	1.2
C_3H_8	9.8	12.9	12.6
Syngas	47.9	44.2	42.9
Products gas yield (wt %)	77.2	78.3	81.1
Liquid products yield (wt %)	22.7	21.0	18.2
Char yield (wt %)	0.9	0.6	0.5
Glycerol conversion (%)	97.2	90.1	96.7

It can be seen in table 6.7 that syngas yield remains under 48, 48.1 and 44.2 mole% for run E64, E66 and E65, respectively. This is because of the low yield of CO, which is also attributed to the temperature range and selection of catalyst (refer to section 5.3.3). i.e. (i) the catalyst was not effective for promoting R-WGS. (ii) the temperature range (up to 550°C) could not offset the activity of catalyst for high yield of syngas product. A high temperature (>700 °C) is needed to produce a higher yield of syngas. On the other hand, the increased methane yield (20.7 mole %) on run E66, indicated that side reactions such as methanation of CO following reactions: $CO + 3H_2 \rightarrow CH_4 + H_2O$ or/and
$CO_2 + 4H_2 \rightarrow CH_4 + 2H_2O$ is a contributing factor for methane formation. Methanation and SCW reforming reactions are closely inter-related. Both arise from reactions occurring under reducing conditions over metals (iron). Both reactions also suffer from the same constraints; for example carbon accumulation and susceptibility to sulphur poisoning if present in the feed. The variation on coke yield is attributed to their mechanism of formation. Carbon is typically a product of CO disproportionation while coke is produced by decomposition or condensation of hydrocarbons on catalyst surfaces and

typically consists of polymerized heavy hydrocarbons. However, the mechanisms by which various carbon species are formed on supported metals and by which different types of coke are formed on metal oxides are only moderately well understood. Nevertheless, coke forms may vary from high molecular weight hydrocarbons to primarily carbons such as graphite, depending upon the conditions under which the coke was formed. A number of books and reviews investigate the formation of carbons and coke on catalysts and the consequent deactivation of the catalysts [**316, 317, 318**]. Furthermore, coke is a non-desorbed secondary reaction by-product, which resulted from poor carbon gasification. Coke can be retained on within the pores or the outer surface of the catalyst as mentioned previously (refer to section 4.2.1) and would, therefore, create a barrier to mass transfer and diffusion into the catalyst. This retention may be due to chemical factors, e.g. strong chemisorptions, but more often to physical ones: low volatility (gas-phase reaction) or solubility (liquid-phase reaction), blockage (trapping) within micropores [**319**]. XRD spectra showed that crystallinity increased with Fe_3O_4 as shown in Fig.4.5 The fresh catalyst consists of more-or-less spherical particles, characteristic of amorphous materials whereas the used catalyst is clustered in aggregates of sharp-edged crystals. For all feedstock, H_2 and CO yield dominate the gas composition indicating a high-quality syngas, but their concentrations strongly affected by temperature and the amount of water in the feed.

6.4.4 Influence of run time on gaseous products of the crude glycerol over Fe_3O_4

A series of CSCWG experiments were performed to study the influence of run time on the product gas yield. The experiments were carried out in a small reactor, and in a similar way as described in section 6.3.4. The gas composition and yield obtained as a function of run time, when magnetite catalysts of 4 mm and 6 mm particle size were used for the CSCWG of crude glycerol are shown in Fig.6.4 and Fig.6.5, respectively.

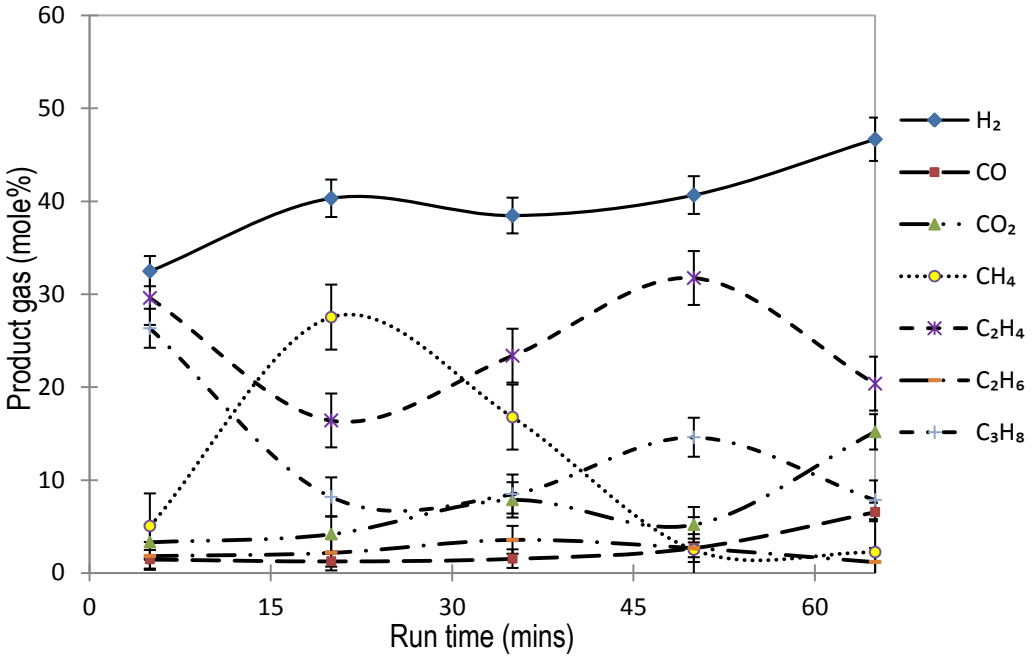

Fig.6.4. Effect of run time on the CSCWG of 15 wt% crude glycerol, run_E66; Small reactor, d_{50}=*4 mm, 10.2 g of Fe_3O_4, irregular shape, 550°C, 250 barg*

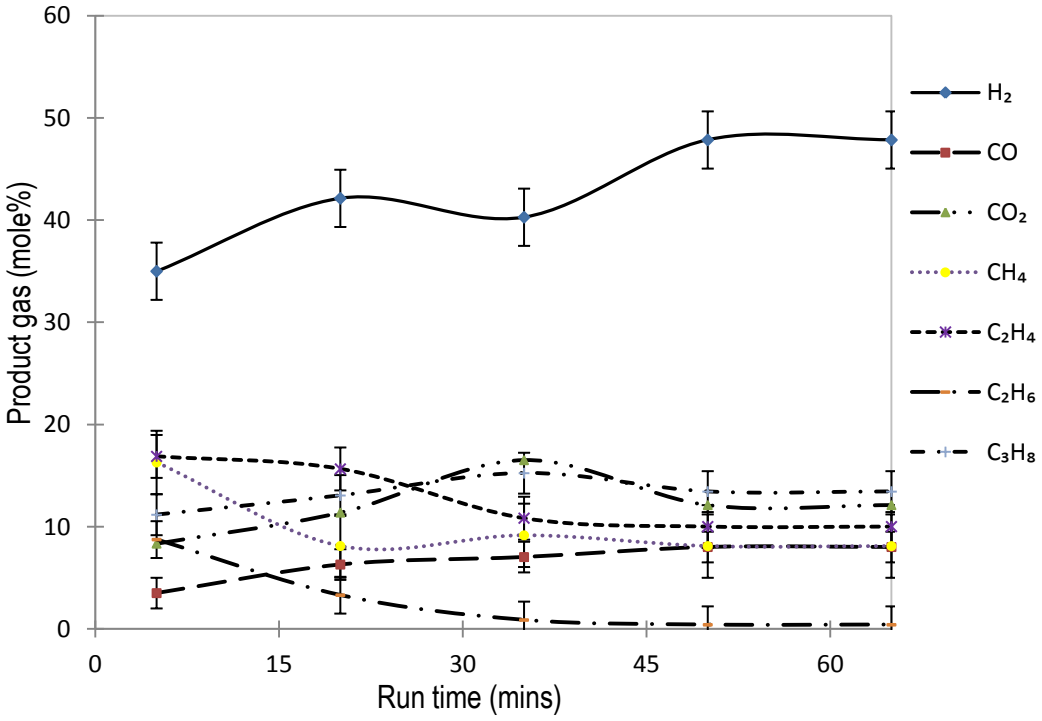

Fig.6.5. Effect of run time on the CSCWG of 15 wt% crude glycerol, run_E73

Small reactor, irregular shape, d_{50}=6 mm, 10.2 g of Fe_3O_4, 550°C, 250 barg

It can be observed that both figures exhibited a similar trend as reported earlier; most gas components for each case showed a non-linear trend with run time. It can be seen in Fig 6.4 and 6.5 that the maximum hydrogen yield was 51 mole% and 47 mole%, respectively. This variation can be attributed to the difference in catalyst particle size and bed porosity. When hydrogen yields increase, coupled with decreasing yields of methane or ethylene, it may be an indication of hydrocarbon reforming. Conversely, when hydrogen yield decreases, coupled with hydrocarbon increases, it is an indication that any coke was hydrogenated into hydrocarbons. These side reactions occur when coke is deposited on the surface of catalyst or accumulated in the catalyst pores, which blocks reactant diffusion and adsorption on the catalyst; hence, the activity of the catalyst is being reduced.

6.4.5 Liquid products obtained from the CSCWG of crude glycerol over Fe_3O_4

The experimental results for the liquid products are given in Table 6.10 and Fig.6.6 for variable weights of catalyst packed in the reactor bed. Although the catalyst loading was varied in other runs, there are only small changes to the individual liquid component yields; the liquid products composition remained largely the same in all runs. The results have confirmed that particle size and loading of catalyst have had minors impact on liquid products formation in SCW. However, it must be pointed out that heat is invariably involved or absorbed in a chemical reaction. The method of packing the catalyst may also affect the rate of heat transfer [**320**], and thus the overall products of the gasification.

Table 6.10. Main liquid products from the CSCWG of crude glycerol over Fe_3O_4

Experimental conditions	15 wt% crude glycerol 550°C, 250 barg, 47 h^{-1}, $\boldsymbol{\varepsilon = 0.2}$, d_{50}= 0.15 mm, 83 g	5 wt% crude glycerol 550°C, 250 barg, 125 h^{-1}, $\boldsymbol{\varepsilon = 0.2}$, d_{50}= 0.15 mm, 83 g	5 wt% crude glycerol 550°C, 250 barg,125 h^{-1}, $\boldsymbol{\varepsilon = 0.5}$, d_{50}= 4 mm, 32.1 g	5 wt% crude glycerol 550°C, 250 barg, 47 h^{-1}, $\boldsymbol{\varepsilon = 0.2}$, d_{50}= 4 mm, 32.1 g	5 wt% crude glycerol 550°C, 250 barg, 125 h^{-1}, $\boldsymbol{\varepsilon = 0.5}$, d_{50}= 4 mm, 10.2 g
Liquid products					mole%
Formaldehyde	19.3	20.9	20.8	20.8	21.2
Acetaldehyde	10.9	2.9	2.9	3.0	3.1
Propionaldehyde	5.3	5.8	5.8	5.9	5.8
Acrolein	10.3	11.1	11.2	11.2	11.1
Valeryaldehyde	3.8	4.4	4.2	4.1	4.4
Methanol	23.9	26.9	26.7	26.3	26.2
Ethanol	2.7	2.7	2.6	2.6	2.6
Allyl alcohol	27.1	29.4	29.6	29.9	29.6
Glycerol Converted	96.8	97.2	96.6	95.9	99.9 %

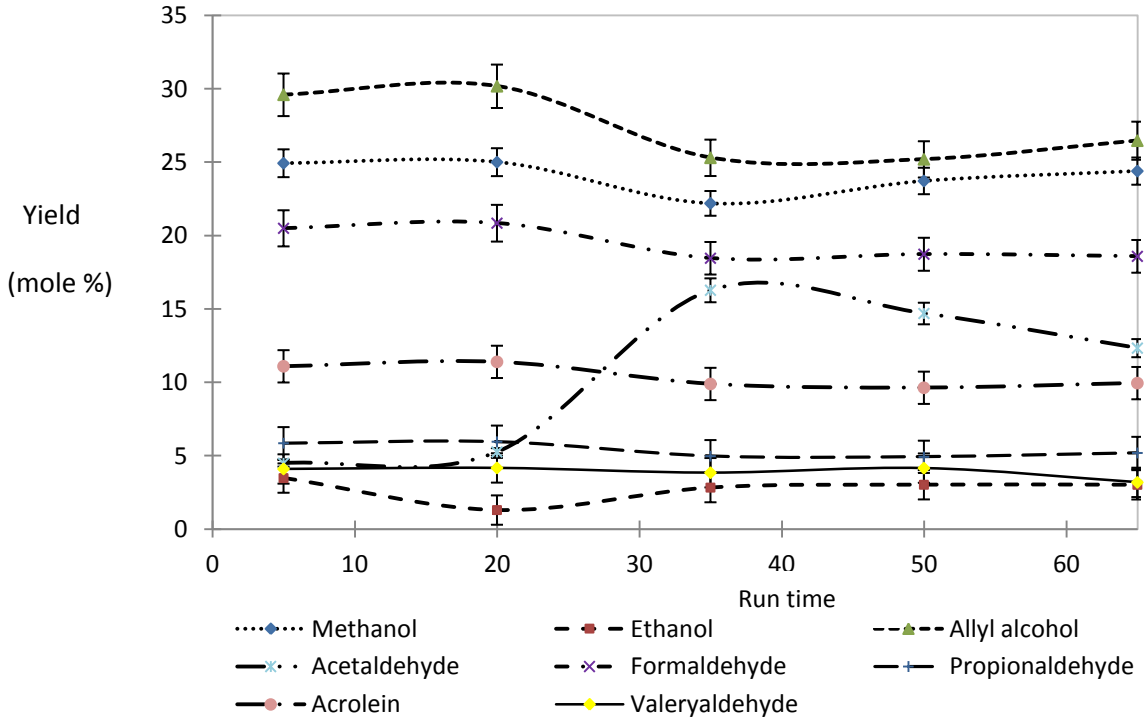

Fig 6.6. Influence of run time on liquid products of 15 wt% crude glycerol, *small reactor, catalyst: Fe_3O_4, d_{50}= 4mm, catalyst loading: 10.2 g, at 550°C, 250 barg.*

With the exception of valeryaldehyde, the liquid products identified over Fe_3O_4 catalyst are the same as those reported in section 5 when Fe_2O_3-Cr_2O_3 was used. The formation of valeryaldehyde might have resulted from an unknown element in the crude glycerol composition or/and in magnetite. However, acetaldehyde, methanol, allyl alcohol, water and formaldehyde remain the dominant liquid products obtained during CSCWG of pure and crude glycerol over Fe_3O_4. Considering the water properties in sub-critical or supercritical conditions, reactions in SCW occur by competing ionic and free radical reaction pathways whose predominance depends on water density and its ionic product. Most liquid products formation was by ionic pathways with some exceptions. For example, a study has shown that allyl alcohol is formed only by free radical mechanism while acetaldehyde and acrolein are formed by an ionic and free radical reaction [**321**]. Increasing the run time to 65 min has led to a sharp increase in acetaldehyde yield, but at 5 min, acetaldehyde yield was low while alcohol yields were higher. However, alcohols products decrease after 20 min, which suggested accelerating degradation of alcohol into gaseous products. For instance, allyl alcohol decreased with increasing run time, indicating that it begins to decompose to other products after 20 min. The decrease in alcohol trend with run time might result from their reformation into methane. This corroborates with the slight increase of methane yield with run time (refer to Figs 6.4 and 6.5).The test results also showed that there was an initial period of intense activity toward liquid product formation, which lasted for about 20 min run time. After 30 min (also observed in a different tests), the catalyst activity toward liquid product had dropped dramatically, producing a high COD effluent. The period of high catalytic activity (>35 min run) contained many reduced yield of the liquid product component compared to run time <35 min (refer to Fig.6.6); it is also expected that the level of mineral in the liquid sample will be reduced because of its reactivity. Furthermore, during the period of low activity, the COD value is higher (8251 mg/l in the liquid effluent compared to <1092 mg/l during high activity); this reduction occurs when the gasification rate improve with time (refer to Figs.6.5 and 6.6); catalytic activity and thermal effect are higher.

6.5 CSCWG of the mixture of pure glycerol + methanol

A series of experiments was performed with a mixture of (pure glycerol + methanol) in order to evaluate the impact of methanol concentration in the crude glycerol. A dosing of 90 wt% pure glycerol and 10 wt% methanol was measured, and mixed to form a homogeneous solution. A concentration of 15 wt% aqueous solutions (90 wt% glycerol + 10wt% methanol): water was prepared, gasified and analysed in the same way as described in section 3. The catalytic parameters, operating conditions and the results are shown in table 6.11

Table 6.11. CSCWG of a mixture of pure glycerol and methanol.

Catalyst: Fe_3O_4, catalyst particle size: 4 mm, catalyst loading: 10.2 g, feed concentration: 15 wt% of (an aqueous solution of 90 wt% pure glycerol +10 wt% methanol), WHSV: 125 h^{-1}, T=550°C, P=250 barg.

Product Yield	Units	Run_Emix1	Run_EMix2	Without Catalyst, E76
H_2	mole%	56.3	51.6	25.4
CO		7.2	5.2	6.1
CO_2		15.3	14.6	9.0
CH_4		2.4	12.6	10.1
C_2H_4		18.6	15.7	48.7
Syngas		63.5	56.8	31.5
Product gas	wt%	97.2	96.3	83.5
Liquid product	wt%	2.7	3.6	16.1
Char	wt%	0.5	0.5	0.4
Conversion of glycerol	%	98.1	96.3	67.4

It can be seen in table 6.9 that the CSCWG of a mixture of (pure glycerol + methanol) at the reported conditions has produced about 96.3 wt% of product gas, 3.5 wt% of liquid product and 0.55 wt% of char. The high yields of product gas, concomitantly with low yield of liquid products, are attributed to the increasing gasification rate due to catalyst choice, optimal operating conditions and more importantly to the presence of methanol in the feed. Hydrogen yield was 54.1 mole%, which is clearly in the same range of yields (54.7, 49.0 and 62.0 mole %) reported in table 6.6 for the similar operating conditions when crude glycerol was used. This indicated that the increased of H_2 and CO_2 yields can be partly attributed to methanol decomposition in SCW. A study has reported that methanol could be reformed in SCW under metal catalyst (Ni) to produce H_2, CO or CO_2 following reactions $CH_3OH \rightarrow CO + 2\ H_2$ or/and $CH_3OH + H_2O \rightarrow CO_2 + 3\ H_2$ [**322**]. The contribution of methanol that can be highly present in crude glycerol on the formation of hydrogen cannot be underestimated. On the other hand, the low yield of methane coupled with slight increase of CO and H_2 indicated possible reforming of methane by hydration following reaction $CH_4 + H_2O \rightarrow CO + 3H_2$. Syngas yield was also higher at 63.5 mole%, due to higher yield of hydrogen.

The methane and ethylene yields have reduced to 2.4 mole% and 18.6 mole%, respectively, compared to hydrocarbons yield reported in table 6.7, which are also attributed to improve the catalytic cracking.

This also indicated that hydrocarbon formation might not have resulted from direct decomposition of methanol. However, the catalytic effect of the stainless steel (316L) reactor wall cannot be underestimated. In effect, the blank test (without catalyst) was run at the same experimental conditions as reported in table 5.1, and the results showed a high yield of product gas (83.6 wt%), which could be evidence of the catalytic activity of the reactor wall (refer to table 5.1). Some studies have demonstrated that the reactor material made of a Ni–Cu alloy or Inconel can have also a significant influence on the decomposition of methanol or/and glycerol [**323, 324**].

6.6 Preliminary study of the CSCWG of digestate

As reported in section 1, various selective organic wastes can be processed in SCWG system into valuable compounds, and digestate is one of those materials. Thus, a compost sample was obtained as the *by*-product of methane and heat production in a biogas plant by anaerobic digestion of organic wastes, and was used to study the CSCWG of digestate over Fe_3O_4 catalyst. Initially, the digestate sample was characterised by semi-quantitative ICP-MS techniques in order to determine the mineral, macro, micro elements content in the sample studied, and results are shown in appendix S. A series of three experiments were performed with low feed concentration of digestate over magnetite catalyst, in the same flow reactor described in section 3. The primary sample was filtered on a mesh with pores size of 1000 μm that is equivalent to the same size of the outlet discharge hole of the pump. This was done to mitigate the blockage on the pump due to the presence of insoluble compounds (debris, woody materials) and some heavy metals like copper (Cu), zinc (Zn), cadmium (Cd), chromium (Cr), mercury (Hg) and lead (Pb) in the sample. Three concentrations of 0.5, 1 and 2 wt%, were prepared as described in section 3, and the feed was preheated to 30°C before it was pressurised and transferred by pumping into the pre-heater (set at 500°C) and subsequently in the reactor. The reactor temperature was set at 550°C, and the system pressure was maintained at 250 barg. The operating conditions, catalytic parameters and the results are shown in table 6.12.

Table 6.12. Results for the CSCWG of digestate over Fe_3O_4;

Experimental conditions	2 wt% digestate 550°C, 250 barg, WHSV=125 h^{-1}, $\boldsymbol{\varepsilon = 0.5}$, d_{50}= 4 mm, 10.2 g	1 wt% digestate 550°C, 250 barg, WHSV=125 h^{-1}, $\boldsymbol{\varepsilon = 0.5}$, d_{50}= 4 mm, 10.2 g	0.5 wt% digestate 550°C,250 barg, WHSV=125h^{-1}, $\boldsymbol{\varepsilon = 0.5}$, d_{50}= 4 mm, 10.2g
Product Yield (mole %)			
H_2	42.3	36.2	29.1
CO	2.4	2.8	1.6
CO_2	9.2	5.3	4.8
CH_4	5.3	2.9	2.8
C_2H_4	24.8	34.1	46.1
C_2H_6	4.5	2.0	3.6
C_3H_8	10.2	16.4	11.8
Syngas	44.7	39	30.7
Product gas (wt %)	69.6	67.4	59.8
Liquid product (wt %)	30.2	32.09	40.1
Char (wt %)	0.2	0.09	0.07
Conversion of the digestate (%)	53.4	70.1	78.2

It can be seen in table 6.12 that the gas composition was identified to contain various components such as H_2, CO, CO_2, CH_4, C_2H_4 and C_3H_8, which indicated that a high degree of polymerisation reactions were occurring due to slow reaction rate. The H_2 yields were lower 42.3 mole% compared to the CSCWG of pure glycerol that gave 61 mole% of H_2-rich gases at 2 wt% feed (Refer to section 5). This is attributed to the poor quality of the digestate feed that might have contributed very little on H_2 formation due to reduced soluble organic matter in the feed. On the other hand, carbon oxides yield were also lower; the yield of the carbon compounds formed depends on two factors: firstly, the operating conditions such as low feed concentration (<2 wt%) and high temperature (550°C) that favour an increasing reaction rate in SCW and the formation of H_2-rich gas (refer to section 4). Secondly, the quality of the digestate in terms of the amount of organic matter contained may have contributed poorly to the product gas yield due to lower organic content. It has been reported [**325**] that the amounts of

organic dry matter and the carbon content of digestate are decreased by the decomposition of easily degradable carbon compounds in the digestors. In addition, H_2 yield increased with reduced feed concentration, which indicates that the formation of hydrogen in the product gas cannot be solely attributed to the decomposition of the organic matter; a significant proportion of the H_2 yield would have resulted from high water concentration in the feed. The ionic product of water increases with high pressure, therefore, providing enough H^+ ions that contribute to H_2 formation by combining with the available protons.

A significant amount of liquid product yields: 30.2, 32.09 and 40.1 wt% was obtained at lower digestate feed concentration 2, 1 and 0.5 wt%, respectively. Concomitantly, the product gas was lower (69.6, 67.3 and 59.8 for the same feed concentration. This was attributed to the poor conversion of the digestate due to the poor feed quality that contain a reduce amount of organic content and various micro and macro elements, as well as metals compounds.

6.7 Catalyst performance: *Comparison of* iron oxide-chromium oxide versus magnetite

The reactor bed was packed with 10.2 g of catalyst. The particle of the catalyst was similar in diameter size (4 mm o/d) but different in shape; spherical and irregular shape for iron oxide-chromium oxide and magnetite, respectively. The experiments were performed in the same way as described in section 5.3. The reaction conditions and the product yields are regrouped in table 6.13.

Table 6.13. Non-catalytic and catalytic performance

Feed: pure glycerol, feed concentration: 15 wt%, WHSV: 125 h^{-1} for E82 and E85, Catalyst size and loading: 4mm and 10.2 g for E82 and for E85, No catalyst was used in run E75, T: 550°C, P: 250 barg.

Catalysts	Units	Without catalyst	Fe_2O_3-Cr_2O_3	Fe_3O_4
Experiments_ ID		E75	E82	E85
Product Yield	mole %			
H_2		25.4	35.1	41.9
CO		6.1	4.4	2.3
CO_2		9.0	4.1	8.4
CH_4		10.1	27.5	15.8
C_2H_4		49.2	28.7	31.3
Syngas		31.5	39.5	44.2
Product gas	wt%	80.6	84.1	87.9
Liquid product	wt%	18.7	15.2	11.6
Char	wt%	0.6	0.5	0.4
Conversion of glycerol feed	%	67.3	96.9	98.1

In all cases, with the utilisation of catalyst, the carbon gasification efficiency or/and glycerol conversion has increased considerably (98.1 %) as compared with those without catalyst (67.3 %). The H_2 and CO_2 yields were higher, and the overall product gases have increased with both catalysts. The gasification rate increases unsteadily, and varies under Fe_2O_3-Cr_2O_3 and Fe_3O_4. Interestingly, Fe_3O_4 seems to be the best catalysts at 10.2 wt% loading. This is because: (a) the Fe_3O_4 catalyst has performed better in term of higher hydrogen yield and maintained activity for more than 9 h run time. (b)The Fe_3O_4 catalyst yielded less undesirable hydrocarbons. Condensable liquid products and carbon deposits were not favoured under these conditions. On the other hand, Fe_2O_3-Cr_2O_3 catalysts deactivated significantly with prolonged run time (172 h on-stream) and on both catalysts carbonaceous have been observed in the reactor. As shown in Fig 6.7, the physical transformation of the used catalyst is further evidence of the reduce activity of the catalyst. The dark colour of the inside of the reactor and the char element (C) identified after EDS analysis are evidence of coke formation. Many factors affect the activity of a catalyst, such as temperature, pressure, method of preparation, degree of subdivision, shape of packing and others. The differences between the performances of these two catalysts could also be attributed to their physico-chemical structure (e.g. O bonding on Fe, crystals arrangement) and the process of preparation. Fe_2O_3-Cr_2O_3 was chemically prepared by impregnation, whereas Fe_3O_4 was obtained naturally without any chemical addition. However, other factors that may have affected the catalysts performance include iron dispersion, time on stream, support stability and mass transfer issues.

(i) Iron dispersion: as a rule, the activity of a catalyst is equivalent to the number of available active sites. At a given metal loading, the number of active sites in a catalyst is a function of the metal dispersion, which is defined as the fraction of the total atoms of the active component that is exposed at the surface. The dispersion is, in turn, inversely proportional to the crystallite size. For instance, in the case of commercial Ni/Al_2O_3 catalysts, the metal dispersion is typically below 15%, corresponding to an average crystallite size of about 6.5 nm or larger [**326**]; the key factors that influence the dispersion of Ni on alumina include the support surface area, the metal loading, and the activation conditions. It may be the case that the support surface area was the only parameter, which could change the metal dispersion. However, it should be noted that both catalysts used (Fe_2O_3+Cr_2O_3 and Fe_3O_4) were non-supported.

(ii) Time on stream: both catalysts had unequal time on stream; 172 and 9 h, respectively for Fe_2O_3+Cr_2O_3 and Fe_3O_4. The mechanical strength of both catalyst in SCWG can only be fully established when both catalysts are exposed on stream to the same duration.

$Fe_2O_3+Cr_2O_3$

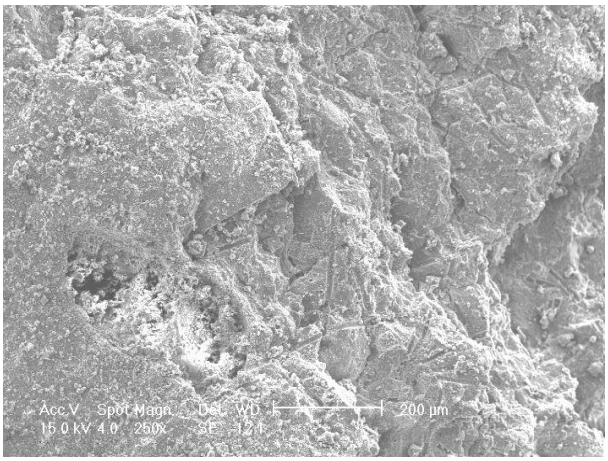

(a) $Fe_2O_3+Cr_2O_3$ -Fresh

Fe_3O_4

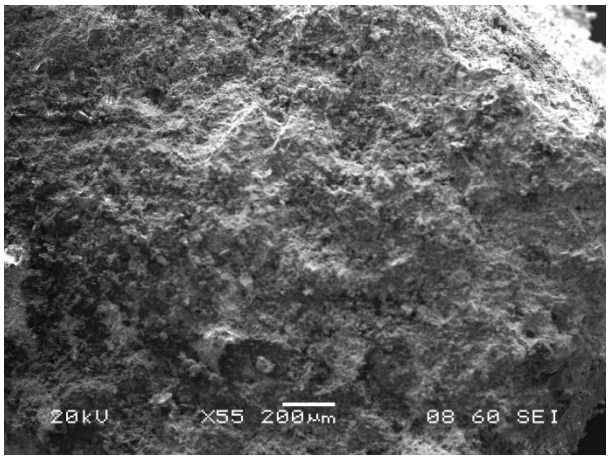

(b) Fe_3O_4 - Fresh

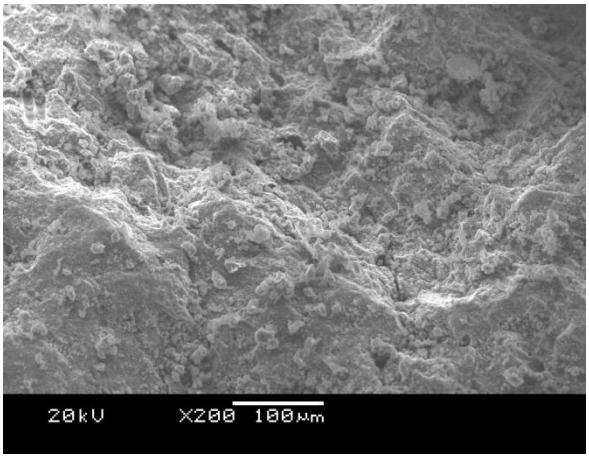

(c) $Fe_2O_3+Cr_2O_3$ –Used (9 h)

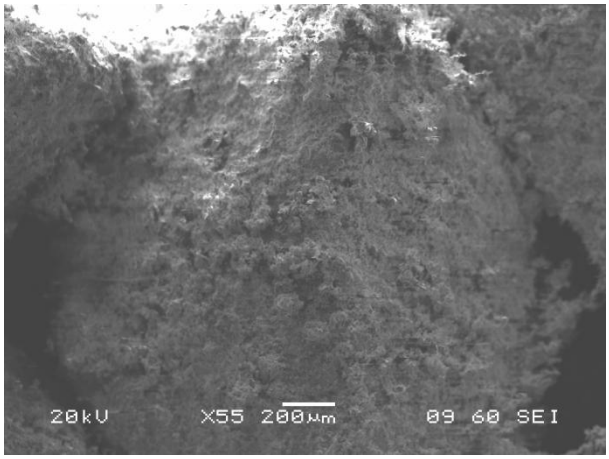

(d) Fe_3O_4 – Used (9 h)

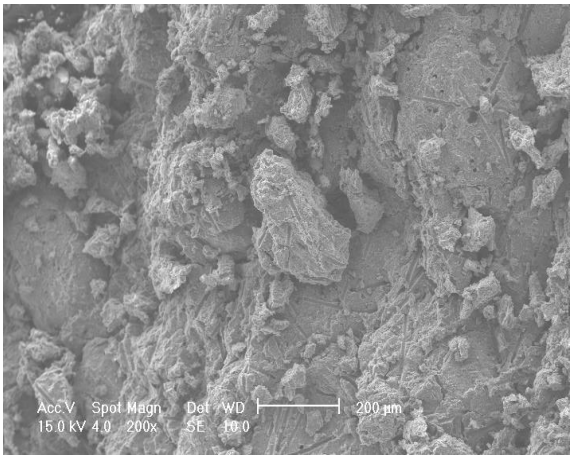

(e) $Fe_2O_3+Cr_2O_3$ –Used (172 h)

Fig.6.7. ESEM images of the fresh of $Fe_2O_3+Cr_2O_3$ (a) and Fe_3O_4 (b) catalysts, and used samples *of $Fe_2O_3+Cr_2O_3$ at 9 h (c), 172 h (e) and Fe_3O_4 (d) catalysts, respectively*
All images are at the same scale of 200 µm, except image (d) at 100 µm.

The ESEM images of Fe_2O_3+Cr_2O_3 shows significant evidence of thermal transformation after 172 h on-stream as reflected by the presence of significant fragmentation into small particles on the surface as shown on Fig.6.7 (c), which can be attributed to the sintering of metals. Similarly, early sign of small fragmentation into small particles was also observed with Fe_3O_4 after only 9 h on-stream as shown on Fig.6.7 (d). This thermal degradation of the catalyst may have contributed to a progressive loss of activity (refer to section 3.3).

The surfaces of both catalyst samples exhibit some porosity as also confirmed by the range of pore sizes detailed in table 6.10. The presence of score marks as it can be seen on images (Fig.6.7 a, c) may have occurred during catalyst preparation. In fact, the manufacturer of the *Fe_2O_3+Cr_2O_3* catalyst has stated "the initial d_{50} = 10 mm diameter pellets were crushed to pass 200 microns sieve, mixed with an addition of 1% graphite, in order to obtain a final pellet of 4 and 6mm diameter pellets". No traces of score marks were observed on fresh and used sample of magnetite, which strengthen the argument that its presence on Fe_2O_3+Cr_2O_3 was not due to the thermal effect in SCW, but to the external factor probably during catalyst preparation.

(vii) Support stability: both catalysts were non-supported. Thus, the impact of support stability on the catalyst performance could not be established. However, they were packed in a similar way, classified as random packing.

(iv) Mass transfer issues. Under similar operating conditions, the rate of mass transfer towards the active sites of a catalyst may depend on the morphological and structural characteristics of the catalyst particulate (pellet, granule, sphere, powder). It becomes apparent that, there was no direct correlation between the catalyst particle size and activity. The data presented in tables 5.3 and 5.4 for the original and crushed catalysts are indicative of this fact. This implies that the mass transfer in the pores was not the rate-determining factor under the experimental conditions used. Therefore, based on these evidences, and also considering the high diffusion coefficients in a supercritical state [**327, 328**], the chemical reaction on the catalytic active site was most likely the rate determining step under the conditions used.

The results in section 5 and 6 showed that in most cases, when hydrogen yield starts to decrease slightly and methane increases concomitantly, it does suggest the onset of catalyst reduced activity. This could be attributed to thermal degradation of catalyst or to coke formation and deposition on the surface of the catalyst particle. However, the analysis of the fresh and used sample on the XRD have revealed that they were no significant change on the magnetite catalyst structure (after 6 hours on stream) to suggest it has degraded. However, coke formation was identified on the surface of catalyst (refer to appendix N), and may be the main cause of loss of activity. In effect, coke formation can occur

by several different ways as shown; for example on the coke-forming reactions: 2 $CO \leftrightarrow CO_2 + C$ or/and $CH_4 \leftrightarrow C + 2\ H_2$. It can be expected that with thermal cracking and catalytic cracking of hydrocarbons, coke is formed as part of the degradation product that would have also included CH_4, H_2O, H_2, CO, CO_2 and light hydrocarbon mixtures. The coke formed on the catalyst surface would be poorly gasified as indicated by the following reactions: $C + H_2O \leftrightarrow H_2 + CO$. This is due to low operating temperature (<550 °C) compared to 700-800°C for high temperature gasification.

The surface area of catalyst is a key parameter that could influence the CSCWG. Fresh sample of iron oxide-chromium oxide has slightly less amount of active metal (69 Fe, 9 % Cr and 6 wt% oxides) as compared to natural magnetite with 73 Fe and 27 wt% oxides. However, the product gas with iron oxide-chromium oxide catalyst was relatively similar to that with magnetite catalyst at the same conditions, except for hydrogen. It can be suggested that magnetite withstands more catalytic activity than iron oxide. Although both catalysts are strong due to high metal content, and could not be easily be eroded if fluidized, they could still undergo degradation under the harsh SCW conditions as reflected by the fragment deposition observed by ESEM on the used samples of iron oxide-chromium oxide. It should be noted that Fe_2O_3+Cr_2O_3 was exposed to 172 h on-stream as compared to (9 h average) with Fe_3O_4. Iron oxide based catalyst was incorporated with Cr_2O_3 in order to strengthen physical hardness, hence reduce degradation by avoiding sintering of metal (Fe) part.

The utilisation of magnetite catalyst appears to be more effective for reforming glycerol or/ and hydrocarbon, but has not resulted in a significant increase in syngas yield, due to the low yield of CO. At the same conditions, hydrocarbon yield has increased with magnetite as compared to iron oxide-chromium oxide. These indicated a high catalytic activity of magnetite for cracking the hydrocarbons. Both catalysts exhibit moderate selectivity for hydrogen production 48.9 and 49.1 mole% for Fe_2O_3+Cr_2O_3 and Fe_3O_4, respectively at the same experimental conditions. The chemical composition of magnetite shows a high oxygen and carbon content; 18 and 27 wt%, respectively. This could contribute to increase the impact of oxidant on carbon reaction by acting like additional catalyst on the gasification resulting to the increasing gas product yield.

These results prove that both catalysts and the experimental conditions are effective in SCWG process. Nevertheless, there was no sign of catalyst deactivation for both catalysts after >6 h on-stream.

Iron oxide-chromium oxide showed good hydrothermal stability, which is probably due to the presence of chromium oxide that was added to strengthen the iron structure. It was expected that the addition of chromium would strengthen the catalyst structure, hence mitigating its degradation process as mentioned in chapter 4. High yield of hydrogen and CO_2 was recorded with magnetite, coupled with low hydrocarbon yields. This indicated that magnetite has high activity for WGS reaction and cracking of

hydrocarbons. The low yield of methane over magnetite catalyst indicated activities toward C-O cleavage.

It is clearly apparent that catalyst deactivation appears to be the main negative factor of this process, and perhaps the only one, which remains to be solved. In this process, it was partly due to coke formation by several different mechanisms on the surface of catalyst and to thermal deactivation through sintering of the catalyst in SCW conditions. Thermally induced loss of catalytic surface area (refer to EDS analysis in appendix N) and active phase–support reactions (refer to XDR pattern) were evidence of this thermal degradation on Fe_2O_3+Cr_2O_3 (172 h on-stream). In addition, the loss of catalytic surface area over Fe_3O_4 had been observed when it was exposed to more than 9 h on stream. When crude glycerol was used, the impurities present (inorganic elements, insoluble compounds) and the interaction of these impurities with the catalyst could lead to loss of activity by chemical deactivation through reversible or irreversible poisoning, which leads to a shortened catalyst lifetime. Chemical deactivation by poisoning would have resulted from strong chemisorption of species on catalytic sites, thereby blocking them for catalytic reaction. This contributes to reduce the micropore area as confirmed by the BET surface analysis result (refer to section 4.4.1).

Other possible sources of catalyst deactivation that were not noticeable in this work include loss of active substance by vaporization; and mechanical deactivation through attrition or erosion [**329**]. The presence of additional X-ray peaks on the used catalysts of iron oxide-chromium oxide and magnetite (XRD analysis) indicated that the reaction of molecules with the catalyst phase to produce unpredictable compounds could have been occurring. However, it was not possible to verify this finding with the available technique of Reitvald analysis because iron fluoresces in copper, so it could not be clearly distinguished. In addition, the high level of background noise further complicated the analysis.
The X-ray patterns of the fresh and used samples of Fe_2O_3-Cr_2O_3 and Fe_3O_4 were significantly different as seen by the variation of peak height and intensity of their X-ray diffraction patterns; note that the same mass of 0.51g was used for both samples (refer to section 3.3). The patterns reveal a poor crystalline structure. However, Energy Dispersive Spectroscopy (EDS) was undertaken to determine the chemical composition of the samples (refer to appendix N).

The loss over time of catalytic activity or selectivity is a problem of immense economical importance in the application of commercial catalytic processes. Reduced catalyst lifetime has a strong negative impact on the process economics; in other words, improved catalyst lifetime has considerable commercial value. Scientists have studied for a long time the synthesis of hydrocarbons from carbon monoxide and hydrogen over iron oxide as catalysts [**330, 331**]. Other studies have demonstrated that the structures of Fe_2O_3 and Fe_3O_4 turn into a complicated mixture of iron oxides, iron carbides, metallic

iron and various forms of free carbon [**332, 333**]. The effects of particle diameter of the different catalysts used as packing material showed that porosity, permeability and thermal conductivity of the catalysts had a significant impact on product yield and product gas composition produced. When magnetite catalyst (d_{50} = 4mm) was used, the amount of gas produced was much higher when compared to a similar particle diameter of iron oxide-chromium oxide. This could be due to improved porosity of the bed (44%) when compared to iron oxide (27%).

Surface area, pore volume and pore size of the catalyst samples was determined from BET measurements. The results are summarised in Table 6.14.

Table 6.14. Summary of the BET analysis

	Unit	F1_Fresh_1	U1_Used_1	Fresh	Used
Sample name		Iron oxide	Iron oxide	Magnetite	Magnetite
Sample weight	g	2.2	1.5	3.3	1.4
Sample particle size (O/D)	µm	4000	4000	1000	1000
Properties					
Area					
BET Surface Area	m^2g^{-1}	58.11	25.83	0.88	0.21
Langmuir Surface Area	m^2g^{-1}	80.38	35.76	1.17	0.33
Micro pore Area	m^2g^{-1}	0.03	2.06	0.62	0.10
External Surface Area	m^2g^{-1}	58.08	23.77	0.26	0.31
Volume					
Single Point Adsorption micropore volume	cm^3g^{-1}	0.21	0.23	0.0073	0.0005
Micro pore volume	cm^3g^{-1}	0.00063	0.0007	0.000285	0.000061
Pore size					
Adsorption average pore size (4V/Å by BET)	Å	151.32Å	364.37Å	334.0217Å	107.6259Å

The BET surface area of the fresh iron oxide was 58.1 m^2g^{-1} and had reduced to 25.8 m^2g^{-1} on the used sample. This significant decline may have resulted from sintering of the catalyst and erosion under SCW conditions. A significant increase in the micro pore area from 0.03 to 2.06 m^2/g could result from strong interactions and reactivity on the catalyst with reactants and gaseous products, which may have contributed to create new micro pores within the catalyst. It is known that diffusion in the pores of catalysts has a strong influence to the reactions that occur on its surface. Reducing the operating

temperature could contribute to increase pore volume and porosity. The average pore diameter of the reducing portion of the catalyst increases with increasing temperature. SCW has been demonstrated to be a powerful technique to reform glycerol, enhanced boosting the reactivity and diffusion rate of the gases on the micro pores as expected (Refer to table 6.11). This may also result to the formation of large pores. On the other hand, the presence of impurities and char on the surface of the catalyst would concomitantly reduce the micropore area. The slight increase in the total pore volume of the fresh and used samples (0.21 and 0.23 cm^3/g respectively) and the minor change to the micropore volume (0.0006 and 0.0007 cm^3/g, respectively) have indicated that pore blockage and filling from char deposition were perhaps negligible. A large size of catalyst pore can facilitate transport and a small size could contain more active catalyst sites.

6.8 Comparison of CSCWG of pure glycerol versus crude glycerol

As reported in chapter 3, crude glycerol was analyzed on GC-FID, and contained 75 wt% glycerol, 11 wt% methanol and others low level of impurities such as free fatty acids, KOH, K_2CO_3 and water. On the other hand, a model compound of glycerol has up to 98 % purity, with little amount of water and other impurities. The performance of CSCWG can be influenced by feedstock selection, feed concentration, catalyst type, particle size and the exposure time between the catalyst and the feed. Two types of feedstock; a model compound (pure glycerol) and a real-organic waste (crude glycerol) were used to evaluate their gasification rates on the SCWG process. Investigations on real-organic wastes provided information on the performance of the SCW gasifier at different operating conditions. On the other hand, the utilisation of a model compound (pure glycerol) has been demonstrated through more fundamental studies to establish the optimal conditions for the CSCWG process.

CSCWG of pure glycerol and crude glycerol were compared over iron oxide-chromium oxide and magnetite, respectively. The results showed that the gas compositions (H_2, CO, CO_2, CH_4 and C_2H_4) are similar with the exception that other light hydrocarbons such as C_2H_4 C_2H_6 and C_3H_8 were also present in the product gas when crude glycerol was gasified. This could be attributed to the presence of impurities in the crude glycerol that polymerise to form tars.

The presence of methanol in the crude glycerol (10 wt %) could also actively participate to the formation of C_2H_4, C_2H_6 and C_3H_8 by decomposition in SCW at the reported conditions. In order to verify this assumption, a mixture solution of pure glycerol and methanol were prepared in the same way as described in section 3.2.1 and were gasified over magnetite catalyst at the same conditions as reported in section 5.3. The result confirmed the presence of additional light hydrocarbons (C_2H_4, C_2H_6

and C_3H_8) in the gas products. Moreover, it has been reported [**334, 335**] that methanol can easily decompose into light hydrocarbons at a temperature below 500°C.

The molar fraction of hydrogen was about 51 mole%, whereas CO was less than 3 mole% when pure glycerol was used as feed over Fe_2O_3-Cr_2O_3 (refer to Fig.5.6). These values increased to 57 mole% for H_2 and 7 mole% for CO when crude glycerol was gasified at the same conditions (refer to table 6.3). The relative high yield of H_2, could also be attributed to the fact that the C:O ratio for glycerol is 1:1, which has a potential influence on the H_2 selectivity. A study had reported that when the oxygenated hydrocarbons had a 1:1 ratio of C:O stoichiometry and the ratio of H_2 to carbon was >1 [refs **336** and **337**] then the selectivity for H_2 increased significantly. This is probably because of the presence of oxygen atoms bonded to each carbon atom, which makes the C-C bonds becoming weaker [**338**]; consequently, it allows for easier scission of biomass molecules to hydrogen and CO. On the other hand, the low CO content may be attributed to two mains reasons. Firstly, the promotion of WGS reaction that reformed CO with water into CO_2, and higher amount of H_2. Secondly, the high excess water in crude glycerol may lead to a preference for the formation of H_2 and CO_2 instead of CO.

6.8.1 Effect of impurities in crude glycerol

The primary impurities in glycerol include spent catalysts, salts after neutralization, residual methanol, and methyl esters, oil/fat, soap and free fatty acids. A study has demonstrated that some impurities such as residual methanol or/and spent catalysts, even in small amounts can strongly catalyse the reaction of carbon with oxidising gases [**339**]. For instance, macro elements such as calcium, phosphorus and carbon are higher in crude glycerol than in pure glycerol and can be as high as 19, 25 and 24 wt%, respectively. Their compositions depend on the primary feedstock type that was used for the production of crude glycerol in biodiesel process. The presence of these macro elements can increase the rate of gasification by acting as a catalyst. Elemental carbon has been used as a catalyst in SCWG process, and increased the gaseous products yield as reported [**340**]. High level of ash is also presented in crude glycerol as compared to pure glycerol. It is estimated that the total ash content in crude glycerol could be up to 6 wt %, depending of the primary feed. However, the full impact of ash in the SCWG has not been yet established. The formation of tar/coke could be due to the presence of heavy impurities such as fats in the crude glycerol, which hardly gasified at the experimental conditions; Fat molecules may diffuse poorly on the surface of the catalyst. It is known that impurities tend to diffuse, and concentrate at crystallite edges during heat treatment at high temperatures [**341**]. The possibility does exist that the catalyst reactivity was higher at the edge of carbon atoms on the magnetite samples because of the reaction being catalysed by impurities

concentrated at these locations. Although, impurities in crude glycerol could have a positive influence on the gas products of SCWG, certain impurities such as salt could play a negative impact by reducing the catalyst lifetime due to deposition on its surface area that would lead to loss of catalyst activity. On the other hand, char (up to 2.7 wt%) and tar formation were higher with crude glycerol than when pure glycerol was gasified, which was due to polymerisation reaction; enhanced by level of the impurities in crude glycerol. Evidence of tar was noticed from a highly viscous liquid product when moderate feed concentration of 15 wt% was used. This caused plugging of the pressure regulator and other fittings.

6.8.2 Effect of energy content in the feed

Energy content in pure and crude glycerol: A study has demonstrated that the energy content of pure glycerol is 19.0 MJ/kg, compared to the crude glycerol, which is about 25.30 MJ/kg [**342**]. This is due to the presence of methanol, other impurities and traces of biodiesel in the composition of the crude glycerol sample. Compared to petrodiesel, whose energy content is around 43.33MJ/kg, biodiesel (B-100) energy content is about 38.02 MJ/kg, which represented 12% lower energy content, as to be expected [**343**]. The full impact of energy content on organic waste feedstock on the SCWG cannot be fully established. However, it is reasonable to expect that high-energy content in the organic feed in SCWG would tend to reduce the activation energy of product formation, hence increasing the reactants conversion.

6.9 Summary of CSCWG of crude glycerol

This chapter has presented the findings of the CSCWG of crude glycerol over iron oxide and magnetite catalysts. The experimental results have demonstrated that crude glycerol; a by-product from biodiesel production can be successfully converted into value added products by catalytic supercritical water gasification. The results are similar with those obtained by others who have reported that CSCWG process over noble metals catalysts can produce a mixture of gaseous products, liquid products consisting of acrolein, formaldehyde, acetaldehyde, as well as char [**344, 345**]. This work had reported similar products formation to pure glycerol where the product gas was made of H_2, CO, CO_2, CH_4 and C_2H_4 with the presence of other volatile hydrocarbons (C_2H_6 and C_3H_8) for crude glycerol. The liquid products composition was also similar to other studies with the exception of allyl alcohol and valeryaldehyde that were also identified in this work. This may be due to the degradation of other unknown compounds present in crude glycerol. In addition, COD for the liquid samples were 1398 mg/l and <65 mg/l for crude glycerol and pure glycerol, respectively, at similar conditions (also see table 4.2). The hydrogen selectivity increased moderately over magnetite loading, compared to iron oxide-

chromium oxide for the same loading of (10.2 g). A high yield of hydrogen 57.4 and 61.1 mole % was obtained over Fe_2O_3-Cr_2O_3 and Fe_3O_4 catalysts, respectively. This fact was attributed to the increase in iron-metal content in Fe_3O_4 particle as compared to Fe_2O_3-Cr_2O_3. On the other hand, syngas yield remained low for both catalysts due to low yield of CO, which suggests a poor reforming of carbon oxides. Most previous work without catalyst have reported low conversion (3–31.4 % at 510°C), whereas with the use of metal catalyst high conversion (80–100%) was attained. This work has demonstrated that high conversion of glycerol (58 % at 550 °C) without a catalyst can be achieved, but also complete conversion (100 %) of pure glycerol over iron oxide –chromium oxide and magnetite catalysts at 550°C can also be achieved. However, the conversion decreases significantly from 100 to 67 % and 100 to 74 % when crude glycerol was used over iron oxide-chromium oxide and magnetite, respectively. A complete conversion of crude glycerol was not attained over magnetite for the same feed concentration tested (15 wt%), as evidenced by the presence of glycerol peak in the liquid samples analysed. This was a result of impurities present in crude glycerol; salt, unconverted oil, fats and soap that are presented in crude glycerol, and can interfer on gasification reaction.

In addition, the work has demonstrated that a metal oxide catalyst can be used to gasify organic waste with high levels of carbon conversion to gas at relatively moderate temperatures of 550°C. In comparaison to other conversion routes for organic wastes, the major advantage of the CSCWG (low-temperature gasification) concept is that it remains a low cost process and easy to large-scale up for bio-energy production. Water participated in SCWG processes and it is critical resource for hydrogen formation. The results presented above have indicated that CSCWG of organic wastes can be used successfully to produce hydrogen. Furthermore, the yield of hydrogen depends on several process variables, such as system pressure, temperature, water to glycerol feed ratio and the choice of catalyst. Low cost catalysts (iron oxide-chromium oxide and natural magnetite) have demonstrated to be highly effective for product gas formation with moderate activity toward hydrogen, and moderately useful for the downstream elimination of the CH_4 and other hydrocarbons. The amount of Fe_2O_3-Cr_2O_3 catalyst loading did not significantly affect product gas yield, but selectivity for hydrogen increased from 40.8 to 49.1 mole% when the catalyst loading was reduced from 32.3 to 10.1 g (d_{50} = 4 mm), respectively. The CSCWG of glycerol over iron oxide-chromium oxide at variable loading has shown a similar effect. On the other hand, hydrocarbon yields were low, 7.3, 2.0, 3.6 mole% for ethylene, ethane and propane, respectively at a reduced catalyst loading of 10.1 g (12 vol% reactor bed), compared to 32.3 g (100 vol% reactor bed). The catalytic reforming by cracking may have contributed on reducing the hydrocarbons yields.

Also, this work has demonstrated that both catalysts (iron oxide-chromium oxide and magnetite) exhibit considerable activity toward hydrogen > 9 h on stream. However, prolonged exposure in SCW showed signs of deactivation as evidenced by the presence of small fragment on the surface after SEM analysis. A deactivation mechanism in SCW conditions has remained the main negative factor for this process and perhaps the only one, which remains to be solved. This was partly due to coke formation, or/and SCW effect on the degradation of metals by sintering.

.

CHAPTER 7. ENGINEERING PROBLEMS IN SCWG AND PROCESS OPTIMISATION

7.1 Introduction to engineering problems in SCWG systems and optimisation

The chapters 5 and 6 have demonstrated that converting organic waste (glycerol) into product gas, condensate liquid product and char can be accomplished in supercritical water at a relatively low temperature (up to 550°C) with metal oxide catalysts (Fe_2O_3-Cr_2O_3 and Fe_3O_4). The CSCWG process offers many advantages over conventional thermal processing routes such as high moisture content in the feedstock (no needed to dry the feedstock, hence energy saving), fast reaction, easier product separation (by simply adjusting the pressure or/and temperature) and clean product gas. Chapter 4 has demonstrated also that if optimal operating conditions and a low cost- effective catalyst are used, the technique can be suitable routes for organic wastes conversion into gaseous and valuable liquid products. Nevertheless, char and tar formation appear to constitute a technological problem. The use of metal oxide catalyst has contributed to the formation of hydrogen –rich gases with reduced amounts of chars and tars. However, the technique still faces many other engineering challenges in order to be a commercially viable route for bio-energy production. Most of these engineering problems remain unsolved for two main reasons: first, the technology is still relatively new (less than 20 years), although it has received a great deal of attention as suitable process for organic wastes gasification (it is safe, non-toxic, readily available, inexpensive and environmentally benign). Secondly, the reaction temperature and pressure are both relatively high to meet the minimum reaction condition. Thus, specific equipment design and construction materials are needed to develop this technology. In light of this, CSCWG is still under intensive investigation at a laboratory and pilot plant scales. In this section, the main challenges are discussed; the mass and energy balance, as well as proposed solutions for process improvement.

7.2 Mass and energy balance calculation

The mass and energy balance calculation are shown in appendix T, and Figure 7.1 summarised the energy flow in and out of the SCWG process as used. This includes the electrical energy supplied to

drive the pump, pre-heating of the feed, follow by heating in the reactor. Energy is lost as a result of cooling and depressurisation of the process stream.

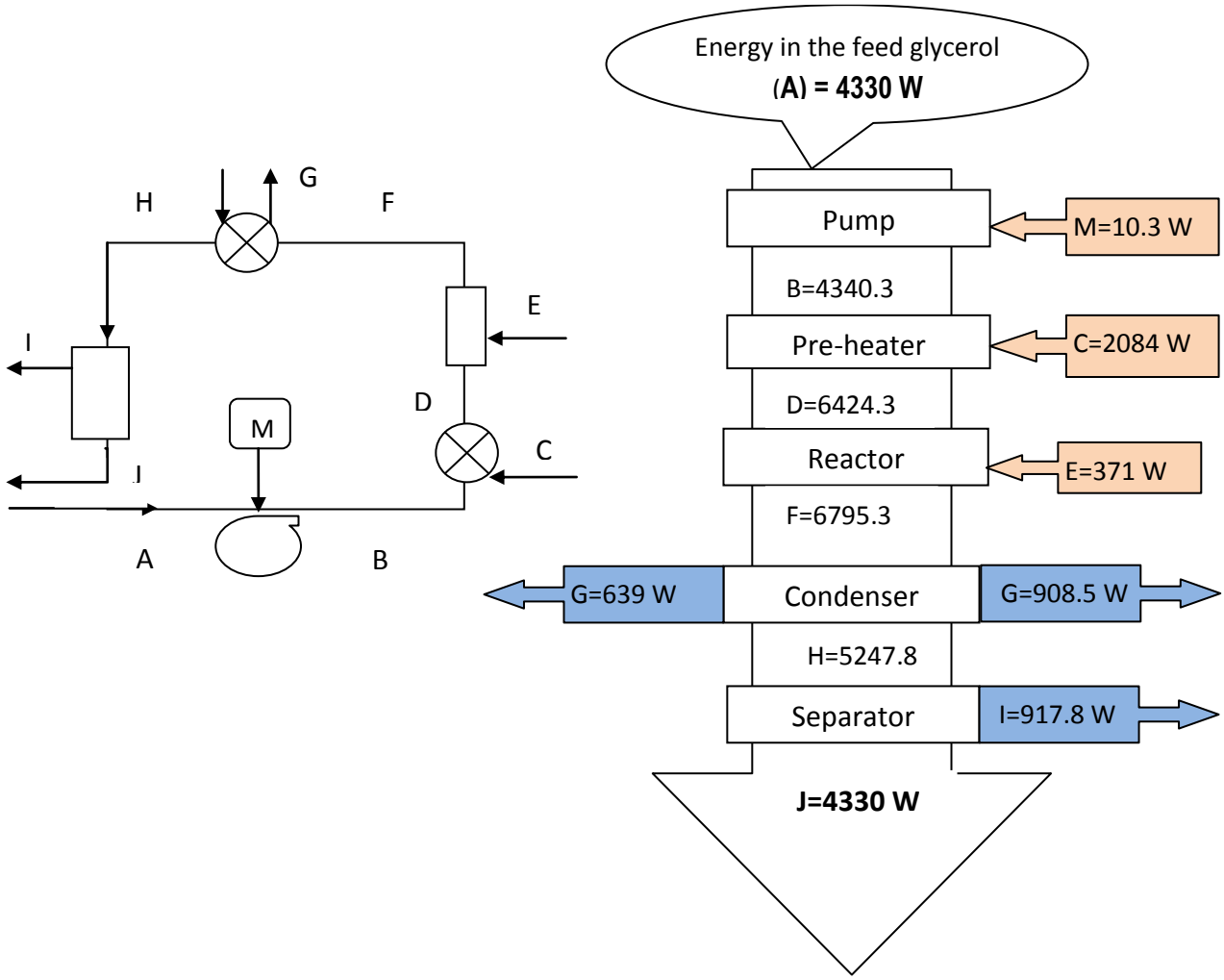

Fig.7.1. Energy scheme: Energy based on 0.109 molemin^{-1} of glycerol or 10.04 gmin^{-1} of glycerol

Energy loading at each stage [Processing conditions: pumping (250 barg, 22C°); pre-heating (250 barg, 500°C); reaction (250 barg, 550 °C); cooling (250 barg, 40°C); separation (40-60 barg, 40°C)]

(A) is the energy (calorific value, W) from the feed glycerol, B→C pumping; C→D pre-heating; D→E isobaric heating; E→G' sub-cooling; G→H depressurisation; H→I Isotherm separation; I→J gas-liquid separation conditions

7.3 Energy and energy recovery

Energy is supplied to the SCWG process in two main ways: by high-pressure pump and heaters (pre-heater and reactor heater). The introduced energies are kinetic and thermal, the latter being the highest because of the intrinsic properties of water towards compressibility and thermal capacity. Energy recovery is an important tool for any process industry. The goal is to minimise energy loss, to improve the thermal efficiency and reduce operating cost of the process. A study has reported that SCWG can realise the goals of energy recovery [**346**], especially for the organic wastes processing.

In the current experimental set-up, the glycerol feed is delivered into the reactor by a high-pressure pump, after being pre-heated to up to 500°C. The reactor is heated up to 550°C to enhance the thermal effect on the chemical reaction. The reactor effluent is subsequently cooled between 20 to 30°C under high-pressure (250 barg) using a condenser that is serviced by chill/cool water (5-10°C). As a result of heat transfer between the hot process stream and the cool service fluid, the temperature of the service fluid leaving the condenser increases to up to 65°C depending on mass flow rate and of the fluid temperature. This provides a potential source for waste heat recovery, which could be reused to pre-heat the feed before it is been pumped using an additional heat exchanger with high thermal efficiency. This was not the case in the current set-up because the high-pressure pump was designed to operate at 20°C for the inlet feed, and therefore it is estimated that a considerable amount of energy is lost during each experiment (up to 22 % of the total energy input). This loss contributes to increase the operating cost, which would become significant over time. It can be noted that during cooling of the effluent stream, part of the gas product dissolved in the water phase, which contributed to potential lost of energy carrier. Although, the product gas is available under high pressure, which make is easy to separate from the liquid phase, significant amount of energy can be lost in both gas and liquid phases. On the other hand, pressure energy can be recovered also using a turbine in a large process plant. It has been reported that rapid heating to supercritical temperatures can be attained by the implementation of a pre-heat coil where the water passes through before being mixed with the feedstock in the reactor [**347**]. The goal of the fast heating rate is to eliminate the undesired reactions associated on the heat-up stage, which can result in solid char and subsequent plugging of the reactor system.

7.4 Engineering problems in SCWG

7.4.1 Feedstock delivery into the reactor

The delivery of soluble organic wastes into the SCWG system would follow fluids transport (gas or/and liquid) mechanism; the theory and its applications are well understood. The transport properties (diffusivity, viscosity) of the SCF are between that of gas and liquid, and have been discussed in chapter 2. In addition, the method of feed delivery into the reactor using the high-pressure diaphragm pump has been discussed also (refer to chapter 2). In spite of its unique transport properties, continuous delivery of non-soluble organic wastes into the SCWG reactor remains one of the biggest challenges of the SCWG system due to two main reasons: firstly, the presence of non-soluble solids in the slurry makes it difficult to transfer by the pumping mechanism. Secondly, the high pressure and temperature regime reduce the reliability of delivery mechanism. On the other hand, for any commercial viable SCWG process, continuous delivery of a high feed concentration is necessary; for instance, as part of process parameters optimisation, high feed concentration is needed to achieve a thermal efficiency and to establish an economic process.

The current delivery system on both small and large-scale rigs was by continuous pumping mechanism of the fluid at the desired pressure and transferred it into the tubular reactor after passing through a preheating furnace. The continuous systems allow for high throughput, which is essential for any potential scale-up to the SCWG process. Additionally, the heating rate in continuous reactors can be much faster than in batch operation due to the small volume of the reactor and ancillaries. The effectiveness of the pumping mechanism is dependent on the fluid properties (solute solubility and viscosity) and the pump choice. Delivery of organic waste into the SCWG system can be accomplished through different feeding mechanisms. It has been reported that various types of pumps, e.g., HPLC pump [**348, 349**], positive displacement pumps [**350, 351**] and syringe pumps [**352, 353**] among others can deliver low viscous organic waste fluid. In this work, a high-pressure (330 barg Max) diaphragm pump was employed to transfer successfully various concentrations of feed glycerol solution into the reactor (up to 30 wt% glycerol as tested). On the other hand, when digestate slurry was used and pumped into the reactor, the pump performance was reduced significantly as evidenced by the loss of flow due to particles in the slurry blocking the pump exist. The presence of non-soluble organics and particles in the solution makes it difficult for this type of process feed to be delivered by a pumping mechanism. However, the problem was alleviated by filtering the slurry using a mesh with pore sizes below the pump exit hole of 1 mm o/d. When the feed digestate concentration was increased to above 5 wt%; the delivery in the reactor was disrupted due to the high concentration of non-soluble particles in

the slurry. In addition, solubility of the digestate in water did not increase after preheating the feed to 40°C due to the presence of non-soluble compounds. Continuous feeding for some biomass that cannot dissolve in the water can be very challenging. A solution to this problem could be to decrease the viscosity of the slurry [**354**]; successfully applied as a pre-treatment method in hot compressed water (150°C, 30 min) for feeding cabbage. Wet biomass, slurries, and suspensions are the most attractive feed options as they have some fluid properties that allow them to be pumped. However, the high feed concentration and the presence of non-soluble particles in the feed make it difficult to be transferred by pumping. There has been very limited research on delivery mechanisms for SCW gasification. A researcher has studied the use of a "cement pump [**355**]" and others have used various pre-treatment techniques including hydrothermal processing [**356**] and liquefaction [**357**]. The delivery of organic waste into the supercritical water gasification reactor therefore remains a technological challenge, which is still receiving more attention.

7.4.2 Plugging

Plugging of the reactor and fittings are common problem in SCWG process, and it can occur at different degrees, depending largely on the process conditions and the feedstock selection. There are two main reasons for plugging in the SCWG system: the first is the coke generated during the incomplete gasification of organic wastes; the second is due to the presence of inorganics such as salts (nitrates, phosphates, sodium), whose solubility are drastically reduced in the SCW. Most of the salts are precipitated, resulting in solid deposition on the reactor wall.

In this work, plugging was observed several times during the experiments of the SCWG of glycerol at high feed concentration (>20 wt %), and at temperature (<450°C). This was due to poor gasification of the reactants, which resulted in tar (refer to Fig.7.1) and coke formation (refer to appendix N). The level of unconverted glycerol (48 wt% of the feed at 400°C reaction temperature) in the liquid product was evidence of poor gasification at lower conditions. The plugging problem occurs mainly in the process fittings, especially on the pressure regulator that was constantly blocked under the above reaction conditions. Plugging caused loss of system pressure, which leads to shutdown of the system in a severe case. This represents a critical problem for the process as also reported by Matsumura and Minowa [**358**]. The problem was alleviated by removing and cleaning the fittings with hot water and with compressed air. In some cases, the problem was mitigated by rising the reaction temperature to above 500°C or/and by pumping water into the system to flush the entire SCWG system. In addition, using deionised water to prepare the feed concentration reduced the amount of salt in the system as evidence by less solid/salt deposition in the reaction environment. It has been reported that plugging

due to carbon and ash build-up usually occurred with sawdust paste after 2-3 h on stream, and plugging removal into the system can be accomplished by pumping a 1.2 M solution of hydrogen peroxide into the reactor for a short time [**359**]. In addition, a study has reported that to handle the plugging problem in the SCWG of biomass, especially for the gasification of high concentration biomass, a novel SCW fluidized bed system [**360**] for biomass gasification has been developed at the State Key Laboratory of Multiphase Flow in Power Engineering (SKLMF) in China. This novel technique is to alleviate the salt issue in a continuous SCWG process is to precipitate the salt by integrating a salt removing column as described in section 2.4.6.2.

7.4.3 Gas-Liquid-char separation

As reported in chapters 5 and 6, the main gas compositions of the SCWG product from pure glycerol were H_2, CH_4, CO, CO_2 and C_2H_4. In order to improve the heating value of the product gas or/and to mitigate the environmental impact of organic waste processing by SCWG, it is essential to remove or reform the CO_2 in the product gas stream. Three approaches are proposed to deal with CO_2 content in the product gas: the first is based on the higher solubility of carbon dioxide than hydrogen in water, enabling a high-pressure separator for hydrogen and carbon dioxide to be integrated in the process. However, the drawback is the complication of the separation steps with multiple separator units, hence increasing operation cost. Secondly, using a CO_2 scrubber based on the same principle of high solubility of CO_2 in water as compared to hydrogen. However, removing CO_2 by dissolving in water does not appear to be the best solution. This is because; CO_2 can be a valuable gas compound if indeed it can be captured, stored and sold. In addition, when dissolving CO_2 in water, some of the hydrogen will also dissolve. Therefore, it will reduce the efficiency of the gas-liquid separation. Thirdly, reforming CO_2 using catalytic absorbing CO_2 materials such as $CaCO_3$ might appear to be the most cost-effective solution especially if syngas is the target product gas. Matsumura et al. [**361**] worked on the specific case of supercritical water gasification; they proposed to mix the formed gas and sub-critical water, which dissolves most of the carbon dioxide. Egan et al. [**362**] attempted to separate the hydrogen with two alumina membranes. They found that hydrogen separation by membrane is possible and it is dependent on the temperature; pressure, pressure ratio across the membrane, and ratio of permeate flow to total flow. However, they also established that the technological and economic issues must be resolved before gas separation membranes are commercially viable. These include improved gas separation efficiency, membrane optimization, sealing of membranes in pressure vessels, high strength of the ceramic material, pore thermal stability, and material chemical stability.

7.4.4 Tar removal

Tar is defined as a viscous, dark coloured material consisting mainly of heavy hydrocarbons, produced during incomplete gasification of the organic wastes. Tar is one of the problems that occur in the SCWG process because the organic waste feedstock does not instantaneously react with SCW into lighter products; the reaction can be slow depending on the operating conditions. The destruction of tar was monitored from 0-20 mins (dark coloured tubes) and then from 35-80 mins (light coloured tubes) as shown in Fig.7.2. It can be seen that the tar is gasified to lighter compounds.

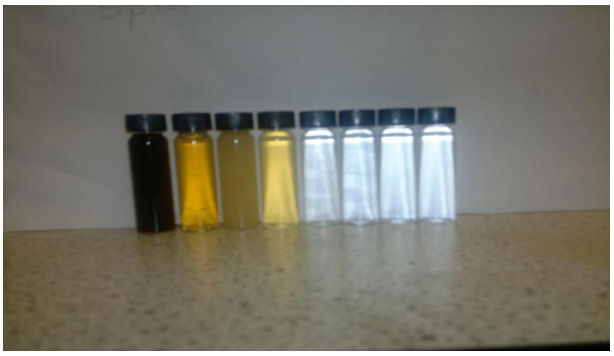

Fig.7.2. Liquid products samples appearance as function of run time,
Sample: crude glycerol. Run times: 0, 5, 20, 35, 50, 65 and 80 mins
small reactor, T=550°C, P=250 barg, Fe_2O_3-Cr_2O_3 (10.1 g)

Several researchers [**363, 364**] have published extensive articles dealing with suppressing tar formation and tar gasification. In this work, the role of the reaction temperature, operating pressure, amount of catalyst, WHSV, and feed concentration were investigated and discussed in Chapter 5, and the best operating conditions for hydrogen production with minimum or /and no tar formation were summarised in chapter 6. Obviously, tar is an undesirable contaminant; it reduces the quality of the product gas when present in the fuel gas. On the other hand, it can be noted that no evidence of tar formation was found when pure glycerol was gasified as reflected by the reduced apparent viscosity, transparent colour and lighter sample of the liquid product. However, when the crude glycerol was gasified at high feed concentration (>15 wt%) , and temperature of < 500°C, traces of tar was observed during the first 20 mins of the run time as evident by the dark colour, apparent viscosity and greasy appearance of the liquid sample (refer to Fig.7.2). However, this observation was dismissed with increasing run time above 30 mins. This suggests that the reaction of crude glycerol in SCW has an initial period of polymerisation reaction due to slow gasification, which then increased with longer run

time due to improved heat transfer in the gasifier. This is attributed to a uniform heat distribution inside the flow reactor, and the quick diffusion of gas molecule through the small pores of the catalyst because of their kinetic energy as function of run time.

7.4.5 Corrosion

The corrosion is an inevitable and a very significant problem for organic waste gasification in SCW as the equipment and reactor are exposed to severe hydrothermal conditions. In addition, organic waste that contents certain inorganic elements such as potassium and sulphur have the potential to exacerbate the corrosion issue. Therefore, it is important to construct the SCWG process with materials highly resistant to corrosion. Alternatively, find ways to protect the reactor material from contacting the reactant and products.

Corrosion in hydrothermal systems up to supercritical temperatures is determined by several solution-dependent and material-dependent factors. Solution-depending factors are the density, the temperature, the pH value, the electrochemical potential of the solution, and the aggressiveness of the attacking anions. Material-dependent parameters include alloy composition, surface condition, material purity, and heat treatment. Corrosion phenomena that are observed include inter-granular corrosion, pitting, general corrosion, stress corrosion and cracking [**365**]. In this work, hastelloy (C-276) materials were used for the full construction of the large-scale rig. The small-scale rig was constructed partly with hastelloy (from the outlet pump to the reactor inlet), and with 316 stainless steel downstream (reactor, condenser, and separator). Hastelloy C-276 is composed of Ni (56 wt %), as well as Mo, Cr, Co, and other metals. The high concentration of nickel in hastelloy provides extended resistance to corrosion, compared to 316 stainless steel. It can be noted that no sign of corrosion was observed on the large-scale system. However, when the small-scale reactor (made from 316 SS material) was used for an extended period (>6 months), evidence of fatigue and corrosion were observed as shown in Fig.7.3. Consequently, increased leak of reactants and gas products from the reactor fittings (refer to picture 7.3) were occurring. To alleviate the risk and the impact of corrosion on the gasification process, the small reactor was subjected to frequent replacement (every 6 months).

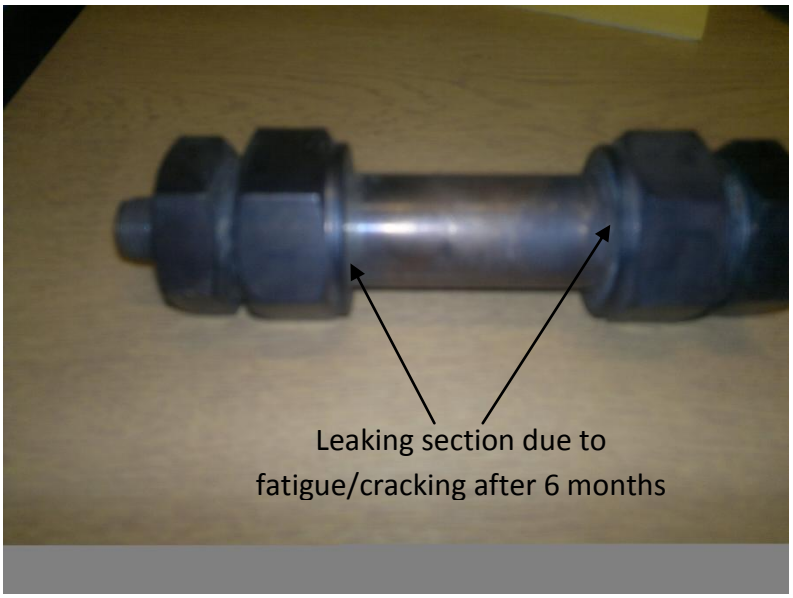

Fig.7.3. Small reactor with sign of fatigue due to fatigue and corrosion

It can be noted that the wall effect and corrosion in SCWG system are interlinked. Depending on the type of construction materials, the wall effect of the reactor can exert a catalytic influence on the gasification chemistry. Evidence of the wall effect was noticed when glycerol was highly gasified (83 wt%) without the presence of catalyst (refer to chapter 5.2). Similarly, a corrosive material will negatively influence the gasification process, and so the catalytic effect of the hastelloy or the 316 SS reactor tubing cannot be neglected in this work. However, the wall effect of the reactor was not explicitly investigated, which therefore forms part of the future work for this project. It has been reported that one approach to study the catalytic role of the reactor wall is to run a sequence of feedstocks, such as glycerol in water, followed by glucose in water, followed by glycerol in water [**366**]. Glycerol is easily gasified, and the gas composition could be affected by the condition of the reactor wall. In this way, glycerol can be used to probe the influence of the reactor wall on the gasification chemistry (refer to table 7.1) for the reactor wall effect.

7.5 SCWG system optimisation

Optimisation is a fundamental and frequently applied task for most engineering activities. However, in many cases, this task is done by trial and error through case studies in a similar manner to that detailed in chapter 5. Like many other SCWG process, improvement from the design stage, to construction and operation are key for the optimisation of the process. This section investigates potential source of process improvement in SCWG including reactor design, separator design, salt removal in the system, optimisation of process conditions, catalyst design and process automation.

7.5.1 Development of reliable kinetic models

The kinetic parameters and rate law are essential for the design of reactors and estimation of product formation. Detailed kinetics should be developed based on the gasification mechanism and reaction path to give guidance to the design of SCWG system. Therefore, a comprehensive gasification mechanism has to be explored including catalyst implication, especially for the qualitative and quantitative analysis of the intermediate and final products. It has been reported in the literature review that the existing kinetic models for SCWG focus solely on gasification yields or feedstock conversion [**367, 368, 369**], without capturing the pathways leading to formation and inter-conversion of gas species. There are no published kinetic models dealing with individual gas yields for SCWG. As a result, little is known about the rates of different potential reaction paths. For instance, the solid-gas reaction($C+ 2H_2 \rightarrow CH_4$) takes place under certain conditions in SCWG, but assuming the amount of char formed is known, it is not known explicitly how much CH_4 is formed from this type reaction, or from methanation or from any other reaction pathways. Moreover, the influence of catalyst on methane formation is not fully established. Thus, it is essential to develop a reliable kinetic model that accounts for the catalyst effect, and the yields of the individual gaseous product in each reaction pathway.

A predictive model should fully describe the behaviour of the CSCWG system in terms of performance based on yield and conversion, accounting for all individual reaction pathways, as well as defining the limitation or constraints of the system. In this work, main reaction pathways (refer to earlier section) were identified and proposed as the basis for the kinetic model development in the CSCWG system. This is similar to the model proposed in the literature for SCWG, which focuses on reactions involving gas species and simplifies reactions involving larger intermediate compounds by defining a generic intermediate species into which all-actual intermediates are regrouped.

7.5.2 Reactor design improvement/catalyst bed construction and stability

The two main disadvantages posed by the use of SCWG are corrosion and salt deposition in the equipment, especially in the gasifier (refer to section 2.3.6). To overcome these two problems, the development of the reactor design could play a key role. It has been reported that the type of reactor used in SCW can be classified into four categories [**370**]: (1) Tank reactor, with the reaction zone in the upper part and a cool zone in the lower part of the tank to dissolve the salts. (2) Wall reactor, with an inner porous pipe, which is rinsed with water to prevent salt deposits at the wall. (3) Film-cooled reactor, which wall is cooled by coaxial introduction of large amounts of water. (4) The tubular reactor, which is the first choice for high-pressure systems. The cooled-wall reactors and transpiring wall reactors are promising designs to overcome salt deposition problems.

Tubular reactors were used in this work, and it is therefore the focus of the reactor design improvement. One criteria that should be considered for the improvement of this type of reactor is the catalyst bed. Both the small and large-scale reactors were not purposely designed with a catalyst bed. The catalyst bed was created on the large scale reactor using a 316L SS tube, which was packed with catalyst and capped at both ends with a screw cap fitted with mesh. Subsequently, the packed tube was inserted into the larger reactor. This is not an ideal design, because of the instability of the catalyst bed and poor heat transfer due to the inclusion of additional wall thickness in the gasifier. These problems can be mitigated if the catalyst bed forms an integral part of the reactor design. On the small reactor, the catalyst bed was created using two portions of mesh with diameter equivalent to the inner diameter of the tubular reactor as shown in Fig.7.4, and is the preferred design.

Table 7.1 shows the effect of spring and mesh loading on the product yields. The spring and mesh were made of 316 SS materials, which are similar to that of reactor wall materials. However, when the reactor was loaded (as shown in Fig.7.4) with the two portions of (spring and mesh) steel for testing, and two experiments were carried out under same conditions reported as for the un-catalysed reaction, the product gas results were similar as shown in table 7.1. This indicated that the spring and mesh tested has no considerable effect on product gas yield and composition, which is attributed to the lower weight of spring and mesh (4.2 g) loaded in the reactor, which did not influence the gasification chemistry. On the other hand, the cracking of hydrocarbons in the product gas and the relative high yield of H_2 indicated that the reactor wall has played a catalytic role on the gasification chemistry, which cannot be neglected.

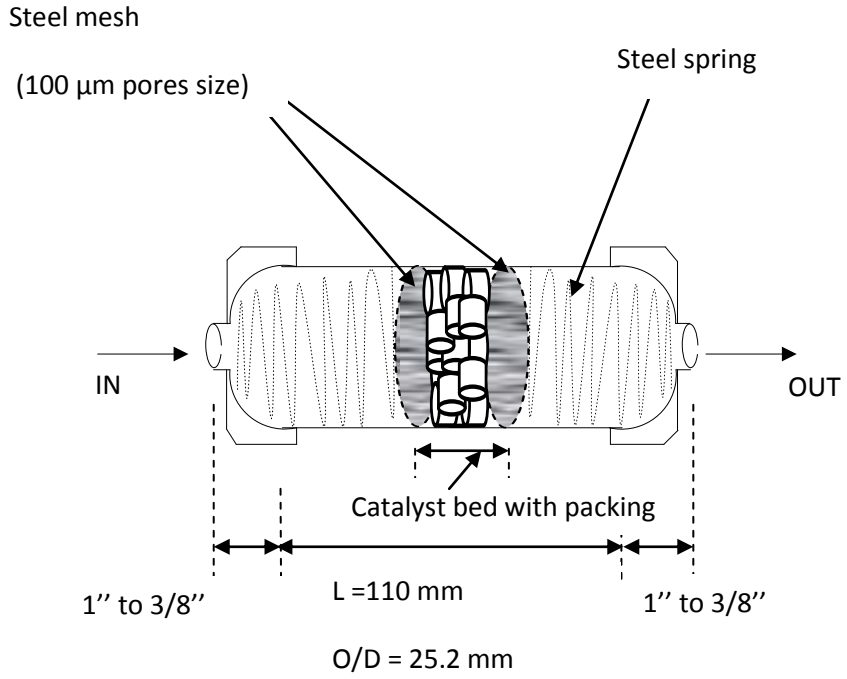

Fig.7.4. Simplified diagram of the small reactor system

Table 7.1. Comparative results of the product gas for the un-catalysed SCWG and CSCWG of pure *glycerol over a 316 stainless steel springs (1.8 g x 2=3.6 g) + meshes (0.3 g x 2= 0.6 g loading) for E13 and E14, feed concentration=15 wt%, feed flow rate = 65 ml min^{-1}, pressure =250 barg, temperature=550°C.*

Experiments	Mole fraction (non-CSCWG)	Mole fraction (non-CSCWG)	(Mole fraction (CSCWG) Over 316 SS spring+mesh	Mole fraction (CSCWG) Over 316 SS spring+ mesh
	E75	E77	E13	E14
Product gas (mole %)				
H_2	24.4	24.9	25.1	24.7
CO	9.8	7.2	6.7	8.8
CO_2	8.2	6.2	10.2	9.2
CH_4	5.6	10.1	9.8	8.6
C_2H_4	51.8	48.7	48.2	48.7
Syngas	34.2	32.1	31.8	33.5
Product gas yields (wt%)	83.5	89.4	89.8	86.5
Liquid product (wt%)	16.1	10.3	9.8	13.1
Char (wt%)	0.4	0.3	0.4	0.4
Glycerol conversion (%)	73.3	78.6	77.3	77.1

It can be seen in Fig.7.4 that catalyst was contained inside the two portions of mesh, and was supported using two springs; placed at both end of the packed bed. Although, the spring was tested before utilisation and was found to have no considerable effect on gas yield and composition, the problem of catalyst bed instability could not be eliminated due to high pressure (up to 300 barg). In addition, the catalytic effect of the reactor wall cannot be neglected, and the degree of wall effect of the reaction is function to the type of reactive metals used in the construction of SCWG reactors [**371**]. On the other hand, the high temperatures and high pressures in SCW systems limit the potential materials for its construction.

The objective of using metals oxide catalyst was to improve yield of product gas, in particular hydrogen, and to reduce the operating temperature of the SCWG as discussed in the literature review. The catalytic effect of the reactor wall was not viewed as a major problem on the CSCWG system. However, the results in table 7.4 also showed that the catalytic effect of the reactor wall has contributed slightly to the higher gasification yields as evidenced by the hydrocarbons cracking and the higher yields of product gas (83.5 and 89.4 wt%, respectively for runs without catalyst E75 and E77). Nevertheless, the catalytic effect of the reactor can be mitigated if it is desired, and a number of methods have been reported in the literature review [**371, 372, 373**]. Some of these methods include the utilisation of quartz reactor due to the inert nature of the material, the installation of ceramic liner inside a metal reactor.

As reported in section 2.3, stainless steels (316L SS) or nickel-base alloys (hastelloy) were used as the main construction materials for the small and large-scale SCWG reactor, respectively. These materials generally have lower mechanical strength than titanium or platinum for instance. Other highly resistant metals have been suggested for reactor construction such as noble metals (gold and platinum, titanium, niobium and tantalum) and different oxide ceramic materials. Gold, platinum, and titanium have been used successfully as liners inside a stainless steel pressure tube [**372, 373**]. Ceramics can be applied in the form of a tube inside an outer high-grade alloy pressure tube [**374**]. In such reactors, the outer tube is only in contact with pressurised de-ionized water.

7.5.3 Gas/liquid separator design improvement

As reported in chapter 3, the theory of gas-liquid separation aims at creating a relative velocity of the droplets in respect to the gas. In this work, the gas-liquid separation method was achieved by gravity settling. A droplet was separated from the gas stream when it reaches one of the walls of the separator column (or other limitations) of the space in which the mixture flows. The captured droplet coalesces in a liquid film on obstacles or walls, and is then drained.

In this work, it appeared that the behaviour of the separator could not be reliably predicted under the reported experimental conditions because settling was achieved with longer time (more than one-hour operation time). For instance, when the gas-liquid sample was left overnight in the separator, a maximum gas product with high hydrogen concentration was separated from the liquid the following day (refer to appendix R). On the small-scale rig, better separation was achieved by operating the separator between 40 to 60 barg. Gas-liquid separation at pressure below 20 barg was very poor. This was due to the feeding position through a 3/8 inch tube, which was located vertically from the top to the middle of the separator that reduced the influence of gravity on the mechanism of separation. For these reasons, it is proposed that the existing separators (gravity by axial flow) design could be improved as follows:

- Feeding position in the column: This design could be improved by feeding from the centre side of the separator, which would eliminate the extended feed tube at the top of the separator, and would enhance settling by gravity, resulting from increased droplet coalescent on the wall.
- Sedimentation (gravity settling): When lowering the velocity of a gas/liquid mixture sufficiently, droplets can experience considerable influence of gravity and will settle down. If it is assumed that, the drag force only opposes the gravity force; and if for Re < 1, Stokes' Law will apply; thus, relative settling velocity can be quantified [**375**].
- Capital and operational costs: the existing separator column was the most simple design column and 316L stainless steel were used as the materials of construction for the small separator. Therefore, it is estimated that this type of separator has a low capital and operational costs, compared to separator with trays or packing materials.

7.5.4 Salt removal system

The presence of insoluble salt in SCW is one of the main issues of SCWG process. Solubility of salt in SCW is reduced significantly due to the physical properties of SCW. This has been discussed intensively in the literature review (refer to chapter 2). Inorganic compounds and their behaviour in SCW systems represent an interesting, but not fully understood aspect.

Inorganic compounds show a tremendously diminished solubility at supercritical conditions due to the changes in the properties of water [**376**]. This behaviour results in precipitation of the inorganic compounds and a formation of a solid phase. The presence of such a solid phase is a possible cause for malfunction of parts of the equipment and scaling of these particles on the walls of the equipment [**377**]. Furthermore, increased erosion and corrosion are to be expected due to the presence of such a solid phase [**378**] in the reaction environment. On the other hand, the diminished solubility of inorganic

compounds can be exploited for a removal of these compounds by applying the principle of difference in solubility between the inorganic compounds as a mean of separation. Two approaches are looked at for the removal of salt in SCW: The first one is pre-treatment by salt removal in water by deionisation. As discussed in the literature review, salt can be removed by filtration of mains water using ion membrane separation. This method can effectively remove up to 90% of inorganics in water depending on the type of membrane and system efficiency. However, as this process is carried out using electricity to power the system. It may increase the operational cost, due to additional energy input. The second one is by the design and integration of salt removal column in a continuous SCWG process. A study has reported on the salt separator design in a continuous operation in SCW process [**379**]. The aim is to achieve high efficiency separation by continuous precipitation of salt to separate it from SCW. The principle is based on varying the salt separator temperature from sub-critical to supercritical across the separator to attain high efficiency (refer to sub-section 2.4.6.2).

7.5.5 CO_2 management

It is desirable that a high-pressure absorption column for CO_2 removal is integrated into the process, so that H_2 could be separated with minimum CO_2 content. However, the drawback is that the liquid phase would include dissolved CO_2 and some part of the H_2. Depressurisation of this liquid will then allow these gases to be released. Since the amount of dissolved H_2 is not negligible, recovery of this dissolved hydrogen would have to be considered in order to optimise the overall process. On the other hand, a viable option for CO_2 management at a commercial scale is CO_2 capturing, which can be used to store or/and transport by pipeline to the offshore and injected into a saline formation located below a natural gas formation. Although geological storage is the most likely near-term CO_2 storage option, there may be potential for CO_2 to be injected directly into the water column and stored in the ocean waters. The under seawater storage option is attractive for countries that do not have sufficient geological storage capacity or lack the geophysical attributes necessary for storage. For instance, the ocean is a natural carbon sink, and most of the CO_2 released into the atmosphere will eventually be taken up by the ocean. Although ocean storage could take a number of forms, the most likely option would be for the CO_2 to be transported by pipeline or vessel from shore and injected deeper in droplet form into the ocean. Ocean storage would be constrained by the availability of CO_2 close to shore, which is estimated to be about 15-20% of total fossil fuel use [**380**]. However, some of the risks associated with the sources of CO_2 storage are found in both the onshore and offshore contexts (such as induced seismicity), several sources of the risk pose a greater likelihood of harm from onshore CO_2

storage. This is because of the higher probability of humans living near the operations, which pose a potential risk to affect groundwater by contamination or hazards to human health.

7.5.6 Catalyst design optimisation (with supported)

The high-pressure effect in SCWG process brings about challenge for the catalyst, such as the effectiveness in CSCWG conditions, strength, durability and lifetime. Therefore, continuous development of a long-life and cheap catalyst is important to increase economical efficiency of CSCWG through improving the gasification yield and lowering the gasification temperature. Although, the catalysts used in the work were low cost, and have showed a good degree of activity toward hydrogen production, signs of catalysts reduce activity (refer to appendix M) were observed after 172 and 9 hours operation for iron oxide-chromium oxide and magnetite, respectively. In addition, these catalysts were non-supported; and it is expected that a supported catalyst contribute to expose the active sites of the metals catalyst, which could enhance its activity in the CSCWG process. Therefore, it is proposed to integrate supporting materials such as activated carbon and alumina on the existing or/and any other future catalyst for CSCWG process.

7.5.7 Process automation: small to large scale operation

The current design of the SCWG-rig was automated only on the pre-heater section, where a PLC control system was used. It is desirable that all major equipments (pump, SCWG reactor, heat exchanger, separation column) are fully automated to reduce the human intervention; this would contribute to reduce operation cost and mitigate risk. Fig.7.5 showed the Labview software, which was designed for this purpose (also, see appendix U). However, due to the increasing cost of the project and limitation in funding available, the design was reduced on viewing processing parameters, instead of controlling.

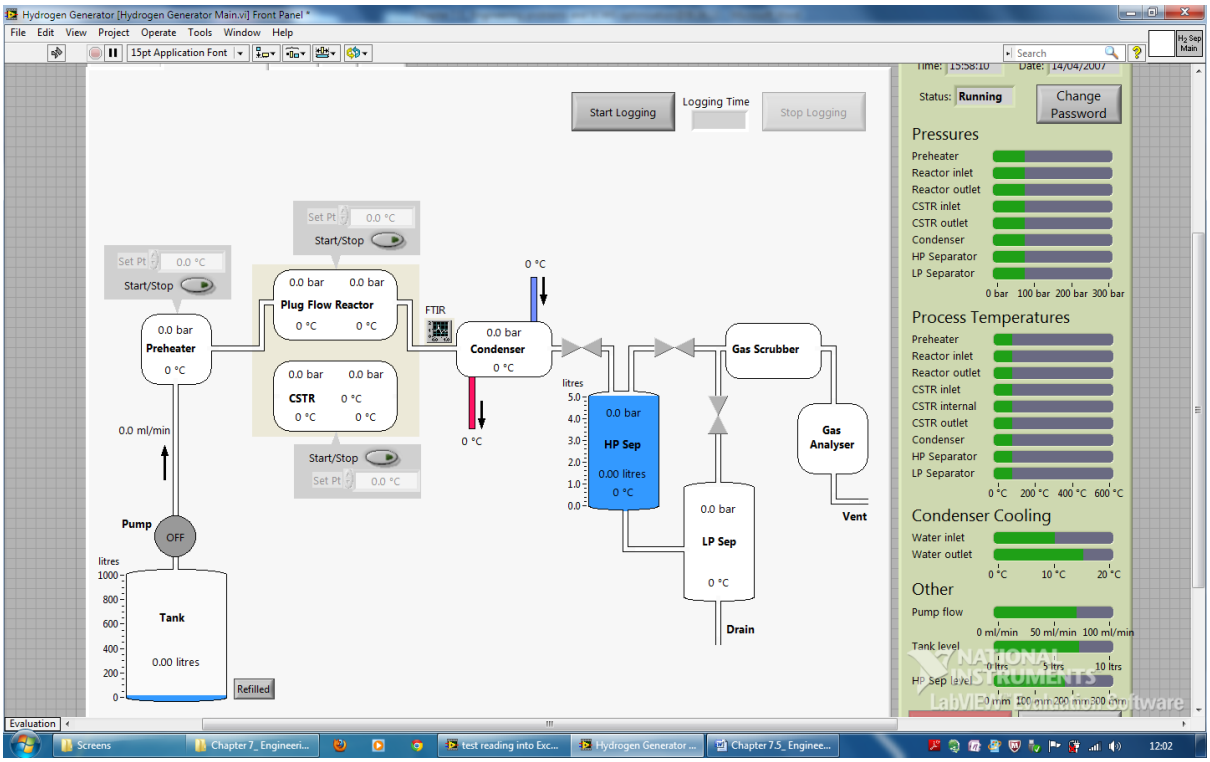

Fig.7.5. Screen shot of Labview

7.6 Summary of the Engineering problems in SCWG systems and optimisation

Reactions at supercritical conditions will continue to receive significant interest for its development and potential applications in industry. However, barriers would have to be overcome, such as reducing the high capital cost of SCW equipment, delivering non-soluble organic material into the reactor continuously as required in industrial scale and improving catalyst cost-effectiveness for optimal yielding of H_2 or/and syngas. The CSCWG is a novel technique for organic waste conversion into useful fuel gases such as H_2, CH_4 and valuable liquid products (acetaldehyde, formaldehyde). The CSCWG of organic wastes was studied over the utilisation of low cost catalysts (iron oxide-chromium oxide and magnetite) and the mains engineering problems were identified and discussed.

In summary,

- Non-soluble organic wastes, delivery into the reactor are one major problem of CSCWG. The choice of delivery mechanism (pump) and pretreatment of the solid organic waste feed can play a big role in mitigating the impact on the SCWG process. Upgrading the pump capability to handle high viscous materials is also a consideration.

- Plugging of the reactor and fittings appear as the main engineering problems of the process. This problem increased with high feed concentration due to tar or polymerisation reaction. However, the problem can be alleviated by increasing the reactor temperature.
- Corrosion of the fittings and equipments particularly the reactor remains another problem to be solved. Corrosion is largely due to alkaline salt deposition on the reactor wall and the acidity of the reaction system that attack the metals. The problem can be partly mitigated by using high-grade nickel content materials such as hastelloy. Integrating a salt removal column in a continuous process would also contribute to solving the problem.

8 CONCLUSIONS AND FUTURE WORK

8.1 Summary of Conclusions

In this work, the degradation of glycerol by CSCWG at temperatures of 400-550°C and pressures of 170-270 barg was investigated using a packed bed reactor (PBR) containing a known amount of Fe_2O_3+Cr_2O_3 or Fe_3O_4 catalysts. Various concentrations (from 2 to 30 wt %) of pure or crude glycerol were prepared in deionised water at ambient conditions. The solution of glycerol was delivered safely at sub or supercritical conditions into the PBR using a high-pressure pump at flow rates from 10-65 mlmin^{-1}, which gave WHSV of 19 -125 h^{-1}, respectively.

The reaction was carried out in a flow reactor (30 ml design capacity) made of 316 SS. The wall effect on the gasification chemistry could not be neglected. It is suggested that the reactor material may increase the gasification chemistry due to high nickel content.

This work has demonstrated that the use of appropriate catalysts (Fe_2O_3+Cr_2O_3 or Fe_3O_4) in the SCWG of the glycerol or organic waste can be carried out successfully at a temperature up to 550°C, when compared to non-catalyst reaction that is usually carried out at 700 to 800°C for hydrogen production. Moderate conversion of pure glycerol (58 % at 550°C) without a catalyst can be achieved, but also high conversion up to 100 % of pure glycerol over Fe_2O_3+Cr_2O_3 or Fe_3O_4 catalysts at 550°C, and up to 15 wt% feed concentration can be attained. In addition, the use of catalyst played a key role on driving the selectivity of the product toward H_2-rich gas while lowering the formation of tar and char. However, various reactions occurred as demonstrated by the range of product composition and yields. Thus, the catalytic cracking of hydrocarbons under sub and supercritical water conditions cannot be limited to one single reaction.

Depending on the catalyst selection and the operating conditions such as temperature, pressure, feed concentration, WHSV and reaction time; a mixture of gaseous (H_2, CO, CO_2, CH_4, C_2H_4), liquid products (ethanol, methanol, allyl-alcohol, formaldehyde, acetaldehyde, propionaldehyde and acrolein) and char are formed. These formations resulted from various reactions (WGS, methanation, gas-solid reaction) and their mechanisms of formation.

The amount of catalyst loading does not significantly affect product gas yield, but selectivity for hydrogen increased from 40.8 to 49.1 mole% when the Fe_2O_3-Cr_2O_3 loading was reduced from 32.3 to 10.1 g (d_{50}= 4 mm), respectively. High gas yield (81.7 wt%) at optimal loading (10.1 g of catalyst representing 21 vol% of the reactor bed volume) of the catalyst as a result of improved contact of reactants over active sites of Fe_2O_3+Cr_2O_3 (3.5 mm cylinder with 4 mm diameter) was observed.

The hydrogen selectivity increased moderately over Fe_3O_4 loading, compared to Fe_2O_3-Cr_2O_3 for the same loading (10.1 g). A high yield of hydrogen (54 mole %) was obtained with smaller d_{50} = 0.15 mm over a maximum loading of 83 g. This was attributed to the higher content of iron-metal in powdered particle as compared to bigger d_{50} (4-6 mm), which led to poor dispersion of materials in the bed. Hydrogen yield was higher (up to 62 mole%) in the product gas when crude glycerol was gasified over Fe_3O_4 compare to 47 mole% for Fe_2O_3-Cr_2O_3 due to high oxides and iron contents in the Fe_3O_4. Carbon monoxide was lower in the gas product stream (<12 mole %), together with a modest increase of CO_2, which indicated the promotion of the WGS reaction. Moderate yield of hydrocarbons were obtained and this decreased with temperature as a result of thermal cracking at 550°C. Lower yields of tar and char by-products were formed, mainly with feed concentrations above 20 wt%, which was due to polymerisation reaction. Syngas of up to 62 mole% and 68.4 mole% over Fe_2O_3-Cr_2O_3 and Fe_3O_4, were obtained with minimum 4:1 mole ratio of H_2:CO as the conditions reported in sub-sections 6.3.3 and 6.2.2, respectively. This lower yield of syngas was due to low yield of CO, which suggests a poor reforming of carbon oxides

High yields of volatile hydrocarbons were also obtained: 14 and 69 mole% for methane and ethylene, respectively, which could be used for energy generation in SOFCs or turbines, reformed to syngas or converted to chemicals by an appropriate route.

The condensate liquid effluent was found to have a reduced COD value (< 11 %), and due to slow gasification reaction, its colour changed with run time from brown (for the first 0-30 min, hence poor gasification) into a clear (for 35-80 min, high conversion into product gas) and transparent in the case of crude glycerol. The calorific value of the gas produced was <26 MJ.m^{-3}, which is lower than natural gas (>35 MJ.m^{-3}). Small amounts of char were obtained (< 2.7 wt %), and carbon was deposited on the catalyst surface as well as on inside the reactor wall.

Pressure had little effect on the gas yields in the subcritical water region, but had a positive effect on H_2 and CO_2 in the supercritical region where char formation also was increased resulting in loss of catalyst activities (after 172 h).

High temperature (up to 550°C) strongly favoured the reforming of hydrocarbons (CH_4 and C_2H_4), which resulted in the production of a hydrogen rich gas (62 mole %). Complete conversion of the model compound, glycerol was achieved at 550°C, 250 barg for up to 15 wt% feed concentration, compared to 91 % conversion for crude glycerol at the same conditions.

Low feed concentration (<5 wt %) also favoured hydrogen formation. High feed concentration (>20 wt%) favoured tar and char formation due to polymerisation reactions resulting from poor gasification. The feed conversion decreases significantly from 100 to 67 % and 100 to 74 % when crude glycerol was processed over either Fe_2O_3+Cr_2O_3 or Fe_3O_4, respectively. A complete conversion of crude

glycerol was not attained over Fe_3O_4 for the same feed concentration tested (15 wt %) as evidenced by the presence of a glycerol peak in the liquid samples. This was attributed to impurities in the crude glycerol that poorly gasified under SCW conditions, rather than the catalyst effectiveness.

The most prominent characteristic of the catalytic cracking for both catalysts was the rate of catalyst coking. Some signs of Fe_2O_3+Cr_2O_3 loss of activity were observed after 172 h on-stream as evidenced by the fragmented catalyst surface as a result of metal sintering. No sign of Fe_3O_4 deactivation was observed under 9 h on-stream and was found to have better activity on hydrogen production than for Fe_2O_3+Cr_2O_3. Neither catalyst was able to promote a favourable balanced syngas ratio of 2:1 for H_2: CO, which would be a suitable feed gas for FTS into mixed alcohols.

8.2 Main conclusions

- **Production of H_2 and syngas**

A high-pressure diaphragm pump was used to deliver glycerol concentration into a SCWG reactor up to 30 wt% concentration tested. Analysis of the gas products indicated that temperature, pressure and feed concentration were the operating parameters that had significant and positive effects on gasification rate. On the other hand, the product gas result showed that feed concentration had a significant adverse impact on the gasification efficiency.

- **Liquid products and char**

The amounts of liquid products and char were influenced by feed concentration, percent of feed conversion and reaction temperature. At concentrations below 15 wt % glycerol, complete conversion was attained for pure glycerol. Crude glycerol could not be entirely gasified below 15 wt% feed concentration due to the presence of heavy materials such as biodiesel, and other impurities in the sample. A SCWG test of a mixture of pure glycerol (90%) methanol (10 wt%) confirmed that the presence of a moderate concentration of methanol (10 wt%) in the crude glycerol resulted in increased gasification rate and hydrogen production.

- **The use of metal oxides catalysts**

The main problem for the use of metal oxide catalysts, which needs to be overcome, is the vulnerability of the catalyst to the corrosive environment of SCW. The characterisation of Fe_2O_3-Cr_2O_3 and Fe_3O_4 catalysts that are used in this study showed that both metal oxides contain a high concentration of Fe metals; 91 wt% and 77 wt%, respectively. The catalytic activity was significantly lost

for used Fe_2O_3-Cr_2O_3 (after 172 h), resulting in a lower conversion. This was primarily due to sintering of the metal rather than oxidation of the metals.

- **Preliminary test of SCWG of digestate over Fe_3O_4**

Initial results of the digestate show that H_2 yields were 42.3, 36.2, 29.1 mole% for digestate feed concentration of 2, 1 and 0.5 wt%, respectively. This indicates that the formation of hydrogen in the product gas cannot be solely attributed to the decomposition of the organic matter; a significant proportion of the H_2 yield would have resulted from high water concentration in the feed. A significant amount of liquid product yields: 30.2, 32. and 40.1 wt% was obtained at lower digestate feed concentrations 2, 1 and 0.5 wt%, respectively. Concomitantly, the product gas was lower 69.6, 67.3 and 59.8 for the same feed concentration.

- **Influence of SCW on metal oxide catalysts**

Fe_2O_3-Cr_2O_3 and Fe_3O_4 have shown signs of performing well as catalysts for SCWG. Fe metal was identified as the most active species in their compositions (Cr, Al, Si, Ni and Cu). Its degree of activity was influenced by the Fe content in the particle, size of particle and the operating conditions of the SCWG process. However, signs of deactivation of iron oxide after 172 h on-stream was observed, which was accompanied by some sintering on Fe, loss of surface area and loss of surface of active Fe. This was attributed to the SCW conditions. Exothermic reactions (e.g. Boudouard reaction and methanation) might be playing a key role on increasing the rate of metal sintering due to heat given out in reaction to the catalyst as well as the severe temperature conditions.

No evidence of Fe_2O_3-Cr_2O_3 and Fe_3O_4 deactivation was observed after 9 h exposure time, but conclusion cannot be made at this stage on the Fe_3O_4 strength in SCW conditions, when compared to Fe_2O_3-Cr_2O_3 at 172 h due to shorter exposure time (9 h) on-stream. Longer hour exposure of Fe_3O_4 on-stream is needed in order to assess it full strength.

8.3 Future work

This work demonstrates the use of a laboratory scale Packed Bed Reactor for the Catalytic Supercritical Water Gasification (CSCWG) of glycerol to produce hydrogen, carbon monoxide, light hydrocarbons and valuable liquid compounds such as methanol, ethanol, allyl alcohol, formaldehyde and acetaldehyde. Previous studies have reported on the use of heterogeneous catalysts (Ru and Rh) to promote hydrogen yield, to reduce the formation of tars and char during the CSCWG reaction. However, the aim of this work was to combine the utilisation of low cost Fe_2O_3-Cr_2O_3 or Fe_3O_4 catalysts to achieve conversion of glycerol or other organic wastes to gaseous products other than focusing on maximizing hydrogen yield.

Although the results showed promising aspects such as complete conversion of glycerol at concentrations up to 15 wt% at 550°C, increasing selectivity toward hydrogen and gaseous product yields could be improved by operating at optimal catalytic and process conditions. In addition, this process allows the utilisation of wet organic slurry as reactant, which addresses the challenges associated with organic waste disposal by reducing conversion costs and reducing process energy requirements. Moreover, the resulting product gases were obtained at high pressures, which can be particularly useful for many applications. In spite of these promising aspects, future investigations are still needed in order to provide comprehension understanding of the process and to bring this technology into commercial applications. Some of these include:

8.3.1 Development of reliable kinetic models

Detailed kinetics should be developed based on the gasification mechanism and reaction path to give guidance to the design of the SCWG system. Therefore, a comprehensive gasification mechanism has to be explored including catalyst implication, especially for the qualitative and quantitative analysis of the intermediate and final products.

8.3.2 Catalytic effect of the reactor wall

The wall effect of the reactor was not investigated explicitly in this work. The wall effect of the reactor cannot be underestimated because the metals selection and its composition in the reactor wall may have contributed to the catalytic effect on the reaction.

8.3.3 Reactor design: catalyst bed support & stability

Stainless steel reactor showed to be poorly suitable for its utilisation in this application. This is because 316L SS has suffered severe corrosion under the conditions employed. A sign of 316 L- SS

reactor failure was observed as evidenced by the materials leaking from the reactor fitting. Future work should be conducted in reactors with walls that do not suffer corrosion and do not interfere with the chemical reaction. On the other hand, change of reactor material to hastelloy or inconel steels has the potential to mitigate corrosion inside the reactor wall. This approach should also be investigated.

8.3.4 Feed transfer into the gasifier

This work has demonstrated also that soluble organic material can be transferred into the gasifier at a desired high pressure using a suitable pump as expected. However, the reactants delivery becomes extremely difficult with high feed concentration (>30 wt %) at ambient conditions and if the organic has a low or negligible solubility. Solving this problem required upgrading the pump for a high temperature delivery. A high feed concentration can be pre-heated to reduce the fluid viscosity and to improve its solubility, which will then facilitate its transfer into the reactor at the desired pressure. One way of achieving this pre-heating can be through the utilisation of a heat exchanger to recover the waste heat from the process stream leaving the reactor. On the other hand, delivery of insoluble organic such as digestate or other ligniocelluosic biomass solution can be more challenging. The existing pump was only able to deliver slurry of digestate at concentration less than 2 wt%. This was due to the presence of insoluble in the feed. This problem can be alleviated by upgrading the existing pump from a pump outlet hole of 1000 microns to 5000 to 10000 microns.

8.3.5 Scaling-up

CSCWG was performed in a small volume Packed Bed Reactors. Any commercial exploitation of this technology will require a large-scale implementation of the CSCWG process, which requires future investigation of some aspects concerning the reactor type such as evaluating the potential of a fluidized bed reactor. Furthermore, mixing in a flow reactor is not fully understood; therefore, experimental and theoretical studies to investigate mixing inside the flow tube, as well as the catalytic behaviour and stability of bed at a large scale would be beneficial.

9 REFERENCES

[1] Haas M. J.; McAloon A. J.; Yee W.C.; Foglia T.A.; A process model to estimate biodiesel production costs. Bioresource Technology, 2006, 97, 671–678.

[2] Mizuno, T.; Goto, M.; Kodama, A.; Hirose, T.; Supercritical Water Oxidation of a Model Municipal Solid Waste. Industrial Engineering Chemistry Research, 2000, 39, 2807-2810.

[3] Clifford, T. Fundamentals of Supercritical Fluids. Oxford University Press, New York, 1998, 22-23.

[4] Hao, X. H.; Guo, L. J.; Mao, X.; Zhang, X. M.; Chen, X. J.; International Journal of Hydrogen Energy, 2003, 28, 55-64.

[5] Simoneit B.R.T.; Hydrothermal effects on organic matter—high versus low temperature components. Organic Geochemistry,1984, 6, 857-864.

[6] Khuwijitjaru P.; Adachi S.; Matsuno R.; Solubility of Saturated Fatty Acids in Water at Elevated Temperatures. Bioscience Biotechnology Biochemical, 2002, 66, 1723–1726.

[7] Ziegler K.J.; Doty R.C.; Johnston K. P.; and Korgel A. B.; Synthesis of Organic Monolayer-Stabilized Copper Nanocrystals in Supercritical Water. Journal of American Chemistry Society, 2001, 123, 7797-7803.

[8] Calzavara Y.; Joussot-Dubien C.; Boissonnet G; Sarrade S.; Evaluation of biomass gasification in supercritical water process for hydrogen production. Energy Conversion and Management, 2005, 46, 615–631.

[9] Lee G.; Mi-Sun K.; Gasification of Glucose in Supercritical Water. Industrial Engineering Chemistry Research, 2002, 41, 1182–1188.

[10] Yoshida T.; Matsumura Y.; Gasification of Cellulose, Xylan, and Lignin Mixtures in Supercritical Water. Industrial Engineering Chemistry Research, 2001, 40, 5469–5474.

[11] Yan B.; Wei C.; Cheng-sheng H.; Cheng X.; Jun-zhang W.; Hydrogen generation from polyvinyl alcohol-contaminated wastewater by a process of supercritical water gasification, Journal of Environmental Sciences, 2007, 19, 1424–1429.

[12] Byrd, A.J.; Pant K. K.; Gupta R.B.; Hydrogen production from glycerol by reforming in supercritical water over Ru/Al_2O_3 catalyst. Fuel, 2008, 87, 2956–2960.

[13] Kyoung S. R.; Cantrell K.; Elliott D.; Hunt P.G.; Catalytic Wet Gasification of Municipal and Animal Wastes. Industrial Engineering Chemistry Research, 2007, 26, 8839–8845.

[14] Vostrikov A. A.; Fedyaeva O.N.; Shishkin A.V.; Dubov D.Y.; Sokol M.Y.; Conversion of municipal sewage sludge in supercritical water. Solid Fuel Chemistry, 2008, 6, 70–80.

[15] García Jarana M.B.; Sánchez-Oneto J.; Portela J.R., Nebot-Sanz E.; Martínez de la Ossa E.J.; Supercritical water gasification of industrial organic wastes. The Journal of Supercritical Fluids, 2008, 46, 329–334.

[16] Yoshida T.; Oshima Y.; Matsumura Y.; Gasification of biomass model compounds and real biomass in supercritical water, Biomass and Bioenergy, 2004, 26, 71–78.

[17] Williams P.T.; Onwudili J.; Subcritical and Supercritical Water Gasification of Cellulose, Starch, Glucose, and Biomass Waste, Energy Fuels, 2006, 20, 1259–1265.

[18] Savage P. E.; Gopalan S.; Mizan T.I.; Martino C. J.; Brock E.E.; Reactions at Supercritical Conditions: Applications and Fundamentals. AIChE Journal, 1995, 41, 1723-1726.

[19] Demirbas M. F.; Biorefineries for biofuel upgrading: A critical review. Applied Energy, 2009, 86, 151–161.

[20] Brunner G.; "Near critical and supercritical water. Part I. Hydrolytic and hydrothermal processes". The Journal of Supercritical Fluids, 2009, 47, 373-381.

[21] Kruse A.; Hydrothermal biomass gasification. The Journal of Supercritical Fluids, 2009, 47, 391–399.

[22] Kestin J.; Sengers J.V.; Kamgar-Parsi B.; Levelt Sengers J.M.H.; *Thermophysical Properties of Fluid H_2O.* Journal of Physical and Chemical Reference Data, *1984, 13, 175-183.*

[23] Ni. M.; Leung D.Y.C.; Leung M.K.H.; Sumathy K.; An overview of hydrogen production from biomass. Fuel Processing Technology, 2006, 87, 461– 472.

[24] Hitchen S. M., Dean J. R.; Properties of supercritical fluids, Applications of Supercritical Fluids in Industrial Analysis, 1993, 1-11.

[25] Veriansyah B.; Tae-Joon P.; Jong-Sung L., Youn-Woo L.; Supercritical water oxidation of wastewater from LCD manufacturing process: kinetic and formation of chromium oxide nanoparticles. The Journal of Supercritical Fluids, 2005, 34, 51-59.

[**26**] Balbuena P.B.; Johnston K. P.; Rossky P.J.; Molecular Dynamics Simulation of Electrolyte Solutions in Ambient and Supercritical Water. Ion Solvation, Journal of Physical. Chemistry, 1996, 100, 2706-2715

[**27**] Jessop P.G.; Leitner W.; Chemical Synthesis using Supercritical Fluid. New York, Wiley-VCH, 1999, ISBN 3-527-29605-0.

[**28**] Stillinger F. H.; Rahman A.; Molecular Dynamics Study of Temperature Effects on Water Structure and Kinetics. Journal of physical chemistry, 1972, 57, 1281-1289.

[**29**] Liong K. K.; Wells P.A.; Foster N.R.; Diffusion in Supercritical Fluids. The Journal of Supercritical Fluids, 1991, 4, 91-108.

[**30**] Debenedetti P.G.; Reid R.C.; Diffusion and mass transfer in supercritical fluids. AIChE. Journal, 1986, 32, 2034-2036.

[**31**] Swaid I.; Schneider G.M.; "Determination of Binary Diffusion Coefficients of Benzene and Some Alkyl benzenes in Supercritical CO, between 308 and 328 K in the Pressure Range 80 to 160 bar with Supercritical Fluid Chromatography," Reports of the Bunsen Society for Physical,1979, 83,969-976.

[32] Puiggen J.; Larrayoz M.A.; Recasens F.; Free liquid-to-supercritical fluid mass transfer in packed beds, Chemical Engineering Science*, 1997,* 52, 195-212.

[33] Dwivedi P. N.; Upadhyay S. N.; Particle-fluid mass transfer in fixed and fluidized beds. Industrial Engineering Chemical Process Design, 1977, 16, 157-165.

[34] Wakao N.; Kaguei S.; Heat and Mass Transfer in Packed Beds. Gordon and Breach, New York, U.S.A. 1982.

[35] Lee A. K. K.; Bulley N. R.; Fattori M.; Meisen A. Supercritical carbon dioxide extraction of canola oilseed in fixed beds, 1986, Journal of American Oil Chemistry Society,1986, 63, 921-928.

[36] Tan C.-S.; Liang S.K.; Liou D.C.; Fluid-solid mass transfer in a supercritical fluid extractor. Chemical Engineering Journal, 1988, 38, 17-21.

[37] Lim G. B; Holder G. D.; Shah Y. T.; Solid-fluid mass transfer in a packed bed under supercritical conditions. Supercritical Fluid Science and Technology, 1989, 406, 379-395.

[38] Lira, G.B.; Holder, G. D.; Shah Y. T.; Mass transfer in gas-solid systems at supercritical conditions. Journal of Supercritical Fluids, 1990, 3,186-197.

[39] Lee C. H.; Holder G. D.; Use of supercritical fluid chromatography for obtaining mass transfer coefficients in fluid solid systems at supercritical conditions. Industrial and Engineering Chemistry Research, 1995, 34, 906-909

[40] Zehnder B.; Trepp C.; Mass-transfer coefficients and equilibrium solubility for fluid supercritical solvent systems by online near IR-spectroscopy. Journal of Supercritical Fluids, 1993, 6,131-139.

[41] Knaff G.; Schliinder E. U.; Mass-transfer for dissolving solids in supercritical carbon dioxide. Part 1: resistance of the boundary layer. Chemical Engineering Process, 1987, 21, 151-159.

[42] Huppert G.L.; Wu B.C.; Townsend S.H.; Klein L. M., Paspek S. C. Hydrolysis in Supercritical Water: Identification and Implications of a Polar Transition State, Industrial and Engineering Chemistry Research, 1989, 28, 161-165.

[**43**] Johnston K.P.; Penninger J.M.L.; New directions in Supercritical Fluid Science and Technology; American Chemical Society, *ACS Symposium Series,* 1989, 406, ISBN 0-8412-1678-91.

[**44**] Savage P.E.; Gopalan S.; Mizan T.I.; Martino C.J.; Reactions at supercritical conditions: applications and fundamentals. AIChE Journal, 1995, 41, 1723-1778.

[45] Wasen U. V.; Swaid I.; Schneider G.M.; Physicochemical Principles and Applications of Supercritical Fluid Chromatography. New analytical methods, Angewandte Chemie International Edition in English, 2003, 19, 575-658.

[46] Savage P. E.; Gopalan S.; Mizan T. I.; Martino C.J.; Brock E.E.; Reactions at Supercritical Conditions: Applications and Fundamentals. AIChE Journal, 1995, 41, 1723-1777.

[47] Iyer S.D.; Michael T.; Klein M.T.; Effect of pressure on the rate of butyronitrile hydrolysis in high-temperature water. Journal of Supercritical Fluids,1997,10, 191-200.

[48] Eldik R. V.; Asano T.; Le Noble W. J.; Activation and Reaction Volumes in Solution, Chemical Reviews, 1989, 89, 549-688.

[49] Brunner G.; "Near critical and supercritical water. Part I. Hydrolytic and hydrothermal processes". *The* Journal of Supercritical Fluids, 2009, 47, 373-381.

[50] Tester J. W.; Holgate H. R.; Armellini F.J.; Webley P.A.; Killilea W. R.; Hong G.T.; Barner H. E.; Supercritical Water Oxidation Technology, Process Development and Fundamental Research, *ACS Symposium Series*, 1993, 518, 35–76.

[51] Ziegler K. J.; Christopher Doty R.C.; Johnston K. P.; Korgel B. A.; Synthesis of Organic Monolayer-Stabilized Copper Nanocrystals in Supercritical Water. Journal of American Society, 2001,123, 7797- 7803.

[52] Rincón J.; Camarillo R., Martín A.; Solubility of Aluminum Sulfate in Near Critical and Supercritical Water. *Journal of Chemical Engineering Data*, 2012, 57, 2084–2094

[53] Poole P. H.; Sciortino F.; Grande T.; Stanley H. E.; Angell C.A.; Effect of Hydrogen Bonds on the Thermodynamic Behavior of Liquid Water, Physical Review Letters. The American Physical Society, 1994, 73, 12-19

[54] Straus J. M.; Schubert G.; Thermal convection of water in a porous medium: Effects of temperature- and pressure-dependent thermodynamic and transport properties. Journal of Geophysical Research, Solid Earth and Planets, 1977, 82, 325–333.

[55] Townsend S. H., Abraham M.A.; Huppert I. G. L.; Klein I. M.; Paspek S.C. Solvent Effects during Reactions in Supercritical Water, Industrial & engineering chemistry research, 1988, 27, 143-149.

[56] Schmieder H.; Dahmen N., Schön J.; Wiegand G.; Industrial and environmental applications of supercritical fluids, Chemistry under Extreme or Non-Classical Conditions, Spektrum, Heidelberg, 1996, 273-278.

[**57**] Shaw R.W.; Brill T.B.; Clifford A.A.; Eckert C.A.; Supercritical water: A medium for chemistry - Chemical Engineering news, 1991.

[58] Jessop P.G.; Ikariya T.; Noyori R.; Homogeneous catalysis in supercritical fluids. Chemical. Reviews, 1999, 99, 475-477.

[59] Baiker A.; Supercritical fluids in heterogeneous catalysis. Chemical Reviews, 1999, 99, 453-473

[60] Darr J.A.; Poliakoff M.; New directions in inorganic and metal–organic coordination chemistry in supercritical fluids. Chemical Reviews, 1999, 99,495-499.

[61] Osada M.; Sato T.; Watanabe M.; Adschiri T.; Arai K.; Low-temperature catalytic gasification of lignin and cellulose with a ruthenium catalyst in supercritical water. Energy Fuels*, 2004, 18, 327–333.*

[**62**] Olofsson G.; LG Hepler L.G.; Thermodynamics of ionization of water over wide ranges of temperature and pressure. Journal of Solution Chemistry, 1975, 4, 128-137.

[63] Delgado J.; Aznar M.P.; Corella J.; "Biomass Gasification with Steam in Fluidized Bed: Effectiveness of CaO, MgO, and CaO−MgO for Hot Raw Gas Cleaning". Industrial & Engineering Chemistry Research, 1997, 36, 1535-1543.

[**64**] Akiya N.; Savage P. E.; Roles of Water for Chemical Reactions in High-Temperature Water. *Chemical Reviews, 2002, 102, 2725–2750.*

[65] Sealock L. J.; Elliott D.C; Baker E.G.; Butner R.S.; Chemical Processing in High-pressure Aqueous Environments. Historical Perspective and Continuing Developments. Industrial Engineering Chemical Research, 1993, 32, 1535-1541.

[66] Kritzer P.; Corrosion in high-temperature and supercritical water and aqueous solutions: a review, Journal of Supercritical Fluids, 2004, 29, 1–29.

[67] Yesodharan S.; Supercritical water oxidation: An environmentally safe method for the disposal of organic wastes. Review Articles, 2002, 82, 1112-1122.

[68] Killilea W.R.; Hong G.T.; Swallow K.C., Thomason T.B.; Supercritical Water Oxidation: Microgravity Solids Separation. Society of Automotive Engineers, 1988, 1, 1–12.

[69] Peterson A.A.; Vogel F.; Lachance R.P.; Froling M.; Antal Jr. M.J.; Tester J.W.; Thermochemical biofuel production in hydrothermal media: a review of sub and supercritical water technologies. Energy & Environmental Science, 2008, 1, 32–65.

[70] Matsumura Y.; Minowa T.; Potic B.; Kersten S.R.A.; Prins W.; Van Swaaij W.P.M.; Van de Beld B.; Elliott D.C.; Neuenschwander G.G.; A. Kruse A.; Antal Jr. M.J.; Biomass gasification in near- and super-critical water: status and prospects. Biomass and Bioenergy, 2005, 29, 269–292.

[71] Elliott D.C.; Phelps M.R.; Sealock Jr. L.J., Baker E.G.; chemical processing in high-pressure aqueous environments. Continuous-flow reactor process development experiments for organics destruction. Industrial and Engineering, Chemistry Research, 1994, 33, 566–574.

[72] Elliott D.C.; Neuenschwander G.G.; Phelps M.R.; Hart T.R.; Zacher A.H.; Silva L.J.; Chemical processing in high-pressure aqueous environments: Demonstration of catalytic gasification for chemical manufacturing wastewater cleanup in industrial plants. Industrial and Engineering Chemistry Research, 1999, 38, 879–883.

[73] Boukis N.; Galla U.; Jesus P.D.; Dinjus E.; Gasification of wet biomass in supercritical water. Results of pilot plant experiments, in 14th European Biomass Conference & Exhibition, 17–21 October, Paris, France, 2005.

[74] Krammer P.; Vogel H.; Hydrolysis of esters in subcritical and supercritical water. Journal of Supercritical Fluids, 2000, 16, 189–206.

[75] Boukis N.; Galla U.; Muller H.; E. Dinjus E.; Biomass gasification in supercritical water. Experimental progress achieved with the Verena pilot plant, in 15th European Biomass Conference & Exhibition, 7–11 May 2007, Berlin, Germany.

[76] Tanak Y.; Shimoda N.; Fukunaga T.; Kawashima S.; Kikuchi R.; Eguchi K.; Influence of solid–acid catalysts on steam reforming and hydrolysis of dimethyl ether for hydrogen production. Applied Catalysis A: General 2006, 304, 40–48.

[77] Chheda J.N.; Huber G.W.; Dumesic J.A.; Liquid-Phase Catalytic Processing of Biomass-Derived Oxygenated Hydrocarbons to Fuels and Chemicals, Angewandte Chemie International Edition, 2007, 46, 7164 – 7183

[78] Jessop P.G.; Ikariya T.; Noyori R.; Homogeneous catalysis in supercritical fluids, Chemical Reviews, 1999, 99, 475-478.

[79] Zhao X.; Cheng K.; Liu D.; Organosolv pretreatment of lignocellulosic biomass for enzymatic hydrolysis, Appl Microbiol Biotechnol, 2009, 82, 815–827.

[80] Lee J.H.; Foster N.R.; Direct Partial Oxidation of Methane to Methanol in Supercritical Water. The Journal of Supercritical Fluids, 1996, 9, 99-105.

[81] Hodes M.; Marrone .P.A.; Hong G.T.; Smith K.A.; Tester J.W.; Salt precipitation and scale control in supercritical water oxidation—Part A: fundamentals and research. Journal of Supercritical Fluids, 2004, 29, 265–288.

[82] Armellini F.J.; Phase Equilibria and precipitation phenomena of sodium chloride and sodium sulfate in sub- and supercritical water, PhD thesis, Massachusetts Institute of Technology, 1993.

[83] Wofford W.T.; Dell'Orco P.C.; Gloyna E.F.; Solubility of potassium hydroxide and potassium phosphate in supercritical water, Journal of Chemical & Engineering Data, 1995, 40,968–973.

[84] Cherubini F.; The biorefinery concept: Using biomass instead of oil for producing energy and chemicals, Energy Conversion and Management, 2010, 51, 1412–1421.

[85] McKendry P.; Energy production from biomass (part 2): conversion technologies. Bioresource Technology, 2002, 83, 47–54.

[86] Wang L.; Weller C. L.; Jones D.D.; Hanna M.A.; Contemporary issues in thermal gasification of biomass and its application to electricity and fuel production, Biomass and Bioenergy, 2008, 32, 573–581.

[87] Zhang S.; Hong R.; Cao. J., Takarada T.; Influence of manure types and pyrolysis conditions on the oxidation behavior of manure char. Bioresource Technology, 2009,100, 4278–4283.

[88] Anitescu G.; Tavlarides L.; Oxidation of Aroclor 1248 in Supercritical Water: A Global Kinetic Study, Industrial and Engineering Chemical Research, 2000, 39, 583-591.

[89] Gloyna E. F.; Li L.; Supercritical water oxidation research and development update. Environmental progress, 1995, 14, 182–192.

[**90**] Devi L., Ptasinski K. J.; Janssen J.J.G.; A review of the primary measures for tar elimination in biomass gasification processes. Biomass and Bioenergy, 2003, 24, 125-140.

[91] Marrone P.A.; Hodes M., Smith K.A.; Tester J.W. Salt precipitation and scale control in supercritical water oxidation—part B: commercial/full-scale applications. Journal of Supercritical Fluids, 2004, 29, 289–312.

[92] Barner H.E.; Huang C. Y.; Johnson T.; Jacobs G., Martch M.A.; Supercritical water oxidation: An emerging technology. Journal of Hazardous Materials, 1992, 31, 1-17.

[93] Spivey J.J.; Catalysis in the development of clean energy technologies.Catalysis Today, 2005,100, 171–180.

[94] Hong G.T.; Killilea W.R.; Thomason T.B.; Method for Solids Separation in a Wet Oxidation Type Process, 1989, U.S. Patent #4,822,497.

[95] Williams P. T.; Onwudili J.; Composition of Products from the Supercritical Water Gasification of Glucose: A Model Biomass Compound. Industrial and Engineering Chemistry Research, 2005, 44, 8739–8749.

[96] Spivey J.J.; Egbebi A.; Heterogeneous catalytic synthesis of ethanol from biomass-derived syngas, *Chemical Society Reviews*, 2007, 36, 1514-1528.

[97] Killilea W.R.; Hong G.T.; Swallow K.C.; Thomason T.B.; Supercritical Water Oxidation: Microgravity Solids Separation, Society of Automotive Engineers, 1988, 1, 1–12.

[98] Roos C. J.; Clean Heat and Power Using Biomass Gasification for Industrial and Agricultural Projects, WSUEEP08-033 Rev. 5, 2010.

[99] Williams P. T.; Jude Onwudili J.; Subcritical and Supercritical Water Gasification of Cellulose,

Starch, Glucose, and Biomass Waste. Energy & Fuels, 2006, 20, 1259-1265.

[100] Antal S.G.; Schulman A. D.; Xu X.; Divilio R.J.; "Biomass Gasification in Supercritical Water," Industrial & Engineering Chemistry Research, 2000, 39, 4040-4053.

[101] Yu D.; Aihara M.; Antal M.J.; "Hydrogen production by steam reforming glucose in supercritical water," *Energy & Fuels*, 1993, 7, 574-577.

[102] Hao X.H.; Guo L.J.; Mao X.; Zhang X.M.; Chen X.J.; Hydrogen production from glucose used as a model compound of biomass gasified in supercritical water. International Journal of Hydrogen Energy, 2003, 28, 55-64.

[103] Elliott D.C.; Sealock L.J.; Baker E.G.; "Chemical processing in high-pressure aqueous environments. Development of catalysts for gasification". *Industrial & Engineering Chemistry Research*, 1993, 32, 1542-1548.

[104] Peterson A. A.; Vogel F.; Lachance R. P.; Froling M.; Antal M. J.; Tester J. W.; Thermochemical biofuel production in hydrothermal media: a review of sub- and supercritical water technologies. *Energy* Environmental Science, 2008, 1, 32–65.

[105] Matsumura Y.; Minowa T.; Potic B.; Kersten S. R. A.; Prins W.; van Swaaij W. P. M.; van de Beld, B.; Elliott D. C.; Neuenschwander G. G.; Kruse, A.; Antal M. J.; Biomass gasification in near- and supercritical water: Status and prospects. *Biomass Bioenergy* 2005, *29*, 269–292

[106] Andries J.; Buhre B. J. P.; Catalytic Synthesis of Ethanol from Biomass-Derived Syngas, *DGMK* Tagungsbericht, 2000, 115–125.

[107] Koizumi N.; Murai, Ozaki K.T., Yamada M.; Development of sulfur tolerant catalysts for the synthesis of high quality transportation fuels, Catal. Today, 2004, 89, 465–478.

[108] Jun K.W., Roh H.S., Kim K.S., Ryu J.S.; Lee K.W.; Catalytic investigation for Fischer–Tropsch synthesis from bio-mass derived syngas. *Apply. Catalyst,* 2004, 259, 221–226

[109] Le Normand F.; Barrault J.; Breault R.; Hilaire L.; Kiennemann A. Catalysis with palladium deposited on rare earth oxides: influence of the support on reforming and syngas activity and *selectivity,* Journal of Physical Chemistry,*1991, 95, 257–269*.

[110] Spivey J. J.; Egbebi A.; Heterogeneous catalytic synthesis of ethanol from biomass-derived syngas. Chemical *Society Reviews*, 2007, 36, 1514-1528.

[111] Corain B.; Basato M.; Zecca M.; Direct synthesis of alcohols from n-olefins and syngas in the liquid phase catalyzed by rhodium supported on cross linked acrylic resins, Journal of Molecular Catalysis, 1992, 73, 23–41.

[112] Tronconi E.; Ferlazzo N.; Forzatti P.; Pasquon I.; Synthesis of alcohols from carbon oxides and hydrogen. Lumped kinetics for the higher alcohol synthesis over a zinc-chromium-potassium oxide catalyst, *Industrial and Engineering Chemical Research*, 1987, *26*, 2122–2129.

[113] Dalmon J.A.; Chaumette P.; Mirodatos C.; Higher alcohols synthesis on cobalt based model catalysts. Catalysis Today, 1992, 15, 101–127.

[114] Xiaoding X.; Scholten J.J.F.; Stability of copper/cobalt catalysts for the synthesis of higher alcohols from syngas, Applied Catalysis A: General, 1992, 82, 91–109.

[115] Camposmartin J.M., Guerreroruiz A., Fierro J.L.G.; Structural and Surface Properties of CuO-ZnO-Cr_2O_3 Catalysts and Their Relationship with Selectivity to Higher Alcohol Synthesis, Journal of Catalyst, 1995,156, 208-218.

[116] Woo H. C.; Park K. Y.; Gul Kim Y. G.; ShikChung J.; Lee J. S.; Mixed alcohol synthesis from carbon monoxide and dihydrogen over potassium-promoted molybdenum carbide catalysts. Applied Catalysis, 1991, 75, 267-280.

[117] Peterson A.A.; Vogel F.; Lachance R. .P.; Froling M.; Antal Jr. M. J.; Tester J. W.; Thermochemical biofuel production in hydrothermal media: A review of sub- and supercritical water technologies. Energy Environmental Science, 2008, 1, 32–65.

[118] Rabe S.; Truong T.; Vogel F.; Low temperature catalytic partial oxidation of methane for gas-to-liquids applications. Applied Catalysis A: General, 2005, 292, 177–188.

[119] Hartley F. R.; Pata S.; Oxidative addition and reductive elimination. The Metal - Carbon Bond: 1995, 2, DOI: 10.1002/9780470771747.

[120] Liu X. H., Li X.H., Fujimoto K.; Controllable Fischer–Tropsch Synthesis by In Situ-Produced 1-Olefins, ChemCatChem, Catalyst Communication, 2007, 8, 1329–1335.

[121] Chen C.; Yuuda H.; X.; Fischer–Tropsch synthesis over one egg shell-type Co/SiO_2 catalyst in a slurry phase reactor. Applied Catalysis A: General, 2011, 396, 116–122.

[122] Tavasoli A.; Abbasloua R. M.; Trepanier M.; Dalai A. K.; Fischer–Tropsch synthesis over cobalt catalyst supported on carbon nanotubes in a slurry reactor, Applied Catalysis A: General, 2008, 345, 134–142.

[123] Brunner G.; “Near critical and supercritical water. Part I. Hydrolytic and hydrothermal processes,” The Journal of Supercritical Fluids, 2009, 47, 373-381.

[124] Kestin J.; Sengers J.V.; Kamgar-Parsi B.; Levelt-Sengers, J.M.H.; *Thermophysical Properties of Fluid H_2O*, Journal of Physical Chemistry Ref. Data, 1984, 13, 175-183.

[125] Peterson A.A.; Vogel F.; Lachance R.P.; Froling M.; Antal Jr. M.J.;Tester, J.W.; Thermochemical biofuel production in hydrothermal media: A review of sub- and supercritical water technologies, Energy & Environmental Science, 2008, 1, 32–65.

[126] Hoogwijka M.; Faaija A., Van den Broeka R.; Berndes G.; Gielenc D.; Turkenburga, W.; Exploration of the ranges of the global potential of biomass for energy. Biomass and Bioenergy, 2003, 25, 119 – 133.

[127] Parikka M.; Global biomass fuel resources. Biomass and Bioenergy, 2004, 27, 613–620.

[128] Ni M.; Leung D.Y.C.; Leung M. K.H.; Sumathy K.; An overview of hydrogen production from biomass. Fuel Processing Technology, 2006, 87, 461 – 472.

[129] Montzka S.A.; Dlugokencky E. J.; J. H. Butler J.H.; Non-CO_2 greenhouse gases and climate change, Nature, 2011, 476, 43–50. Doi: 10.1038/nature10322.

[130] Strachan N.; Kannan R.; Hybrid modelling of long-term carbon reduction scenarios for the UK. Energy Economics, 2008, 30, 2947–2963.

[131] Vassilev S. V.; Baxter D.; Andersen L.K.; Vassileva C.G.; “An overview of the chemical composition of biomass”. Fuel, 2010, 89, 913-933.

[132] Pagliaro M.; Rossi M.; The Future of Glycerol. New Usages for a Versatile Raw Material, RSC Publishing, Cambridge, UK, 2008.

[133] Wendisch V.F.; Lindner S.N.; Meiswinkel T.M.; Use of glycerol in biotechnological applications, 2011, 1, 305-334.

[134] Johnson D.T.; Taconi K.A.; The Glycerin Glut: Options for the Value-Added Conversion of Crude Glycerol Resulting from Biodiesel Production. Environmental Progress, 2007, 26, 338-348.

[135] Pagliaro M.; Ciriminna R.; Kimura H.; M. Rossi; Pina. C.D.; From Glycerol to Value-Added Products. Chemical International Edition,2007, 46, 4434-4440.

[136] Boocock D.G.B.; Konar S. K.; V. Mao V.; Lee C.; Sonia Buligan, Fast formation of high-purity methyl esters from vegetable oils. Journal of the American Oil Chemists Society, 1998, 75, 1167-1172.

[137] Kumari V.; Shah S.; N. Gupt M.; Preparation of Biodiesel by Lipase-Catalyzed Transesterification of High Free Fatty Acid Containing Oil from Madhuca indica. Energy & Fuels, 2007, 21, 368-372.

[138] T. Valliyappan T. D.; Ferdous N. N.; Dalai B.A.K.; Production of Hydrogen and Syngas via Steam Gasification of Glycerol in a Fixed-Bed Reactor. Top Catal, 2008, 49, 59–67.

[139] Lang X.; Dalai A.K.; Bakhshi N.N.; Reaney M.J.; Hertz M.J.; Conversion of Degummed Soybean Oil to Biodiesel: Optimization of Degumming Methods and Evaluation of Fuel Properties. International Journal of Green Energy, 2010, 7, 6-11.

[140] Cortright R.D.; Davda R.R.; Dumesic J.A.; Hydrogen from catalytic reforming of biomass-derived hydrocarbons in liquid water. Nature, 2002, 418, 964-967.

[141] Rahmat N.; Abdullah A. Z.; Mohamed A.R.; Recent progress on innovative and potential technologies for glycerol transformation into fuel additives: A critical review, Renewable and Sustainable Energy Reviews, 2010, 14, 987–1000.

[142] Claude S.; Research of new outlets for glycerol – recent developments in France, Fett/Lipid 101, 1999, 3, 101–104.

[143] Guerrero-Pérez M.O.; Rosas J. M.; Bedia J.; Rodríguez-Mirasol J.; Cordero T.; Recent Inventions in Glycerol Transformations and Processing, Recent Patents on Chemical Engineering, 2009, 2, 11-21.

[144] Tsukuda E.; Sato S.; Takahashi R.; Sodesawa T.; Production of acrolein from glycerol over silica-supported heteropoly acids. Catalysis Communications, 2007, 8, 1349–1353.

[145] Ott L.; Bicker M.; Vogel H.; Catalytic dehydration of glycerol in sub- and supercritical water: a new chemical process for acrolein production. *Green Chemistry,* 2006, 8, 214-220.

[146] Deleplanque J.; Dubois J-L.; Devaux J.-F.; Ueda W.; Production of acrolein and acrylic acid through dehydration and oxydehydration of glycerol with mixed oxide catalysts. Catalysis Today, 2010, 157, 351–358.

[147] Wanga F., Dubois J.-L.; Ueda W.; Catalytic dehydration of glycerol over vanadium phosphate oxides in the presence of molecular oxygen. Journal of Catalysis, 2009, 268, 260–267.

[148] Golinska H.; Rojasa E.; López-Medina R.; Calvino-Casilda V.; Ziolek M.; Banares M.A.; Guerrero-Pérez M.O.; Designing new V–Sb–O based catalysts on mesoporous supports for nitriles production. Applied Catalysis A: General, 2010,380, 95–104.

[149] Liebiga C.; Paula S.; Katrynioka B.; Guillona C.; Couturiere J.-L.; Dubois J.-L.; Dumeignila F.; Hoelderich W.F.; Glycerol conversion to acrylonitrile by consecutive dehydration overWO3/TiO2 and ammoxidation over Sb-(Fe,V)-O. Applied Catalysis B: Environmental, 2013, 132, 170–182.

[150] Clacens J.-M.; Pouilloux Y.; Barrault J.; Selective etherification of glycerol to polyglycerols over impregnated basic MCM-41 type mesoporous catalysts. Applied Catalysis A: General, 2002, 227,181–190.

[151]Barrault J.; Clacens J.-M.; Pouilloux Y.; Selective oligomerization of glycerol over mesoporous catalysts. Topics in Catalysis, 2004, 27, 1–4.

[152] Watanabe T.; Sugiura W.; Satoa M.; Yamada N.; Nakanishi K.; Diacylglycerol production in a packed bed bioreactor. Process Biochemistry, 2005, 40, 637–643.

[153] Meher L.C.; Vidya-Sagar D.; Naik S.N.; Technical aspects of biodiesel production by transesterification. Renewable and Sustainable Energy Reviews, 2006, 10, 248–268.

[154] Dıaz I.; Mohino F.; Pérez-Pariente J.; Sastre E.; Synthesis of MCM-41 materials functionalised with dialkylsilane groups and their catalytic activity in the esterification of glycerol with fatty acids. Applied Catalysis A: General, 2003, 242,161–169.

[155] Jaecker-Voirol J.; Durand I.; Hillion G.; Delfort B.; Montagne X.; Glycerin for New Biodiesel Formulation. Formulation d'un nouveau biocarburant Diesel à base de glycérol, *Oil & Gas Science and* Technology – Reviews, 2008, 63, 395-404.

[156] Behr A.; Eilting J.; Irawadi K.; Leschinski J.; Lindner F.; Improved utilisation of renewable resources: New important derivatives of glycerol. Green Chemistry, 2008, 10, 13-30.

[157] Zhou C.-H. ; Beltramini J.N.; Yong-Xian Fanaand G. Q.; Chemoselective catalytic conversion of glycerol as a biorenewable source to valuable commodity chemicals, Chemical Society Reviews, 2008, 37, 527–549.

[158] Ruppert A. M.; Meeldijk J. D.; Kuipers B .W.M.; Ben H. E.; Weckhuysen B.M.; Glycerol Etherification over Highly Active CaO-Based Materials: New Mechanistic Aspects and Related Colloidal Particle Formation. Chemical European Journal, 2008, 14, 2016 – 2024.

[159] Scott E.; Peter F.; Sanders J.; Biomass in the manufacture of industrial products—the use of proteins and amino acids, Apply Microbiology Biotechnology, 2007, 75, 751–762.

[160] Van Haveren J.; Scott E. L.; Sanders J.; Bulk chemicals from biomass. Biofuels, Bioproduct. Biorefining, 2008, 2, 41–57.

[161] Homann T.; Tag C.; Biebl H.; Deckwer W.-D.; Schink B.; Fermentation of glycerol to 1,3-propanediol by *Klebsiella* and *Citrobacter* strains. Applied Microbiology and Biotechnology, 1990, 33, 121-126.

[162] Boenigk R.; Bowien S.; Gottschalk G.; Fermentation of glycerol to 1,3-propanediol in continuous cultures of Citrobacter freundii. Applied Microbiology and Biotechnology, 1993, 38, 453-457.

[163] Huang L.; Zhu Y.-L.; Zheng H.-Y.; Li Y-W.; Zeng Z.-Y.; Continuous production of 1,2-propanediol by the selective hydrogenolysis of solvent-free glycerol under mild conditions. Chemical Technology Biotechnology, 2008, 83, 1670–1675.

[164] Guo L.; Zhou J.; Mao J.; Guo X.; Zhang S.; Supported Cu catalysts for the selective hydrogenolysis of glycerol to propanediols. Applied Catalysis A: General, 2009, 367, 93–98.

[165] Hu W.; Knight D.; Lowry B.; Varma A.; Selective Oxidation of Glycerol to Dihydroxyacetone over Pt-Bi/C Catalyst: Optimization of Catalyst and Reaction Conditions, Industrial and Engineering Chemistry Research, 2010, 49, 10876–10882.

[166] Simonetti D.A.; Kunkes E.L.; Dumesic J.A.; Gas-phase conversion of glycerol to synthesis gas over carbon-supported platinum and platinum–rhenium catalysts. Journal of Catalysis, 2007, 247, 298–306.

[167] Simonetti D.A.; Rass-Hansen J.; Kunkes E. L.; Soares R.R.; Dumesic J.A.; Coupling of glycerol processing with Fischer–Tropsch synthesis for production of liquid fuels. *Green Chemistry,* 2007, 9, 1073-1083.

[168] Huber G. W.; Shabaker J. W., Dumesic J. A.; Raney Ni-Sn Catalyst for H_2 Production from Biomass-Derived Hydrocarbons. Science, 2003, 300, 2075-2077.

[169] Luoa N.; Fua X.; Cao F.; Xiaoa T.; Edwards P.P.; Glycerol aqueous phase reforming for hydrogen generation over Pt catalyst – Effect of catalyst composition and reaction conditions. Fuel, 2008, 87, 3483–3489.

[170] Palkovits R.; Nieddu I.; Kruithof C.A.; Klein G.R.J.M.; Weckhuysen B.M. Palladium-based telomerization of 1,3-butadiene with glycerol using methoxy-functionalized triphenylphosphine. Ligands ChemIcal Eurpean Journal, 2008; 14, 8995-9005.

[171] Guerrero-Pérez M. O.; Rosas J.M.; Bedia J.; Rodríguez-Mirasol J.; Tomás Cordero T.; Recent Inventions in Glycerol Transformations and Processing. Recent Patents on Chemical Engineering, 2009, 2, 11-21.

[172] Pachauri N.; He B.; "*Value-added Utilization of Crude Glycerol from Biodiesel Production: A Survey of Current Research Activities*". ASABE Annual International Meeting, 9 - 12 July 2006.

[173] Demirbas A.; Importance of biodiesel as transportation fuel. Energy Policy, 2007, 35, 4661–4670.

[174] Matsumura Y.; Minowa T.; Potic B.; Kerstenc S.R.A.; Prinsc W.; Van Swaaij P.M.; Van de Beld B.;. Elliotte D.C., Neuenschwander G.G.; Kruse A.; Antal Jr. M. J.; Biomass gasification in near- and super-critical water:Status and prospects. Biomass and Bioenergy, 2005, 29, 269–292.

[175] Maya A.; Salvadó J.; Torras C.; Montané D.; Catalytic gasification of glycerol in supercritical water. Chemical Engineering Journal, 2010, 160, 751–759.

[**176**] Van Bennekon J.G.; Kirillov V.A.; Amosov Y.I.; Krieger T.; Venderbosh R.H.; Assink D.; Lemmens K.P.J., Heeres H.J. Explorative catalyst screening studies on reforming of glycerol in Supercritical Water. The Journal of Supercritical Fluids, 2012, 70, 171-181.

[177] Bu¨hler W.; Dinjus E.; Ederer H.J.; Kruse A.; Mas C.; Ionic reactions and pyrolysis of glycerol as competing reaction pathways in near- and supercritical water. Journal of Supercritical Fluids, 2002, 22 37–53.

[178] Yu-Wu Q.M.; Weiss-Hortala E.; Barna R.; Boucard H.; Bulza S.; Glycerol and bioglycerol conversion in supercritical water for hydrogen production. Environmental Technology, 2012, 33, 2245–2255.

[179] Luo N.; Fu X.; Cao F.; Xiao T.; Edwards P.P.; Glycerol aqueous phase reforming for hydrogen generation over Pt catalyst – Effect of catalyst composition and reaction conditions. Fuel, 2008, 87 3483–3489.

[180] Huber G. W.; Shabaker J. W.; Dumesic J. A.; Raney Ni-Sn Catalyst for H_2 Production from Biomass-Derived Hydrocarbons. Science,2003, 300, 2075-2078.

[181] Iriondo A.; Barrio V.L.; Cambra J.F.; Arias P.L.; Güemez M.B.; Navarro R.M.; Sánchez-Sánchez M.C.; Fierro J. L. G.; Hydrogen production from glycerol over nickel catalysts supported on Al_2O_3 modified by Mg, Zr, Ce or La. Top Catal, 2008, 49, 46-58.

[182] Kong L.; Li G.; Zhang B.; He W.; Wang H.; Hydrogen production from biomass wastes by hydrothermal gasification, Energy Source. Part A, 2008, 30, 1166- 1178.

[183] Guo Y.; Wang S.Z.; Xu D.H.; Gong Y.M.; Ma H.H.;Tang X.Y.; Review of catalytic supercritical water gasification for hydrogen production from biomass. Renewable and Sustainable Energy Reviews,2010, 14, 334–343.

[184] Adhikari S.; Fernando S.D.; Haryanto A.; Hydrogen production from glycerol: An update. Energy Conversion and Management, 2009, 50, 2600–2604.

[185] Pompeo F.; Santori G.; Nichio N.N.; Hydrogen and/or syngas from steam reforming of glycerol.Study of platinum catalysts. International journal of hydrogen energy, 2010, 35, 8912-8920.

[186]. Byrd A.J.; Pant K.K.; Gupta R.B.; Hydrogen production from glycerol by reforming in supercritical water over Ru/Al_2O_3 catalyst. Fuel,2008, 87, 2956–2960.

[187] Maya A.; Salvadó J.; Torras C.; Montané D.; Catalytic gasification of glycerol in supercritical water. Chemical Engineering Journal, 2010, 160, 751–759.

[188] Ni M.; Leung D.Y.C.; Leung M.K.H.; Sumathy K.; An overview of hydrogen production from biomass. Fuel Processing Technology, 2006, 87, 461 – 472.

[189] Guo L.J.; Lu Y.J.; Zhang X.M., Ji C.M.; Guan Y.; Pei A.X.; Hydrogen production by biomass gasification in supercritical water:A systematic experimental and analytical study. Catalysis Today, 2007, 129, 275–286.

[190] Sricharoenchaikul V.; Assessment of black liquor gasification in supercritical water. Bioresource Technology, 2009, 100, 638–643.

[191] Chuntanapum A.; Matsumura Y.; Char Formation Mechanism in Supercritical Water Gasification Process: A Study of Model Compounds. Industrial and Engineering Chemistry Research, 2010, 49, 4055–4062.

[192] Karayıldırım T.; Sınag A.; Kruse A.; Char and Coke Formation as Unwanted Side Reaction of the Hydrothermal Biomass Gasification. Chemical Engineering Technology, 2008, 31, 1561–1568.

[193] Jesus P. D.; Boukis N.; Kraushaar-Czarnetzki B.; Dinjus E.; Influence of process variables on gasification of corn silage in supercritical water. Industrial and Engineering Chemistry Research, 2006, 45, 1622–1630.

[194] Yoshida T.; Partial Oxidative and Catalytic Biomass Gasification in Supercritical Water: A Promising Flow Reactor System. Industrial and Engineering Chemistry Research, 2004, 43, 4097-4104.

[195] Feng W.; Van der Kooi H. J.; Swaan-Arons J.; Biomass conversions in subcritical and supercritical water:driving force, phase equilibria, and thermodynamic analysis. Chemical Engineering and Processing, 2004, 43,1459–1467.

[196] Bröll D.; Kaul C.; Krämer A.; Krammer P.; Richter T.; Jung M.; Vogel H.; Zehner P.; Chemistry in Supercritical Water. Angewandte Chemie International Edition, 1999, 38, 2998-3014.

[197] Xu X.; Matsumura Y.; Stenberg J.; Antal Jr. M.J.; Carbon-Catalyzed Gasification of Organic Feedstocks in Supercritical Water. Industrial and Engineering Chemistry Research, 1996, 35, 2522-2530.

[198] Kruse A.; Gawlik A.; Biomass Conversion in Water at 330−410 °C and 30−50 MPa. Identification of Key Compounds for Indicating Different Chemical Reaction Pathways. Industrial and Engineering Chemistry Research, 2003, *42*, 267–279.

[199] Watanabe M.; Sato T.; Inomata H.; Smith R. L.; Arai Jr. K.; Kruse A.; Dinjus E.; Chemical Reactions of C_1 Compounds in Near-Critical and Supercritical Water. Chemical Reviews, 2004, 104, 5803−5821.

[200] Guo S.; Guo L.; Cao C.; Yin J.; Lu Y.; Zhang X.; Hydrogen production from glycerol by supercritical water gasification in a continuous flow tubular reactor. International journal of hydrogen energy,2012, 37, 5559-5568.

[201] Qadariyah L.; Sumarno M.; Machmudah S.; Wahyudiono S. M.; Goto M.; Degradation of glycerol using hydrothermal process. Bioresource Technology, 2011, 102, 9267-9271.

[202] Shu-Lai-Mok W.; Antal Jr. M. J.; Formation of Acrylic Acid from Lactic Acid in Supercritical Water, Journal of Organic Chemistry,1989,54, 4596-4602.

[203] Tsukuda E.; Sato S.; Takahashi R.; Sodesawa T.; Production of acrolein from glycerol over silica-supported heteropoly acids. Catalysis Communications, 2007, 8, 1349–1353.

[204] Subramani V.; Gangwal S.K.; A Review of Recent Literature to Search for an Efficient Catalytic Process for the Conversion of Syngas to Ethanol. Energy & Fuels, 2008, 22, 814-839.

[205] Fang K.; Li D.; Lin M.; Xiang M.; Wei W.; Sun Y.; A short review of heterogeneous catalytic process for mixed alcohols synthesis via syngas. Catalysis Today, 2009 147, 133–138.

[206] Bermejo D.M.; Cocero M.J.; Supercritical Water Oxidation: A Technical Review, AIChE Journal, 2006, 52, 3933 – 3951.

[207] Sippula O.; Lind T.; Jokiniemi J.; Effects of chlorine and sulphur on particle formation in wood

combustion performed in a laboratory scale reactor. Fuel, 2008, 87, 2425–2436.

[208] Ni M.; Leung D. Y.C.; Leung M.K.H.; Sumathy K.; An overview of hydrogen production from biomass. Fuel Processing Technology, 2006, 87, 461 – 472.

[209] Schmieder H.; Abeln J.; Boukis N.; Dinjus E.; Kruse A.; Kluth M.; Petrich G.; Sadri E.; Schacht M.; Hydrothermal gasification of biomass and organic wastes. Journal of Supercritical Fluids, 2000,17, 145–153.

[210] Elliott D.C.; Catalytic hydrothermal gasifi cation of biomass. Biofuels, Bioproducts, Biorefining, 2008, 2, 254–265.

[211] Luterbacher J.S.; Fröling M.; , Vogel F.; Maréchal F.; Jefferson W. Tester J.W.; Hydrothermal Gasification of Waste Biomass: Process Design and Life Cycle Assessment. *Environmental Science* Technology*, 2009, 43, 1578–1583.*

[212] Kruse A.; Dinjus E.; Influence of Salts during Hydrothermal Biomass Gasification: The Role of the Catalysed Water-Gas Shift Reaction. Journal of Physical Chemistry, 2005, 219, 341-366.

[213] Schmieder H.; Abeln J.; Supercritical Water Oxidation: State of the Art, Chemical Engineering Technology, 1999, 22, 11-19.

[214] Kritzer P.; Dinjus E.; An assessment of supercritical water oxidation (SCWO). Existing problems, possible solutions and new reactor concepts. Chemical Engineering Journal, 2001, 83, 207–214.

[215] Hodes M.; Marrone P.A.; Hong G.T.; Smith K.A.; Tester J.W.; Salt precipitation and scale control in supercritical water oxidation—Part A: fundamentals and research. Journal of Supercritical Fluids, 2004, 29, 265–288.

[216] Schubert M.; Regler J.W.; Vogel F.; Continuous salt precipitation and separation from supercritical water. Part 1 salts. Journal of Supercritical Fluids, 2010, 52, 99–112.

[217] Marrone P.A.; Hodes M.; Smith K.A.; Tester J.W.; Salt precipitation and scale control in supercritical water oxidation—part B: commercial/full-scale applications. Journal of Supercritical Fluids, 2004, 29, 289–312.

[218] Veriansyah B.; Kim J.-D.; Supercritical water oxidation for the destruction of toxic organic wastewaters: A review. Journal of Environmental Sciences, 2007, 19, 513–522.

[219] Schubert M.; Regler J.W.; Vogel F.; Continuous salt precipitation and separation from supercritical water. Part 1 salts. Journal of Supercritical Fluids, 2010, 52, 99–112.

[220] Gao N.; Lia A.; Quan C.; Gao F.; Hydrogen-rich gas production from biomass steam gasification in an updraft fixed-bed gasifier combined with a porous ceramic reformer. International journal of hydrogen energy, 2008, 33, 5430–5438.

[221] Shie J.-L.; Chang C.-Y.; Chena C.-Y.; Dai-Gee Shaw D.-G.; Chen Y.-H.; Kuan W.-H.; Ma H.-K.; Energy life cycle assessment of rice straw bio-energy derived from potential gasification technologies. Bioresource Technology, 2011, 102, 6735–6741.

[222] Elliott D. C.; Catalytic hydrothermal gasification of biomass, Biofuels, Bioproducts, Biorefining, 2008, 2, 254–265.

[223] Calzavara Y.; Joussot-Dubien C.; Boissonnet G.; Sarrade S.; Evaluation of biomass gasification in supercritical water process for hydrogen production. Energy Conversion and Management, 2005, 46, 615–631.

[224] Xu D., Wang S.; Hu X. Chen C., Zhang Q.; Gong Y.; Catalytic gasification of glycine and glycerol in supercritical water. International journal of hydrogen energy, 2009, 34, 5357–5364.

[225] May A.; Salvadóa J.; Torras C.; Montané D.; Catalytic gasification of glycerol in supercritical water. Chemical Engineering Journal, 2010, 160, 751–759.

[226] Byrd A.J.; Pant K.K.; Gupta R.B.; Hydrogen production from glycerol by reforming in supercritical water over Ru/Al_2O_3 catalyst. Fuel, 2008, 87, 2956–2960.

[227] Chakinala A. G.; Brilman D.W.; Van Swaaij -Wim P.M.; Kersten S.R.A.; Catalytic and Non-catalytic Supercritical Water Gasification of Microalgae and Glycerol. Industrial and Engineering Chemical Research, 2010, 49, 1113–1122.

[228] Sa´nchez E.A.; D'Angelo M.A.; Comelli R.A.; Hydrogen production from glycerol on Ni/Al_2O_3 catalyst. International journal of hydrogen energy, 2010, 35, 5902–5907.

[229] Feng J.; Fu H.; Wang J.; Li R.; Chen H.; Li X.; Hydrogenolysis of glycerol to glycols over ruthenium catalysts: Effect of support and catalyst reduction temperature. Catal Communication, 2008, 9, 1458-1464.

[230] Kinga D.L.; Zhang L.; Xia G.; Karim A.M.; Heldebrant D.J.; Wang X.; Peterson T.; Yong Wanga Y.; Aqueous phase reforming of glycerol for hydrogen production over Pt–Re supported on carbon, Applied Catalysis B: Environmental, 2010, 99, 206–213.

[**231**] Cornell R. M.; Schwertmann U.; the iron oxides structure, structure, properties, reactions, occurrences and uses, 2nd edition, Wiley VCA, 2003, ISBN 3-527-3027.

[232] Trambouze P. ; Euzen J.-P.; Chemical reactors: from design to operation, 2004, 16, Editions OPHRYS, 656-659, ISBN 2710811243, 9782710811244.

[233] Bangala D. N.; Abatzoglu N.; Chornet E.; Steam Reforming of Naphthalene on Ni-Cr/Al_2O_3 Catalysts Doped with MgO, TiO_2, and La_2O_3. AIChE Journal, 1998, 44, 927-937.

[**234**] Arauzo J.; Radlein D.; Piskorz J.; Scott D.S.; Catalytic pyro-gasification of biomass. Evaluation of modified nickel catalysts, Industrial and Engineering Chemistry Research, 1997, 36, 67-69.

[**235**] Furusawa T.; Sato T.; Sugito H.; Miura Y.; Ishiyama Y.; Sato M.; Itoh N.; Suzuki N.; Hydrogen production from the gasification of lignin with nickel catalysts in supercritical water. International Journal of Hydrogen Energy, 2007, 32, 699 – 704.

[**236**] Thompson P.; Cox D. E.; Hastings J.B.; Rietveld refinement of Debye-Scherrer synchrotron X-ray data from Al_2O_3. Journal of Applied Crystallography, 1987, 20, 79-83.

[237] Sing K. S. W.; Everett D. H.; Reporting physisorption data for gas/solid systems with Special Reference to the Determination of Surface Area and Porosity, Pure & Applied Chemistry, 1985, 57, 603—619.

[**238**] Mizuno N.; Misono M.; Heterogeneous Catalysis. Chemical Reviews, 1998, 98, 199-217.

[**239**] Germain J.; Fréchet J.M.J.; Svec F.; Hypercrosslinked polyanilines with nanoporous structure and high surface area: potential adsorbents for hydrogen. *Journal of Materials and Chemistry* 2007, 17, 4989-4997.

[**240**] Franke O.; Schulz-Ekloff G.; Rathousky J.; Starek J.; Zukal A.; Unusual type of adsorption isotherm describing capillary condensation without hysteresis. Journal of Chemical Society, Chemical Communication, 1993, 724-726.

[**241**] Branton P. J.; Hall P. G.; Sing K. S. W.; Physisorption of nitrogen and oxygen by MCM-41, a model mesoporous adsorbent, Journal of Chemical Society, Chemical Communication, 1993, 1257-1258.

[242] Wendisch V.F.; Lindner S. N.; Meiswinkel T. M.; Use of glycerol in biotechnological applications, 2011, 305-334.

[**243**] Rahmat N.; Abdullah A. Z.; Mohamed A.R.; Recent progress on innovative and potential technologies for glycerol transformation into fuel additives: A critical review. Renewable and Sustainable Energy Reviews, 2010, 14, 987–1000.

[244] Yuksel A.; Koga H.; Sasaki M.; Goto M.; Hydrothermal Electrolysis of Glycerol using a Continuous Flow Reactor. Industrial and Engineering Chemistry Research, 2010, 49, 1520-1525.

[245] Montané D.; May A.; Salvadó J.; Catalytic Gasification of Glycerol in Supercritical Water for Hydrogen Production, WHEC, 2010, 5, 16-21.

[246] Van Bennekon J.G.; Assink D.; Heeres H.J. Reforming of Methanol and Glycerol in Supercritical Water. Journal of Supercritical Fluids, 2011, 58, 99-113.

[247] May A.; Salvedo J.; Torras C.; Montane D.; Catalytic gasification of glycerol in supercritical water. Chemical Engineering Journal, 2010, 160, 751-759.

[248] Weingartner H.; Ulrich Franck E.; Supercritical Water as a Solvent. Angewandte Chemie International Edition, 2005, 44, 2672 – 2692.

[249] Dileo G.J.; Neff M.E.; Kim S.; Savage P.E.; Supercritical water gasification of phenol and glycine as models for plant and protein biomass. Energy & Fuels, 2008, 22, 871-877.

[250] Xiaodong X.; Yukihiko M.; Jonny S.; Michael J.; Carbon-catalysed Gasification of Organic Feedstock in Supercritical Water. Industrial and Engineering Chemistry Research, 1996, 35, 2522-2530.

[251] Adam J.B.; Pant K.K.; Ram B.G.; Hydrogen Production from Glycerol by Reforming in Supercritical Water over Ru/Al_2O_3 Catalyst. Fuel, 2008, 87, 2956–2960.

[252] Xu D.; Wang S.; Hu X.; Chen C.; Zhang Q.; Catalytic Gasification of Glycerine and Glycerol in Supercritical Water. International Journal of Hydrogen Energy, 2009, 34, 5357-5364.

[253] Voll F.A.P.; Rossi C.C.R.S.; Silva C.; Guirardello R.; Sourza R.O.M.A.; Cabrall V.F.; Cardozo-Filho L.; Thermodynamic Analysis of Supercritical Water Gasification of Methanol, Ethanol, Glycerol, Glucose and Cellulose. International Journal of Hydrogen Energy, 2009, 34, 9737-9744

[254] May A.; Salvadó J.; Torras C.; Montané D.; Catalytic gasification of glycerol in supercritical water. Chemical Engineering Journal, 2010, 160, 751–759.

[255] Gutiérrez Ortiz F.J.; Serrera A.; Galera S.; Ollero P.; Experimental study of the supercritical water reforming of glycerol without the addition of a catalyst. Energy, 2013, 56, 193-206.

[256] Yoshida T.; Oshima Y.; Matsumura, Y.; Gasification of biomass model compounds and real biomass in supercritical water. Biomass and Bioenergy, 2006, 26, 71–78.

[257] Osada M.; Sato O.; Arai, K.; Shirai M.; Stability of Supported Ruthenium Catalysts for Lignin Gasification in Supercritical Water. Energy & Fuels, 2006, 20, 2337-2343.

[258] Antal M. J.; Allen S.; Lichwa J.; Schulman D.; Xu X.; Hydrogen production from high-moisture content biomass in supercritical water, proceedings of the US-DOE hydrogen program review. NREL/CP-570-26938, 1999, 2-24.

[**259**] Sundari R.; Vaidya P.D.; Reaction Kinetics of Glycerol Steam Reforming Using a Ru/Al_2O_3 Catalyst. Energy Fuels, 2012, 26, 4195−4204.

[**260**] Fan X.; Burton R. Zhou Y.; Glycerol (By-product of Biodiesel Production) as a Source for Fuels and Chemicals – Mini Review. The Open Fuels & Energy Science Journal, 2010, 3, 17-22.

[**261**] Lu Y.; Li S.; Guo L.; Zhang X.; Hydrogen production by biomass gasification in supercritical water over Ni/gAl_2O_3 and Ni/CeO_2-gAl_2O_3 catalysts. International Journal of hydrogen energy, 2010, 35, 7161-7168.

[**262**] Mark E.; Dry M.; The fischer-tropsch process - commercial aspects. Catalysis Today, 1990, 6, 183–206.

[**263**] Schulz H.; Short history and present trends of Fischer–Tropsch synthesis, Applied Catalyst. A: General, 1999, 186, 2-13.

[**264**] Sato T.; Kurosawa S.; Smith Jr. R.L.; Adschiri T.; Arai K.; Water gas shift reaction kinetics under noncatalytic conditions in supercritical water. Journal of Supercritical Fluids, 2004, 29,113–119.

[265] Goula M. A.; Kontou S. K.; Tsiakaras P. E.; Hydrogen production by ethanol steam reforming over a commercial Pd/_-Al_2O_3 catalyst, Applied Catalysis B: Environmental, 2004, 49,135–144.

[266] Haryanto A.; Fernando S.; Murali N.; Current status of hydrogen production techniques by steam reforming of ethanol, a review. Energy Fuels, 2005, 19, 2098-2106.

[267] San S.H.; Park D.; Duffy G.J.; Edwards J.H.; Roberts D.G.; Llyushechkin A.; Morpeth L.D.; Nguyen T.; Kinetics of High-Temperature Water-Gas Shift Reaction over two Iron-based Commercial Catalysts using Simulated Coal-derived Syngas. Chemical Engineering Journal, 2009, 146, 148–154.

[268] Paul A.W.; Jefferson W.T.; Fundamental Kinetics of Methane Oxidation in Supercritical Water. Energy and Fuels, 1991, 5, 411- 419.

[**269**] Adhikari S.; Fernando S.D.; Haryanto A.; Hydrogen production from glycerol: An update, Energy Conversion and Management, 2009, 50, 2600–2604.

[270] Adhikari S.; Fernando S.D.; Haryanto A.; Production of hydrogen by steam reforming of glycerin over alumina supported metal catalysts. Catal Today, 2007,129, 355–64.

[271] Matsumura Y.; Minowa T.; Biljana P.; Kersten S.R.A., Wolter P.; Willibrordus P.M.; Bert van de B.; Douglas C.E.; Neuenschwandere G.G.; Andrea K.; Antal J.M.; Biomass gasification in near- and supercritical water: Status and Prospects, Biomass and Bioenergy,2005, 29, 269–292.

[272] Coll R.; Salvado J.; Farriol X.; Montane D.; Steam Reforming Model Compounds of Biomass Gasification Tars: Conversion at Different Operating Conditions and Tendency towards Coke Formation. Fuel Process Technology, 2001, 74, 19–31.

[273] Hirai T.; Ikenaga N.O.; Miyake T.; Suzuki T.; Production of Hydrogen by Steam Reforming of Glycerin on Ruthenium Catalyst. Energy Fuels, 2005, 19, 1761–1762.

[274] Richard K.H.; Jefferson W.T.; Oxidation Kinetics of Carbon Monoxide in Supercritical Water, Energy and Fuels, 1987, 1, 417- 423.

[**275**] Penninger J.M.L.; Marco R.; Reforming of aqueous wood pyrolysis condensate in supercritical water. International Journal of Hydrogen Energy, 2006, 31, 1597 – 1606.

[**276**] Antal M.J.; Glen Allen S.; Schulman D.; Xu X.; Biomass Gasification in Supercritical Water. Industrial and Engineering Chemistry Research, 2000, 39, 4040-4053.

[**277**] Xu X.; Matsumura Y.; Stenberg J.; Antal M.J.; Carbon-Catalyzed Gasification of Organic Feedstock in Supercritical Water. Industrial and Engineering Chemistry Research, 1996, 35, 2522-2530.

[278] Adam J.B.; Pant K.K.; Ram B.G.; Hydrogen Production from Glycerol by Reforming in Supercritical Water over Ru/Al_2O_3 catalyst. Fuel, 2008, 87, 2956–2960.

[279] Xue E.; O'Keeffe M.; Ross J.R.H.; Water–Gas Shift Conversion using a Feed with a Low Steam to Carbon Monoxide ratio and Containing Sulfur. Catal Today, 1996, 30, 107–118.

[**280**] Van Bennekom J.G.; Venderbosch R.H.; Assink D.; Heeres H.J.; Reforming of methanol and glycerol in supercritical water. Journal of Supercritical Fluids, 2011, 58, 99– 113.

[**281**] Bett J.A.; Kinoshita K.; Stonehart P.; Crystallite Growth of Platinum Dispersed on Graphitized Carbon Black. Journal of catalysis, 1976, 41, 124-133.

[282] Rideal and Taylor; "Catalysis in Theory and Practice", First Edition, London, Macmillan Co., 1919. 63-67.

[283] Buhler W.; Dinjus E.; Ederer H.J.; Kruse A.; C. Mas C.; Ionic reactions and pyrolysis of glycerol as competing reactions pathways in near-and supercritical water; Journal of Supercritical Fluids, 2002, 22, 37-53.

[284] Brunner G.; Near critical and supercritical water. Part I. Hydrolytic and hydrothermal processes, Journal of Supercritical Fluids, 2009, 47, 373–381.

[285] May A.; Salvadó J.; Torras C.; Montané, D.; Catalytic gasification of glycerol in supercritical water. Chemical Engineering Journal, 2010, 160, 751–759.

[286] Subramani V.; Gangwal S.K.; "A Review of Recent Literature to Search for an Efficient Catalytic Process for the Conversion of Syngas to Ethanol". Energy & Fuels, 2008, 22, 814-839.

[287] Hu J.; Dagle R. A.; Holladay J. D.; Cao C.; Wang Y.; White J. F.; Elliott D. C.; Stevens D. J.; Alcohol synthesis from CO or CO_2. US Patent application publication No. US2007/0161717, 2007

[288] Takeuchi K.; Matsukaki T.; Arakawa H.; Sugi Y.; "Synthesis of ethanol from syngas over Co-Re Sr/SiO_2 Catalysts". Applied Catalysis, 1985, 18, 325-334.

[289] Subramani V.; Gangwal S.K.; "A Review of Recent Literature to Search for an Efficient Catalytic Process for the Conversion of Syngas to Ethanol" .Energy & Fuels, 2008, 22, 814-839.

[290] Nimlos M.R.; Blanksby S.J.; Qian X.; Himmel M.E.; Johnson D.K.; Mechanisms of Glycerol Dehydration. Journal of Physical Chemistry, 2006, 110, 6145-6156.

[291] Buhler W.; Dinjus E; Ederer H.J.; Kruse A.; Mas C.; Ionic reactions and pyrolysis of glycerol as competing reaction pathways in near- and supercritical water. Journal of Supercritical Fluids, 2002, 22 37 – 53.

[292] Bai S.; Yonker C. R.; Pressure and Temperature Effects on the Hydrogen-Bond Structures of Liquid and Supercritical Fluid Methanol. Journal of Physical Chemistry, 1998, 102, 8641-8647.

[293] Johnson D.T.; Taconi K.A.; The glycerine glut: options for the value-added conversion of crude glycerol resulting from biodiesel production. Environmental progress, Wiley Interscience, 2007, 26 1-11.

[294] Chai S.; Wang H.; Liang Y.; Xu B.; sustainable production of acrolein: Gas-phase dehydration of glycerol over Nb_2O_5 catalyst. Journal of Catalysis, 2007, 250, 342-349.

[295] Smith A.M.; Mao J.; Metabolic fate of acrolein under aerobic and anaerobic aquatic conditions, Journal of Agricultural and Food Chemistry,1995, 43, 2497- 2503.

[296] Katryniok B.; Paul S.; Capron M.; Dumeignil F.; Towards the Sustainable Production of Acrolein by Glycerol Dehydration. ChemSusChem, 2009, 2, 719–730.

[297] Ramayya S.; Brittain A.; DeAlmeida C.; Mok W.; Antal Jr. M.J.; Acid-catalysed dehydration of alcohols in supercritical water. Fuel, 1987, 66, 1365-1372.

[298] Pagliaro M.; Ciriminna R.; Kimura H.; Rossi M.; Della Pina C.; From Glycerol to Value-Added Products. Angewandte Chemie International Edition, 2007, 46, 4434 – 4440.

[299] Demirbas M.F. Biorefineries for biofuel upgrading: A critical review, Applied Energy, 2009, 86, 151-161.

[300] Montané D.; May A.; Salvadó J.; Catalytic Gasification of Glycerol in Supercritical Water for Hydrogen Production, WHEC, 2010, 5, 16-21.

[301] Van Bennekon J.G.; Assink D.; Heeres H.J.; Reforming of Methanol and Glycerol in Supercritical Water. Journal of Supercritical Fluids, 2011, 58, 99-113.

[302] Guo Y.; Wang S.Z.; Xu D.H.; Gong Y.M.; Ma H.H.; Tang X.Y.; Review of Catalytic Supercritical Water Gasification for Hydrogen Production from Biomass. Energy Reviews, 2010, 14, 334 –343.

[303] Wen G.; Xu Y.; Ma H; Xu Z.; Tian Z.; Production of hydrogen by aqueous-phase reforming of glycerol. International journal of hydrogen energy, 2008, 33, 6657–6666.

[304] He L.; Salamanca-Parra J. M.; Blekkan E. A.; De Chen D.; Towards efficient hydrogen production from glycerol by sorption enhanced steam reforming, Energy Environmental Science, *2010,* 3, *1046-1056*

[305] Thompson J.C.; He B.; Characterisation of crude glycerol from biodiesel production from multiple feedstocks. Applied Engineering in Agriculture, 2006, 22, 261-265.

[306] Sınag A.; Kruse A.; Schwarzkopf V.; Key Compounds of the Hydropyrolysis of Glucose in Supercritical Water in the Presence of K_2CO_3. Industrial and Engineering Chemistry Research, 2003,42, 3516-3521.

[307] Matsumura Y.; Minowa T.; Potic B.; Kersten S.A.; Prins W.; Willibrordus P.S.; Biomass gasification in near- and supercritical water: status and prospects. Biomass Bioenergy, 2005, 29, 269–292.

[308] Calzavara Y.; Joussot D.C.; Boissonnet G.; Sarrade S.; Evaluation of biomass gasification in supercritical water process for hydrogen production. Energy Conversion Management, 2005, 46, 615–631.

[309] May A.; Salvadó J.; Torras C.; Montané D.; Catalytic gasification of glycerol in supercritical water. Chemical Engineering Journal, 2010, 160, 751–759.

[310] Buhler W.; Dinjus E.; Ederer H.J.; Kruse A.; Mas C.; Ionic reactions and pyrolysis of glycerol as competing reactions pathways in near-and supercritical water. Journal of Supercritical Fluids, 2002, 22, 37-53.

[311] Brown M.J.; Parkyns N.D.; Progress in the partial oxidation of methane to methanol and formaldehyde. Catalysis Today, 1991, 8, 305–335.

[312] Osada M.; Watanabe M.; Sue K.; Adschiri T.; Arai K.; Water density dependence of formaldehyde reaction in supercritical water. Journal of Supercritical Fluids, 2004, 28, 219–224.

[313] Xu X.; De Almeida C.; Antal, Jr. M.J.; Mechanism and Kinetics of the Acid-Catalyzed Dehydration of Ethanol in Supercritical Water. The Journal of Supercritical Fluids, 1990, 3, 228-232.

[314] Takashashi K.; Takezawa N.; Kobayashi H.; Third World Congress on Oxidation Catalysis, Apply Catal, 1982, 2, 363-364.

[315] Watanabe M.; Sato T.; Inomata H.; Smith R. L.; Jr., Arai K.; Kruse A.; Dinjus E.; Chemical Reactions of C_1 Compounds in Near-Critical and Supercritical Water. Chemical Reviews, 2004, 104, 5803−5821.

[316] Rodríguez J.C.; Marchi A.J.; Borgna A.; Monzón A.; Effect of Zn Content on Catalytic Activity and Physicochemical Properties of Ni-Based Catalysts for Selective Hydrogenation of Acetylene. Journal of Catalysis, 1997, 171, 268-278.

[317] Rostrup-Nielsen J.R.; Trimm D.L.; Natural Gas Conversion Vii: Proceedings of the 7th Natural Gas Conversion. Journal of Catalysis, 1977, 48, 155-159.

[318] Menon P.G.; Mol.J.; Progress in Catalysis, ISBN 0-444-89556-6, 1990, 59, 207-208.

[319] Guisnet M.; Ramoa Ribeiro F.; Deactivation and Regeneration of solid catalysts, 2011, 9, 1-17, IBSN: 139978-1-84816-637-0

[320] Suen T.J.; Chen T. P.; Chu P. S.; Influence of External Factors in Catalytic Reactions, Dehydrogenation of Ethyl Alcohol with Copper Catalyst. Industrial and Engineering Chemistry, 1942 - ACS Publications, 674-683.

[321] Chai S.-H.; Wang H.-P.; Liang Y.; Xu B.-Q.; Sustainable production of acrolein: investigation of solid acid–base catalysts for gas-phase dehydration of glycerol. *Green Chemistry*, 2007, 9, 1130-1136.

[322] Van Bennekoma J.G.; Venderbosch R.H.; Assink D.; Heeres H.J.; Reforming of methanol and glycerol in supercritical water. Journal of Supercritical Fluids, 2011, 58, 99– 113.

[323] Gadhe J.B.; Gupta R.B.; Hydrogen production by methanol reforming in supercritical water: suppression of methane formation. Industrial and Engineering Chemistry Research, 2005, 44, 4577–4584.

[324] Boukis N.; Diem V.; Habicht W.; E. Dinjus E.; Methanol reforming in supercritical water, Industrial and Engineering Chemistry Research, 2003, 42, 728–735.

[325] Li Y.; Park S.Y.; Zhu J.; Solid-state anaerobic digestion for methane production from organic waste. Renewable and Sustainable Energy Reviews, 2011, 15, 821–826.

[326] Azadi P.; Afif E.; Azadi F.; Farnood R.; Screening of nickel catalysts for selective hydrogen production using supercritical water gasification of glucose. Green Chemistry, 2012,14, 1766-1769.

[327] Franck E.U.; Thermophysical Properties of Supercritical Fluids with Special Consideration of Aqueous Systems. Fluid Phase Equilibrium, 1983, 31, 211-223.

[328] Antal Jr. M.J.; Brittain A.; DeAlmeida C.; Ramayya S.; Heterolysis and homolysis in supercritical water. Supercritical Fluids, 1987, 3, 78-82.

[329] Wang W.; Wang S.; Ma X.; Gong J.; Recent advances in catalytic hydrogenation of carbon dioxide. Chemical Society Reviews, 2011, 40, 3703–3727.

[330] Berry F.J.; Smith M.R.; Mössbauer A.; Investigation of iron-containing catalysts prepared at low temperatures and active for carbon monoxide hydrogenation. Journal of Chemical Society, 1989, 85, 467-471.

[331] Sakurai H.; Haruta M.; Carbon dioxide and carbon monoxide hydrogenation over gold supported on titanium, iron, and zinc oxides. Applied Catalysis A: General, 1995, 127, 93–105.

[332] Krebs H.J.; Bonzel H.P.; A model study of the hydrogenation of CO over polycrystalline iron, Surface Science, 1979, 88, 269-271.

[333] Dwyer D.J.; Somorjai G.A.; The catalytic reduction of carbon monoxide over iron surfaces: A surface science investigation. Journal of Catalysis, 1978, 52, 291-293.

[334] Bjørgen M.; Olsbye U.; Petersen D.; Kolboe S.; The methanol-to-hydrocarbons reaction: insight into the reaction mechanism from benzene and methanol co-reactions, over zeolite H-beta. Journal of Catalysis, 2004, 221, 1–10.

[335] Stöcker M.; Methanol-to-hydrocarbons: catalytic materials and their behavior. Microporous and Mesoporous Materials, 1999, 29, 3–48.

[336] Davda R.R.; Shabaker J.W.; Huber G.W.; Cortright R.D.; Dumesic J.A.; A review of catalytic issues and process conditions for renewable hydrogen and alkanes by aqueous-phase reforming of oxygenated hydrocarbons over supported metal catalysts, Applied Catalysis B: Environmental, 2005, 56, 171–186.

[337] Cortright R. D.; Davda R. R.; Dumesic J. A.; Hydrogen from catalytic reforming of biomass-derived hydrocarbons in liquid water. Nature, 2002, 418, 964-967.

[338] Wawrzetz A.; Peng B.; Hrabar A.; Jentys A.; Lemonidou A.A.; Lechery J.A.; Towards understanding the bifunctional hydrodeoxygenation and aqueous phase reforming of glycerol. Journal of Catalysis, 2010, 269, 411–420.

[339] Yang F.; Hanna M.A.; Sun R.; Value-added uses for crude glycerol, a by-product of biodiesel production. Biotechnology for Biofuels, 2012, 5,*13-27*.

[340] Xu X.; Matsumura Y.; Stenberg J.; Antal Jr. M.J.; Carbon-Catalyzed Gasification of Organic Feedstocks in Supercritical Water. Industrial and Engineering Chemistry Research,1996,35, 2522-2530.

[341] Laine N. R.; Vastola S.J.; Walxer Jr. P. L.; The importance of active surface area in carbon-oxygen gasification, 1967, 67, 2030-2035.

[342] Pachauri N.; He B.; "*Value-added Utilization of Crude Glycerol from Biodiesel Production: A* Survey of Current Research Activities*". ASABE Annual* International Meeting, 2006, 2-6.

[**343**] Swanson K.J.; Madden, M.C.; Ghio A.J.; Biodiesel Exhaust: The Need for Health Effects Research. Environmental and Health Perspective, 2007,115, 496–499.

[344] Byrd A.J.; Pant K.K.; Gupta R. B.; Hydrogen production from glycerol by reforming in supercritical water over Ru/Al_2O_3 catalyst. Fuel, 2008, 87, 2956–2960.

[345] Nakagawa Y.; Tomishig K.; Heterogeneous catalysis of the glycerol hydrogenolysis. Catalysis Science Technoogy*, 2011, 1, 179-190.*

[346] Guo L.; Cao C.; Lu Y.; Supercritical Water Gasification of Biomass and Organic Wastes Biomass, 2010.

[347] Hendry D.; Venkitasamy C.; Wilkinson N.; Jacoby W.; Exploration of the Effect of Process Variables on the production of High-value Fuel Gas from Glucose via Supercrticical Water Gasification. Bio-resource Technology, 2010, 102, 3480-3487.

[348] Asghari F.S.; Yoshida H.; Kinetics of the decomposition of fructose catalyzed by hydrochloric acid in subcritical water: Formation of 5-hydroxymethylfurfural, levulinic, and formic acids, Industrial and Engineering Chemistry Research, 2007 46, 7703–7710.

[349] Matsumura Y.; Minowa T.; Potic B.; Kersten S.R.A.; Biomass gasification in supercritical water. Industrial and Engineering Chemistry Research, 2000, 39, 4040–4053.

[350] Li Y.; Guo L.; Zhang X.; Jin H.; Lu Y.; Hydrogen production from coal gasification in supercritical water with a continuous flowing system. International Journal of hydrogen energy, 2010, 35, 3036–3045.

[351] Lee I.G.; Ihm S.K.; Catalytic Gasification of Glucose over Ni/Activated Charcoal in Supercritical Water. Industrial and Engineering Chemistry Research, 2009, 48, 1435–1442.

[352] Youssef E.A.; Chowdhury M.B.I.; Nakhla G.; Charpentier P.; Effect of nickel loading on hydrogen production and chemical oxygen demand (COD) destruction from glucose oxidation and gasification in supercritical water. International Journal of Hydrogen Energy, 2010, 35, 5034-5042.

[353] Hendry D.; Miller A.; Jacoby W.; Turbulent operation of a continuous reactor for gasification of alcohols in supercritical water. Industrial and Engineering Chemistry Research, 2012, 51, 2578–2585.

[354] Schmieder H.; Abeln J.; Boukis N.; Dinjus E.; Kruse A.; Kluth M.; Petrich G.; Sadri E.; Schacht M., Hydrothermal gasification of biomass and organic wastes. Journal of Supercritical Fluids, 2000, 17, 145 – 153.

[355] Antal M. J.; Glen Allen S.; Schulman D.; Xiaodong X.; Biomass Gasfication in Supercritical Water. Industrial and Engineering Chemistry Research, 2000, 39, 4040-4053.

[356] Matsumura Y.; Minowa T.; Fundamental Design of a continuous biomass gasification process using supercritical water fluidized bed. International Journal of Hydrogen Energy, 2003, 29, 701-707.

[357] Matsumura Y.; Evaluation of supercritical water gasification and bio-methanation for wet biomass utilization in Japan. Energy Conversion and Manage, 2002, 43, 1301-1310.

[358] Yoshida T.; Oshima Y.; Matsumura Y.; Gasification of biomass model compounds and real biomass in supercritical water. Biomass and Bioenergy, 2004, 26, 71-78.

[359] Antal M. J.; Glen A.S.; Schulman D.; Xu X.; Biomass Gasification in Supercritical Water. Industrial and Engineering Chemistry Research, 2000, *39,* 4040-4053.

[360] Lu Y.J.; Jin H.; Guo L.J.; Zhang X.M.; Cao C.Q.; Guo X.; Hydrogen production by biomass gasification in supercritical water with a fluidized bed reactor. International journal of hydrogen energy 33 (2008) 6066–6075

[361] Matsumura Y.; Minowa T.; Xu X.; Nuessle F.; Adschiri T.; Antal J.M.; High pressure carbon dioxide removal in supercritical water gasification of biomass. Industrial and Engineering Chemistry Research, 1997, 864-878.

[362] Egan B.; Fain D. E.; Roettger G.E.; Separating hydrogen from coal gasification with alumina membranes. Journal of Engineering Gas Turbines Power, 1991; 114:367.

[363] Abu El-Rub Z.; Bramer E.A.; Brem G.; Review of Catalysts for Tar Elimination in Biomass Gasification Processes. Industrial and Engineering Chemistry Research, 2004, 43, 6911–6919.

[364] Jun H.; Kim H.; The reduction and control technology of tar during biomass gasification/pyrolysis: An overview, Renewable and Sustainable Energy Reviews, 2008, 12, 397–416.

[365] Kritzer P.; Corrosion in high-temperature and super critical water and aqueous solutions: a review. The Journal of Supercritical Fluids, 2004, 29, 1–29.

[366] Dehui Y.; Masahiko A.; Antal Jr. M.J.; Hydrogen production by steam reforming glucose in supercritical water. *Energy Fuels*, 1993, 7, 574–577.

[367] Schwald W.; Bobleter O.; Hydrothermolysis of cellulose under static and dynamic conditions at high temperatures. Journal of Carbohydrate Chemistry, 1989, 8, 565–578.

[368] Matsumura Y.; Biomass gasification in near- and supercritical water: Status and prospects. Energy Conversion Management, 2002, 43, 1301–1310.

[369] D'Jesus P.; Boukis N.; Kraushaar-Czarnetzki B.; Dinjus E.; Influence of process variables on gasification of corn silage in supercritical water. Industrial and Engineering Chemistry Research 2006, 45, 1622–1630.

[370] Anand G.; Chakinala D. W. F. Wim van Swaaij P.M.; Sascha R. A. K.; Catalytic and Non-catalytic Supercritical Water Gasification of Microalgae and Glycerol, Industrial and Engineering Chemistry Research, 2010, 49, 1113–1122.

[371] Kritzer P.; Corrosion in high-temperature and supercritical water and aqueous solutions: a review. Journal of Supercritical Fluids, 2004, 29, 1–29.

[372] Boukis N.; Franz G.; Friedrich C.; Habicht W.; Ebert K.; Corrosion screening tests with Ni-base alloys in supercritical water containing hydrochloric acid and oxygen, Proceedings of the ASME Heat Transfer Division, The American Society of Mechanical Engineers,1996,4, 159-167.

[373] Watanabe Y.; Kobayashi T.; Adschiri T.; Significance of water density on corrosion behavior of alloys in supercritical water, National Association of Corrosion Engineers, Houston, TX, Paper no. 1369, 2001.

[374] McMillan P.F.; New materials from high-pressure experiments, Progress Article abstract. Nature Materials, 2002, 1, 19 – 25.

[375] Happel J.; Brenner H.; Low Reynolds number hydrodynamics with special applications to particulate media, Columbia University, CEAC, New York, 1983.

[376] Knox D.E.; Solubilities in supercritical fluids, Pure Applied. Chemistry, 2005, 77, 513–530.

[377] Hodes M. ; Philip A. M.; Glenn T. H.; Kenneth A. S.; Jefferson W. T.; Salt precipitation and scale control in supercritical water oxidation—Part A: fundamentals and research. The Journal of Supercritical Fluids, 2004, 29, 265–288.

[378] Kritzer P.; Corrosion in high-temperature and supercritical water and aqueous solutions: a review, The Journal of Supercritical Fluids, 2004, 29, 1-29.

[379] Schubert M.; Regler J.W.; Vogel F.; Continuous salt precipitation and separation from supercritical water. Part 1: Type 1 salts, Journal of Supercritical Fluids, 2010, 52, 99–112.

[380] Howard H.; Ocean Carbon Sequestration, presented at the Workshop on Carbon Sequestration Science, 2001.

[**381**]Yaws C.L.; Chemical properties handbook: physical, thermodynamic, environmental, transport, safety, and health related properties for organic and inorganic chemicals. McGraw-Hill,1999,441-560.

[**382**] Thompson J.C.; He B.B.; Characterization of crude glycerol from biodiesel production from multiple feedstocks. Applied Engineering in Agriculture, 2006, 22, 261-265.

[383] Allen R.G.; Pereira L.S.; Raes D.; Smith M.; Crop evapo-transpiration - Guidelines for computing crop water requirements - Food and Agriculture Organization of the United Nations, 1998, 56-59.

[384] Demirbas A.; Calculation of higher heating values of biomass fuels. Fuel, 1997, 76, 431-434.

[385] Ambrosini D.; D. Paoletti D.; Rashidnia N.; Overview of diffusion measurements by optical techniques. Optics and Lasers in Engineering, 2008, 46, 852–864.

[386] Dahmen N.; Kordikowski A.; Schneider G.M.; Determination of binary diffusion coefficients of organic compounds in supercritical carbon dioxide by supercritical fluid chromatography. Journal of Chromatography, 1990, 505, 169-178.

[**387**] Aris R.; On the Dispersion of a Solute by Diffusion, Convection and Exchange between Phases. Proceedings of the Royal Society of London, 1956, 235, 67-69.

[388] Chun-Jiang J.; Ling-Dong S.; Feng L.; *et al.;* Large-scale synthesis of single-crystalline iron oxide magnetic nanorings. Journal of the American Chemical Society, 2008, 130, 16968–16977

APPENDICES

Appendix A. Expressions of the diffusion

According to the Fick's first law of diffusion, the diffusional flux (moles/cm^2/s) of a given molecule is determined from (eq.A.1)

$$J = -\frac{DA(\Delta C)}{\Delta x} \qquad (A.1)$$

Where D is the diffusion coefficient (cm²/s), A is the surface area of the membrane, ΔC is the change in concentration of the solution (mole/cm³) and Δx is the distance travels by the solute from one point x=0 to x=L (in cm). The mass transfer coefficient is proportional to the flux divided by the concentration difference between an interface and the bulk. Equation 2.1 shows that the rate of the diffusion coefficient is dependent substantially on the molecular diffusion and the medium in which it is diffusing. For a porous material, the diffusion coefficient (D) can be obtained from the molecular diffusion coefficient (D_i), the catalyst particle porosity (ε) and tortuosity (τ) as shown in equation 2. 2.

$$D = \frac{\varepsilon}{\tau} D_i \qquad (A.2)$$

For a spherical shaped molecule, which are usually much larger than the solvent molecule in which it diffuses, Stokes Einstein used an analogy to Stoke's law [**385**] to show that:

$$D' = \frac{kT}{6\pi r \varepsilon} \qquad (A.3)$$

Where D' is the translational diffusion coefficient, which is directly proportional to (kT), or to the absolute temperature, ε is the viscosity, k the Boltzmann constant and r the hydrodynamic radius of the diffusion molecule.

A study has reported the determination of diffusion coefficients (D_{12}) of organic compounds in supercritical carbon dioxide for a binary diffusion system using a supercritical fluid chromatographic apparatus and a peak-broadening method [**386**]. Aris and co-workers [**387**] were the first to study the theory of diffusion in flowing fluids. They established that the effective diffusion coefficient $\boldsymbol{D}_{eff}$ is given by equation 2.4.

$$D_{eff} = D_{12} + \frac{r^2 u^2}{48 D_{12}} \qquad (A.4)$$

Where u is the average solvent velocity, r the inner radius of the tube and (D_{12}) is the binary diffusion coefficient.

Appendix B. Catalyst particle size distribution

The results of the particle size distribution are showed in Figs.H1 and H2 for iron oxide and magnetite samples, respectively.

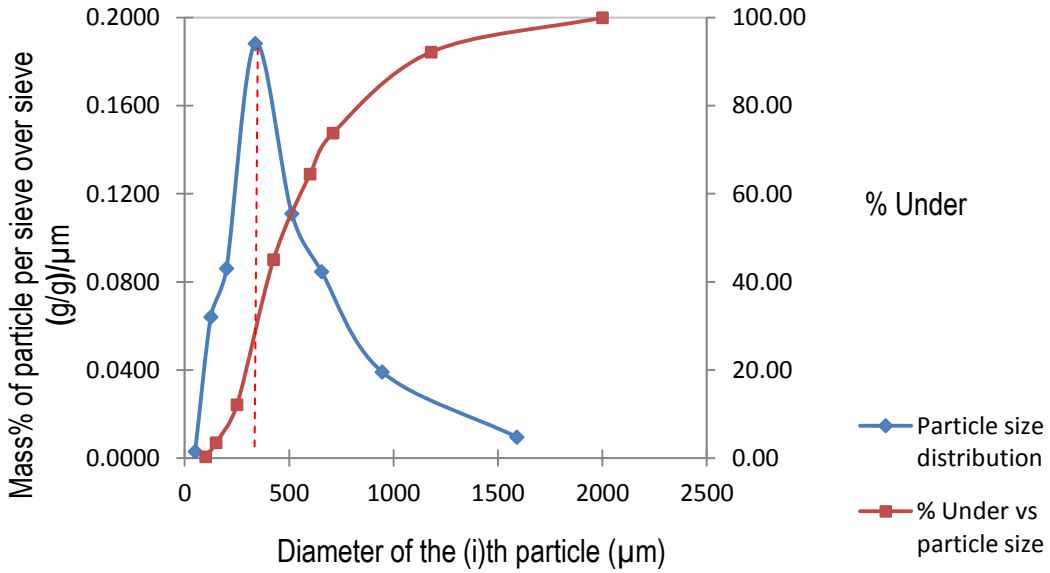

Fig.H.1. Particle size distribution of Fe_2O_3-Cr_2O_3 catalyst

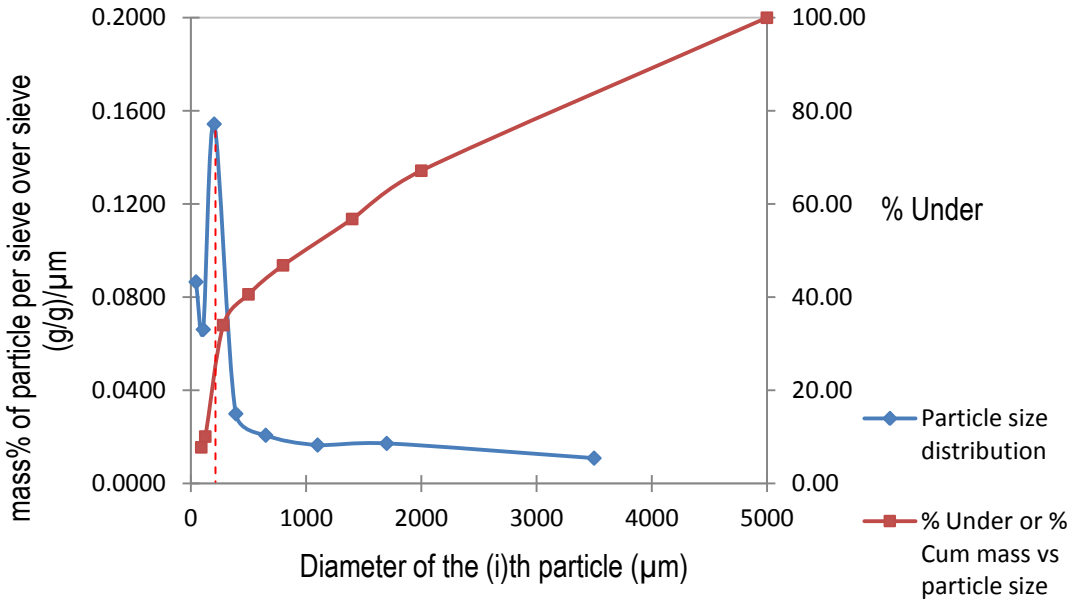

Fig. H.2. Particle size distribution of Fe_3O_4 catalyst

A single number such as diameter can be used to describe a catalyst size [e.g. 3.5 mm cylinder shape with d_{50} = 4 mm] for a fresh sample of Fe_2O_3-Cr_2O_3. This is because every dimension is identical. After,

crushing of the particle, its shape and size were changed to non-spherical shape and variable size which can be described using multiple length and width measures. However, particles in a known sieve size were assumed spherical, with its diameter being the average of two consecutive sieves. For particle size distributions, the median is called the D50 (or x50 when following certain ISO guidelines) as indicated by the red dot line in the Figs.H1 and H2, which represented the size in microns that split the distribution with half above and half below this diameter. For Fe-Cr and magnetite, D50 were 200 μm and 350 μm, respectively with an error of ± 5% on the x (size) axis. This error includes all sources such as sampling and sample preparation. However, the same error goes up to ± 10% when translated to the y (percent) axis because of the steepness of the distribution curve.

Appendix C. Pilot plant process flow sheet

Appendix D. Diaphragm pump calibration curves

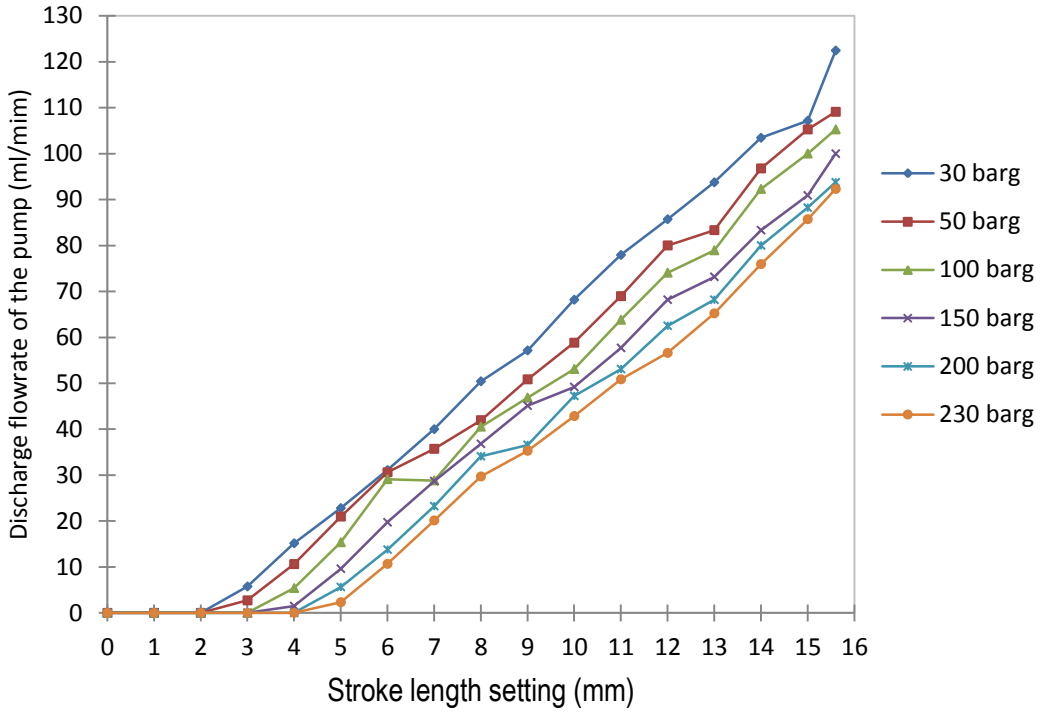

Fig.A.1. Calibration graph of the pump using mains water at 20.5 °C

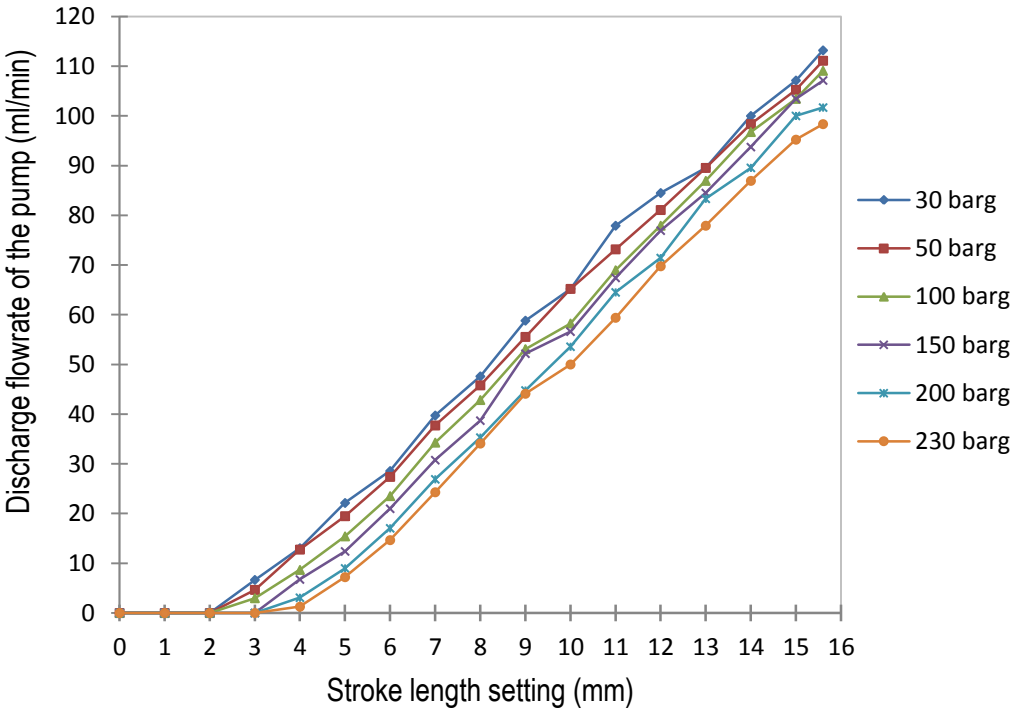

Fig.A.2. Calibration graph of the pump using 2 wt % glycerol at 19.7 °C

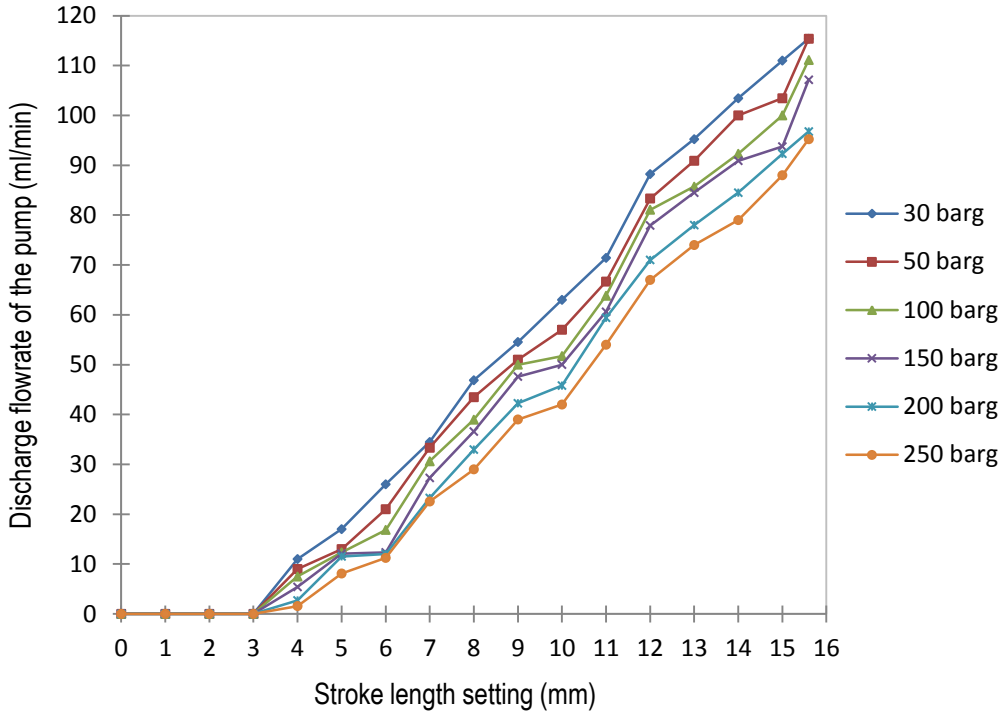

Fig.A.3. Calibration graph of the pump using 5 wt % glycerol at 15.9 °C

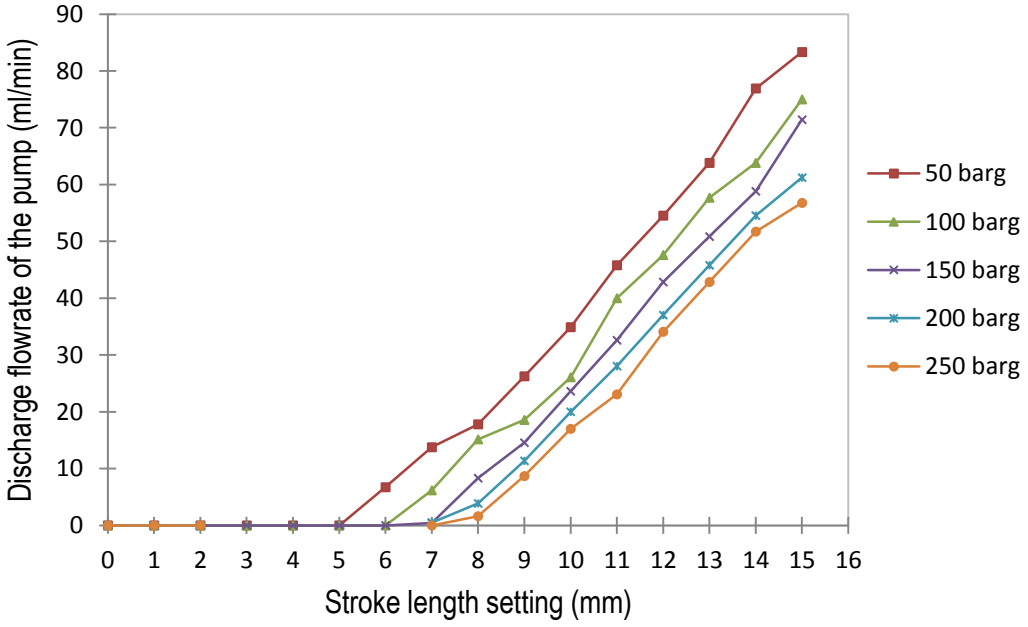

Fig.A.4. Calibration graph of the pump using 10 wt % glycerol at 17.6 °C

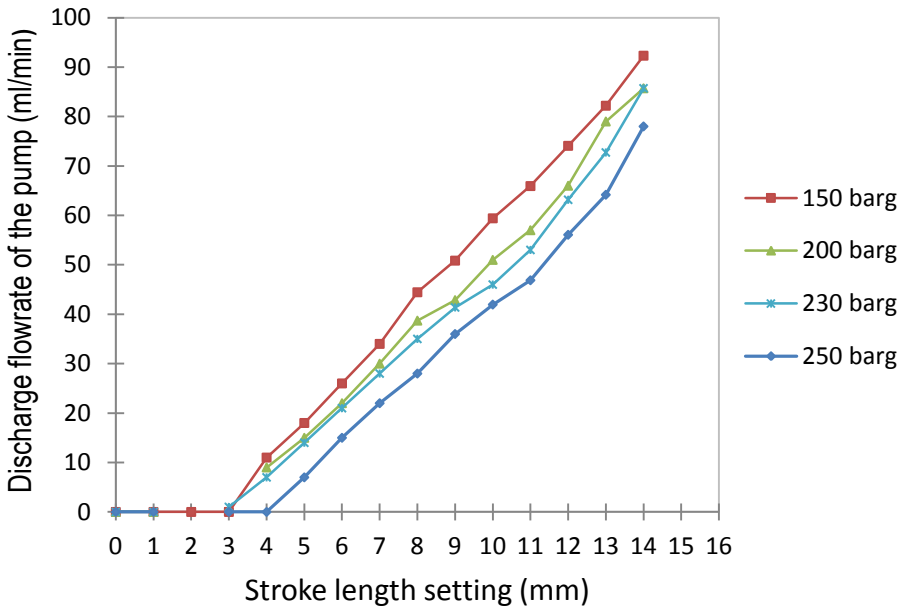

Fig.A.5. Calibration graph of the pump using 15 wt % glycerol at 18 °C

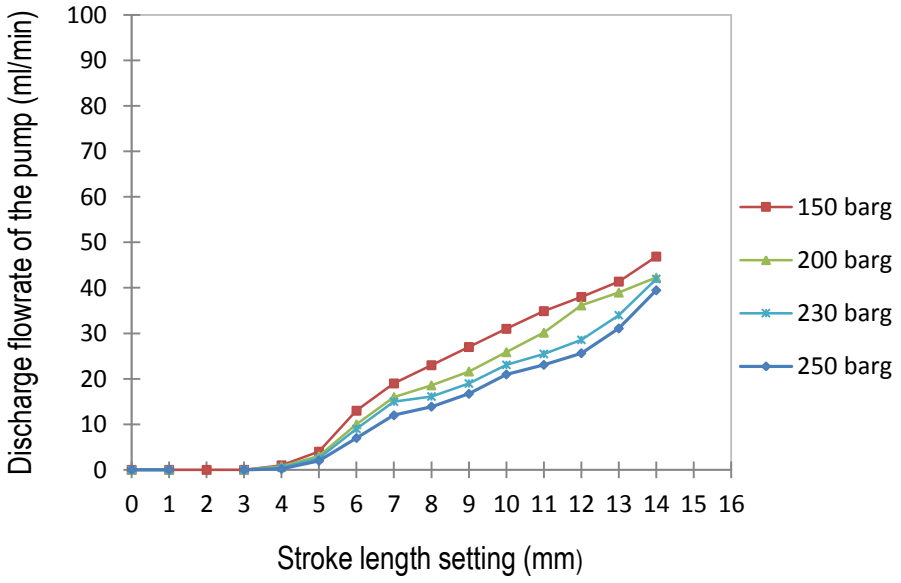

Fig.A.6. Calibration graph of the pump using 20 wt % glycerol at 17.7 °C

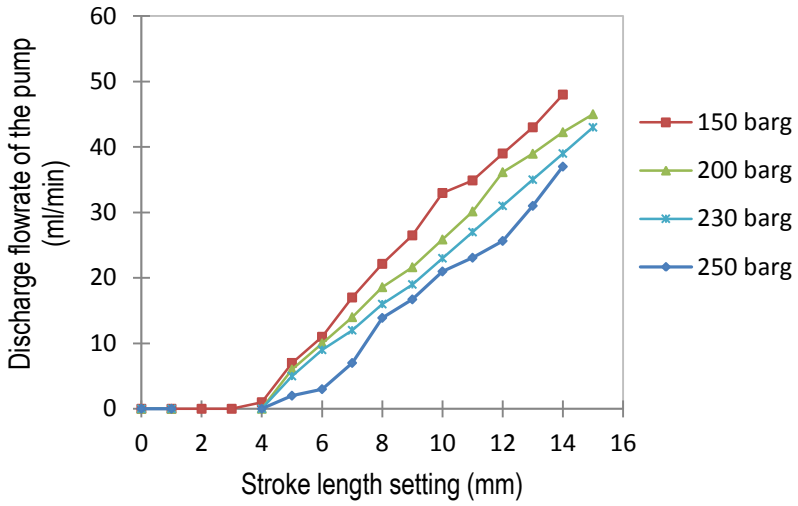

Fig.A.7. Calibration graph of the pump using 30 wt % glycerol at 25.3°C

In summary, the following information can be noted from the above calibration graphs

- As expected, the feed flow rate increases gradually at a high stroke length because the piston of the pump travel for longer distance; therefore more fluid is been pumped.
- As expected, feed flowrate increases linearly with the stroke length increases. The change in the shape of the curve was down to pressure fluctuation and errors (less than 5% margin error).
- As expected, feed flowrate decreases slightly as the glycerol concentration in the slurry increases
- Stroke length has negligible or no effect on pressure change
- As the fluid became more viscous, the minimum stroke length requirement became higher
- Minimum flow rate is a function to the stroke length adjustment and to the desired outlet pressure
- Maximum flowrate was achieved at high stroke length (15.6 mm) independent to the feed concentration
- Feedstock temperature affects the flowrate delivery by the pump; increasing the glycerol feed temperature(before pumping) resulted in an increase of delivery flowrate. The temperature increased is a key factor that reduce the viscosity; the fluid became lighter due to change in its transport properties (diffusivity, viscosity), and therefore travels more rapidly, enhancing an increase in flowrate. Refer to Fig.A.3. for 5 wt% glycerol at different temperatures 15.6 °C and 18.7°C).

Appendix E. Standard operating and emergency procedure of the plant

E1. Pre-experimental Operating instructions

- Ensure the water is filled in the flash feed tank- T01
- Switch on the local isolator A for reactor –RO1
- Start the preheater-HO1 by switching ON/OFF button located on the heater control unit.
- Open pumps discharge outlet valve V03
- Ensure the discharge flow control valve-FCV01 is opened
- Start the cooling water flow by opening the valves V34, FCV02 and BV-2 while ensuring the cooling water discharge valve BV-1 is also opened.
- Start the pump – PO1 by switching the local ON/OFF button
- Set the reactor pressure and system pressure using the pressure control valve PCV01
- Control the reactor temperature by adjusting the settings on the heater instrument.
- Control the reactor pressure and system pressure by adjusting the PCV01
- Control the outlet temperature of the process fluid by manually adjusting the cooling water- flow control valve FCV02.
- Control the process fluid inlet pressure (240 bar max) to the High-pressure separator HP-S01 using PCV01.
- Control the process fluid inlet pressure (17 bar max) to the Low pressure separator LP-S02 using PCV02

E2. Operation of the rig

- Following the pre experimental operating instructions, ensure the rig is at equilibrium – by monitory pressure and temperature for about 40 min.
- Ensure the water/biomass slurry is filled in the flash feed tank –T01.
- Control pressure through the system & High pressure separator pressure HP-S01 (138 bar max outlet) by adjusting the PCV01
- Control pressure (17 bar max inlet) of the low pressure separator by adjusting the PCV02
- Control the liquid product level into the high-pressure separator HP-S01 by adjusting the process flow control valve; FCV01, V20 and V21.
- Vent the gas at the HP-S01 through normal venting line-outlet stream from PCV01
- In case of PVC01 and RV03 not working or Emergency- open valve V17 to vent the gas through the emergency venting line.
- Vent the gas at the LP-S01 through normal venting line-outlet stream from PCV02

In case of PCV02 and RV04 not working or in Emergency- open valve V25 to vent the gas through the emergency venting line.

- Use V19, V27 to collect liquid sample from separator HP-SO1 and HP-SO2 respectively for analysis using HPLC
- Open the liquid discharge valve-V28 of the separator-LP-S02 to evacuate the water into the drain system.

E3. Normal Shutdown Procedure

- At the end of an experiment, switch OFF the pump using the local ON/OFF –red button located on the lab wall behind the table.
- Switch OFF the pre-heater by pressing the OFF button on the heater instrument located on the table.
- Switch OFF the isolator by pressing the OFF button on the ISOLATOR A located on the table for reactor RO1.
- Depressurise the reactor RO1 by gradually opening all the valves between the reactor and heat exchanger and to the separator.
- Depressurise the high pressure separator HP-S01 by gradually opening all the gas release and venting valves
- Depressurise all the gas lines by ensuring all the valves on the gas lines are opened fully.
- Stop the cooling water flow by closing valve V34 and BV-2
- Open the reactor cover to lessen down using the surrounding air.
- Exist the Lab view and switch OFF the laptop.

E4. Emergency shutdown procedure

- Stop the pump P01 by pressing the OFF button located on the wall just behind the rig table.
- Turn OFF the heater by switching OFF the heater instrument button.
- Use the emergency shutdown button located on the lab wall behind the rig table by turning the button into the OFF position.
- Maintain the cooling water flow through the condenser.
- Turn OFF the control box using the switch button located on the wall just behind the rig table for Lab-view Emergency shutdown.

Appendix F. Preparation of Fe_2O_3-Cr_2O_3

A co-incipient wetness impregnation (IWI) method was used for catalyst preparation as follows: A solution of iron nitrate and chromium nitrate was prepared in demineralised water and heated to 40 °C with stirring. At 40 °C, a solution of 10% wt sodium carbonate was added slowly, over a period of 2 h, to the stirred solution until the pH increased to 8.2. This addition was done in order to obtain the weight ratio of Fe/Cr and Na/Fe/Cr. When the addition of sodium carbonate had stopped, and a pH of 8.2 had been reached the slurry was heated to 60 °C with stirring and maintained at 60 °C for 1 h. At the end of 1 h, the slurry was filtered and the filter cake re-slurried with demineralised water at 60 °C a further 4x with filtration between each slurry wash. In this manner, the sodium content of the filter cake was reduced below 0.1% wt. These impregnated samples (wet and washed then filtered) were then dried at 90 °C for 12 h. Subsequently, it was calcined at 340 °C for 4 h. The calcined powder was then sieved to < 100 micron, mixed with 2 % wt graphite, and then pelleted into tablets of 10 mm diameter. The 10 mm diameter pellets were then crushed to pass 200 microns sieve, mixed with an addition of 1% graphite, and finally pelleted to give a pellets with d_{50} = 4 and 6 mm. The pellets were activated by calcination in the air to 480°C. The composition of the final pellet is presented in table F.1 according to the catalyst supplier. The above pellets were then heated/steam to reduce the surface area and crushed - sieved to obtain a range of particle sizes and surface areas as required.

Appendix_ Iron oxide-chromium oxide composition as analysed by the manufacturer.

Table F.1. Composition of the Fe_2O_3-Cr_2O_3 sample after preparation as indicated by the supplied

Elements	Composition wt %
Fe_2O_3	88.7
Cr_2O_3	9.1
C	2.2
Na	0.07

Appendix G. Determination of density and viscosity of the glycerol

Table G. Fluid properties (density and viscosity) used in the experiments as measured

Fluids	Density (g/cm^3)	Viscosity (Pa.s)
Pure glycerol (20 °C)	1.25	1.36
Crude glycerol (20 °C)	1.12	1.23
Deionised water (30 °C)	0.996	0.000798

It can be noted that the lower viscosity and density of the crude glycerol were due to the high concentration of methanol and water in the crude glycerol.

CRUDE CLYCEROL@ 20 C

shear stress Pa	shear rate 1/s	viscosity Pa.s	time s	temperature °C	normal stress Pa	strain	normal force N	normal stress coefficient Pa.s^2	time global s	gap micro m
1.265	0.9977	1.268	30.906	20	78.14	30.541	0.0491	78.5	67.906	700
1.896	1.585	1.196	65.968	20	83.9	48.42	0.05272	33.41	102.968	700
3.18	2.513	1.265	100.89	20	89.41	76.173	0.05618	14.16	137.89	700
4.912	3.981	1.234	135.97	20	96.05	121.1	0.06035	6.062	172.968	700
7.777	6.31	1.233	170.81	20	95.33	190.59	0.0599	2.394	207.812	700
12.26	9.997	1.226	205.98	20	100.4	306.15	0.06307	1.004	242.984	700
		1.23								

PURE GLYCEROL@20 C

shear stress Pa	shear rate 1/s	viscosity Pa.s	time s	temperature °C	normal stress Pa	strain	normal force N	normal stress coefficient Pa.s^2	time global s	gap micro m
1.326	1.001	1.325	31.531	20	-2.883	31.187	-1.81E-03	-2.88	42.531	1000
2.122	1.586	1.338	66.578	20	-7.081	48.06	-4.45E-03	-2.816	77.578	1000
3.372	2.511	1.343	101.91	20	-11.26	77.285	-7.08E-03	-1.786	112.906	1000
5.369	3.981	1.349	137.5	20	-6.253	123.76	-3.93E-03	-0.3946	148.5	1000
8.526	6.309	1.351	172.83	20	-15.89	194.32	-9.99E-03	-0.3994	183.828	1000
13.52	9.998	1.352	208.61	20	-15.15	313.12	-9.52E-03	-0.1516	219.609	1000

Appendix H. Porosity and permeability of the bed

Permeability of the packed bed with different particle diameter of the packing material was determined using equation 3.6 and results are shown in Table G.

$$P° = (dp^2 \times \varepsilon^2) / ((180 \times (1-\varepsilon)^2) \text{ (equation 10.1)}$$

Where dp – is the diameter of the particle, cm and ε is the porosity of the packed bed

Table G: Porosity and permeability of the packed bed with different packing size of the packing material

Packing material	Particle size (d_{50})	Porosity (ε)	Permeability (P°)
	mm	%	cm^2
Iron oxide	6	-	-
Iron oxide	4	27	$1.21 * 10^{-4}$
Iron oxide	1	33	$1.34 * 10_{-5}$
Iron oxide	0.5	35	$4.02 * 10^{-6}$
Iron oxide	0.125	38	$3.26 * 10^{-7}$
Magnetite	4	44	$5.48 * 10^{-4}$
Magnetite	2	51	$2.41 * 10^{-4}$
Magnetite	1	53	$7.06 * 10^{-5}$
Magnetite	0.5	54	$1.91 * 10^{-5}$
Magnetite	0.15	55	$1.29\ 10^{-6}$

Appendix I. Gases compounds - Calibration with external standard using GC- TCD and FID

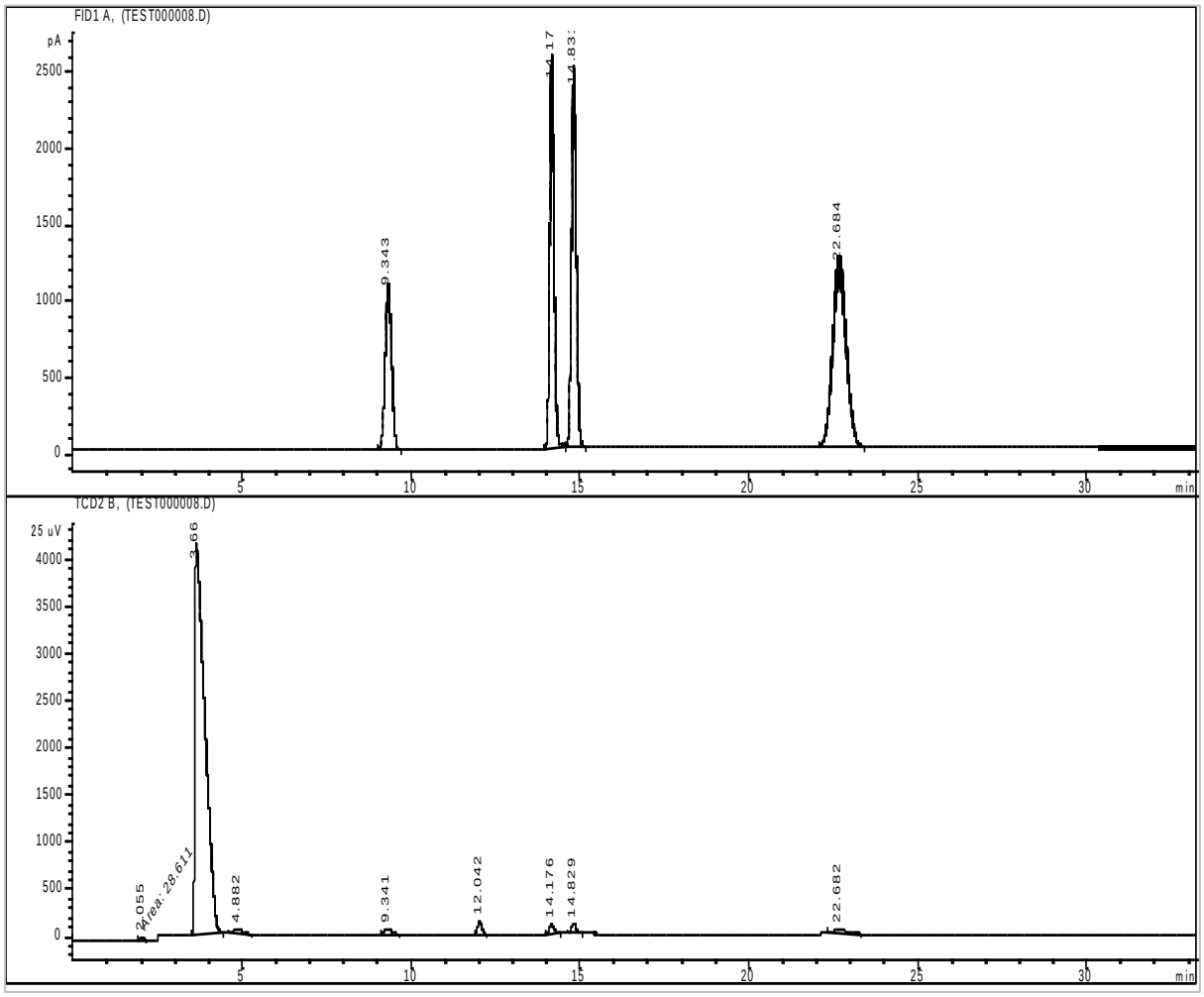

Fig.I1. Chromatograms of the external standard calibration for the gas compounds using GC with two detectors FID (hydrocarbons) and TCD (permanent gases). *For peak identification: please refer to retention time and table I1.*

Table I1. Peak areas of the external standard calibration

Sample ID	% Composition	Vol Sample	Dilution Vol	Conc of Ext Std	Mass of Ext Std	Retention Time	Peak Area
		Ext. Std	Nitrogen	Std	In injection 2µl		Ext. Std
		Sample					
	(%)	% vol		(g/l)	(g)	(min)	
Hydrogen	1	1		0.0854	1.71E-07	2.055	28.6
Carbon monoxide	0.99	0.99		1.173	2.35E-06	4.882	1043.5
Methane	1.01	1.01		0.685	1.37E-06	9.341	852.8
Carbon dioxide	1.01	1.01		1.881	3.76E-06	12.042	1376.8
Ethylene	0.98	0.98		1.163	2.33E-06	14.176	1160.9
Ethane	0.93	0.93		1.183	2.37E-06	14.823	1278.4
Propane	0.92	0.92		1.716	3.43E-06	22.682	1721.7
Nitrogen			92.17	109.265	0.00021	3.66	84966.7
Total		7.83	92.17		0.000234		

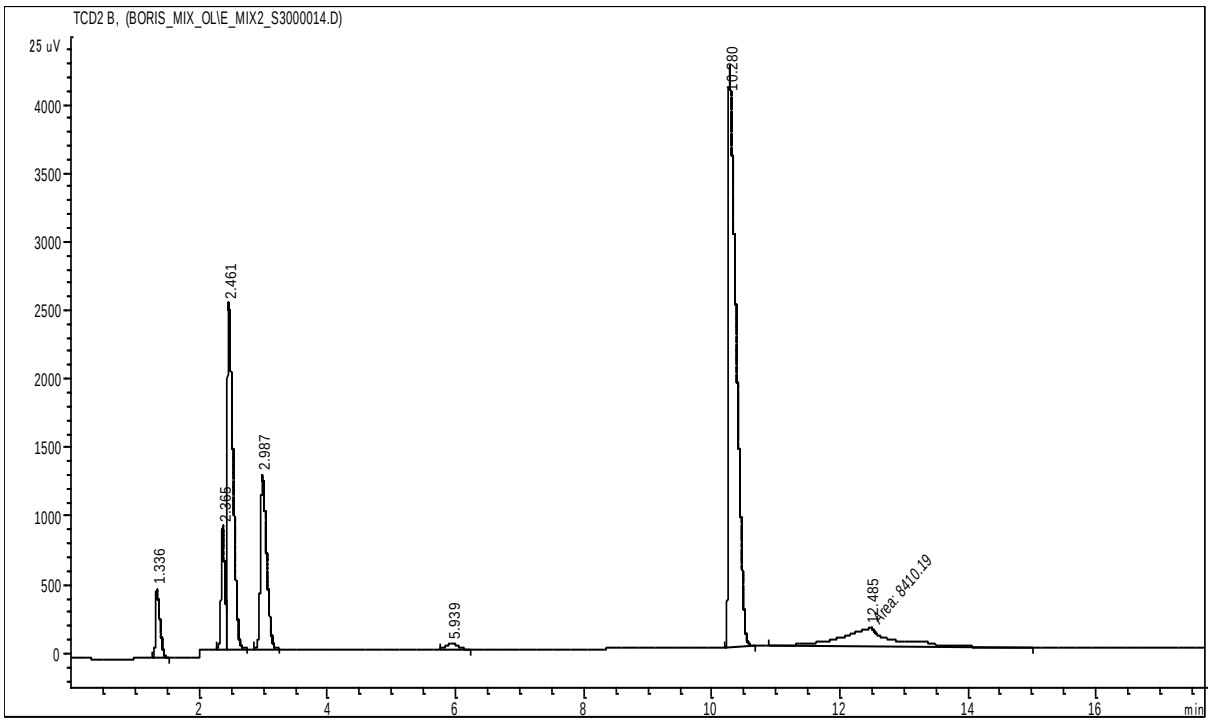

Fig.I2. Typical chromatograms of the gas sample (run E_24) carried out at the same conditions reported for the calibration. *For peak identification: please refer to retention time and table I1.*

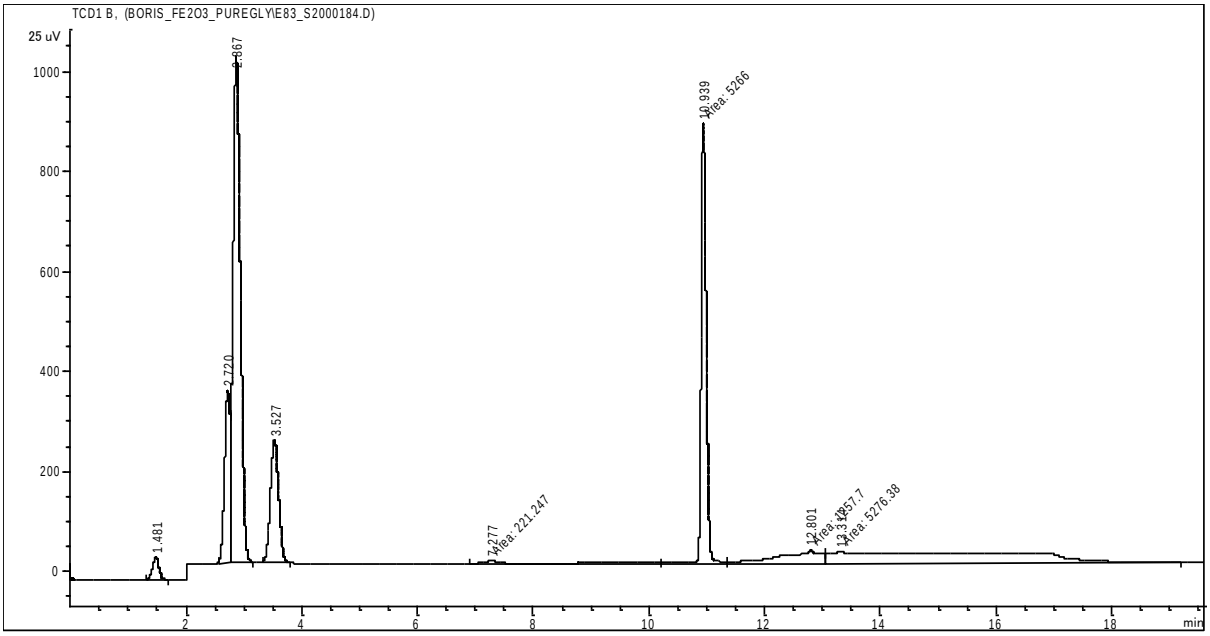

Fig.I3. Typical chromatograms of the gas sample (run E_54) carried out at the same conditions reported for the calibration

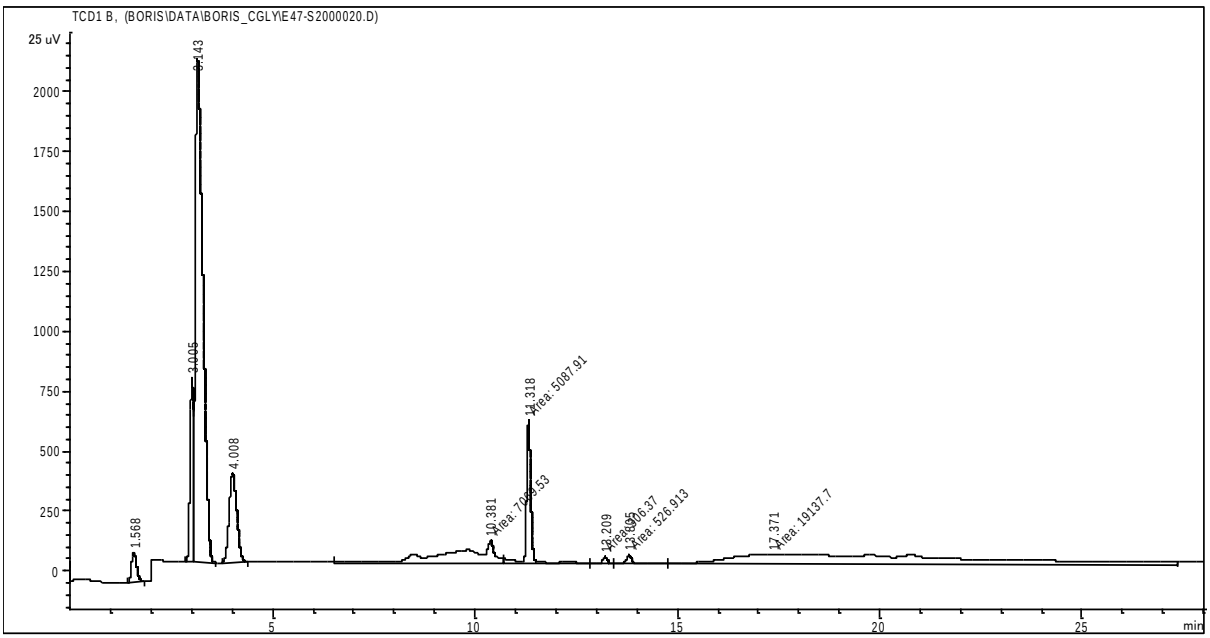

Fig.I4. Typical chromatograms of the gas sample (run E_74) carried out at the same conditions reported for the calibration. *For peak identification: please refer to retention time and table I1.*

Appendix J. Liquid compounds –calibration with internal standard using GC-FID

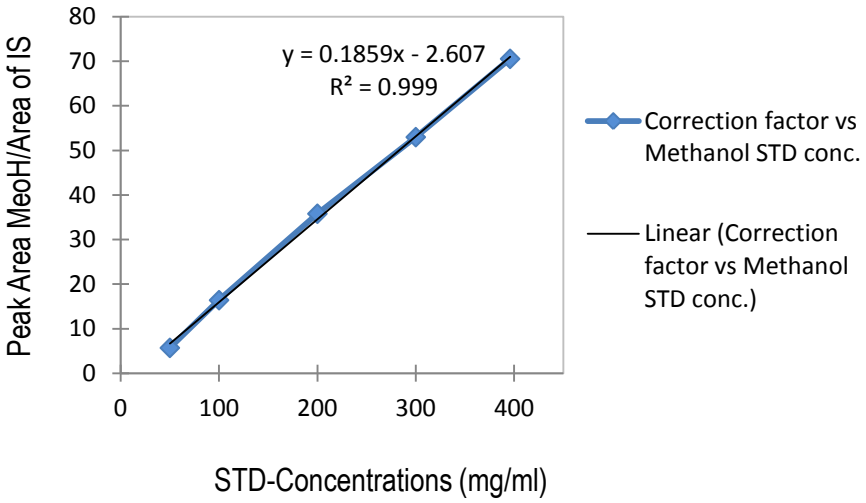

Fig.J.1. Methanol calibration curve

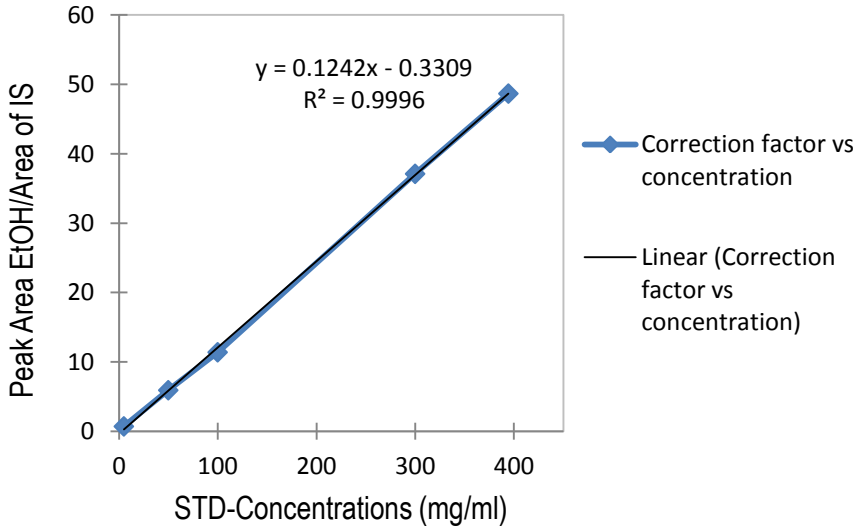

Fig.J.2. Ethanol calibration curve

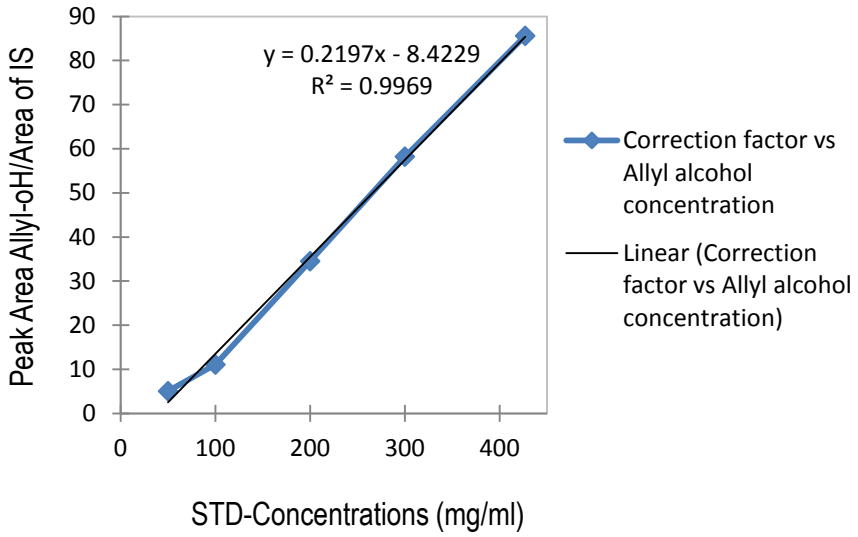

Fig.J.3. Allyl alcohol calibration curve

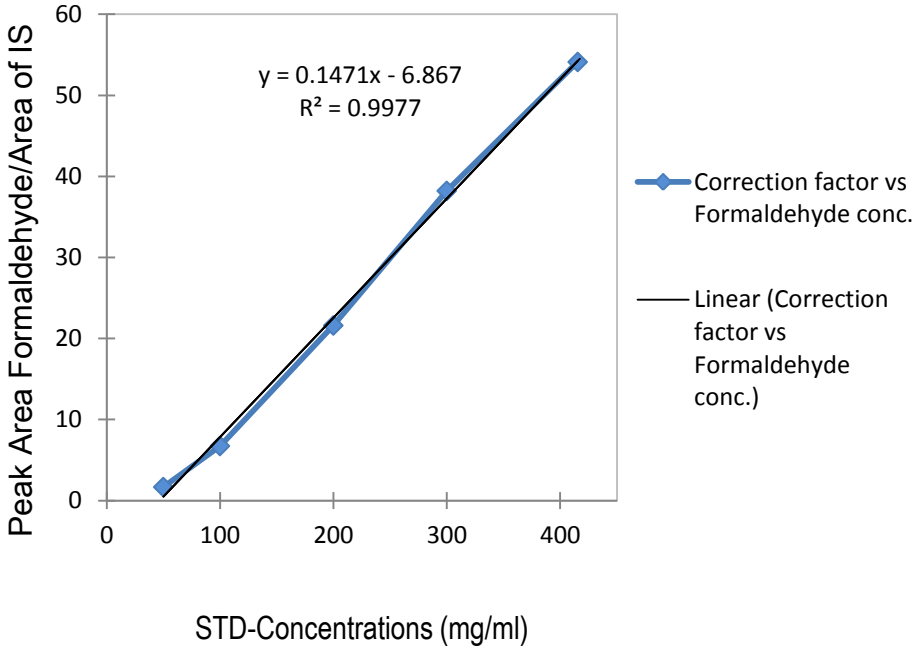

Fig.J.4. Formaldehyde calibration curve

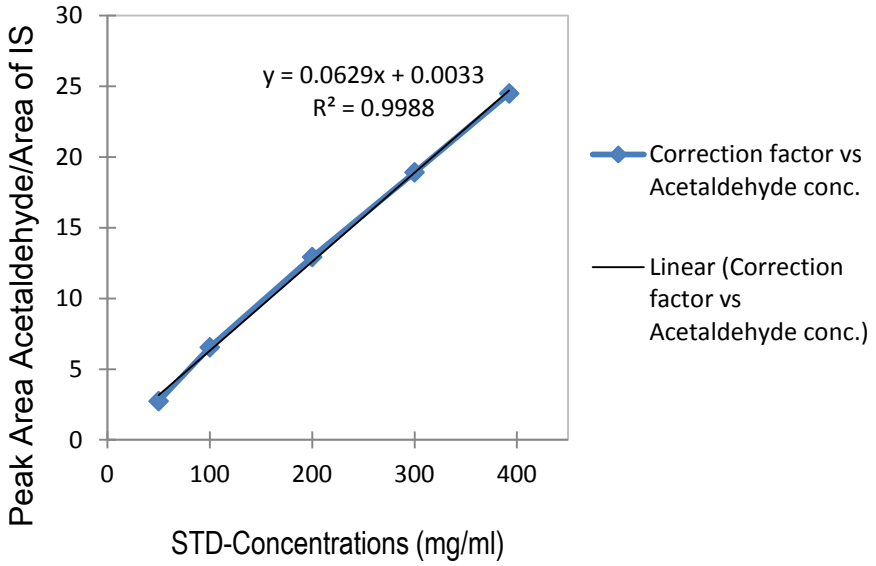

Fig.J.5. Acetaldehyde calibration curve

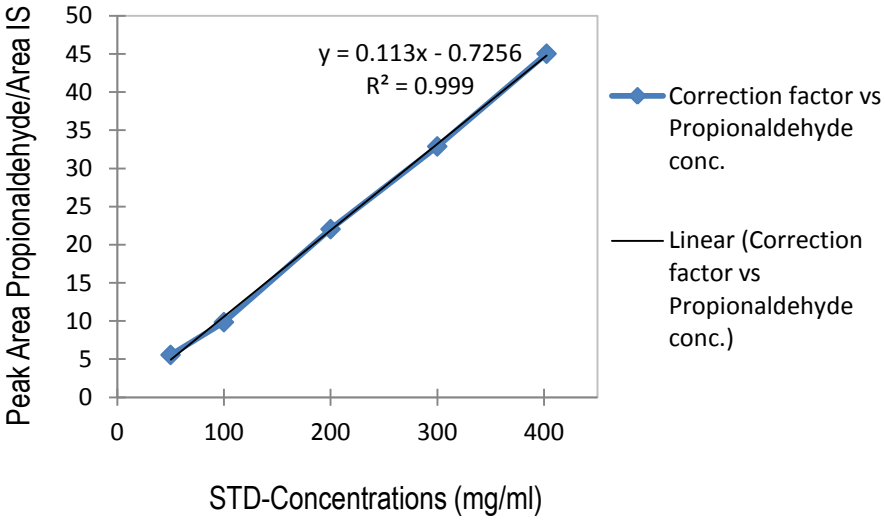

Fig.J.6. Propionaldehyde calibration curve

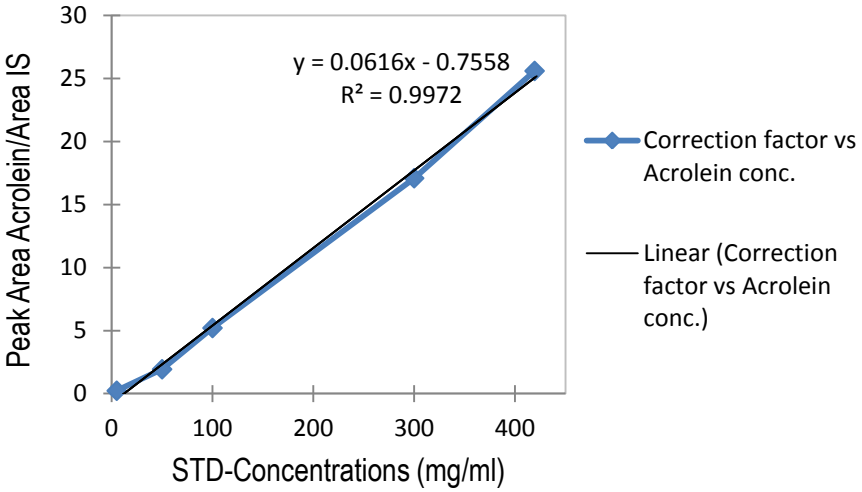

Fig.J.7. Acrolein calibration curve

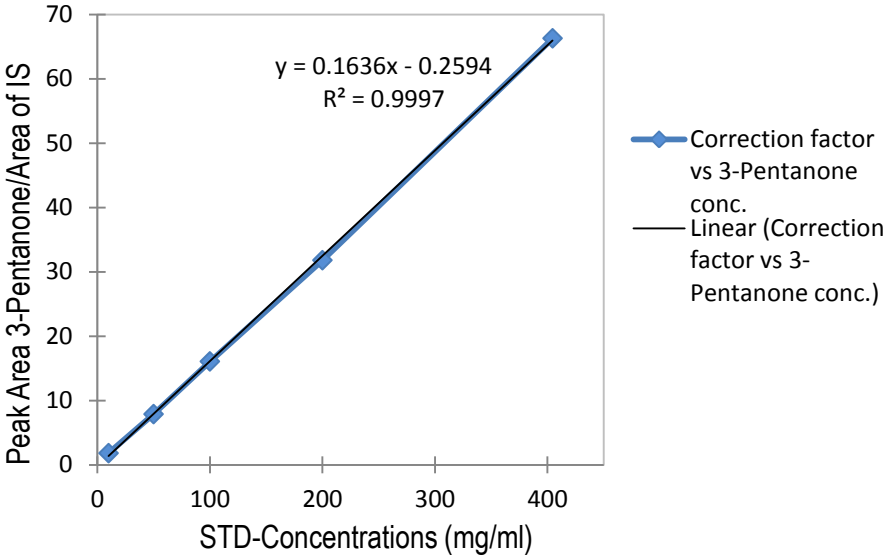

Fig.J.8. 3-Pentanone calibration curve

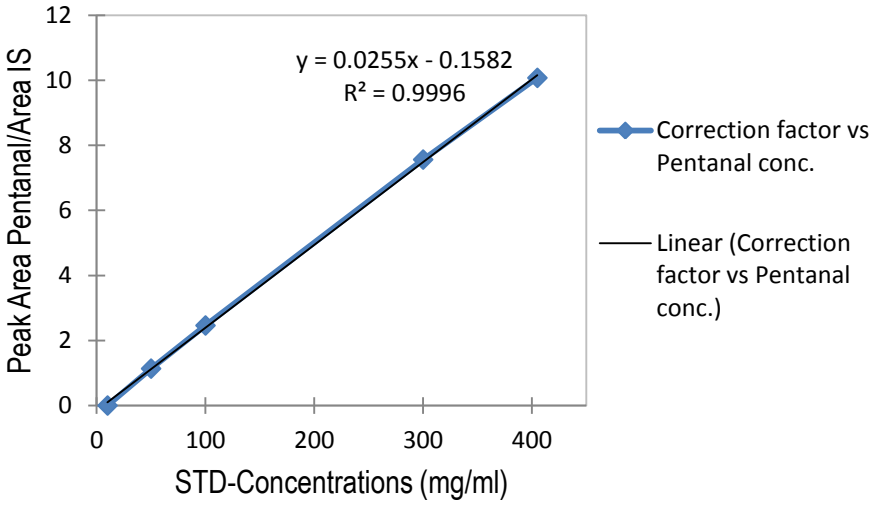

Fig.J.9. Pentanal calibration curve

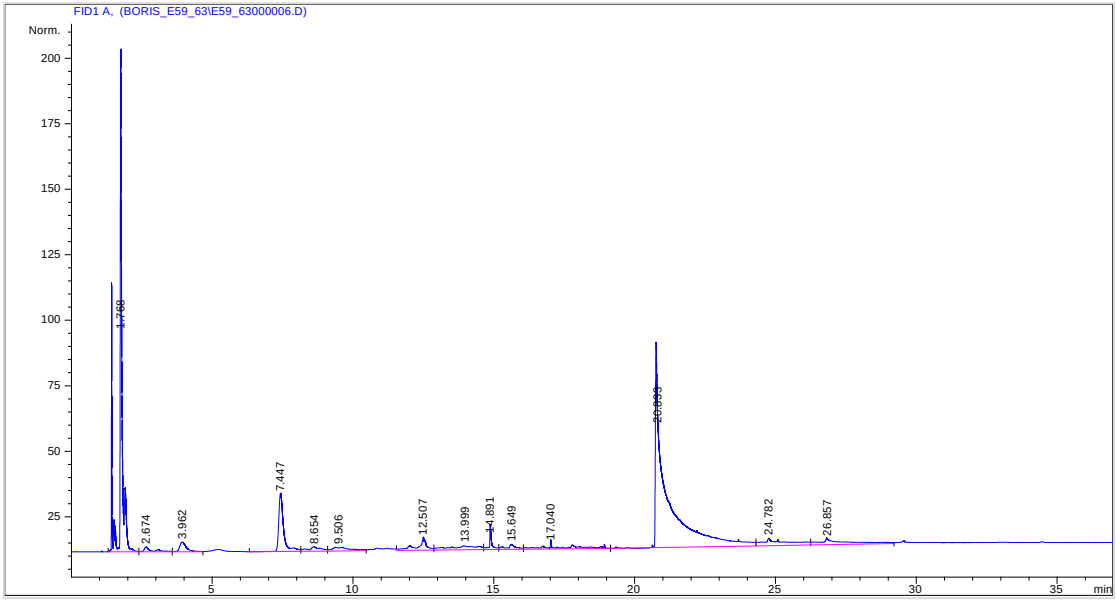

Fig.J10.1. Typical peaks of experimental sample analysis (E59_S6)

CSCWG of pure glycerol over iron oxide-chromium oxide catalyst

For peak identification: please refer to retention time matching with standard (± 0.5)

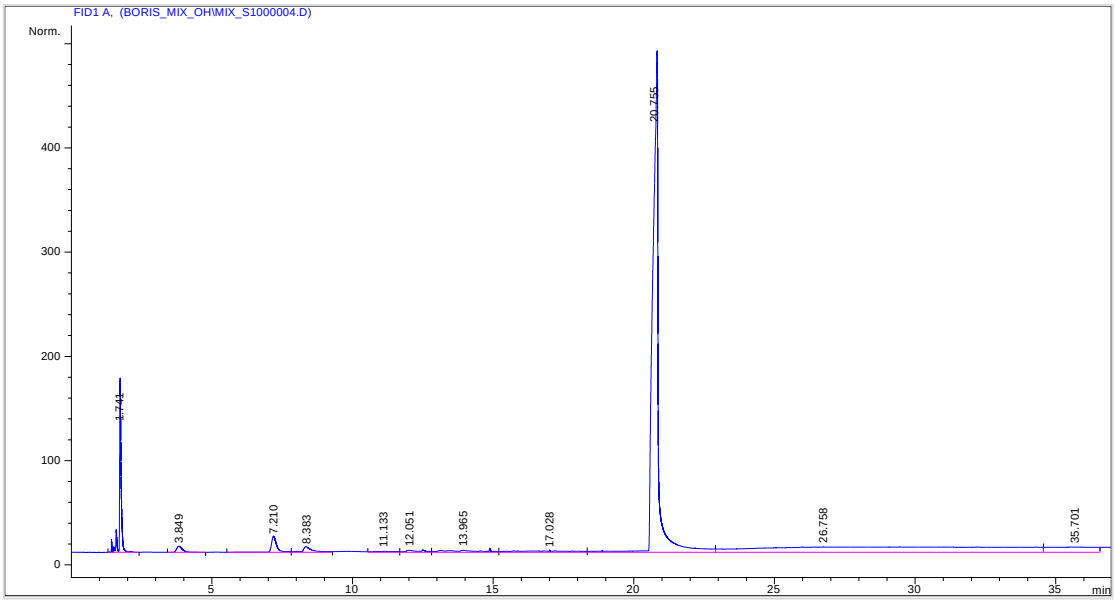

Fig.J10.2. Typical peaks of experimental sample analysis (EMix_S6)

CSCWG of a mix of pure glycerol + methanol over magnetite catalyst

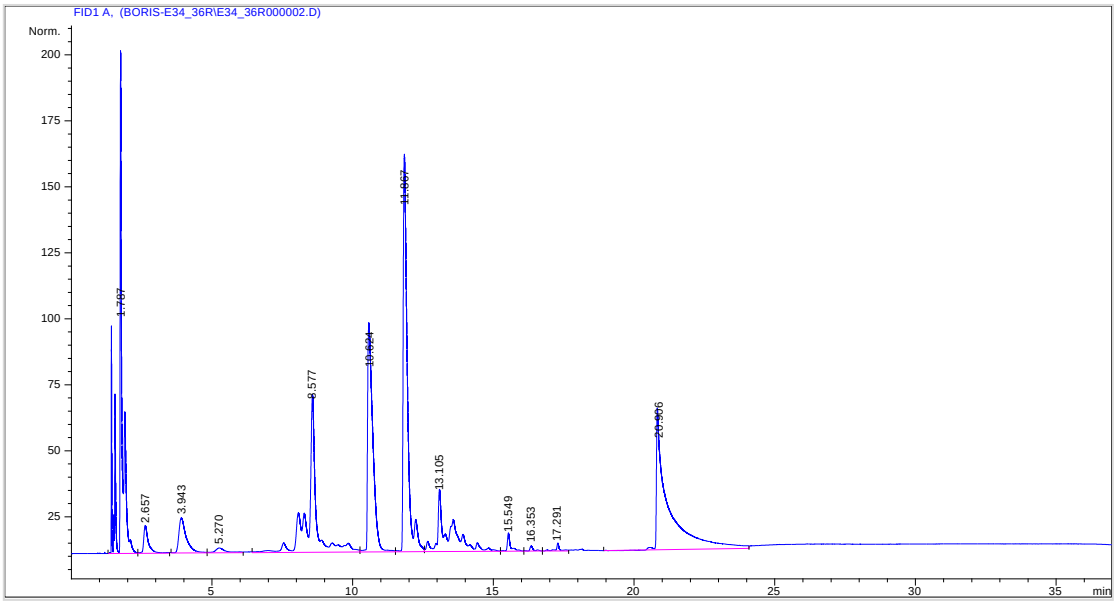

Fig.J10.3. Typical peaks of experimental sample analysis (E34_S6)

CSCWG of crude glycerol over iron oxide -chromium oxide catalyst

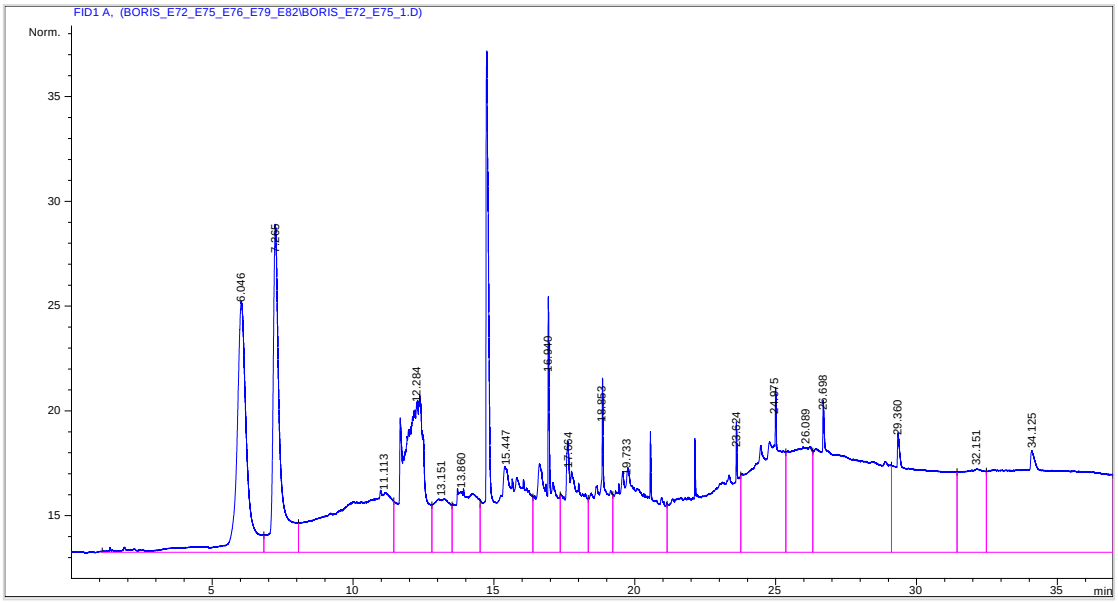

Fig.J10.4. Typical peaks of experimental sample analysis (E72_S1)

CSCWG of crude glycerol over magnetite catalyst

For peak identification: please refer to retention time matching with standard (± 0.5)

Appendix K. Determination of purity of the crude glycerol and methanol concentration

The purity of the crude glycerol was determined using the calibration- linear graphs as showed in Fig. K.1 and the results are shown in table K.1.

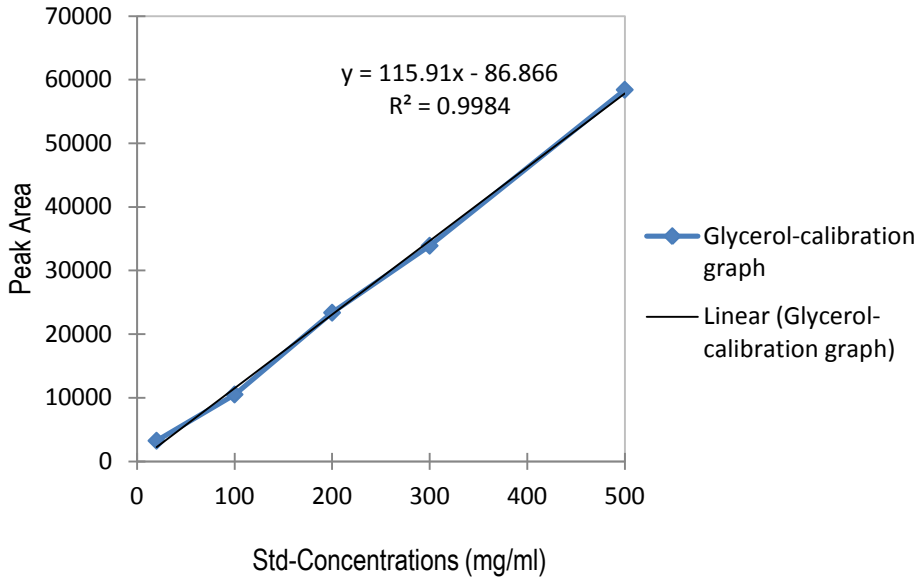

Fig. K.1. Calibration graph of model compounds glycerol by GC-TCD

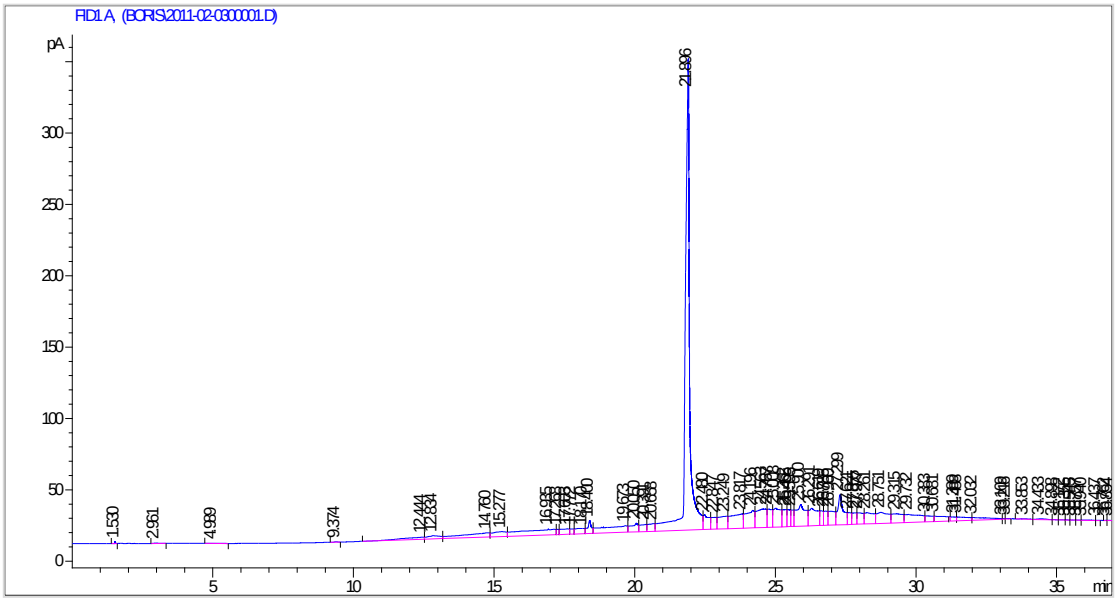

Fig. K.2. Peak of model compounds glycerol by GC-TCD,
Glycerol retention time = 21.893 ±0.5min

Table K.1. Results of the standard glycerol calibration at different concentrations

Retention time	Pure glycerol	Concentration in water	Peaks Area
mins	wt%	mg/ml or g/l	Area units
20.9	2	20	3230
21.6	5	50	5250
21.8	10	100	10505
21.0	15	150	16930
22.1	20	200	23361
22.1	50	500	58400

A known concentration of crude glycerol was prepared similarly as previously reported, and also as for standard calibration. 1ml in volume of this concentration was filtered using syringe filter with 0.22 µm pore size, and was filled into a vial of 2 ml capacity. The analysis was carried out using GC-FID. The GC –FID parameters were the same as for all standards and liquid sample analysis. The retention time of the standard glycerol was used to identify the retention time of the pure glycerol with a margin of ± 0. 5 (min). The purity of the crude glycerol was determined using the following equation:

Purity of crude glycerol = $\frac{\text{peak areas crude glycerol}}{\text{peak areas pure glycerol}} * \frac{\text{Concentration of pure glycerol}}{\text{concentration of crude glycerol}}$*100%

Table K.2. Results of the purity of crude glycerol

Concentration of crude glycerol	Peak areas of the crude glycerol	Concentration of crude glycerol	Peak areas of the glycerol standard	Purity of the crude glycerol
wt%	Area units	wt%	Area units	%
2	2336	2	3230	72.3
5	3813	5	5250	72.6
15	12721	15	16930	75.1
15	12597	15	16930	74.4

Determination of methanol content in the crude glycerol

Three concentrations of crude glycerol: 5, 10 and 15 wt % of crude glycerol were prepared as described in section 2. 1 ml of each sample solution was measured and placed in a vial, and analysed.

The concentration of the methanol in the crude glycerol was determined using the methanol calibration curve (refer to Fig.K.2, and the results are shown in table K.2.

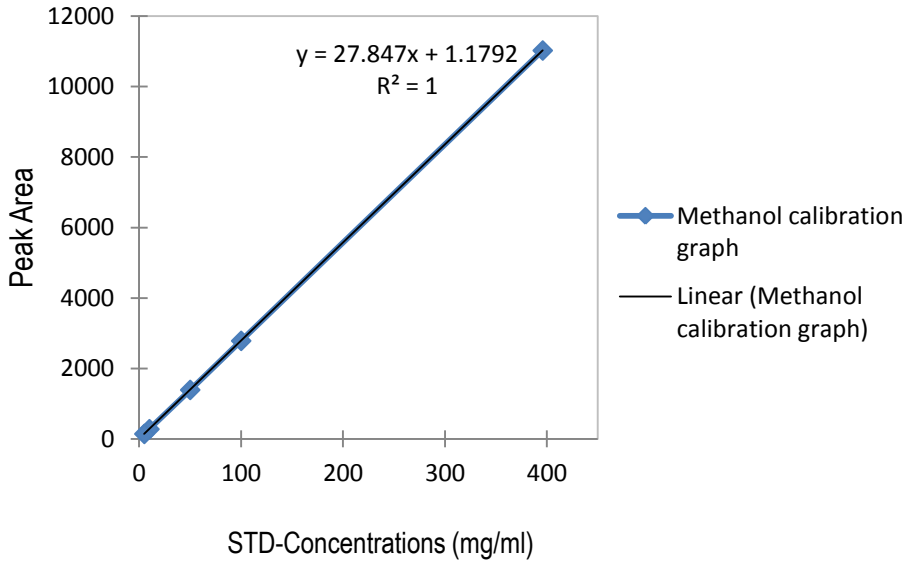

Fig. K.2. Calibration graph of methanol standard by GC-TCD

Table K.2. The results of methanol concentration in crude glycerol

Concentration of crude glycerol	Concentration of crude glycerol	Peak areas of methanol in crude glycerol	Concentration of methanol in crude glycerol using standard equation of methanol	Volume of the sample analysed	wt% of methanol in the crude glycerol
wt%	$mgmL^{-1}$	Area	$mgmL^{-1}$	mL	wt%
5	50	144.2	5.1	1	$\frac{5.1mg}{50mg}*100=10.2\%$
10	100	279	9.9	1	$\frac{9.9mg}{100mg}*100=9.9\%$
15	150	376	13.4	1	$\frac{13.4mg}{150mg}*100=8.9\%$

Appendix L. Crystallographic structure of the catalyst determination by X-ray diffraction (XRD) analysis

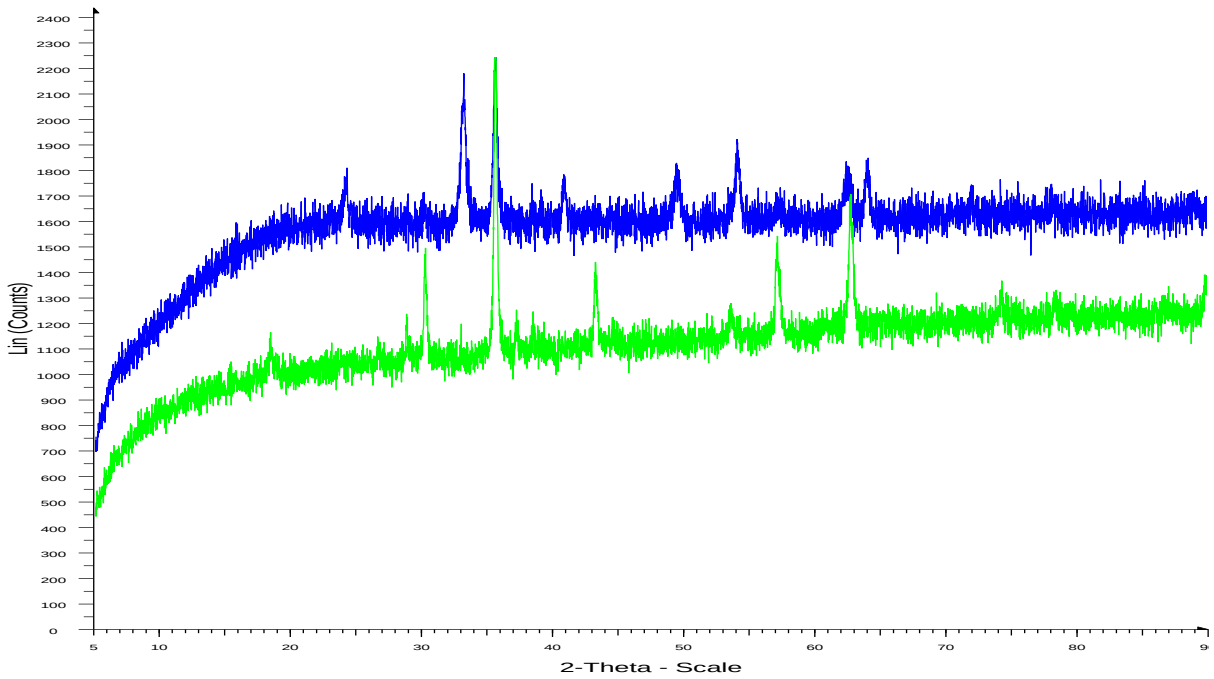

Fig. L.1: XRD patterns of fresh (a) and used (b) samples of non-supported Fe_2O_3+Cr_2O_3 catalysts *(4 mm o.d. particle size)*

Fresh Catalyst 2 theta values: 32 Cr, 35 Fe, 39 Cu, 50 Al, 54 Si, and 63 Ca

Used Catalyst 2 theta values: 30 Cr, 35 Fe, 42 Cu, 54 Al, 57 Si, and 63 Ca

The Fe_2O_3 Powder Diffraction Data was analysed by comparing its data to the indexed diffraction pattern for $CrFe_2O_3$ found in the JCPDS database [**388**], Miller indices (h k l; indicating the set of lattice planes responsible for that diffraction peak) were assigned to each peak in the diffraction pattern as shown below.

2θ	**32.8**	**35.4**	**39.9**	**50.4**	**54.3**	**57.7**	**63.8**
h k l	1 0 0	1 1 0	1 1 1	2 0 0	2 1 0	2 1 1	2 2 0

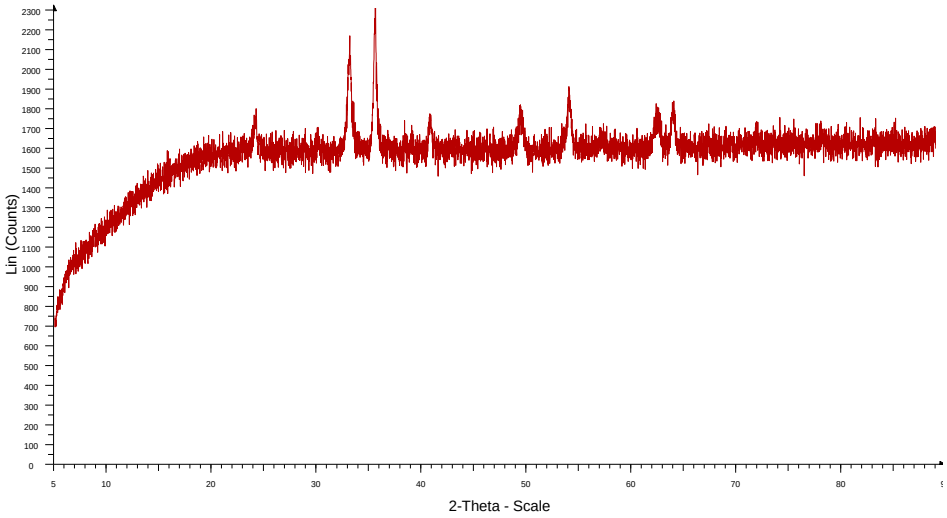

Fig.L.2. XRD patterns of fresh (a) and used (b) samples of non-supported Fe_2O_3+Cr_2O_3 catalysts *(d_{50}= 6 mm)*

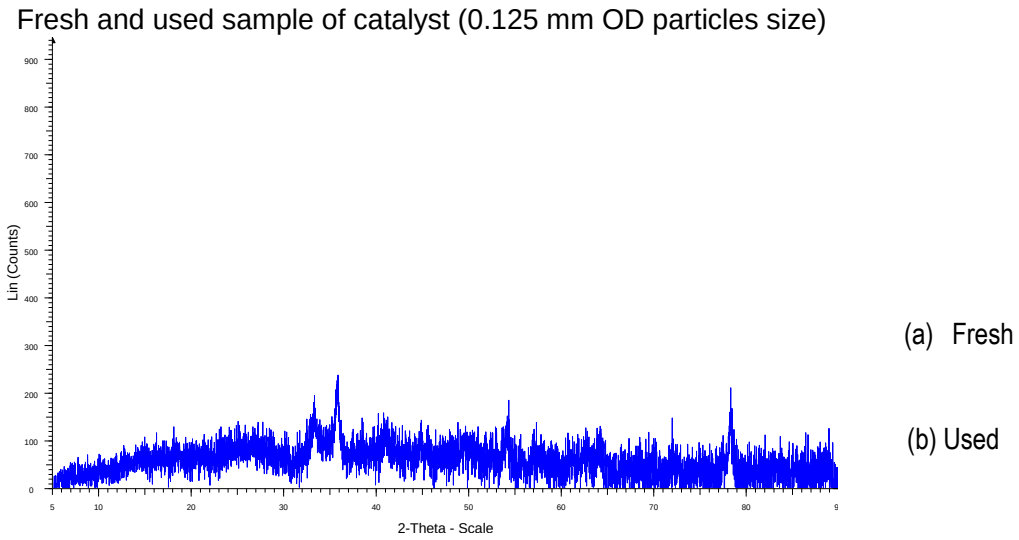

Fig.L.3. XRD patterns of fresh (a) and used (b) samples of non-supported Fe_2O_3+Cr_2O_3 catalysts *(d_{50}=0.125 mm)*

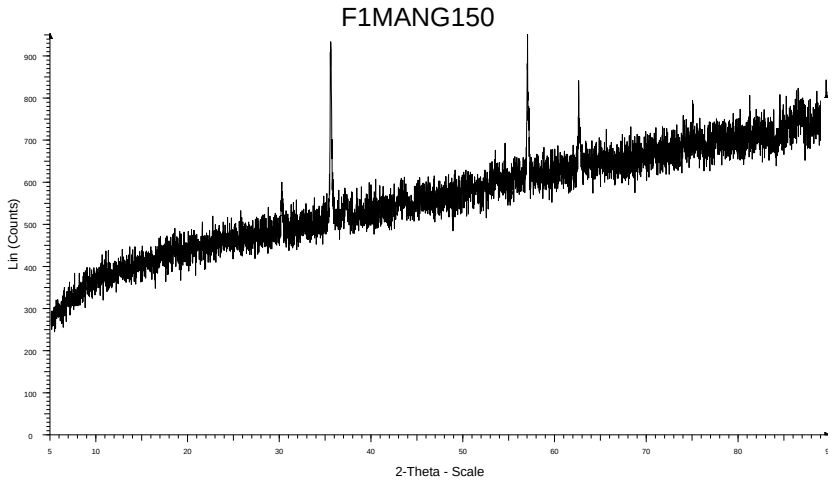

Fig.L.4. XRD patterns of fresh (a) and used (b) samples of non-supported Fe_3O_4 catalysts *(d_{50}= 0.15 mm)*

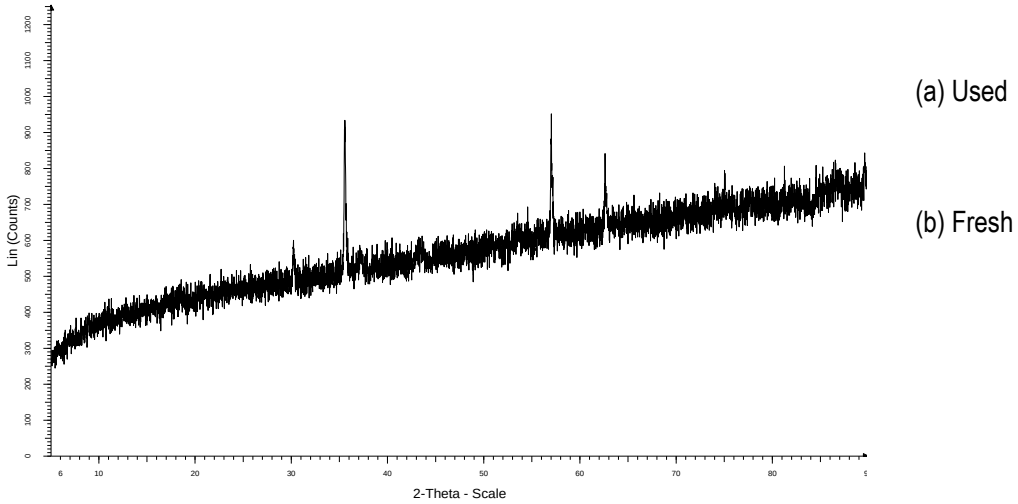

Fig.L.5. XRD patterns of used(a) and fresh (b) samples of non-supported Fe_3O_4 catalysts *(d_{50}= 4 mm)*

Fresh Catalyst 2 theta values: 32 Cr, 35 Fe, 39 Cu, 50 Al, 54 Si, and 63 Ca

Used Catalyst 2 theta values: 8 unknown, 30 Cr, 35 Fe, 42 Cu, 54 Al, 57 Si, and 63 Ca

The Fe_3O_4 Powder Diffraction Data was analysed by comparing its data to the indexed diffraction pattern for $CrFe_2O_3$ found in the JCPDS database [**388**], Miller indices (h k l; indicating the set of lattice planes responsible for that diffraction peak) were assigned to each peak in the diffraction pattern as shown below.

2θ	**32.8**	**35.4**	**39.9**	**50.4**	**54.3**	**57.7**	**63.8**
h k l	1 0 0	1 1 0	1 1 1	2 0 0	2 1 0	2 1 1	2 2 0

Appendix M. Image analysis by SEM

Table M.1. SEM on the fresh and used samples of Fe_2O_3+Cr_2O_3 catalyst

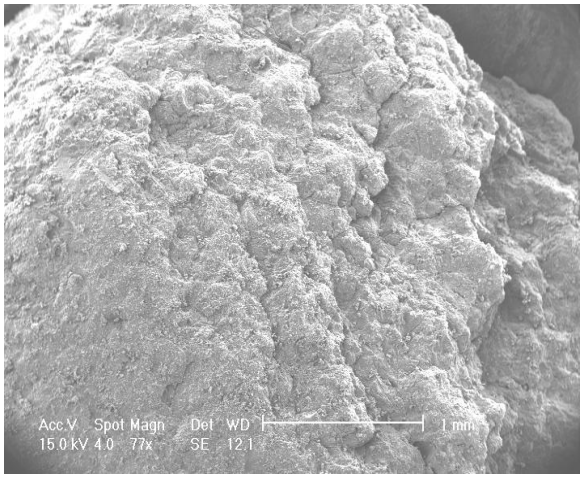

Fresh of Fe_2O_3+Cr_2O_3 catalyst, d_{50} =6000 microns

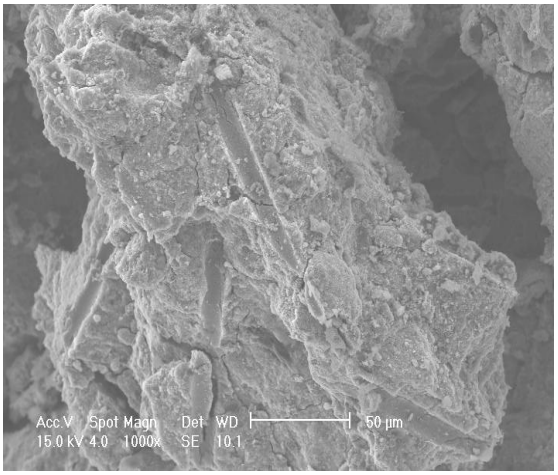

Used of Fe_2O_3+Cr_2O_3 catalyst (14 h), d_{50} = 6000 microns

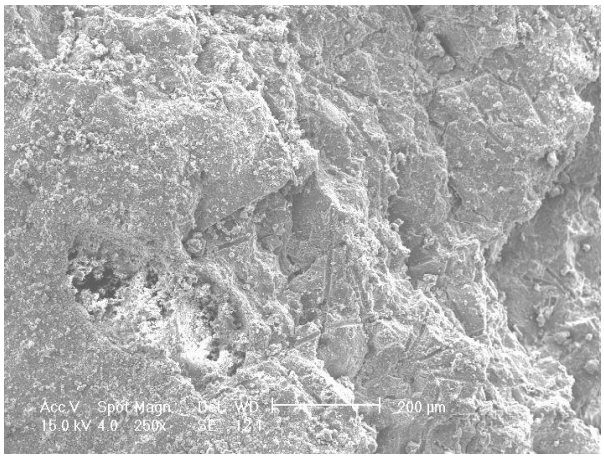

Fresh of Fe_2O_3+Cr_2O_3 catalyst, d_{50}=4000 microns

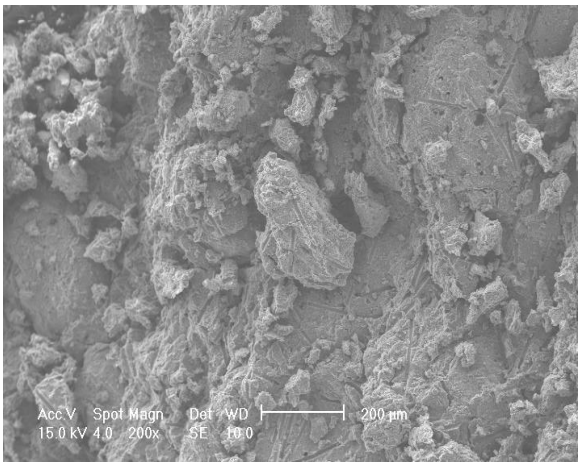

Used of Fe_2O_3+Cr_2O_3 catalyst (172 h), d_{50}= 4000 microns

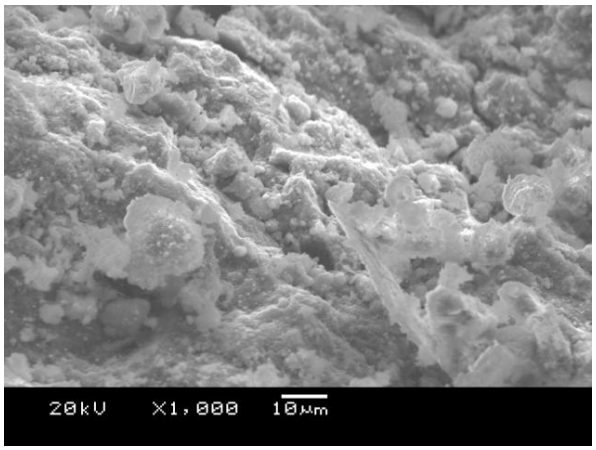

Fresh of Fe_2O_3+Cr_2O_3 catalyst, d_{50}=2000 microns

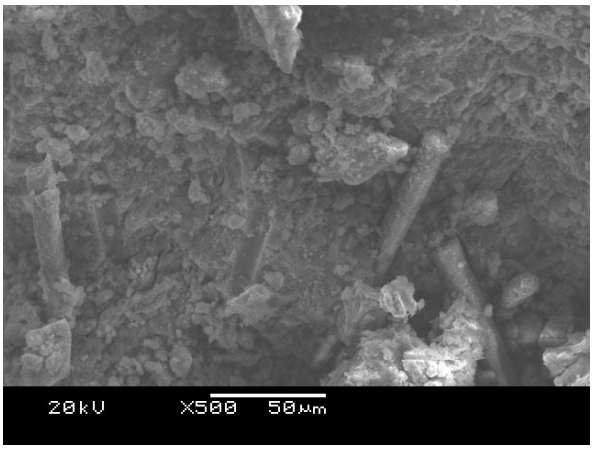

Used of Fe_2O_3+Cr_2O_3 catalyst (12 h), d_{50}= 2000 microns

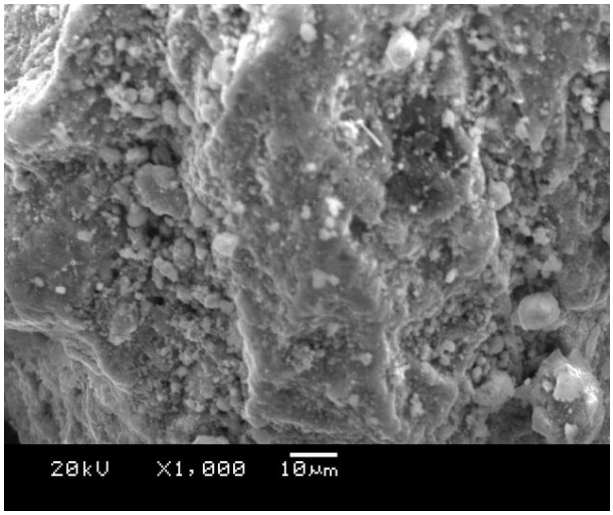

Fresh of Fe_2O_3+Cr_2O_3 catalyst, d_{50}=1000 microns

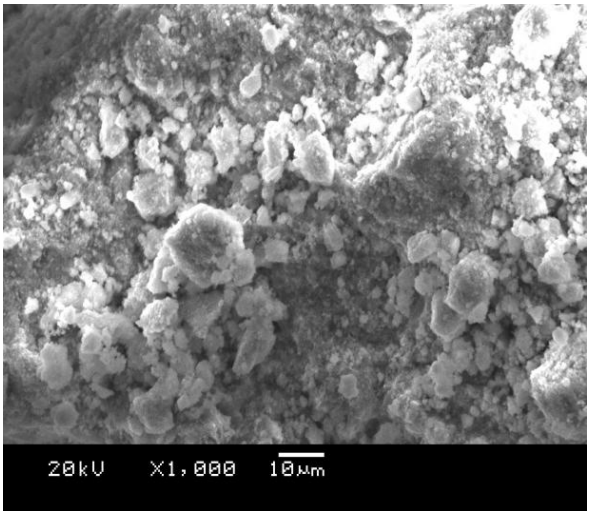

Used of Fe_2O_3+Cr_2O_3 catalyst (9 h), d_{50}= 1000 microns

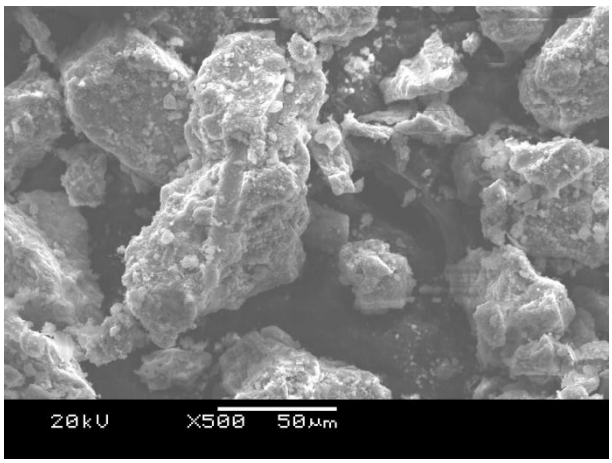

Fresh of Fe_2O_3+Cr_2O_3 catalyst, d_{50}= 500 microns

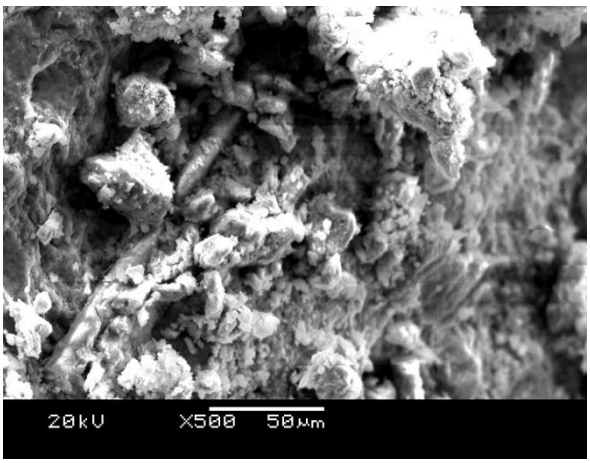

Used of Fe_2O_3+Cr_2O_3 catalyst (9 h),d_{50}=500 microns

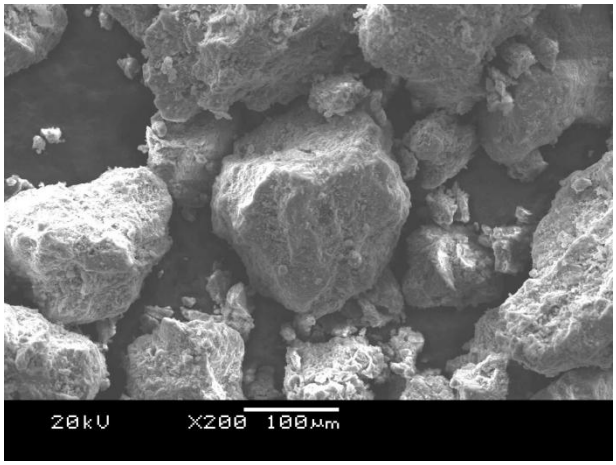

Fresh of Fe_2O_3+Cr_2O_3 catalyst, d_{50} =125 microns

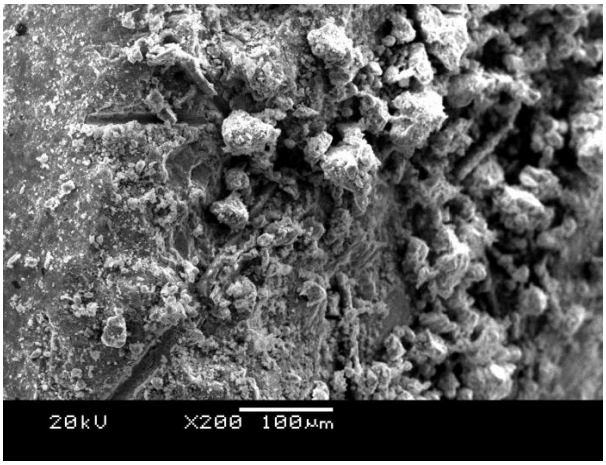

Used of Fe_2O_3+Cr_2O_3 catalyst (9 h), d_{50}=125 microns

Table M.2. Image analysis by SEM on the fresh and used samples of Fe_3O_4 catalyst

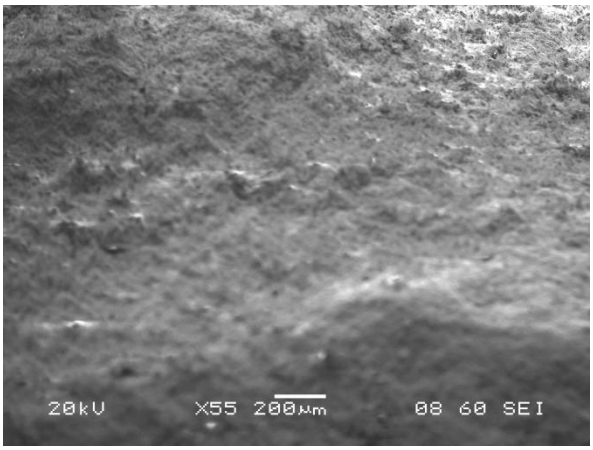

Fresh of Fe_3O_4, d_{50}=4000 microns

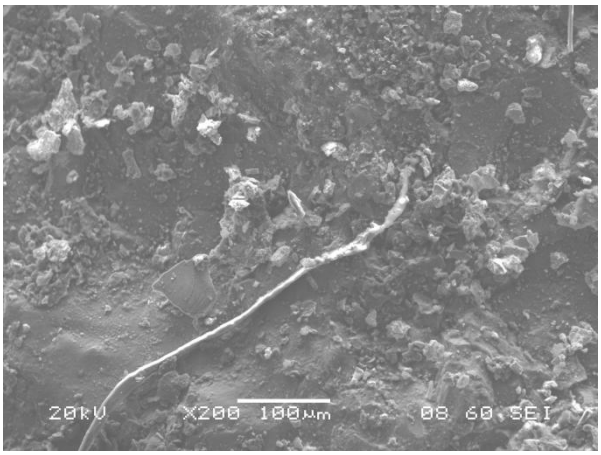

Used of Fe_3O_4, d_{50} = 4000 microns

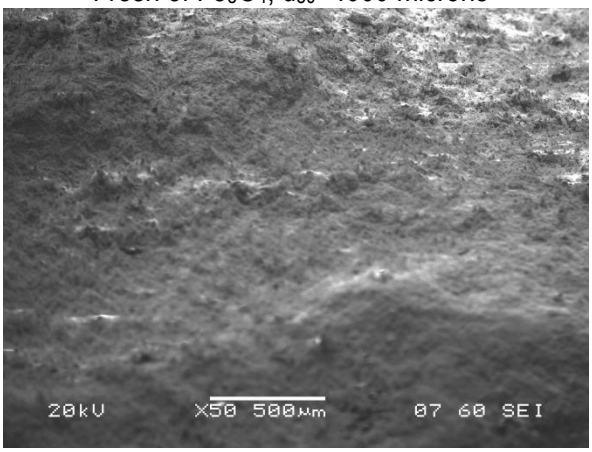

Fresh of Fe_3O_4, d_{50}= 2000 microns

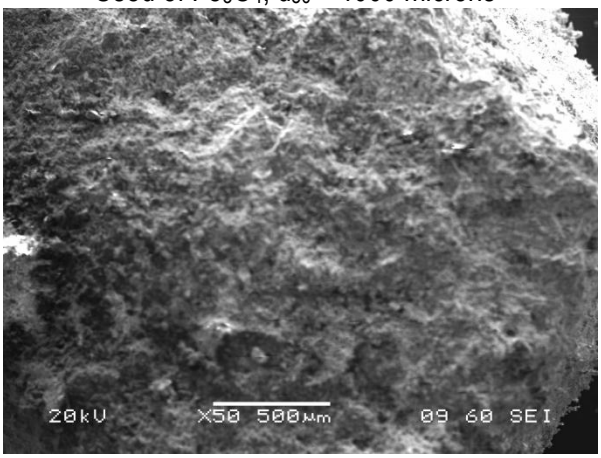

Used of Fe_3O_4, d_{50}= 2000 microns

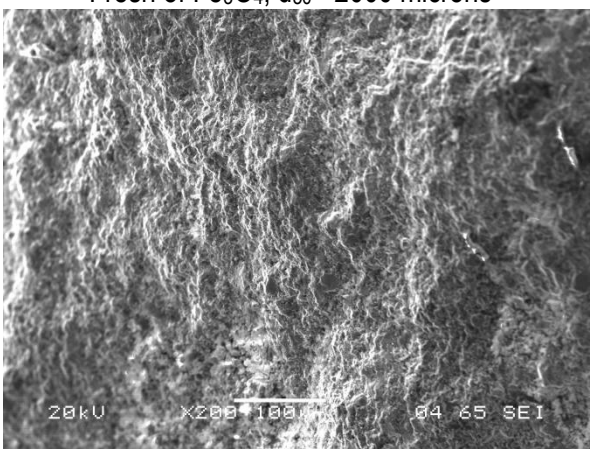

Fresh of Fe_3O_4, d_{50} = 500 microns

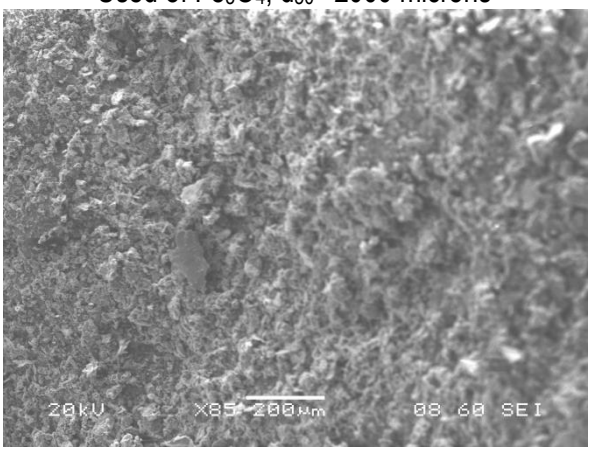

Used of Fe_3O_4, d_{50} = 500 microns

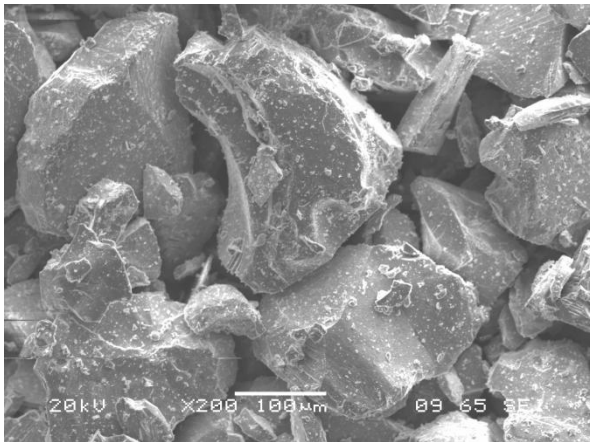

Fresh of Fe_3O_4, d_{50} =125 microns

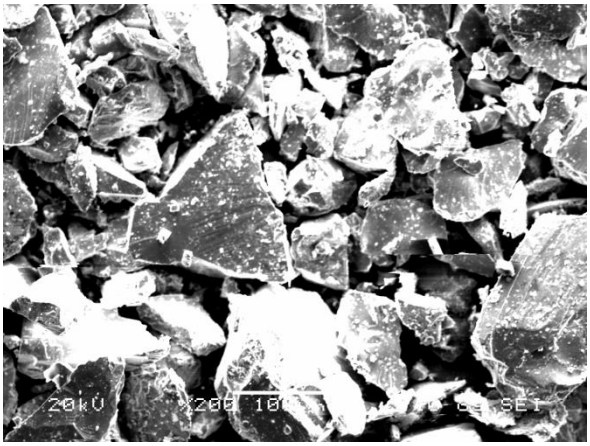

Used of Fe_3O_4, d_{50} = 125 microns

Appendix N. Elemental analysis by Energy Dispersive X-ray Spectrometry (EDS)

N1. EDS of fresh and used sample of Fe_2O_3+Cr_2O_3

Element	Weight %	Atomic %
C K	4.60	14.83
O K	18.89	41.68
Al K	0.37	0.49
Si K	0.53	0.67
Cr K	7.46	5.07
Fe K	66.17	41.83
Cu L	2.58	1.43
Totals	100.00	

Fresh of Fe_2O_3+Cr_2O_3 catalyst, d_{50}= 4000 microns

Element	Weight %	Atomic %
C K	7.7	16.35
O K	18.04	38.29
Al K	0.37	0.47
Si K	0.61	0.73
Ca K	0.35	0.30
Cr K	6.34	4.14
Fe K	54.40	33.08
Ni K	2.76	1.60
Cu L	9.43	5.04
Totals	100.00	

Used of Fe_2O_3+Cr_2O_3 catalyst (172 h), d_{50} = 4000 microns

Element	Weight %	Atomic %
C K	4.57	14.76
O K	10.55	25.57
Al K	0.34	0.49
Si K	0.39	0.54
Ca K	0.32	0.31
Cr K	5.91	4.41
Fe K	75.56	52.48
Cu K	2.36	1.44
Totals	100.00	

Fresh of Fe_2O_3+Cr_2O_3 catalyst (d_{50}=2000 microns)

Element	Weight %	Atomic %
C K	7.19	20.88
O K	12.53	27.34
Al K	0.70	0.90
Si K	1.26	1.57
Ca K	1.07	0.93
Cr K	6.84	4.59
Fe K	67.72	42.31
Cu K	2.70	1.48
Totals	100.00	

Used of Fe_2O_3+Cr_2O_3 catalyst (12 h), d_{50}= 2000 microns

Element	Weight %	Atomic %
C K	3.96	13.63
O K	6.59	17.01
Al K	1.91	2.93
Si K	1.44	2.12
Ca K	1.20	1.24
Cr K	6.83	5.43
Fe K	76.78	56.81
Cu K	1.28	0.83
Totals	100.00	

Element	Weight%	Atomic %
C K	6.61	21.41
O K	8.09	19.68
Al K	0.42	0.61
Si K	0.46	0.63
Ca K	0.15	0.14
Cr K	5.92	4.43
Fe K	70.49	49.12
Ni K	1.28	0.85
Cu K	4.14	2.54
Tb L	2.44	0.60
Totals	100.00	

Fresh of Fe_2O_3+Cr_2O_3 catalyst (d_{50}=1000 microns)

Used of Fe_2O_3+Cr_2O_3 catalyst (9 h), d_{50}= 1000 microns

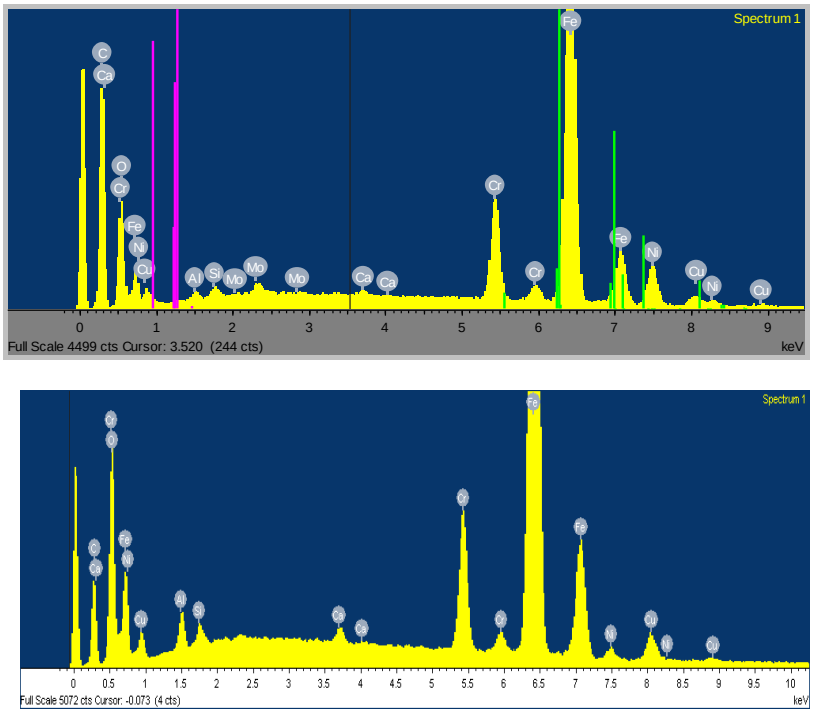

Y-axis: intensity, X-axis: resolution in keV

N2. EDS of fresh and used sample of Fe_3O_4

Element	Weight %	Atomic %
C K	3.52	11.19
O K	12.37	29.49
Mg K	0.55	0.86
Al K	0.96	1.36
Si K	0.91	1.23
Ca K	0.33	0.31
V K	0.15	0.11
Fe K	80.66	55.09
Ni K	0.56	0.36
Totals	100.00	

Fresh of Fe_3O_4 (d_{50}= 2000 microns)

Element	Weight %	Atomic %
C K	6.03	16.25
O K	14.51	29.38
Na K	0.34	0.48
Mg K	3.09	4.12
Al K	1.80	2.16
Si K	6.61	7.63
P K	0.46	0.48
K K	0.54	0.45
Ca K	1.85	1.49
Ni K	0.17	0.12
Fe K	64.59	37.46
Totals	100.00	

Used of Fe_3O_4 (d_{50}=2000 microns)

Element	Weight %	Atomic %
C K	1.86	6.42
O K	10.84	28.12
Mg K	0.20	0.34
Al K	0.24	0.37
Si K	0.23	0.35
Fe K	86.63	64.41
Totals	100.00	

Fresh of Fe_3O_4 (d_{50}= 500 microns)

Element	Weight %	Atomic %
C K	7.69	23.63
O K	8.80	20.30
Mg K	0.31	0.46
Al K	0.43	0.59
Si K	0.41	0.53
Ca K	0.20	0.19
Ti K	0.30	0.23
V K	0.19	0.14
Cr K	0.19	0.13
Fe K	80.74	53.33
Ni K	0.73	0.46
Totals	100.00	

Used of Fe_3O_4 (d_{50} =500 microns)

Element	Weight %	Atomic %
C K	2.01	7.33
O K	7.72	21.12
Mg K	0.30	0.55
Al K	0.34	0.55
Si K	0.20	0.31
Ti K	0.30	0.27
Fe K	89.13	69.87
Totals	100.00	

Fresh of Fe_3O_4 (d_{50} =125 microns)

Element	Weight %	Atomic %
C K	2.12	6.97
O K	12.57	30.96
Mg K	0.47	0.77
Al K	1.35	1.97
Si K	0.58	0.82
Fe K	82.90	58.51
Totals	100.00	

Used of Fe_3O_4(d_{50}= 125 microns)

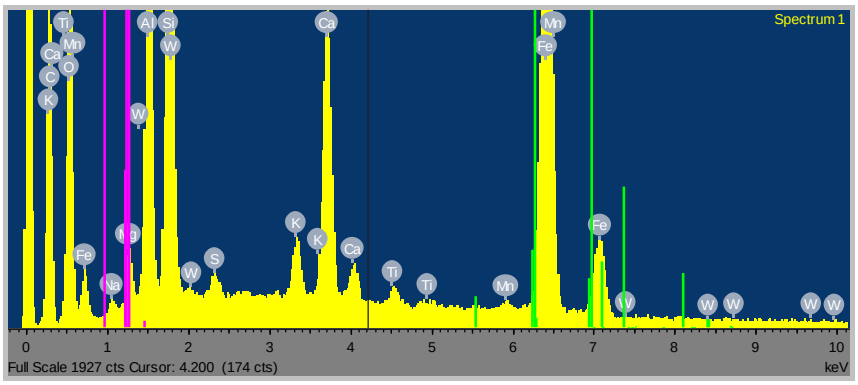

Y-axis: intensity, X-axis: resolution in keV

Appendix O. TGA results

Table O.1. Fresh sample of Fe_2O_3-Cr_2O_3 with d_{50}= 4 mm

Temperature / °C	Mass %	Mass of sample = 101.6mg	Mass losses or gained
°C	%	mg	mg
30	100	101.6	0
50	99.75624	101.3523	0.247659
100	98.75461	100.3347	1.265321
150	98.35383	99.92749	1.672507
200	98.11404	99.68387	1.916132
250	97.9435	99.5106	2.089401
300	97.79795	99.36272	2.237279
350	97.729	99.29267	2.307333
400	97.6896	99.25263	2.347366
450	97.64432	99.20663	2.393372
500	97.56566	99.12672	2.473285
550	97.41938	98.97809	2.621908
600	96.40848	97.95102	3.648983

Table O.2. Used sample of Fe_2O_3-Cr_2O_3 with d_{50}=4 mm

Temperature / °C	Mass %	Mass of sample = 82.3 mg	Mass loss or gained
°C	%	mg	mg
30	100	82.3	0
50	98.90381	81.39784	0.902161
100	89.27709	73.47505	8.824953
150	82.8545	68.18925	14.11075
200	83.18783	68.46359	13.83641
250	84.10301	69.21678	13.08322
300	84.4708	69.51947	12.78053
350	84.52277	69.56224	12.73776
400	84.51122	69.55273	12.74727
450	84.48713	69.53291	12.76709
500	84.46702	69.51635	12.78365
550	84.4469	69.4998	12.8002
600	84.39573	69.45768	12.84232

Table O.3. Fresh sample of Fe_3O_4 with d_{50}=1 mm diameter

Temperature / °C	Mass %	Mass of sample = 49.7 mg	Mass losses or gained
°C	%	mg	mg
30	100	49.7	0
50	99.9992	49.5118	0.1882
100	99.99841	49.15161	0.36024
150	99.99781	49.07019	0.08142
200	99.99701	49.8246	0.75441
250	99.99642	49.87983	0.05523
300	99.99582	49.8386	0.044123
350	99.99522	49.74669	0.091911
400	99.99462	49.73328	0.01341
450	99.99403	49.71984	0.01344
500	99.99343	48.99786	0.72198
550	99.99283	48.98111	0.01675
600	99.99204	48.96102	0.02009

Table O.4. Used sample of Fe_3O_4 with d_{50}=1 mm diameter

Temperature / °C	Mass %	Mass of sample = 49.4 mg	Mass losses or gained
°C	%	mg	mg
30	100	49.4	0
50	99.78097	49.2918	0.108201
100	99.30892	49.05861	0.341394
150	99.15019	48.98019	0.419808
200	99.03765	48.9246	0.475402
250	98.94702	48.87983	0.520174
300	98.86356	48.8386	0.561402
350	98.67751	48.74669	0.653312
400	98.65032	48.73326	0.666744
450	98.62313	48.71982	0.680175
500	98.57869	48.69787	0.702127
550	98.50568	48.66181	0.738193
600	98.09922	48.46101	0.938988

Appendix P. Additional results of the BET analysis

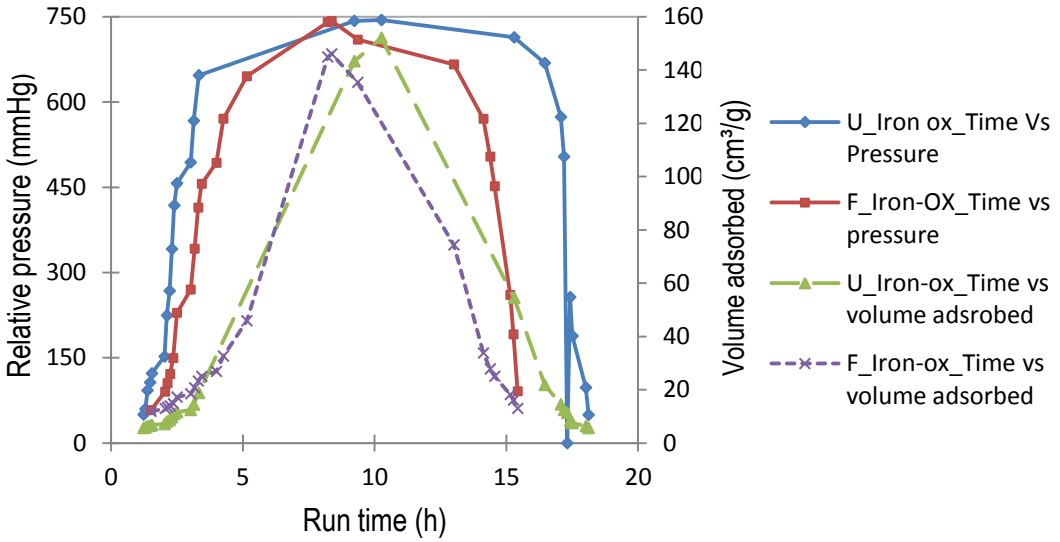

Fig.P1. Additional results of BET analysis of Fe_2O_3+Cr_2O_3 sample (4mm diameter)

Where U is the used sample and F a fresh sample

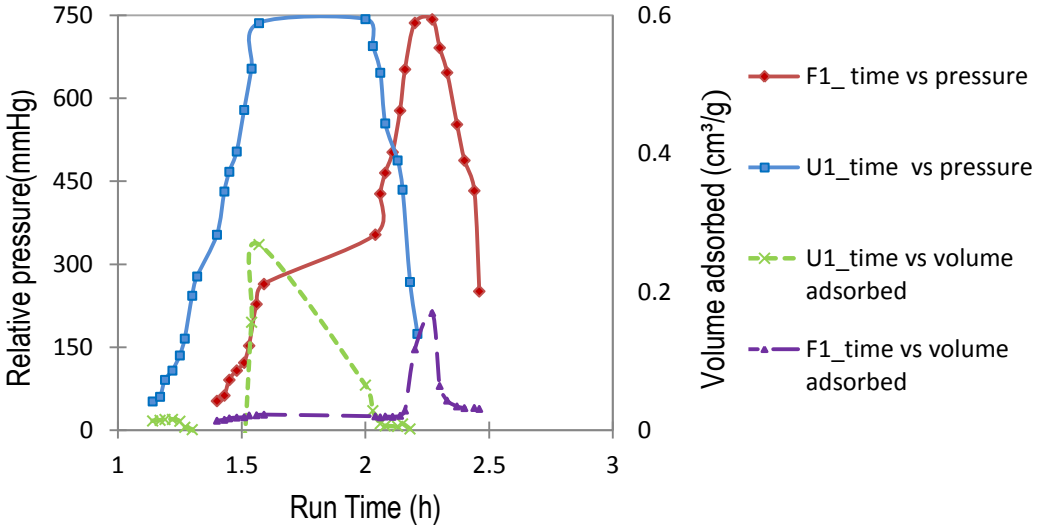

Fig.P.2. Additional results of BET analysis of Fe_3O_4 sample (4 mm diameter)

Where U is the used sample and F a fresh sample

Appendix Q. Pulse Chemisorptions of CO over Fe_2O_3-Cr_2O_3 catalyst

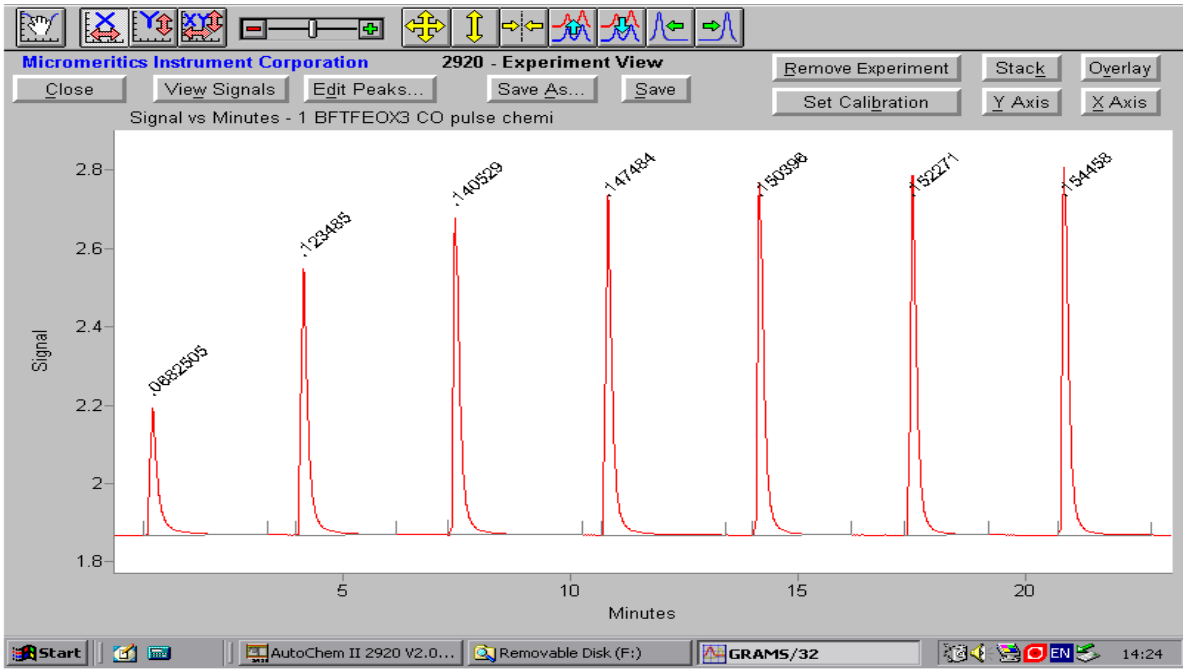

Fig.Q.1. Pulse Chemisorptions of CO on virgin sample of Fe_2O_3-Cr_2O_3, time vs signal

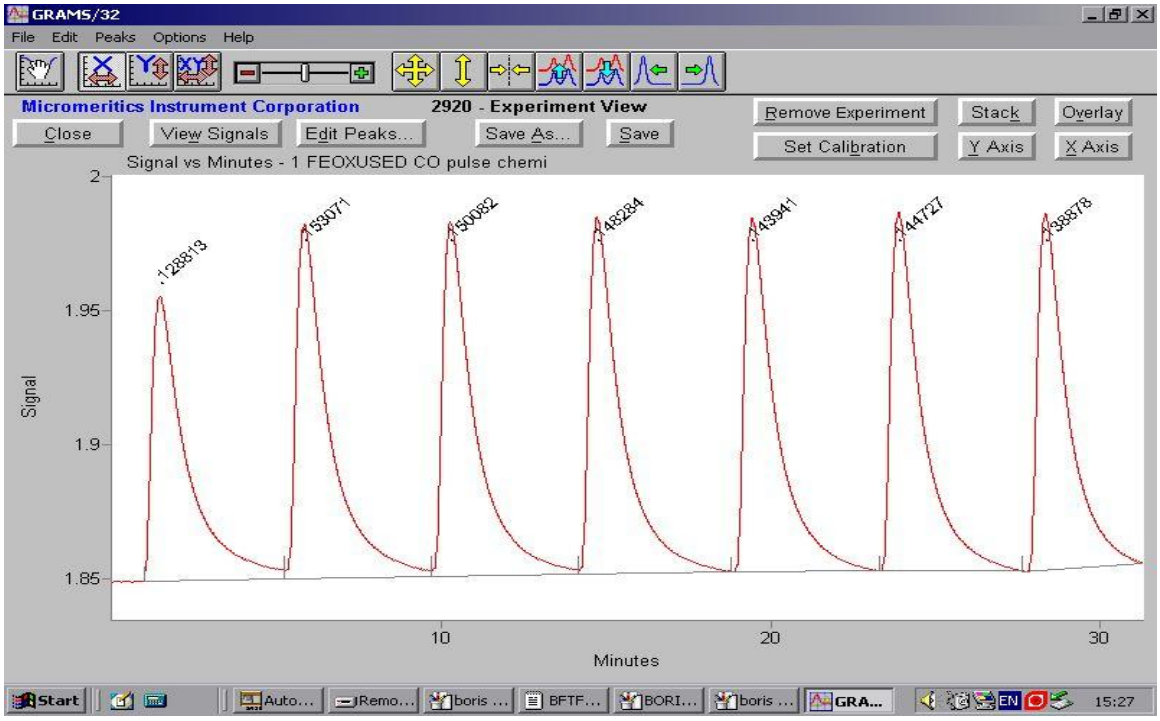

Fig.Q.2. Pulse Chemisorptions of CO on used sample of Fe_2O_3-Cr_2O_3, time vs signal

Fig.Q.1 (graph of Time vs TCD signal) shows that initially after the first few injection of CO, the detector did no recorded a change in signal suggesting that the CO was totally consumed. From 2 to 12 mins

times, the peak areas were significantly different in size (0.088, 0.12, 0.140, and 0.147) as showed in Fig.Q.1 and Q.2. This was attributed to the fact that CO was adsorbed at different rate/degree (as a function of time), which is represented by variable peak area. In addition, high CO absorbed could indicate a strong inter-action between catalyst surfaces and the absorbate gas (CO). In effect, when the sample tends to approach saturation, peaks representing concentration of unreacted molecules of CO appear and peaks that are constant in the area suggested a possible completion of reaction after CO injection.

The quantity of molecules chemisorbed was the difference between the total amount of reactant gas injected, the sum amount that did not react with the active sites of the sample catalyst as measured by the detector.

Appendix R. Investigation of the H_2 yield: spike change

To study the spike change of the hydrogen yield as a function of the date of sample collection and analysis, a series of experiments were conducted under the influence of variable process parameters. Five samples of each run were collected during the experiment after 5 min run time and subsequently every 15 min. All samples were analysed the same day and the following day. The aim was to study the H_2 spike that was observed frequently during the gas samples analysis. At the end of reaction time, the system was shutdown and the gas-liquid products were contained in the separator, by closing the control valves of gas and liquid product streams, respectively. This was left overnight (1 night) before the gas sample was then collected for analysis. The hydrogen yield results analysed the day of the experiment and after 1 night after are shown in table R.1.

Table R.1. Hydrogen yield, as analysed the day of the experiment and 1 night after the sample was produced and kept in the separator.

	H_2	H_2	H_2	H_2	H_2
Runs	Lowest Same day mole%	Cumulative value mole%	Highest same day mole%	1 night after mole%	margin mole%
E56	46.3	57.78	66.29	59.2	1.42
E59	37.7	49.1	60.53	74.92	25.82
E60	12.1	21.68	27.54	39.38	17.7
E62	16.1	37.83	62.14	65.99	28.16
E65	32.46	76.45	46.65	90.47	14.02
E66	31.81	38.15	44.48	38.15	0

It can be seen in table R.1, that when the sample was collected and analysed the same day of the experiment, the yield of hydrogen was lower, compared to the yield of hydrogen after the sample was left overnight in the separator. This could be due to effect of turbulence of the gas-liquid in the separator during the experiment, which results to poor gas-liquid separation, hence low concentration of hydrogen in the gas product. The separator was designed and mounted vertically; the feed into the separator was placed at the top of the separator. In this condition, gas-liquid will tend to move in the same direction due to poor gravity settling; the contra-flow of the two fluids (gas-liquid products) therefore interferes with the flow paths and separation was slower; therefore gas will separate more slowly from the liquid. In fact, an improve gravity settling will have feed flowing horizontally in the separator; gas will separate more quickly from the liquid because the gas is moving in an upward direction into the vapour section of the separator and the liquid /particles are tending to fall to the vessel bottom under the influence of gravity and coalescent. However, other factors effect such as fluid temperature (23-30 °C), pressure (40-60 barg), and density of the fluids influenced the gas-liquid separation.

Appendix S. Semi-Quantitative ICP-MS results of the digestate sample

A sample of digestate produced by acidogenesis (Nitric acid) was characterised to determine its elemental composition by semi-quantitative analysis using an Inductively Coupled Plasma mass spectrometry technique (The Agilent 4500 Series). The results are shown below in table S.1.

Table S.1. Results of the ICP-MS of the digestate

Components	Concentration (ppb)	Components	Concentration (ppb)
Li	80	Pd	33
B	280	Ag	15
Na	35000	Cd	10
Mg	44000	In	5.5
Al	110000	Sn	700
P	930	Sb	22
K	12000	Ba	1800
Ca	400000	La	66
Ti	1300	Ce	91
V	160	Pr	17
Cr	520	Nd	71
Mn	4500	Sm	6.0
Fe	220000	Eu	2.0
Co	62	Gd	9.6
Ni	560	Dy	4.9
Cu	2400	Ho	1.0
Zn	7600	Er	2.2
Ga	98	Yb	1.9
Ge	29	Hf	4.5
As	38	W	8.6
Rb	50	Pt	4.7
Sr	1700	Pb	1900
Y	24	Bi	14
Zr	150	Th	7.8
Nb	1.7	U	5.9
Mo	30		

Results are approximate only (± 20%)

Appendix T. Mass and energy balance calculation

The following assumptions were made for the chemical reaction and mass balance calculation:

- *There is water in the feedstock, or water in the feed is not consumed completely. In effect, the gas product contains some moisture. The liquid product also contains water: the amount of water depends on feed concentration and type of reforming reactions at the process parameters.*
- *The chemical equation does not account for char formation. However, this is not the case in practice. In fact, char is deposited on the catalyst surface (refer to appendix M for ESEM analysis). The amount of char depends on char reforming reaction and process temperature.*
- *Side reactions are negligible in the formation of the products. However, this is not the case, many side reactions can occur depending on a number of factors (process operating parameters*, catalyst selection). These side reactions could significantly affect the product yield. Some of these side reactions are methanation, WGS, RWGS, and Char reforming in water.
- *All CO produced in the primary reaction (eq.t.1) is consumed completely in secondary side reaction (eq.t.2); however, this is not the case. In fact, considerable amounts of CO can be present in the product gas stream due to reverse-WGS reforming although catalyst choice would limit this. The amount of CO depends on the type of reaction being promoted and the used catalyst.*

T.1. Chemical reactions and Mass balance

Many reactions occur in SCWG of glycerol such as hydrolysis, WGS, gas-solid reactions and gas phase reactions. In accordance to the above assumptions, the prominent reaction for hydrogen production is the WGS reaction that is used to derive the overall chemical reaction for the decomposition of glycerol in SCW as shown in equations t.1, t.2 and t.3.

Decomposition of glycerol $C_3H_8O_3 + H_2O \longrightarrow \cancel{3CO} + 4H_2 + H_2O$ (t.1)

WGS-reaction: $\cancel{3CO} + 3H_2O \longrightarrow 3CO_2 + 3H2$ (t.2)

Overall reaction: $C_3H_8O_3 + 4H_2O \longrightarrow 3CO_2 + 7H_2 + H_2O$ (t.3)

RMM (g/mole)	92.1	18	44.01	*2.01*	18.1

Basis: 1 min

15 wt% glycerol solution was made by measuring 875 g of pure glycerol (≈700 ml in volume since the density of glycerol at 25°C is 1.25 g/ml) and adding 4.96 litres of deionised water at 21.6°C. Total solution = 5660 ml

Flow rate = 65 ml/min,

Amount of glycerol in 65 ml/min = 875 g * $\frac{65\ \mathrm{ml/min}}{4960\ \mathrm{ml}+700\ \mathrm{ml}}$ = 10.04 g/min of glycerol.

Amount of water in 65 ml/min = 4960 g * $\frac{65\ \mathrm{ml/min}}{4960\ \mathrm{ml}+700\ \mathrm{ml}}$ = 56.96 g/min of water

Number of mole = $\frac{10.04\ \mathrm{g/min}}{92.1\ \mathrm{g/mole}}$ = 0.109 mole/min of glycerol

For one mole of glycerol, 3 moles of CO_2 is produced:

Mass of CO_2 =3*0.109 mole/min*44.01 g/mole = $14.39\ g/min$

For one mole of glycerol, 7 moles of H_2 is produced:

Mass of H_2 =7*0.109 mole/min*2.016 g/mole = $1.538\ g/min$

For one mole of glycerol and 4 mole of reacting water, 1 mole of H_2O will leave with product:

Mass of H_2O =1*0.109 mole/min*18.01 g/mole = $1.963\ g/min$

Three moles of CO are needed to produce three moles of CO_2 (refer to section 7.2)

Mass of CO =3*0.109 mole/min* 28.01 g/mole = $9.159\ g/min$

Table T.1. Theoretical Mass balance

Reactants	Products
Glycerol : 10.04 g/min	H_2 = $1.538\ \ g/min \equiv \frac{1.538\ g/min}{2.016\ g/mole}\ 0.763\ \ mole/min$ (63.68 mole% H_2) $\rightarrow \frac{0.763\ mole/min * 1\ mole\ of\ glyceol}{0.109\ mole/min\ of\ glycerol}$ = 7 moles of H_2/mole of glycerol
Water : 56.960 g/min	CO_2 = $14.391\ \ g/min \equiv \frac{14.391\ g/min}{44.1\ g/mole}\ \ 0.326\ \ mole/min$ (27.21 mole% CO_2) hence $\frac{0.326\ mole/min * 1\ mole\ of\ glyceol}{0.109\ mole/min\ of\ glycerol} \approx$ 3 moles of CO_2/mole of glycerol
Vapour	H_2O = 1.963 $g/min = \frac{1.963\ g/min}{18.01\ g/mole}$ =0.109 mole/min (9.09 mole% H_2O)
	Total gas products= 17.892 g/min →26.6 wt% of total products
	Liquid products
	Assume no char; however, this is not the case char is formed but was not explicitly quantified.
	Total liquid products = 49.468 g/min→73.4 wt%
Total = 67.36 g/min	Total = 17.892 + 49.468 = 67.36 g/min of gas/liquid products

Table T.2. Summary of the theoretical and experimental mass balance

Operating conditions of the experiments: system pressure = 250 barg, Pre-heater set point =500°C, reactor set point = 550°C, feed concentration = 15 wt% pure glycerol (875 g of glycerol + 4950 g of water), feed flowrate =65 ml/min. catalyst conditions: particle size: 4 mm iron oxide-chromium or magnetite, loading = 10.1 g.

		Experimental mass balance	Experimental mass balance	Experimental mass balance	Theoretical mass balance (ideal case)
	Units	Run_75	Run_55	Run_85	
Type of packing materials		No catalyst	Iron oxide	Magnetite	No catalyst
Product gas	mole%				
H_2		25.4	37.7	41.9	63.6
CO		6.1	4.5	2.3	-
CO_2		9.0	13.3	8.4	27.2
CH_4		10.1	20.4	15.8	0.0
C_2H_4		49.2	23.9	31.3	0.0
H_2O(vapour)					9.1
Conversion of glycerol	%	67.3	96.9	98.1	100
Product yields	wt%				
Product gas yield		80.6	84.1	87.9	26.6
Liquid product		18.7	15.2	11.6	73.4
Char		0.6	0.5	0.4	-

T.2. Energy

The energy balance calculation is presented below, and shown in Table 7.3. Before analysing the data, it is important to remind the hypotheses used to perform the calculations.

Assumptions:

- *The mass balances are based on the experimental results.*
- *The calculated energy need for the reaction is based on an ideal case study as shown in equation 7.3, and there are no energy losses. Thus, the energy need could be therefore underestimated compared to a real process.*
- *The calculated energy recovery is based also on an ideal case study without any other form of heat losses (e.g. heat losses to the surrounding, heat losses from evaporating water and heat transfer by radiation), which is a very favourable assumption.*
- *The energy balance calculations are based on the SCWG of glycerol for hydrogen production using equation (T.3)*

$$C_3H_8O_3 + 4H_2O \rightarrow 3CO_2 + 7H_2 + H_2O \qquad (t.3)$$

Other chemical reactions:

$$C_3H_8O_3 + 4H_2O \rightarrow 2CO_2 + 3H_2 + 3H_2O + CH_4 \quad (t.4)$$

$$C_3H_8O_3 + 4H_2O \rightarrow CO + CO_2 + 2H_2 + 4H_2O + CH_4 \quad (t.5)$$

However, other exothermic (e.g. $C + H_2 \rightarrow CH_4$) and endothermic (e.g. $C + CO_2 \rightarrow 2CO$) reactions are occuring as evidence by the wide composition and yields of products obtained. These reactions have been discussed in section 5, 6 and also refer to section 2.3.3.

- The calorific value (CV) of a fuel is defined as the quantity of heat produced by its combustion at STP, and in this case it is based on all gas produced during its combustion.
- Glycerol and water are treated as individual components in the mixture, and are not considering mixture properties. For example, the heat capacities are calculated for each components (water, glycerol) and are not for the actual (water + glycerol) mixture.
- Specific capacity (Cp) of water is 4.12 kJ/kg.K or 74.98 kJ/kmol.K

T.2.1. Calculations of the calorific value of the product gas

Although, the product gas is not an ideal gas; it was assumed to be an ideal gas and the calorific value (CV) is defined in equation T.6 by Wrobel and Wright [**382**].

$$CV = X_1*CV_1 + X_2*CV_2 + \ldots X_n*CV_n \quad (t.6)$$

Where X_1, X_2 … Xn are the mole fractions of the gas compounds in the product gas, and CV_1, CV_2, CV_n are the calorific values of the gas compounds at 15 °C and at atmospheric pressure.

Table T.3: Summary of the caloric value of the product gas

Operating conditions of the experiments: system pressure = 250 barg, reactor temperature 550°C, feed concentration = 15 wt% pure glycerol

Product gas	CV at 15 °C and atm. Pressure (MJ/m³) [384]	Mole fraction (no catalyst)	CV (MJ/m³) (no catalyst)	(E55) Mole fraction (Fe_2O_3-Cr_2O_3)	CV (MJ/m³)	(E85) Mole fraction (Fe_3O_4)	CV (MJ/m³)
H_2	12.9	24.9	3.1	0.38	4.9	0.42	5.4
CO	11.9	7.2	0.8	0.04	0.5	0.03	0.2
CO_2	-	7.8	-	0.13	-	0.08	-
CH_4	59.7	13.3	7.7	0.21	11.9	0.16	9.5
C_2H_4	37.7	46.5	17.3	0.24	9.0	0.31	11.7
C_2H_6	66.1		-	-	-	-	-
C_3H_8	93.9		-	-	-	-	-
Total			28.9	1	26.3	1	26.8

It can be seen that the CV of the product gas for un-catalysed is higher than that of catalysed, which is attributed to the presence of higher concentration of hydrocarbons in the product gas of the un-catalysed SCWG reaction. On the other hand, it is evident in table 7.3 that the gasification of glycerol using SCW has resulted in low calorific value gas stream [3-5 MJ/m³] if the CV is based on H_2-gas only. The CV is higher for catalysed-SCWG (4.9 MJ/m³), compare to 3.1 MJ/m³ for un-catalysed. This is because of the higher concentration of H_2 in the product gas of CSCWG, which resulted from a combination of primary and secondary reactions that include cracking of hydrocarbons.

T.2.2. Energy balance calculation

Note that the chemical properties of the compounds such as specific heat capacity, heat of formation and enthalpy were taken from the chemical properties handbook [**381**]. The results of the energy balance are summarised in table 7.4.

A. Energy in feed glycerol

Feed concentration = 15 wt% glycerol (875 g of glycerol and 4950 g of water), feed flow rate =65 ml/min, which gives a value of 10.04 g/min of glycerol + 56.96 g/min of water at 22°C

Caloric value (CV) of glycerol = 25 MJ/kg at STP [**382**] (0°*C* and under a pressure of *1,013 mbar)*

Energy in glycerol input =$25\frac{MJ}{kg}$*10.04*$10^{-3}\frac{kg}{min}$ = 0.251 MJ/min = 251 kJ/min=4.18 kW

CV of water = 0.0042 MJ/kg at STP [**382**]

Energy in water input = $0.0042\frac{MJ}{kg}$*56.96*$10^{-3}\frac{kg}{min}$ =0.000239 MJ/min = 0.239 kJ/min=0.00398 kW, thus, energy in the feed glycerol (15 wt% glycerol at 65 ml/min) is Q_{feed} = 4.33+0.00398 =4.33 kW = 4330 W

B. Pump energy

Hydraulic Pump Power (P_h): The ideal hydraulic power to drive a pump depends on the mass flow rate, the liquid density and the differential height. The flow is lifted from a static point of one height to an other, or the friction head loss component of the system can be calculated as

$(P_h)= \frac{Q\ \rho\ g\ h}{3.6*10^6*\varepsilon}$ (equation t.7)

Where, P_h = power (kW), Q = flow capacity (m^3/h), ρ = density of fluid (kg/m^3), g = gravity (9.81 m/s^2), h = differential head (m)

Based on run E85, the actual flowrate was Q = 65 ml/min (or 0.0039 m^3/h) of glycerol slurry at 250 barg, design capacity: Q= 4.71litre/h, which is 0.004 71 m^3/h of water slurry at 300 barg. The pump dynamic head is 1.4571*250 bar (refer to pump data sheet), density of 15 wt% glycerol at 25°C was

1.12 g/ml (or 1120 kg/m^3) as measured, $\text{and } \varepsilon$ is the pump efficiency (~0.3, refer to calibration curve-Appendix A).

The pressure can be converted from barg to head in meter as follows, h = $\frac{\mathbf{10.197}*\boldsymbol{Pressure}}{\boldsymbol{\rho}}$ *(eq.t.8)*

h = $\frac{10.197*Pressure}{\rho}$ = *259.86 m*

P_h= $\frac{Q\ \rho\ g\ h}{3.6*10^6*\varepsilon}$ = $\frac{0.0039*1120*9.81*259.86}{3.6*10^6*0.3}$= 0.0103 kW (~10.3 W), compared to its design power of 1.1 kW

C. <u>Pre-heater; energy involved to pre-heating the feed from 25 to 500°C</u>

Basis: 1 mole of glycerol in the feed

Reagent 1: glycerol

Q_1= Energy required for taking liquid glycerol from 25°C to boiling temperature (290°C)

Q_1= $\int_{25}^{290} mCp\ dT$

Q_1= 1 mole*$\int_{25}^{290}(132.145 + 8.601 * 10^{-1}\,T - 1.974*10^{-3}\,T^2 + 1.806*10^{-6}\,T^3)\,dT$ [**381**]

= $[132.145T + 0.8601T^2 - 0.000658\,T^3 + 0.0000004515T^4]$

= (38322.05 + 72334.41 – 16047.96 + 3193.37) – (3303.625+537.562 – 10.281 + 0.1764)

= 97801.87 – 3831.08

= 93970.79 J

<u>Q_1=93.39 kJ</u>

Heat of vaporisation (Hvap) of glycerol at 290°C is 66.13 kJ/mol [**381**]

Q_2= Energy required to vaporise the liquid glycerol at 290°C.

Q_2=H_{vap}*1mol<u>= 66.13 kJ</u>

Q_3= Energy required to take glycerol vapour from 290°C to 550°C

Q_3= 1 mole* $\int_{290}^{550}(9.656 + 4.283 * 10^{-1}\,T - 2.679*10^{-4}\,T^2 + 3.179*10^{-8}\,T^3 + 2.774*10^{-11}\,T^4)\,dT$ [**381**]

= [9.656T + 0.214T² - 0.0000893T³ + 7.947*10$^{-9}\,T^4$ + 5.548*10$^{-12}\,T^5$]

= (5310.8 + 64735 – 14857.28 + 727.24 + 279.22) – (2800.24 + 17997.4 – 2177.93+ 56.207+ 11.379)

= 56194.98 – 18687.296

Q_3= 37507.68 J

Q_3 = 37.507 kJ

Heat required for feed glycerol, $Q_{glycerol}$= Q_1+Q_2+Q_3 = 93.39 + 66.13 + 37.507 = 197.027 kJ

Reagent 2: water

Q_{W1}= Heat required for feed water = m$C_p\ \Delta$T (Cp=74.98*10^{-3} kJ/mol.K [**381**])

Q_{W1}= 4 mole*74.98*10$^{-3}\frac{\text{kJ}}{\text{mol.K}}$* (100-25) =22.494 kJ

Heat of vaporisation of water at (250 barg, 100 °C) is 0.3404 kJ/mol [**383**]

Q_{W2}= m*H_{vap} = 4 mole * 0.3404 kJ/mol = 1.362 kJ

Energy required for taking water vapour from 100°C to 550°C

Q_{W3}= m*$\int_{100}^{550} Cp\ dT$

Q_{W3}= 4 mole*$\int_{100}^{550}(33.933 - 8.412 * 10^{-3} T^3 + 2.991*10^{-5} T^2 - 1.782*10^{-8} T^3 + 3.693*10^{-12} T^4)$ dT [**381**]

Q_{W3}= 9.412 kJ

Total heat energy required for the feed water

Q_{water}= Q_{W1}+Q_{W2}+Q_{W3} =22.494 + 1.362 + 9.412 = 33.266 kJ

Total heat energy required for reactants (glycerol + water) in SCWG process:

Q_{feed} =$Q_{glycerol}$l + Q_{water} = 197.027 + 33.266 = 230.293 kJ = <u>4.33 kW</u>

Heat of the reaction

$C_3H_8O_3 + 4H_2O \rightarrow 3CO_2 + 7H_2 + H_2O$

$(\Delta Hr)_{reaction}$ = $Q_{reaction}$= $\sum$ (ΔHr) product - $\sum$ (ΔHr) reactant

$\Delta H_r°$ = [(3× $\Delta H_f°$ (CO_2)) + (7× $\Delta H_f°$(H_2)) + (1*$\Delta H_f°$(H_2O)] (products) - [(1 × $\Delta H_f°$($C_3H_8O_3$) + (4× $\Delta H_f°$(H_2O)] (reactants)

$\Delta H_r°$ = [(3*(-393.52)) + (7*(0) + (1*(-241.82)] – [(1*(-672.39) + (4*(-285.83)] (refer to **reference 381**)

= [(-1180.56 + 0 – 241.82)] – [(- 672.39 – 1143.32)]

= -1422.38– (-1815.71)

$He_r°$ = <u>393.33 kJ</u> (endothermic reaction)

Q_{INPUT} = total energy required for the reaction = Qfeed + Qreaction = 230.293 + 393.33 = 623.623 kJ

Q_{INPUT} <u>= 623.623 kJ</u>

Theoretical Energy output

$C_3H_8O_3 + 4H_2O \rightarrow 3CO_2 + 7H_2 + H_2O$ (t.3)

7 moles of hydrogen are produced (theoretical value), representing 63.68 mole% of the product gas.

CV of H_2 at 15°C is 12.78 MJ/m³ [**384**],

At STP, one mole of gas occupies 24.8 dm³ (0.0248 m³), hence 7 moles of H_2-gas would occupied a volume of V_g= $\frac{7\ \text{mole} * 0.0248}{1\ \text{mole}}$ m³ = 0.1736 m³

So the heating value of the produced hydrogen =0.1736 m³ * 12.78 MJ/m³= 2.22 MJ = <u>2220 kJ</u>

Total energy input for the reaction = Q_{INPUT} = 623.6 kJ

Net energy gained assuming all gas burns= 2220 - 623.6 = 1596.4 kJ per mole of glycerol reacted. (~39 % of the energy input)

For the breakeven value of energy (input=output, assuming no heat losses), the minimum mole of H_2 yield = $\frac{mole\ of\ H_2}{1\ mole\ of\ glycerol\ feed} * \frac{623.6\ kJ\ of\ energy\ input}{2220\ kJ\ of\ \ heating\ value\ produced} = 3.55$ moles H_2/mole of glycerol feed.

Actual energy output - runs E85 (refer to section 6.7)

Mole fraction of H_2 produced in run E85 was 0.419 (refer to table 6.11)

Actual number of mole of H_2 = 7mole of H_2 *0.419 = 2.933 mole of H_2 produced

CV of H_2 at 15°C is 12.78 MJ/m³ [**384**],

At STP, one mole of gas occupies 24.8 dm³ (0.0248 m³), hence 2.933 of H_2-gas would occupied a volume of $V_g = \frac{2.933\ \text{mole} * 0.0248}{1\ \text{mole}}$ m³ = 0.07274 m³

So the actual heating value of the hydrogen produced =0.07274 m³ * 12.78 MJ/m³= 0.929 MJ

= 929 kJ, compared to the theoretical value of 2220 kJ

Total energy input for the reaction = Q_{INPUT} = 623.6 kJ, which is 10.4 kW

Net energy gained from the reaction = 929 - 623.6 = 305.4 kJ per mole of glycerol reacted.

D. Pre-heater energy-continued

By integration and basis of 1 min

Reagent 1: glycerol; (Calculation is based on the 15wt% feed concentration given in section A).

Q_1= Energy required taking liquid glycerol from 25°C to boiling temperature (290°C)

Flowrate = 10.04 g/min, RMM = 92.1 g/mole

$Q_1 = \int_{25}^{290} mCp\ dT$

$Q_1 = 10.04\ \frac{g}{min} * \frac{1}{92.1}\frac{mole}{g} * \int_{25}^{290}(132.145 + 8.601 * 10^{-1}\,T - 1.974*10^{-3}\,T^2 + 1.806*10^{-6}\,T^3)\,dT$ [**381**]

$= 0.109\ \frac{mole}{min}\left[132.145T + 0.8601T^{\,2} - 0.000658\,T^{\,3} + 0.0000004515T^4\right]\frac{J}{mole\ K}$

= 0.109 (38322.05 + 72334.41 – 16047.96 + 3193.37) – (3303.625+537.562 – 10.281 + 0.1764)

= 0.109 (93970.79) = 10242.816 J/min

Q_1=10.242 kJ/min

Heat of vaporisation (H_{vap}) of glycerol at 290°C is 66.13 kJ/mol.

Q_2= Energy required to vaporise the liquid glycerol at 290°C.

$Q_2 = 66.13\frac{kJ}{mole} * 0.109\ \frac{mole}{min}$ = 7.208 kJ/min

Q_3= Energy required to take glycerol vapour from 290°C to 500°C

Q_3= 10.04 $\frac{g}{min} * \frac{1}{92.1}\frac{mole}{g} * \int_{290}^{500}(9.656 + 4.283 * 10^{-1}\,T - 2.679*10^{-4}\,T^2 + 3.179*10^{-8}\,T^3 + 2.774*10^{-11}\,T^4)\,dT$ [1]

= $0.109\ \frac{mole}{min}$ [9.656T + 0.214T² - 0.0000893T³ + 7.947*10$^{-9}\,T^4$ + 5.548*10$^{-12}\,T^5$]

= $0.109\ \frac{mle}{min}$[(4828 + 53500 – 11162.5 + 496.68+ 173.37)- (2800.24 + 17997.4 – 2177.93+ 56.207+ 11.379)]

Q_3= $0.109\ \frac{mole}{min}$ (33326.13$\frac{J}{mole}$) = 3414.54 J/min

Q3 = <u>3.414 kJ/min</u>

Heat required for feed glycerol, $Q_{glycerol}$= Q_1+Q_2+Q_3 =10.242 + 7.208 + 3.414 = <u>20.864 kJ/min</u>

Reagent 2: water

Mass flowrate of water in 15 wt% feed of glycerol at 65 ml/min is 56.96 g/min

Q_{W1}= Heat required for feed water = m Cp ΔT (74.98*10^{-3} kJ/mol.K, (**refer to reference 381**)

Q_{W1}= 56.96 $\frac{g}{min} * \frac{1}{18.1}\frac{mole}{g}$[74.98*10$^{-3}\frac{\text{kJ}}{\text{mol.K}}$] (100-25)

<u>Q_{W1}=17.69 kJ/min</u>

Heat of vaporisation of water at (250 barg, 100 °C) is 0.3404 kJ/mol (**refer to reference 381**)

Q_{W2}= m* H_{vap}= 56.96 $\frac{g}{min} * \frac{1}{18.1}\frac{mole}{g}$ * 0.3404 kJ/mol

<u>Q_{W2}= 1.071 kJ/min</u>

Energy required for taking water vapour from 100°C to 500°C

Q_{W3}= m*$\int_{100}^{550} Cp\ dT$

Q_{W3}=56.96 $\frac{g}{min} * \frac{1}{18.1}\frac{mole}{g}$ *$\int_{100}^{500}(33.933 - 8.412 * 10^{-3}\,T^3 + 2.991*10^{-5}\,T^2 – 1.782*10^{-8}\,T^3 + 3.693*10^{-12}\,T^4)\,dT$ [381]

= 3.146 $\frac{mole}{min}$ [33.933T – 4.206*10^{-3} T² + 9.97*10^{-6} T³ – 4.45*10^{-9}T⁴ + 7.386*10^{-13}T⁵]

=3.146 $\frac{mole}{min}$ [(16966.5 – 1051.5 + 1246.25 – 278.125 + 23.08) – (3393.3 – 42.06+9.97-0.445+0.007386)]

Q_{W3}= 3.146 $\frac{mole}{min}$ (13545.435$\frac{J}{mole}$) = 42613.9 J/min

<u>Q_{W3} = 42.613 kJ/min</u>

Total heat energy required for the feed water

Q_{water}= Q_{W1}+Q_{W2}+Q_{W3} = 17.69 + 1.071 + 42.613 = <u>61.37 kJ/min</u>

Total heat energy required for reactants (glycerol + water) in SCWG process:

Q_{feed}=$Q_{glycerol}$ + Q_{water}= 20.864.53 kJ/min + 61.37 kJ/min = <u>82.238 kJ/min</u>

Heat of the reaction

$C_3H_8O_3 + 4H_2O \rightarrow 3CO_2 + 7H_2 + H_2O$

$(\Delta Hr)_{reaction} = Q_{reaction} = \sum (\Delta Hr)$ product - $\sum (\Delta Hr)$ reactant

$\Delta H_r° = [(3\times \Delta H_f° (CO_2)) + (7\times \Delta H_f°(H_2)) + (1*\Delta H_f°(H_2O)]$ (products) - $[(1 \times \Delta H_f°(C_3H_8O_3) + (4\times \Delta H_f°(H_2O)]$ (reactants)

$\Delta H_r° = [(3*0.109\frac{mole}{min}(-393.52)) + (7*(0) + (1*0.109\frac{mole}{min}(-241.82)] - [(1*0.109\frac{mole}{min}(-672.39) + (4*0.109\frac{mole}{min}(-285.83)]$ (refer to **reference 381**)

= [(-128.68 + 0 – 26.358] – [(- 73.29 – 124.62)]

= -155.068 – (- 197.91)

$He_r°$ = 42.842 kJ/min (endothermic reaction)

Qpre-heater (input) = 82.238 + 42.842 =125.08 kJ/min = <u>2.084 kW, which is 2084 W</u>

E. <u>Reactor energy</u>

The process stream leaving the pre-heater enters the reactor at ~400°C (as measured) where is heated at temperature of 550°C

$Q_{r(glycerol)}$ =Energy required to take glycerol vapour from 400°C to 550°C

$Q_{r1\ (glycerol)} = 10.04\ \frac{g}{min} * \frac{1}{92.1}\frac{mole}{g} * \int_{400}^{550}(9.656 + 4.283 * 10^{-1}\ T - 2.679*10^{-4}\ T^2 + 3.179*10^{-8}\ T^3 + 2.774*10^{-11}\ T^4)\ dT$ [**381**]

$=0.109\ \frac{mole}{min}\ [9.656T + 0.214T^2 - 0.0000893T^3 + 7.947 * 10^{-9}\ T^4 + 5.548 * 10^{-12}\ T^5]_{400}^{550}$

$= 0.109\ \frac{mole}{min}$ [(5310.8 + 64735 – 14857.28 + 727.24 + 279.22) – (3862.4 + 34240 – 5715.2+ 203.44+ 56.81)]

$= 0.109\ \frac{mole}{min}$ (85909.54 – 32647.45) $\frac{J}{mole}$= 5805.56 J/min

= <u>5.805 kJ/min</u>

Energy required for taking water vapour in the preheated feed from 400°C to 550°C

$Q_{r2(water\ vapour)} = m^* \int_{400}^{550} Cp\ dT$

$Q_{r2(water\ vapour)}$ =56.96 $\frac{g}{min} * \frac{1}{18.1}\frac{mole}{g} * \int_{400}^{550}(33.933 - 8.412 * 10^{-3}\ T + 2.991*10^{-5}\ T^2 - 1.782*10^{-8}\ T^3 + 3.693*10^{-12}\ T^4)\ dT$ [381]

Q_{r2} =3.14 $\frac{mole}{min}$ [33.933T – 4.206*10^{-3} T^2 + 9.97*10^{-6} T^3 – 4.45*10^{-9}T^4 + 7.386*10^{-13}T^5]

= 3.14 $\frac{mole}{min}$[(18663.15–1272.315 +1658.75- 407.20+37.17)–(13578.2-672.96+638.08-113.92+7.56)]

= 3.14 $\frac{mole}{min}$(18679.55 – 13436.96) $\frac{J}{mole}$ = 16461.73J/min

= <u>16.461 kJ/min</u>

Q_r = 5.805 kJ/min + 16.461 kJ/min = <u>22.266 kJ/min = 0.371 kW= 371 W</u>

Total reactor energy input,

Q_{INPUT} = total energy required for the reaction = Q_{feed} + $He_r°$ + Q_r

= 82.238 kJ/min + 42.842 kJ/min + 22.266 kJ/min

Q_{INPUT} = 147.346 kJ/min

<u>= 2.456 kW</u>

<u>= 2456 W</u>

F. <u>Cooler: Energy lost from cooling the process stream from 550 to 31°C</u>

- First heat balance

15-wt% glycerol solution was made by measuring 875 g of pure glycerol (≈700 ml in volume since the density of glycerol at 25°C is 1.25 g/ml) and adding 4.96 litres of deionised water at 21.6 °C with density of 0.997 g/ml). Total solution = 5660 ml

Flow rate of process stream = 65 ml/min,

Amount of glycerol in 65 ml/min = 875 g * $\frac{65\ ml/min}{4960\ ml+700\ ml}$ = 10.04 g/min of glycerol.

Amount of water in 65 ml/min = 4960 g * $\frac{65\ ml/min}{4960\ ml+700\ ml}$ = 56.96 g/min of water

Process stream temperature leaving the reactor = 550°C, process stream outlet from the cooler = 31°C

Calculate energy in stream at 550°C using Q= m * Cp * ΔT

Assume 10.04 g/min flow rate of process stream.

Q = 0.0104$\frac{kg}{min}$ * 4.12$\frac{kJ}{kg.K}$ (550- 31) + 0.056$\frac{kg}{min}$ ∗2.43 $\frac{kJ}{kg.K}$(550-31) =

= 22.23$\frac{kJ}{min}$ + 70.62$\frac{kJ}{min}$

=92.85 $\frac{kJ}{min}$

=1.5475 kW

= 1547.5 W

Energy lost from cooling ($Q_{Lost\text{-}cooling}$)

$Q_{Lost\text{-}cooling}$ = 2456 - 1547.5 = 908.5 W

Energy lost from depressurisation (Q_{Lost}-pressure)

Q_{Lost} -pressure = 1547.5 – 908.5 = 639 W

- *Second heat balance*

At steady state, energy from the first heat balance can be used to determine mass flow rate of coolant.

Energy in process stream, Q= 1879 W = $m_c * c_p * \Delta T$,

Inlet service water (average mains water in winter period) temperature = 6°C, outlet service water = 41°C

Mass flowrate of coolant, m_c = $\frac{1879}{4120*(41-6)}$ = 0.0129 $\frac{kg}{s}$ = 0.777$\frac{kg}{min}$ = 777 $\frac{g}{min}$ (this value changes when the temperature of the mains water in the summer also is changed to an average of 16°C)

Appendix U. Screen shot of Labview

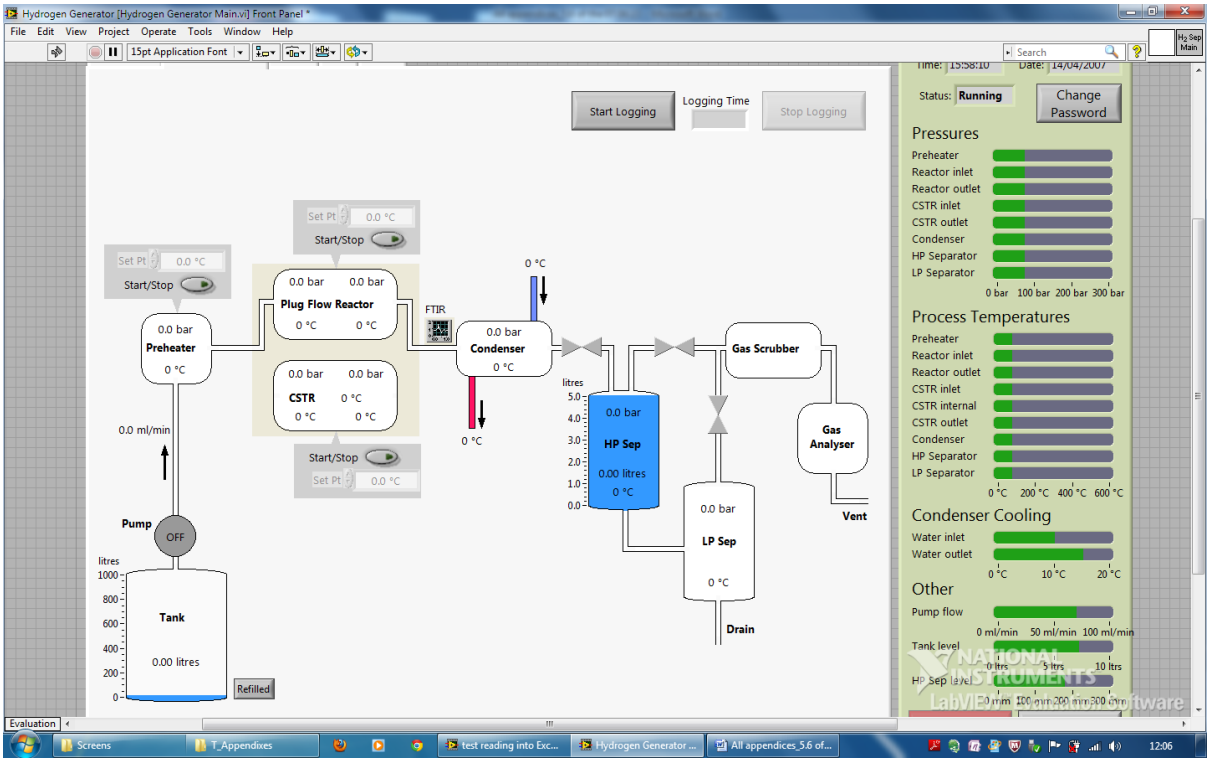

Appendix V. Materials and experimental procedure used for COD analysis

Reagents. All the reagents used were of analytical reagent grade and supplied by sigma –Aldrich in tube of 40 ml volume (part n° 14555). Reagents are CSB/COD, and were composed as followed: potassium dichromate, mercury II sulphate, acid sulfuric.

COD reactor supplied by Haache Ltd was used for the oxidation reaction at a maximum heating temperature of 150°C.

COD analyser. The COD measurement was carried out on Specroquant NOVA 60, with a maximum range concentration of 500-10000 mgL^{-1}. All cell tests were pre-programmed, and the device automatically recognised the cell that has been inserted. It uses the measured absorbance to calculate the concentration in a matter of seconds.

COD Determination Method. Standards of glycerol were prepared at different concentrations (0.5, 1%, and 2.5%). Condensate liquid samples were collected from the CSWCG rig during liquid sample collection for each run and were stored in the fridge below 4°C for more that 10 days prior to the COD analysis. The method (024) associated to the range of concentration was programmed and saved on the analyser as the analytical method.

COD Analytical procedure:

- Measure 1ml of standard or 1ml of the waste condensate liquid sample
- Add to the tube containing the reagent and mix well by hand shaking
- Place the tube into the COD reactor and heat (up to 2 h) at maximum temperature of 150°C
- Allow to cool for approximately 10 to 15 min
- Shake the tube well after cooling
- Place the tube on the COD analyser after selecting the analytical method and read the COD measurement.

Appendix W. Papers published